## Title

Understanding the mechanistic crosstalk between endoplasmic reticulum-associated degradation and lipid homeostasis



## Author

To, Milton

## Publication Date

2020

Peer reviewed|Thesis/dissertation

# Understanding the mechanistic crosstalk between endoplasmic reticulum-associated degradation and lipid homeostasis

By

Milton To

A dissertation submitted in partial satisfaction of the

requirements for the degree of

Doctor of Philosophy

In

Comparative Biochemistry

in the

Graduate Division

of the

University of California, Berkeley

Committee in charge:

Professor James Olzmann, Chair
Professor Sona Kang
Professor Daniel Nomura

Spring 2020

Abstract

Understanding the mechanistic crosstalk between endoplasmic reticulum-associated degradation and lipid homeostasis

by

Milton To

Doctor of Philosophy in Comparative Biochemistry

University of California, Berkeley

Professor James Olzmann, Chair

The endoplasmic reticulum (ER) mediates the folding, maturation, and deployment of the secretory proteome. Proteins that fail to achieve their native conformation are retained in the ER and targeted for clearance by ER-associated degradation (ERAD), a sophisticated process that mediates the ubiquitin-dependent delivery of substrates to the 26S proteasome for proteolysis. Recent findings indicate that inhibition of long-chain acyl-CoA synthetases with triacsin C, a fatty acid analogue, impairs lipid droplet (LD) biogenesis and ERAD, suggesting a role for LDs in ERAD. However, whether LDs are involved in the ERAD process remains an outstanding question.

We use chemical and genetic approaches to disrupt diacylglycerol acyltransferase (DGAT)–dependent LD biogenesis. We provide evidence that LDs are dispensable for ERAD in mammalian cells. Instead, our results suggest that triacsin C causes global alterations in the cellular lipid landscape that disrupt ER proteostasis by interfering with the glycan trimming and dislocation steps of ERAD. Prolonged triacsin C treatment activates both the IRE1 and PERK branches of the unfolded protein response and ultimately leads to IRE1-dependent cell death. These findings identify an intimate relationship between fatty acid metabolism and ER proteostasis that influences cell viability.

During ERAD, ubiquitinated substrates are extracted from membrane-embedded dislocation complexes by the AAA ATPase VCP and targeted to the cytosolic 26S proteasome. In addition to its well-established role in the degradation of misfolded proteins, ERAD also regulates the abundance of key proteins such as enzymes involved in cholesterol synthesis. However, due to the lack of generalizable methods, our understanding of the scope of proteins targeted by ERAD remains limited. To overcome this obstacle, we develop a VCP inhibitor substrate trapping approach (VISTA) to identify endogenous ERAD substrates. VISTA exploits the small-molecule VCP inhibitor CB5083 to trap ERAD substrates in a membrane-associated, ubiquitinated form. This strategy, coupled with quantitative ubiquitin proteomics, identified previously validated (e.g., ApoB100, Insig2, and DHCR7) and novel (e.g., SCD1 and RNF5) ERAD substrates in cultured human hepatocellular carcinoma cells. Moreover, our results indicate that RNF5 autoubiquitination on multiple lysine residues targets it for ubiquitin and VCP-dependent

clearance. Thus, VISTA provides a generalizable discovery method that expands the available toolbox of strategies to elucidate the ERAD substrate landscape.

In this dissertation, we discuss the intricacies between disruptions in cellular lipid homeostasis and its effects on ERAD. Furthermore, our development of VISTA enables proteomic profiling of endogenous ERAD substrates, many of which have been previously linked to lipid metabolism. Together, these studies provide novel tools and insight to elucidate a complex relationship between protein quality control in the ER and proper maintenance of the cellular lipid environment.

Dedication

For Pritella

Table of Contents

List of Figures

Acknowledgements

I thank everyone who has been there to share this journey with me. This dissertation would not have been possible without a great many people.

To James Olzmann: You have been a fantastic mentor for me through the years. It has been a privilege being a part of your lab and seeing it grow from the early days into what it is now. You were always there to challenge me and to support me. Thank you for believing in me and giving me more responsibilities than I thought I could handle.

To the members of the Olzmann Lab, past and present: You are the ones who have made my day to day graduate experience. Through long days and late nights, you have been there to share this experience. We shared sweat, tears, food, thoughts, stories, food, smells, laughs, lessons, data, diseases, disappointments, cells, plasmids, reagents, food, drinks, songs, pictures, videos, and so much more. I would not have had it any other way. Hi Truc.

To the wonderful members of the Comparative Biochemistry Program, NST department, and UC Berkeley community (hello, Alyssa Rosenbloom): Thank you for providing such a passionate research environment. I am extremely fortunate to be a surrounded by such a supportive group of people. To the less-wonderful members: Thanks for being there, I guess.

My graduate experience has been a wonderful journey thanks to all of you. Though the future holds many uncertainties, I draw my strength from the experiences I have shared with all of you. You all made the magic real.

# Chapter 1: Protein quality control and endoplasmic reticulum-associated degradation

## 1.1 Introduction

Proper folding of newly synthesized proteins is an essential step of all life. Inevitably, mutations, errors in transcription or translation, or environmental stress can yield terminally misfolded proteins. In order to compensate, cells have evolved complex mechanisms to ensure proper folding and function [1,2]. Misfolded proteins are most often degraded by the proteolytic pathway known as the ubiquitin-proteasome system (UPS), which occurs through the sequential actions of an E1 activating enzyme, an E2 conjugating enzyme, and an E3 ubiquitin ligase [2–4]. Typically, the C-terminus of ubiquitin, a 76-amino acid protein, is covalently attached to the ε-amine group of a lysine residue on the protein to be degraded. Following monoubiquitination of the misfolded protein, polyubiquitin chains are formed by the successive attachment of ubiquitin to any of the seven lysine residues of the preceding ubiquitin [5]. While ubiquitination can function in a wide variety of cellular regulation, it is most commonly understood as a marker for protein degradation.

## 1.2 Endoplasmic reticulum-associated degradation

The endoplasmic reticulum (ER) is a eukaryotic organelle where nearly one-third of the proteome is synthesized, folded, and modified prior to trafficking to downstream cellular compartments. Misfolded proteins in the ER are spatially separated from the UPS machinery in the cytoplasm. In a process known as ER-associated degradation (ERAD), a unique set of proteins in the ER is responsible for recognition of misfolded substrates and their delivery across the lipid bilayer of the ER for degradation by the cytosolic UPS [6]. ERAD is responsible for degrading a diverse set of substrates, including soluble luminal proteins, transmembrane proteins, and in some cases, cytoplasmic proteins. Although the precise mechanisms from substrate to substrate can vary and are yet to be elucidated, ERAD occurs through a series of spatially and temporally regulated steps: 1) recognition of the substrate for degradation 2) dislocation (also known as retrotranslocation) of the substrate across the ER bilayer 3) ubiquitination of the substrate and 4) degradation by the 26S proteasome.

### 1.2.1 Substrate recognition

The first step of ERAD involves the ability of the system to recognize a substrate for degradation. The vast majority of proteins entering the secretory pathway undergo N-linked glycosylation, the covalent addition of a core oligosaccharide unit containing three glucoses, nine mannoses, and two N-acetyl-glucosamines [7,8]. The terminal glucoses of the glycan are then trimmed by α-glucosidase I and α-glucosidase II, leaving a monoglucosylated glycan which can bind to the ER chaperones calnexin and calreticulin to assist in folding [6,8]. While progressive trimming of the final glucose residue by α-glucosidase II releases proteins from calnexin and calreticulin, UDP-glucose glycoprotein glucosyltransferase can reglucosylate the glycan, resulting in a folding cycle of binding and release from ER chaperones [8,9]. Terminally misfolded proteins in the ER can exit this cycle through the progressive trimming of mannose residues by ER mannosidases, and the trimmed glycans are recognized and bound by the ER lectins OS-9 and XTP-3 for delivery to the dislocation complex and subsequent degradation [6,8,10–12]. Although this folding cycle provides an intriguing mechanism by which misfolded proteins can be recognized, ERAD must also recognize proteins that are not glycosylated. While there is evidence for

glycosylation-independent ERAD pathways, ER mannosidases are also able to bind non-glycosylated ERAD substrates and facilitate their degradation [13–15].

### 1.2.2 Dislocation

Following recognition of an ERAD substrate for degradation, the substrate is then brought to a proteinaceous dislocation complex for access to the cytoplasmic UPS machinery. The dislocation complex appears to be composed of many adapter proteins surrounding a membrane-embedded E3 ubiquitin ligase [16]. Integrated proteomics analysis of these E3 complexes show that ERAD networks are organized into functional modules and adapter proteins to help accommodate for the diverse biochemical properties of ERAD substrates, including soluble luminal proteins and membrane proteins with many different topologies [17]. However, the mechanism by which substrates gain cytoplasmic access was unclear, with studies suggesting a role for the Derlin proteins, signal peptide peptidase, the Sec61 translocon, E3 ligases, and even lipid droplets in the dislocation of ERAD substrates [18–23]. A later study using reconstituted proteoliposomes found that autoubiquitination of the E3 ubiquitin ligase Hrd1 was sufficient to drive dislocation of an ERAD substrate [24]. This study suggested that transmembrane domains of the Hrd1 E3 ubiquitin ligase, and possibly other E3 ubiquitin ligases within the ER membrane, forms a pore by which ERAD substrates can access the cytoplasmic UPS machinery. The formation of the Hrd1 pore was later confirmed by structural analysis using cryo-electron microscopy in which five of eight transmembrane domains of Hrd1 form an aqueous cavity bridging the ER lumen to the cytosol [25]. Evidence of the Hrd1 pore formation was also supported by high-resolution electrophysiology, which also found a conformational change of the pore that was regulated by the autoubiquitination of Hrd1 [26]. While this model provides an elegant mechanism by which ERAD substrates can gain cytoplasmic access, it does not necessarily exclude the possibility of other mechanisms.

Although Hrd1 allows for cytoplasmic access of a luminal ERAD substrate, physical extraction from the lipid bilayer is catalyzed by p97/VCP, an ATPase associated with diverse cellular activities (AAA+ ATPase). Several ERAD proteins commonly found in complex with E3 ubiquitin ligases contain a variety of VCP-recruitment domains, suggesting that recruitment of p97/VCP is tightly coupled to ERAD by direct interaction with the dislocon [27]. p97/VCP drives dislocation through the ER membrane by harnessing energy from the hydrolysis of adenosine triphosphate (ATP) [27]. Structural studies reveal that p97/VCP forms a hexameric ring-like structure consisting of two stacked rings with a central pore region that contracts from ~61 to ~54 Å following ATP hydrolysis [28]. While the pore size is large enough to accommodate ERAD substrates, the relatively small magnitude of the contraction suggests that substrates may not be threaded through the pore itself. However, later biochemical data using site-specific photocrosslinking show that ATP hydrolysis indeed moves ERAD substrates from the D1 ring through the central pore through the D2 ring [29]. A later study using cryo-EM showed that the unfolding of ubiquitin allows for the physical processing of substrates through p97/VCP [30]. Together, this provides an elegant mechanism by which ERAD substrates are fed through the dislocation channel embedded in the ER membrane and pulled from the dislocon into the cytoplasm by p97/VCP using energy derived from the hydrolysis of ATP.

### 1.2.3 Ubiquitination

In addition to its role in the physical extraction of ERAD substrates, p97/VCP is also implicated in substrate unfolding to assist in degradation. Intriguingly, the unfoldase activity of p97/VCP appears to be dependent on the ubiquitination state of its substrate [29]. Ubiquitination of ERAD substrates can be catalyzed by dozens of E3 ubiquitin ligases in the ER membrane [31]. In some cases, multiple E3 ubiquitin ligases may coordinate to facilitate the degradation of substrates. The E3 ligases gp78 and Trc8 appear to cooperate in the ubiquitination and degradation of HMG-CoA reducatase [32]. In the case of a truncated major histocompatibility complex (MHC) class I heavy-chain molecule, Hrd1 is required for ubiquitination and dislocation, but the E3 ubiquitin ligase gp78 functions downstream of Hrd1 in coordination with the BAG6 chaperone complex [33]. Furthermore, cytoplasmic ubiquitination machinery may be involved. A recent genomic screen implicated the recruitment of the cytoplasmic E2 UBE2D3 and E3 ligases UBR4 and KCMF1 in the degradation of Insig-1 [34]. Moreover, the E3 ligases themselves can be ubiquitinated and degraded as a form of self-regulation, either by autoubiquitination or by ubiquitination by another E3 ligase [35,36]. Although ubiquitination of the E3 ligases can lead to degradation of the E3, ubiquitination of the lysine residues in the RING-finger domain of Hrd1 is required for proper substrate dislocation [24]. The overall interactions and potential compensation among the dozens of E3 ubiquitin ligases remains unclear and warrants further research.

### 1.2.4 A role for deubiquitinating enzymes

While E3 ubiquitin ligases play crucial roles in accelerating the degradation of ERAD substrates, their activities can be counteracted by the activity of deubiquitinating enzymes (DUBs). The human genome contains approximately 100 DUBs that can deconstruct polyubiquitin chains and remove ubiquitin from a target substrate [37]. While autoubiquitination of Hrd1 triggers dislocation of ERAD substrates, the ubiquitination can also drive degradation. Thus, the activity of the DUB must be carefully regulated to maintain proper activity of Hrd1. A recent study showed that deubiquitination of Hrd1 by the membrane-bound DUB Ubp1 stabilized levels of Hrd1, revealing a novel mechanism by which Hrd1 is regulated [38]. Furthermore, the activity of Ubp1 can be modulated by many of the interactors of Hrd1.

Removal of ubiquitin chains does not necessarily inhibit degradation of ERAD substrates. Expression of a dominant negative mutant of YOD1, a DUB associated with the p97/VCP dislocation complex, resulted in an impairment in the dislocation of several ERAD substrates, suggesting that trimming of polyubiquitin chains is required for proper dislocation [39]. Reconstitution of this process using Otu1 and Cdc48, the yeast homologs of YOD1 and p97/VCP respectively, verified the importance of polyubiquitin chains to recruit p97/VCP, but also the importance of deubiquitination for proper p97/VCP function [40]. A later study reconciled this apparent paradox [29]. In this study, polyubiquitinated substrates bind p97/VCP through the p97/VCP cofactors Ufd1 and Npl4, allowing the substrate to be threaded through the central pore of p97/VCP and accounts for the unfoldase activity. Trimming of the polyubiquitinated substrate by Otu1 leaves a shorter oligoubiquitin chain that can be unfolded and threaded through p97/VCP along with the rest of the substrate. Upon release of the substrate from the p97/VCP complex, the unfolded oligoubiquitin chain likely refold and allow for targeting to the proteasome. Together, this provides mechanistic insight for the requirement of both ubiquitination and deubiquitination of a substrate for ERAD.

### 1.2.5 Proteasomal degradation

ERAD substrates that have undergone dislocation and ubiquitination are ultimately targeted to the 26S proteasome for degradation. The 26S proteasome serves as the primary proteolytic system for protein degradation in eukaryotes and consists of a 20S barrel-like core peptidase and 19S regulatory lids on both ends [41]. Substrates are delivered to the proteasome through the recognition of ubiquitin on the substrate on the lid of the proteasome [42]. Once the substrate is engaged with the proteasome, it can be deubiquitinated by Rpn11, a DUB within the lid of the proteasome, and fed into the proteolytic core of the proteasome [42].

Of note, many ERAD substrates contain hydrophobic domains that become exposed to the cytoplasm following dislocation and unfolding. For Insig-1, a membrane protein degraded by ERAD, dislocation is coupled to proteasomal degradation by recruitment of proteasomes to the substrate prior to extraction from the membrane [43]. However, chaperones can also mediate dislocation and degradation in ERAD by maintaining the solubility of proteins during dislocation, and prior to degradation [44,45]. Unassembled TCRα chain is targeted for ERAD, and requires the Bag6 chaperone holdase complex to maintain solubility of ubiquitinated TCRα prior to degradation [46]. In this study, depletion of Bag6 or its cofactor Trc35 resulted in the formation of detergent insoluble aggregates.

Another path to sequester exposed hydrophobic domains of ERAD substrates has been suggested through lipid droplets, an organelle composed of a neutral lipid core bounded by a phospholipid monolayer. Lipidated ApoB-100 in the ER lumen, a key protein of very low density lipoprotein, appears to be dislocated from the lumen onto the surface of lipid droplets for proteasomal degradation [47]. In addition, lipid droplet proteins such as PLIN2 is degraded by the ERAD E3 ligase MARCH6 [48]. Together, these studies suggest that an intricate relationship between ERAD and lipid droplets exists, but the dynamics and control of these relationships have yet to be elucidated.

## 1.3 The unfolded protein response

Accumulation of misfolded proteins in the ER (known as ER-stress) activate a signal transduction pathway known as the unfolded protein response (UPR). The mammalian UPR activates a series of 3 distinct pathways, IRE1, ATF6, and PERK, to compensate for an excess of unfolded proteins and restore normal proteostasis [49,50]. Initially, the adaptive response of the UPR slows translation while upregulating genes involved in ER expansion, folding, and ERAD. However, under prolonged ER-stress, the UPR activates apoptosis to remove folding-defective cells [51].

### 1.3.1 Canonical activation and response

In yeast, the UPR is controlled by the activity of IRE1, which can directly bind to unfolded proteins, activating kinase and ribonuclease domains, resulting in regulated IRE1-dependent decay of cellular mRNA and noncanonical splicing of the transcription factor HAC1 (XBP1 in mammals) [49,52]. To further reduce the protein load of a cell undergoing ER stress, the ER-resident kinase PERK is activated and phosphorylates eukaryotic initiation factor 2α to inhibit general protein

translation [53]. Although activation of PERK temporarily inhibits global translation, it allows for the translation of certain genes, such as the transcription factor ATF4, to upregulate genes involving the restoration of cellular proteostasis [54]. Structural analysis of PERK reveal that the luminal domain is similar to that of IRE1, suggesting that both PERK and IRE1 can sense unfolded proteins using a similar mechanism [55]. The third branch of the UPR involves the transcription factor ATF6, which is constitutively expressed in the ER membrane. Upon ER stress, ATF6 is transported to the Golgi apparatus, where it is cleaved, released into the cytoplasm, and transported to the nucleus where it can upregulate the transcription of downstream targets [56].

Initial activation of the UPR upregulates genes involved in cell survival, such as genes involved in ERAD, expansion of the ER, and chaperones to assist in folding. However, cells unable to adapt to ER stress will eventually undergo UPR-induced apoptosis [57]. For example, activation of IRE1 can also lead to activation of Jun-N-terminal kinase and p38 MAPK, resulting in the activation of downstream pro-apoptotic factors [58]. Additionally, IRE1, ATF6, and PERK can all induce the expression of CHOP and induce apoptosis [59]. While previous work has elucidated the structure and mechanisms driving the transcriptional response of these three pathways, the factors driving the UPR between cell survival and cell death remain poorly understood.

### 1.3.2 Activation by lipid perturbations

While the UPR was historically studied in the context of unfolded proteins, emerging data reveal that the UPR can be activated to compensate for lipid disruptions in the ER membrane, known as lipid bilayer stress [60–62]. Genetic disruptions of phosphatidylcholine and phosphatidylethanolamine induced the UPR and caused severe imbalances in lipid composition in yeast [63]. In this study, the effects of the UPR was able to compensate for the otherwise lethal effects of chronic phosphatidylcholine deficiency, acting primarily to restore lipid homeostasis rather than protein homeostasis. Interestingly, uncoupling the lipid bilayer stress from proteotoxic stress reveals that the luminal domain of IRE1 is responsible for sensing proteotoxic stress, while the transmembrane domain of IRE1 senses lipid bilayer stress, and these two stresses result in divergent transcriptional response [64]. Together, this provides an complex and incompletely understood, relationship between protein quality control and lipid homeostasis.

## 1.4 ERAD in human health and disease

ERAD in human health and disease reflects a delicate balance between folding and degradation. Impairment of ERAD can lead to the accumulation of misfolded proteins. As demonstrated in the aberrant accumulation of mutant forms of transthyretin, failure of ERAD to degrade certain mutants can lead to amyloidosis [65]. However, ERAD can also degrade functional proteins as well. In the most common mutation in patients with cystic fibrosis, deletion of a phenylalanine at position 508 in the cystic fibrosis transmembrane conductance regulator (CFTR), the resulting protein is still functional, but is degraded by ERAD before it can reach the plasma membrane [66]. The search for treatments for this mutation have been focused on both folding of CFTR, as well as selective inhibition of ERAD [67,68]. Insight into how and why proteins are degraded can therefore have wide implications in human health and disease.

### 1.4.1 ERAD in lipid metabolism

The ER is the site of synthesis for many cellular lipids, including cholesterol, phospholipids, and neutral lipids [69]. In addition to its role in degrading mutant misfolded proteins, ERAD is also responsible for the regulated turnover of endogenous proteins. One of the best-studied cases of ERAD serving in quantity control is in that of cholesterol metabolism. Cholesterol is an essential component for human life and plays vital roles in a wide variety of cellular processes including the maintenance of membrane integrity and biogenesis of steroid hormones, bile acids, and oxysterols [70]. However, it has also long been known that increased cholesterol levels are a risk factor in cardiovascular disease [71]. For decades, statins have been used to inhibit HMG-CoA reductase, the rate-limiting enzyme in cholesterol synthesis, and control excess cholesterol levels [72]. However, ERAD can modulate the activities of several key enzymes to control the overall levels of cellular cholesterol through regulated degradation.

Under high sterol conditions, ERAD degrades HMG-CoA reductase, the rate-limiting enzyme in cholesterol synthesis, in order to decrease the rate of cholesterol biosynthesis [73]. Furthermore, at least several other key proteins in the cholesterol synthesis pathway are degraded by different ERAD pathways, including squalene monoxygenase and the Insig proteins [74]. Regulated degradation of proteins in this pathway shows the potential of ERAD serving as a key regulator of cellular metabolism. In addition to control of cholesterol metabolism through regulated degradation, ERAD proteins can affect triacylglycerol metabolism through non-degradative mechanisms. Under levels of high fatty acids, UBXD8, a p97/VCP recruitment factor essential for ERAD of several proteins, is recruited to the surface of lipid droplets, where it interacts with the lipase ATGL and prevents lipolysis [75]. However, the mechanism by which UBXD8 senses cellular lipids has yet to be elucidated. The relationship between lipid metabolism and protein quality control will be examined more closely in Chapter 2.

### 1.4.2 Hijacking ERAD

Although ERAD plays a vital role in both quality and quantity control of healthy cells, ERAD machinery can be manipulated by exogenous factors such as viruses and toxins. Toxins such as cholera and ricin enter the cell via endocytosis. Toxicity of cholera and ricin then depend on ERAD machinery to gain access to the cytoplasm [76,77]. Herpesviruses can also take advantage of ERAD as a form of immune evasion. The viral proteins US2 and US11 trigger the degradation of major histocompatibility class I (MHC-I) via recruitment of MHC-I to the TRC8 and TMEM129 E3 ubiquitin ligase complexes respectively [78–80]. While yeast use only two E3 ubiquitin ligases for ERAD, mammalian cells have evolved dozens of ER-membrane E3 ubiquitin ligases. Although TRC8 and TMEM129 have potential as therapeutic targets, little is known about their substrates and functions in healthy cells. Understanding the many different E3 ligase complexes and their relationship to normal cellular function is crucial to developing targeted therapeutics.

### 1.4.3 Unknown mechanisms of ERAD in diseases

While the past decades of research on ERAD have elucidated a general idea of the requisite steps as well as examples of key regulation points, much remains unknown about ERAD and its role in human health and disease. For example, the E3 ubiquitin ligase Hrd1 (also known as

synoviolin) is thought to be a causative factor for arthropathy in synovial cells [81]. However, while studies looking specifically for Hrd1 substrates have identified a large number of candidates, there is still a missing link between the substrates of Hrd1 and a mechanistic cause for arthropathy [82,83].

ERAD has also been implicated in several types of cancers through unknown mechanisms. Levels of the Hrd1 luminal adapter SEL1L were previously found to be significantly correlated with progression of colorectal cancer [84]. A study of 110 human gliomas also found expression of SEL1L to have a significant role in malignant gliomas [85]. Although the ER lectins OS-9 and XTP-3 have been implicated in cancer metastasis through regulation of HIF-1α expression, OS-9 does not play a role in HIF-1α degradation [86,87].

One proposed hypothesis for the role of ERAD in cancer lies in proteotoxic stress. The increased growth rate of cancer cells may result in more misfolded proteins, by which cells can compensate by inducing the UPR and upregulating ERAD [88]. Supporting this hypothesis, the proteasome inhibitor bortezomib has been used successfully in treating multiple myeloma [89]. Inhibition of p97/VCP has also been shown to have anticancer properties [90]. However, proteasome inhibition appears to have limited antitumor activity in solid tumors, suggesting that compensatory pathways may exist [91,92]. A mechanistic understanding of the many pathways within ERAD would allow for more targeted approaches in therapeutic development.

## 1.5 Figures

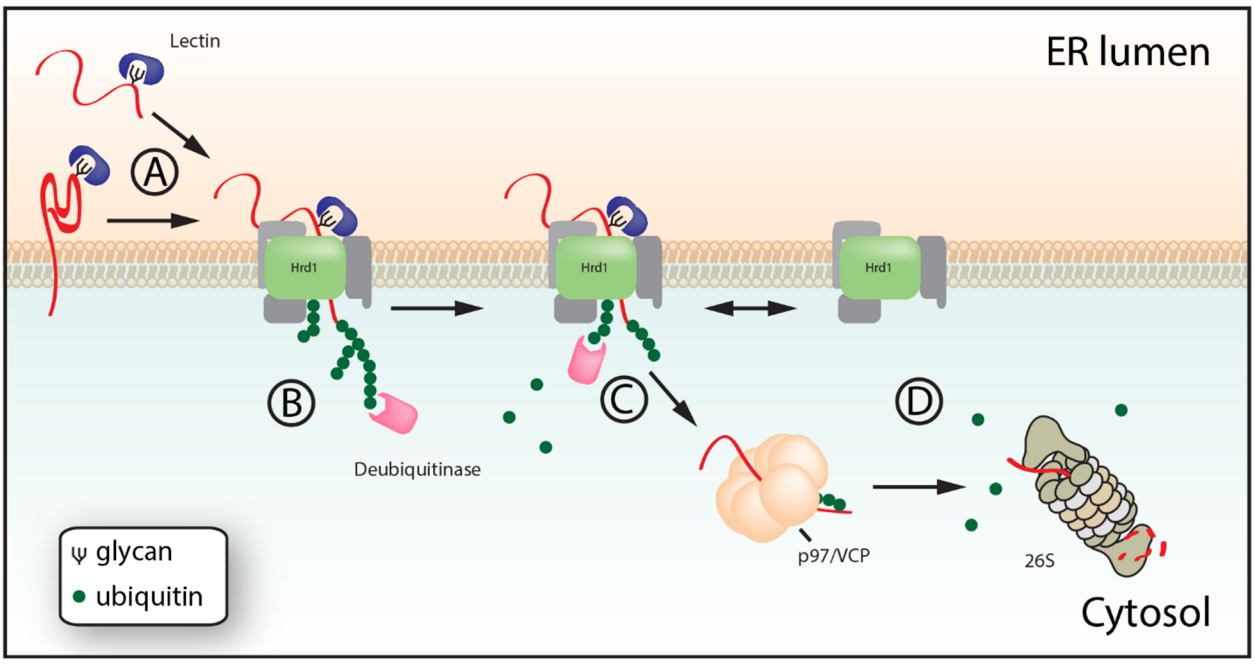


Figure 1-1: Overview of ERAD. (A) Proteins in the ER lumen or membrane are recognized by lectins or other adaptors for delivery to the Hrd1 (or potentially other E3 ubiquitin ligase) complex. (B) Substrates can pass through the pore of Hrd1 to gain access to the cytoplasm. Upon gaining access to the cytoplasm, the substrate is polyubiquitinated by one or more E3 ubiquitin ligase. Deubiquitinases trim the polyubiquitin chains on the substrate, leaving a short oligoubiquitin chain. (C) The substrate is physically pulled from the E3 ligase complex by the AAA+ ATPase p97/VCP. The substrate passes through the central pore of the p97/VCP complex, unfolding the attached oligoubiquitin chain. Once through, ubiquitin presumably refolds quickly. Hrd1 can also be extracted and degraded in this manner. While deubiquitinases can stabilize Hrd1, autoubiquitination is required for its activity. (D) Ubiquitinated and unfolded substrates are fed into the 26S proteasome, where ubiquitin chains are removed, and substrates are degraded into short polypeptides.

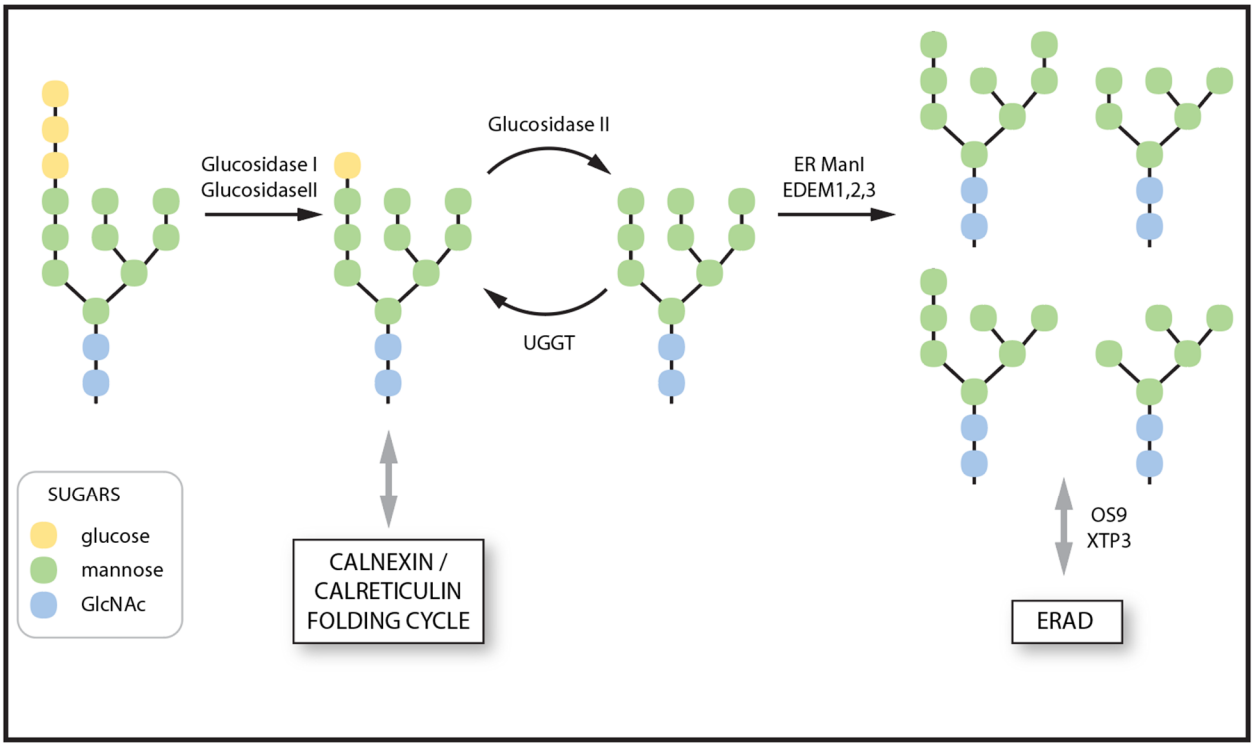


Figure 1-2: Glycan trimming in protein folding and ERAD. The vast majority of proteins entering the secretory pathway are modified by this core glycan unit. The terminal glucoses are quickly removed by α-glucosidase I and II. When glucose is present on the glycan, it is recognized by the ER chaperones calnexin and calreticulin to assist in protein folding. Progressive trimming of the mannose residues by ER ManI and the EDEMs recruit the ER lectins OS9 and XTP3 for delivery to ERAD. UGGT, UDP-glucose glycoprotein glucosyltransferase; GlcNAc, N-acetylglucosamine.

## Chapter 2: Lipid disequilibrium disrupts ER proteostasis by impairing ERAD substrate glycan trimming and dislocation

Contents in this chapter are modified with permission from the previously published research article:

To M*, Peterson CW*, Roberts MA, Counihan JL, Wu TT, Forster MS, Nomura DK, Olzmann JA. Lipid disequilibrium disrupts ER proteostasis by impairing ERAD substrate glycan trimming and dislocation. Mol Biol Cell. 2017 Jan 15;28(2):270-284.
*These authors contributed equally

## 2.1 Introduction

As the entry point into the secretory pathway, the endoplasmic reticulum (ER) is host to an extensive cohort of enzymes and chaperones that coordinate the folding, modification, and deployment of a large fraction of the proteome. Failure of secretory proteins to achieve their native structure due to mutations, errors in transcription or translation, protein damage, or inefficient folding can have dire consequences for cellular physiology and has been implicated in the etiology of numerous human diseases [93]. Incorrect protein folding not only can result in a reduction in protein activity (i.e., loss of function), but it can also lead to the generation of cytotoxic protein aggregates (i.e., gain of function). To ensure the fidelity of the secretory proteome, the ER has evolved a quality control system that detects terminally misfolded and unoligomerized proteins and targets them for clearance via a process known as ER-associated degradation (ERAD) [6,70,94]. The cell also responds to perturbations in ER homeostasis by activating the unfolded protein response (UPR) [95,96], a set of signaling pathways that enhance the overall folding capacity of the ER.

ERAD involves a series of spatially and temporally coupled steps that mediate substrate recognition, dislocation (also known as retrotranslocation) across the ER membrane into the cytoplasm, ubiquitination, and targeting to the proteasome for proteolysis [6,70,94]. Although the mechanism by which substrates are triaged for degradation is incompletely understood, it is clear that the structure of substrate-conjugated N-linked glycans provides a "molecular code" that plays a determining role in the fate of secretory proteins [97]. During insertion into the ER, the majority of the secretory proteome is modified by covalent attachment of a triantennary glycan moiety [98]. Progressive trimming by ER-resident mannosidases exposes an α-1,6–linked mannose, which acts as a signal for ERAD and is recognized by the mannose 6-phosphate receptor homology (MRH) domain of the ER lectin, OS-9, and possibly a second ER lectin, XTP3-B [12]. These two ER lectins interact with the Hrd1 luminal adaptor SEL1L [99–101], facilitating substrate delivery for dislocation. Most models posit that the AAA ATPase VCP (also known as p97) then extracts substrates from proteinaceous pores in the membrane, possibly formed by the E3 ubiquitin ligase Hrd1 [23,24,40], the derlin family of proteins [19,102–104], or in some cases, the Sec 61 translocon [21,105].

In addition to its role as a protein-folding compartment, the ER functions as a major site of lipid metabolism, mediating the synthesis of important lipids (e.g., phospholipids, sterols, and neutral lipids) and the biogenesis of lipid storage organelles called lipid droplets (LDs) [106–108]. LDs are ubiquitous, conserved organelles composed of a neutral lipid core (e.g., triacylglycerol [TAG] and sterol esters) encircled by a phospholipid monolayer. Whereas the hydrophobic core of LDs is devoid of proteins, the bounding phospholipid monolayer is decorated with a unique proteome that regulates LD growth, breakdown, and trafficking. LDs function as dynamic repositories of lipids, protecting the cell from fatty acid–induced toxicity [109] and providing the cell with an "on demand" source of lipids for membrane biogenesis [110], energy production via β-oxidation [111], and use as ligands in lipid signaling pathways [112,113]. Several unexpected roles have also been identified for LDs, such as the regulation of the hepatitis C life cycle [114,115], the sequestration of histones [116,117], and the control of cytosolic inclusion body clearance [118].

Reports have identified a number of intriguing links between ERAD and LDs. A subset of proteins implicated in ERAD, including UBXD8, UBXD2, VCP, AUP1, and Ube2g2, were

identified in proteomic analyses of buoyant, LD-enriched biochemical fractions [119–121] and the localization of these proteins to the LD surface was confirmed by fluorescence microscopy [47,75,100,122–125]. This subset of ERAD factors has been implicated in the regulation of LD abundance, size, and clustering [47,75,100,122–125], but whether these effects on LDs are related to their functions in ERAD remains to be determined. ERAD substrates have also been observed on the LD surface (e.g. ApoB100 [47,126]) and in ER subdomains that are closely juxtaposed to LDs (e.g., 3-hyd¬roxy-3-methylglutaryl-coenzyme A reductase (HMGCR) [127]). In addition, ER stress induces LD biogenesis [128,129] and loss of LDs activates the UPR [130–133].

Indirect experimental evidence supporting a functional role for LDs in ERAD came from studies employing triacsin C, a polyunsaturated fatty acid analogue that inhibits long-chain acyl-CoA synthetases (ACSLs) [134,135] and blocks LD biogenesis [136,137]. These studies found that triacsin C impaired the degradation kinetics of several ERAD substrates, including the null Hong Kong (NHK) mutant of α-1 antitrypsin [125], a truncated variant of ribophorin I [125], class I MHC heavy chain [125], and HMGCR [124,127]. Together these findings led to multiple models of how LDs might be involved in ERAD [18,47,124,125,127,129]: 1) LD biogenesis is coupled to the dislocation of luminal ERAD substrates via the formation of transient pores in the membrane or the dislocation of integral membrane ERAD substrates via capture in the membrane of an exiting LD, 2) ERAD substrate dislocation and ubiquitination preferentially occur in LD-associated ER subdomains, and/or 3) ERAD substrates are sequestered on the surface of LDs as an intermediate step en route to the proteasome. Although these models are attractive, triacsin C is not a specific inhibitor of LD biogenesis, as it also affects unrelated processes that require activated fatty acids (e.g., de novo phospholipid synthesis [134]). Moreover, the degradation kinetics of several ERAD substrates was unaffected in a strain of yeast lacking LDs [130,138], indicating either that LD formation is not essential for ERAD or that there are unrecognized differences between the ERAD process in yeast and mammalian cells. Thus, the functional relationship between ERAD and LDs remains unresolved.

In this study, we focused our attention on the effect of triacsin C on ERAD and the potential requirement of LDs for ERAD in mammalian cells. Our results demonstrate that, as in yeast [130,138], LDs are dispensable for ERAD in mammalian cells. However, our data indicate that triacsin C causes widespread changes in the cellular lipid composition, impairs ERAD substrate glycan trimming and dislocation, and induces the UPR, culminating in cell death. These findings support a fundamental connection between fatty acid metabolism and ER proteostasis.

## 2.2 Results

### 2.2.1 Inhibition of long-chain acyl-CoA synthetases with triacsin C impairs select ERAD pathways

To examine the effect of triacsin C on ERAD, we analyzed the degradation kinetics of a panel of substrates that reflect a range of topologies and use distinct degradation pathways (Figure 2-1A). The panel included an endogenous ERAD substrate, CD147, which is a glycosylated type I transmembrane protein that is recognized as an unassembled subunit of an oligomeric complex and is constitutively degraded by a Hrd1/SEL1L pathway [101]. We also tested two exogenously expressed mutant substrates: the NHK mutant of α-1 antitrypsin — a soluble, luminal substrate

degraded by a Hrd1/SEL1L pathway [99,139]) — and the ΔF508 mutant cystic fibrosis transmembrane conductance regulator (CFTRΔF508) — a polytopic integral membrane substrate degraded by multiple E3 ligase pathways [140–142].

To determine the kinetics of triacsin C treatment on ERAD disruption, we performed a time course of triacsin C incubation and analyzed the degradation of CD147 during emetine translation shutoff (Figure 2-1, B–D). As expected [101,143], CD147 migrated as two primary species: a high–molecular weight plasma membrane form bearing complex glycans (CD147(mature [Mat.])) and a lower–molecular weight ER form bearing the core-glycan structure (CD147(CG); Figure 2-1C). CD147(CG) was degraded during the 6-h emetine chase (Figure 2-1, C and D). Addition of triacsin C at time 0 of the emetine chase had no effect on CD147(CG) degradation (Figure 2-1, C and D). Increasing stabilization of CD147(CG) was observed as the triacsin C preincubation time was lengthened, with a maximal stabilization occurring after a 16-h triacsin C pretreatment (Figure 2-1, C and D). Using the 16-h triacsin C pretreatment, we analyzed the degradation kinetics of our full panel of ERAD substrates (Figure 2-1, E–J). The Hrd1 substrate CD147(CG) was stabilized by triacsin C pretreatment (Figure 2-1, E and F). Although the majority of newly synthesized CD147 is degraded by ERAD, a small fraction can correctly assemble and mature by trafficking through the Golgi to the plasma membrane [101,143]. To account for both fates of CD147, we performed radioactive pulse-chase experiments (Supplemental Figure 2-S1A). Over the 6-h time course of our experiment, no CD147 maturation was detected, and triacsin C pretreatment stabilized CD147(CG). These results indicate that the effect of triacsin C is due to impairment of CD147 degradation rather than maturation. The Hrd1 luminal substrate NHK–green fluorescent protein (GFP) was also stabilized by triacsin C pretreatment (Figure 2-1, G and H). No secretion of NHK-GFP was observed in this cell line (Supplemental Figure 2-S1B). In contrast to CD147 and NHK-GFP, CFTRΔF508 degradation kinetics was unaffected by the triacsin C pretreatment (Figure 2-1, I and J). These data demonstrate that treatment with the ACSL inhibitor triacsin C impairs select ERAD pathways.

### 2.2.2 Triacsin C does not generally inhibit the ubiquitin-proteasome system

Our finding that triacsin C inhibits the degradation of a subset of ERAD substrates suggests that triacsin C treatment does not generally inhibit the ubiquitin-proteasome system (UPS). In agreement with this notion, ubiquitinated proteins accumulated in cells treated with the proteasome inhibitor MG-132, but not with triacsin C (Figure 2-2A). To assess more directly the effect of triacsin C on the degradation of cytosolic proteins, we used flow cytometry to measure the degradation kinetics of a cytosolic UPS reporter (Figure 2-2B). This reporter consists of the Venus fluorescent protein fused to a destabilized domain (Venus-DD), a variant FK506-binding domain from FKBP12 that, in the absence of the small molecule shield-1, is misfolded and rapidly degraded via the UPS [144–146]. Triacsin C had no significant effect on the constitutive degradation of Venus-DD (Figure 2-2B), indicating that triacsin C does not generally affect the degradation of cytosolic UPS substrates.

After dislocation, ERAD substrates are deglycosylated by the cytosolic peptide:N-glycanase (PNGase) and cleared by the UPS [6,97]. Thus, the presence and accumulation of a deglycosylated form of ERAD substrates reflect inefficient coupling of dislocation with proteasomal degradation. Incubation with the proteasome inhibitor MG-132 during an emetine

chase resulted in the accumulation of deglycosylated CD147 (CD147(-CHO)), indicating the buildup of cytosolically dislocated CD147 (Figure 2-2C). CD147 deglycosylated in vitro by incubation with the glycosidase PNGase F resolved at the same molecular weight as the CD147 band that accumulated in MG-132–treated cells, and no additional lower–molecular weight forms appeared (Supplemental Figure 2-S2), confirming the identity of the CD147(-CHO) species. A portion of CD147 also migrated in a high–molecular weight smear, likely representing ubiquitinated CD147 (Figure 2-2C). In contrast to MG-132, triacsin C pretreatment solely stabilized CD147(CG); deglycosylated CD147 and ubiquitinated CD147 were absent (Figure 2-2C). Together, these data indicate that triacsin C impairs ERAD upstream of the proteasome and does not cause a global defect in the UPS.

### 2.2.3 Triacsin C does not impair protein secretion

Dysregulated lipid metabolism can alter organelle morphology and function [63,147,148], and disruptions in ER-to-Golgi trafficking reduce the degradation of some ERAD substrates [149–151]. To examine the function of the secretory pathway, we analyzed the secretion of hemagglutinin-tagged transthyretin (TTR-HA), a tetrameric protein that is normally secreted into the serum, where it functions as a carrier of the thyroid hormone thyroxine. Similar levels of TTR-HA were immunoprecipitated from media isolated from cells incubated in the presence or absence of triacsin C (Figure 2-2, D and E), indicating that triacsin C pretreatment does not affect TTR secretion. Furthermore, the overall morphology of the ER (Figure 2-2F) and Golgi complex (Figure 2-2G) remained unperturbed by a triacsin C pretreatment at the resolution of fluorescence deconvolution microscopy. Together, these results indicate that the secretory system remains functionally and morphologically intact after a 16-h triacsin C treatment.

### 2.2.4 Triacsin C impairs CD147 glycan trimming

Our initial results indicated that triacsin C affects ERAD upstream of the proteasome (Figure 2-2). To determine more precisely the steps in ERAD that are compromised, we focused our attention on the degradation of the endogenous substrate CD147, which was strongly stabilized by triacsin C (Figure 2-1). Glycan trimming is often believed to be one of the most upstream events in ERAD, potentially acting as a timing mechanism that releases a substrate from futile calnexin/calreticulin folding cycles and facilitates targeting for degradation by enabling direct interactions with the ERAD-implicated lectins [97]. The various trimmed CD147(CG) glycoforms are not resolved on small SDS–PAGE gels. Therefore, to examine a potential effect of triacsin C on CD147(CG) glycan trimming, we separated CD147 on large-format SDS–PAGE gels (Figure 2-3A). On these larger gels, the variety of CD147 glycoforms becomes evident, and CD147(CG) is resolved as approximately five bands (Figure 2-3A). Treatment of lysates in vitro with PNGase F collapsed all CD147 forms into a single band of ~29 kDa (Figure 2-3D), consistent with the conjecture that the variations in the CD147 banding pattern reflect the diversity of CD147 glycoforms.

During the course of an emetine translation shutoff experiment, the upper CD147(CG) bands were rapidly lost (Figure 2-3, A and B, vehicle), whereas the lower bands displayed a slight lag period before clearance (Figure 2-3, A and C, vehicle). These results are consistent with the conversion of CD147(CG) from a slower-migrating, untrimmed form into a faster-migrating,

trimmed form before degradation. Treatment with the mannosidase inhibitor kifunensine (Figure 2-3, A–C, kifunensine) or the glucosidase inhibitor deoxynojirimycin (Supplemental Figure 2-S3) stabilized CD147(CG) in the slower-migrating form, providing evidence that these bands represent an untrimmed form of CD147(CG). It is worth noting that CD147(CG) continued to be degraded in the presence of kifunensine (Figure 2-3A, kifunensine), albeit at a slower rate, indicating either that glycan trimming is not a strict requirement for CD147(CG) degradation or that kifunensine inhibition of glycan trimming is incomplete. Cotreatment with kifuensine and deoxynojirimycin did not result in additional stabilization (Supplemental Figure 2-S3). Analysis of CD147(CG) in cells pretreated with triacsin C revealed a significantly reduced rate of CD147(CG) conversion from untrimmed to the trimmed glycoform (Figure 2-3, A–C, triacsin C), similar to the effect of kifunensine. In contrast, blocking CD147(CG) degradation at a downstream step with the VCP inhibitor CB-5083 resulted in the accumulation of a lower–molecular weight, presumably highly trimmed form of CD147(CG) (Figure 2-3, A–C, CB-5083). These data suggest that triacsin C impairment in ERAD is caused, at least in part, through inhibition of substrate glycan trimming.

### 2.2.5 Triacsin C disrupts CD147 delivery to the Hrd1 dislocation complex

CD147 is degraded via an ERAD pathway that requires Hrd1, SEL1L, and, to some extent, the lectins OS-9 and XTP3-B [101]. The Hrd1 dislocation complex is a membrane-embedded, macromolecular complex [17,100]. Several properties of membrane lipids can influence the interactions and functions of membrane-embedded protein complexes [152,153]. To determine whether ACSL inhibition affects the composition of the Hrd1 dislocation complex, we used a quantitative triple stable isotope labeling with amino acids in cell culture (SILAC) strategy to measure the dynamics of Hrd1 interactions in response to triacsin C treatment (Figure 2-4A and Supplemental Tables 1-S1 and 1-S2). The results from this experiment are displayed in a two-dimensional plot (Figure 2-4A), which groups nonspecific background, as well as constitutive and dynamic interactors. Of the 145 proteins detected, 15 passed our criteria for high-confidence interactors (SILAC ratio M:L > 2-fold). In addition to the identification of Hrd1 itself (the bait), the strongest interactors (SILAC ratio M:L > 20-fold) were known members of the Hrd1 complex—SEL1L, FAM8A1, ERLIN2, OS-9, and XTP3-B. Other noteworthy interactors that were captured included proteins involved in protein folding and degradation, such as VCP, PDI, GRP94, Hsp47, calnexin, and ubiquitin. The significance of Hrd1 association with RPN1 (also known as ribophorin I), PGRC1, and EMD is unknown. These proteins are not known to be involved in protein quality control and may represent endogenous substrates of the Hrd1 complex. Several previously reported Hrd1 complex members (UBXD8, AUP1, derlin-1, derlin-2) were not detected in our SILAC experiment, possibly due to their lower abundance. Therefore, we examined the association of these interactors with Hrd1 by immunoblotting of affinity purified S-tagged Hrd1 complexes (Figure 2-4B). Analysis of the results from both the SILAC (Figure 2-4A) and immunoblotting (Figure 2-4B) experiments indicate that few Hrd1 interactions were affected by triacsin C treatment. The core Hrd1 complex, characterized by SEL1L, FAM8A1, XTP3-B, OS-9, and ERLIN2, remained intact after triacsin C treatment. There were minor trends toward increased associations with VCP and ubiquitin, as well as decreased association with Hsp47.

To examine a potential effect of triacsin C on the delivery of CD147 to the Hrd1 complex, we analyzed endogenous Hrd1 complexes immunoprecipitated from vehicle- and triacsin C–treated cells. Hrd1 bound only the ER-localized core glycosylated form of CD147 (Figure 2-4, C

and D), supporting the specificity of the interaction with CD147. Of interest, triacsin C treatment caused a pronounced decrease in the amount of CD147(CG) that coprecipitated with Hrd1 (Figure 2-4, C and D). Thus, our results indicate that whereas the overall composition of the Hrd1 dislocation complex is mostly unaffected, triacsin C treatment reduces the delivery of the substrate CD147 to the Hrd1 complex.

### 2.2.6 Triacsin C impairs the dislocation of a luminal glycosylated ERAD substrate

Given the effects of triacsin C on CD147 glycan trimming (Figure 2-3) and association with Hrd1 (Figure 2-4, C and D), we predicted that triacsin C would affect substrate dislocation. The accumulation of deglycosylated CD147 in response to MG-132 treatment provides one potential method to assess dislocation. However, MG-132 also stabilized CD147(CG), and the appearance of deglycosylated CD147 was minimal and difficult to detect (Figure 2-2C). Therefore, to assess quantitatively the effects of triacsin C on dislocation, we used a more sensitive and robust fluorescent ERAD dislocation assay based on the reconstitution of split Venus (Figure 2-4E) [154]. In this assay, the N-terminal half of deglycosylation-dependent Venus is fused to the H2-Kb signal sequence (SS-dgdV1Z), targeting it to the ER lumen [154] SS-dgdV1Z is glycosylated, recognized as an aberrant protein, and dislocated into the cytosol for degradation [154]. In the presence of MG-132, SS-dgdV1Z accumulates in the cytosol and associates with the C-terminal half of Venus (VZ2), reconstituting the mature fluorescent protein and enabling dislocation to be measured by flow cytometry [154]. Of importance, the fluorescence is deglycosylation dependent [154], ensuring that any fluorescence detected results from the dislocation of dgdV1Z from the ER lumen into the cytosol.

Incubation of 293T.FluERAD cells stably expressing SS-dgdV1Z and VZ2 with MG-132 resulted in a large increase in Venus fluorescence (Figure 2-4F, 16.4-fold increase). In agreement with a role for VCP in SS-dgdV1Z dislocation [154], ), coincubation with CB-5083 and MG-132 nearly completely blocked the increase in fluorescence (Figure 2-4F, 1.6-fold increase). Similar to the effect of kifunensine treatment (Figure 2-4F, 7.6-fold), triacsin C treatment partially blocked the increase in fluorescence in response to MG-132 (Figure 2-4F, 7.3-fold). Thus, triacsin C significantly reduces the dislocation of a luminal glycosylated ERAD substrate.

### 2.2.7 Lipid droplets are dispensable for CD147 ERAD

The observation that triacsin C inhibits ERAD [124,125,127] (Figure 2-1) is in agreement with a role for LDs in ERAD; however, triacsin C is not a selective inhibitor of LD biogenesis (Figure 2-5A). Although a selective inhibitor of LD biogenesis has not been identified, ablation of the diacylglycerol acyltransferase (DGAT) enzymes (DGAT1 and DGAT2), which catalyze the final and committed step in TAG synthesis (Figure 2-5A), causes a complete blockade of LD biogenesis in adipocytes [155]. Therefore, to examine a role for LDs in ERAD, we exploited a recently developed DGAT1 inhibitor, T863 (DGAT1i) [156], and mouse embryonic fibroblast (MEF) cell lines lacking DGAT2 (DGAT2-/-) [155,157] to simultaneously disrupt both DGAT enzymes. The DGAT2-/- MEFs exhibited a low amount of LDs under basal conditions, which increased dramatically after a 6-h treatment with 200 μM oleate (Figure 2-5, B and C), indicating that DGAT2-/- MEFs are still able to generate LDs in response to an oleate challenge, due to the presence of DGAT1. Treatment with either triacsin C or DGAT1i reduced the amount of LDs in non–oleate-treated cells and completely blocked the increase in LD biogenesis in response to oleate (Figure 2-5, B and C). The levels of

the LD protein perilipin-2 (PLIN2) are known to correlate with LD abundance, and, in the absence of LDs, PLIN2 is degraded by the ubiquitin-proteasome system [158–160]. Analysis of PLIN2 levels and cellular distribution indicate that triacsin C and DGAT1i treatments block oleate-induced increases in PLIN2 levels and PLIN2-immunoreactive LDs (Supplemental Figure 2-S4). Together these data demonstrate that the DGAT2-/- MEFs provide a facile means to acutely manipulate LD biogenesis at an upstream step (i.e., with triacsin C) or a downstream step (i.e., with DGAT1 inhibitor).

As observed in HEK293 cells, CD147(CG) was degraded in DGAT2-/- MEFs during an emetine translation shutoff experiment and was stabilized by a triacsin C pretreatment (Figure 2-5, D and E). The rate of CD147(CG) degradation was greater in the DGAT2-/- MEFs than in the HEK293 cells (half-life ∼25 min vs. ∼2 h). DGAT1i pretreatment, despite inhibiting LD biogenesis (Figure 2-5, B and C), had no effect on the kinetics of CD147 degradation (Figure 2-5, D and E). These results argue against a requirement for LDs in CD147 degradation and suggest that triacsin C affects ERAD through a mechanism independent of LDs.

### 2.2.8 Metabolomic profiling reveals global alterations in the cellular lipid landscape of triacsin C treated cells

To understand the effects of triacsin C on cellular lipid homeostasis, we performed targeted single reaction monitoring (SRM)–based liquid chromatography–tandem mass spectrometry (LC-MS/MS) steady-state lipidomic profiling of >100 lipid metabolites, encompassing a wide array of lipid classes, including neutral lipids, fatty acids, acyl carnitines (ACs), N-acyl ethanolamines, sterols, phospholipids, sphingolipids, lysophospholipids, and ether lipids (Figure 2-6 and Supplemental Table 2-S3). Among the 118 lipids, 71 exhibited significant changes ($p < 0.05$) after a 16-h triacsin C treatment (Figure 2-6, A–K). As expected, we observed a prominent decrease in the levels of many neutral lipids—monoacylglycerols (MAGs), diacylglycerols (DAGs), and TAGs (Figure 2-6, B and C). Not all species of TAG were reduced (e.g., C16:0/C20:4/C16:0 TAG and C18:0/C18:0/C18:0 TAG; Figure 2-6, B and C), suggesting that there may be protected pools of TAGs or that some ACSLs that are incompletely inhibited mediate the formation of these specific TAGs [134]. We also observed an anticipated decrease in AC levels, particularly in C16:0 AC (Figure 2-6, B and E). Although free fatty acids might be expected to accumulate due to the inhibition of ACSLs and consequent lack of conversion into the CoA intermediate for cellular use, no changes in fatty acid levels were detected (Figure 2-6B). This may be due to a compensatory efflux of free fatty acids [134], which could result in an underestimate of total free fatty acid levels, or increased flux through ACSL enzymes that are not inhibited.

Broad changes in additional cellular lipids were also observed, including decreases in many phospholipids, phospholipid ethers, neutral ether lipids, and lysophospholipid ethers (Figure 2-6, B–K). The decreases in lipid levels presumably resulted from impairments in synthesis caused by the inability of ACSLs to activate fatty acids, a requirement for conjugation. Particularly striking was the general decrease in nearly all phosphatidylinositol and phosphatidylinositol ether lipids (Figure 2-6, B, F, and J). This is interesting, given the recent finding that phosphatidylinositol maintains ER homeostasis in yeast by sequestering fatty acids when LD biogenesis is inhibited [131]. Our results suggest that phosphatidylinositol may represent an especially dynamic phospholipid pool that reflects the levels of fatty acid flux.

Several lipid species displayed significant increases, including many lysophospholipids (Figure 2-6, B, D, and H), which can act as signaling molecules, and several phospholipids (Figure 2-6, B–K). The increase in some lipids is consistent with the possible increased flux of fatty acids through ACSL enzymes that are not inhibited or are incompletely inhibited by triacsin C. The ratio of phosphatidylcholine (PC) to phosphatidylethanolamine (PE) has been implicated in ER homeostasis [63,161,162], and although we observed alterations in PC and PE levels (Figure 2-6, B and F), the ratio between the two lipid species was relatively unchanged. An increase in ceramides (C16:0 ceramide and C18:0 ceramide) was detected (Figure 2-6, B and G), which is notable, given their role in cellular stress responses and UPR activation [163]. Together our results indicate that triacsin C treatment not only affects the levels of neutral lipids sequestered in LDs, but it also causes widespread alterations in the cellular lipid landscape (Figure 2-6). The levels of several of the altered lipids have been suggested to affect ER homeostasis (e.g., phosphatidylinositol and ceramides).

### 2.2.9 Triacsin C activation of the PERK and IRE1 arms of the UPR has opposing effects on cell viability

Disruptions in ERAD and in lipid homeostasis can activate the UPR [163,164]. Inositol-requiring enzyme-1 (IRE1), an ER transmembrane serine/threonine kinase and endonuclease, is a primary mediator of the UPR that splices XBP1 mRNA to enable the translation of the XBP1 transcription factor [95]. Analysis using reverse transcription PCR revealed that incubation with triacsin C induced XBP1 splicing (Figure 2-7A). The spliced form of XBP1 was detectable at low levels as early as 8 h, and it became much more prominent at 16 and 24 h (Figure 2-7A). A second arm of the UPR is controlled by the ER-resident kinase PKR-like ER kinase (PERK), which phosphorylates the α subunit of eukaryotic translation-initiation factor 2 (eIF2α). Phosphorylation of eIF2α represses global translation while simultaneously promoting the translation of the ATF4 transcription factor to up-regulate stress-responsive genes such as the proapoptotic transcription factor C/EBP homologous protein (CHOP) [165]. To examine the potential effect of triacsin C on PERK induction of stress-responsive genes, we exploited a clonal HEK293 reporter cell line expressing an 8.5-kb CHOP gene fragment fused to GFP (CHOP::GFP) [166,167]. Treatment with tunicamycin, an inhibitor of N-linked glycosylation that induces the UPR, resulted in a robust and rapid accumulation in GFP fluorescence (Figure 2-7C and Supplemental Figure 2-S5). Treatment with triacsin C also caused an increase in GFP fluorescence but with different temporal dynamics. During the first 8 h, no increase in GFP fluorescence was observed (Figure 2-7C). This lag period was followed by an increase in GFP fluorescence levels at 16 and 24 h (Figure 2-7C).

The IRE1 and PERK arms of the UPR play well-characterized protective roles through the induction of genes involved in protein folding and membrane expansion and through the repression of translation [95]. Of note, UPR up-regulation protected yeast from ER trafficking and ERAD defects induced by lipid disequilibrium [63]. However, persistent activation of IRE1 or PERK can lead to cell death [168,169]. To determine the role of the IRE1 and PERK pathways in the cellular response to triacsin C treatment, we analyzed the effects of the IRE1 inhibitor 4μ8c (IRE1i) and PERK inhibitor GSK2606414 (PERKi). IRE1i completely blocked triacsin C–induced XBP1 cleavage (Figure 2-7, A and B), and PERKi significantly attenuated the induction of the CHOP::GFP reporter (Figure 2-7D). Inhibition of PERK increased the amounts of cell death

induced by triacsin C at 8, 16, and 24 h (Figure 2-7E), indicating that PERK plays a predominantly protective role under these conditions. In contrast, inhibition of IRE1 had little effect during triacsin C treatment and increased the amount of cell death at 24 h (Figure 2-7E). These findings indicate that both the IRE1 and PERK arms of the UPR are induced by triacsin C, but that the outputs of these two signaling pathways have opposing effects on cell viability.

## 2.3 Discussion

Although there are several intriguing connections between LDs and ERAD, whether LDs are directly involved in the ERAD mechanism has remained an outstanding question. Our data argue that LD biogenesis is not a fundamental requirement for ERAD. Instead, our results support a model (Figure 2-7F) in which triacsin C inhibition of ACSLs causes widespread changes in the cellular lipid composition that impair specific steps in ERAD, resulting in disruptions in ER proteostasis, activation of the UPR, and eventual cell death. Thus, dysregulated fatty acid metabolism negatively affects ER homeostasis and protein quality control independently of LDs. To inhibit LD biogenesis but avoid the broad effects that ACSL inhibition has on lipid homeostasis, we pursued an approach that would disrupt a downstream step in TAG synthesis. To this end, we characterized a combined chemical (DGAT1 inhibition) and genetic (DGAT2-/-) approach to inhibit both of the DGAT enzymes, which are required for the conversion of DAG to TAG and the generation of LDs [155,170]. This strategy enabled acute disruption of LD biogenesis, reducing LD abundance under basal and oleate-stimulated conditions as effectively as triacsin C does. In contrast to triacsin C, disruption of LD biogenesis by inhibiting the DGATs had no effect on the kinetics of CD147 ERAD. These results are consistent with previous analyses of ERAD in yeast models of LD disruption [130,138], which together demonstrate that LD biogenesis is not integral to the ERAD mechanism in yeast or mammalian cells. The possibility that LDs may function in the degradation of specific substrates or in ERAD under specific conditions is still worth consideration. For example, for ApoB100, an extremely large, hydrophobic protein, the association with LDs might provide a specialized ERAD mechanism to reduce aggregation [47,126]. LDs may also contribute to ERAD only under particular conditions, such as periods of disrupted proteostasis. Under conditions in which proteasomal capacity is limiting, the LD surface could act as a transient site for the sequestration of ERAD and other UPS substrates [126,129].

Our findings are in agreement with previous reports that triacsin C impairs ERAD [124,125,127]. Indeed, we found that triacsin C inhibited the degradation of two glycosylated Hrd1 substrates—the luminal substrate NHK and the endogenous integral membrane substrate CD147. The highest amount of substrate stabilization required a 16-h pretreatment with triacsin C, suggesting that ACSL activity is not required acutely during ERAD but instead that ACSL activity is required to establish a particular cellular environment conducive for ERAD. To define more precisely the step in ERAD that is affected by triacsin C, we tested individual steps of ERAD in the context of triacsin C treatment. Our results indicate that the triacsin C–induced defect in protein degradation is upstream of the proteasome and is confined to a subset of ERAD pathways. This conclusion is supported by several findings: 1) ubiquitinated proteins did not accumulate in response to triacsin C, 2) triacsin C did not stabilize a cytosolic UPS substrate, 3) triacsin C affected a subset of ERAD substrates—CD147 and NHK—but not CFTRΔF508, and 4) triacsin C impaired the dislocation of a luminal glycosylated substrate. Moreover, analyses of the glycosylation state of CD147 during degradation indicate that triacsin C treatment impaired CD147 glycan trimming and delivery to

the Hrd1 complex, suggesting that the primary impairment in ERAD is due to the failure to expose the trimmed glycan structure necessary for degradation commitment. Our proteomics data indicate that the composition of the Hrd1 complex is largely unaltered in triacsin C–treated cells; however, it is possible that alterations in the ER lipid composition could modulate the structure and/or function of the complex. The enzymes involved in the trimming of CD147's glycans are unknown, but this step is most likely catalyzed by ER-resident mannosidases ERManI and/or EDEM1-3. Disruptions in lipid composition could influence substrate localization to ERManI-containing ER subdomains [171] or could affect EDEM membrane association, which is known to affect EDEM glycan trimming activity toward certain substrates [172]. It is also possible that the inhibition of ACSLs could influence protein acylation, and both calnexin [173–175] and the ERAD E3 ligase gp78 [176] have been reported to be palmitoylated. Whether other ERAD factors are regulated by lipid modifications is unknown.

Activation of the UPR initiates signaling pathways with opposing outputs, a protective response that seeks to reestablish ER homeostasis and an apoptotic response that promotes cell death in the face of persistent ER stress [50,51,168,177]. Consistent with disruptions in ER homeostasis, treatment with triacsin C induced XBP1 splicing (IRE1 arm) and CHOP::GFP expression (PERK arm) and eventually caused cell death. Treatment of cells with the UPR inducer tunicamycin causes a rapid and transient up-regulation of IRE1 signaling that is paralleled by a slower increase in apoptotic PERK signaling at later times [168]. Of interest, in response to triacsin C, we see very different temporal dynamics and effects of UPR induction. Both the PERK and IRE1 arms exhibited similar activation kinetics and, after an initial lag period, steadily increased until the end of our experiments. Despite increasing CHOP reporter expression, PERK actions were overall protective in response to triacsin C. This finding indicates that CHOP expression alone is not conclusive evidence of a proapoptotic signaling output, consistent with the observation that forced CHOP expression was insufficient to induce cell death [178]. In contrast to PERK, IRE1 signaling appeared to promote cell death, and the inhibition of IRE1 attenuated triacsin C–induced apoptosis, possibly by inhibiting excessive regulated Ire1-dependent decay (RIDD) of important secretory transcripts [169] or activation of a JNK apoptotic signaling pathway [179]. These results highlight the complex relationship between the UPR and cell death and reveal that the mode of UPR activation (e.g., tunicamycin vs. triacsin C) has a profound effect on the ultimate effects of each UPR branch. Alterations in phospholipids can directly induce UPR signaling [60,163], and whether the changes in the lipid environment, the defects in ER protein quality control, or both are responsible for triacsin C activation of the UPR is unclear. In addition, how the UPR is customized to fit a particular ER stressor is not evident. It is possible that the temporal coordination of individual UPR branches influences the end output (i.e., protection vs. cell death) or that different ER stressors provide a unique "second hit" (e.g., disruptions in lipid homeostasis or depletion in ER calcium pools) that sensitizes cells to IRE1- or PERK-dependent cell death pathways.

Our study reveals an intimate relationship between cellular lipid homeostasis and ER protein quality control. Our findings raise the possibility that certain lipid environments and/or modifications may affect ER proteostasis by regulating specific steps of the ERAD process. It is worth noting that a multitude of diseases, ranging from obesity to neurodegenerative diseases, are associated with altered lipid homeostasis and upregulated UPR [180]. In addition, targeting lipid metabolic enzymes to decrease fatty acid availability (e.g., inhibition of FASN) is being actively pursued as a therapeutic strategy for the treatment of cancer [181–183]. Therefore, elucidating the

connections between ER lipid and protein homeostasis could have significant ramifications for our understanding of the pathogenic mechanisms underlying a wide number of diseases.

## 2.4 Materials and Methods

### 2.4.1 Plasmids, antibodies, and reagents

The pcDNA3.1(-) plasmids for expression of TTR-HA, the null Hong Kong mutant of α-1 antitrypsin (NHK-HA and NHK-GFP), and S-tagged Hrd1 (Hrd1-S) were previously described [17,99]. The CFTRΔF508 plasmid was kindly provided by Doug Cyr (University of North Carolina at Chapel Hill, Chapel Hill, NC).

Antibodies employed in this study include anti-CD147 (A-12, G-19, 8D6; Santa Cruz Biotechnology), anti-Hrd1 (A302-946A; Bethyl), anti-HA (HA7; Sigma-Aldrich), anti–S-peptide (EMD Millipore), anti-tubulin (Abcam), anti–glyceraldehyde-3-phosphate dehydrogenase (EMD Millipore), anti-GFP (Roche), anti-CFTR (University of North Carolina at Chapel Hill, CFTR Antibodies Distribution Program), anti–ubiquitin conjugates (FK2; EMD Millipore), anti-AUP1 (Proteintech), anti-SEL1L (T-17; Santa Cruz Biotechnology) and anti-KDEL (Enzo). Anti–derlin-1 and anti–derlin-2 antibodies were kind gifts from Yihong Ye (National Institutes of Health, Bethesda, MD). Rabbit polyclonal anti-UBXD8 antibodies were generated against a histidine-tagged fragment of UBXD8 (amino acids 97–445) by Proteintech Group. All IRDye680- and IRDye800-conjugated secondary antibodies for Western blotting were obtained from LI-COR. Alexa Fluor–conjugated secondary antibodies for immunofluorescence microscopy were obtained from Thermo Fisher Scientific.

Reagents employed in this study include triacsin C (Enzo Life Sciences), emetine dihydrochloride hydrate (Sigma-Aldrich), CB-5083 [90] (Cleave Biosciences), oleate (Sigma-Aldrich), kifunensine (Cayman Chemical), deoxynojirimycin (Sigma-Aldrich), MG-132 (Selleck Chemicals), T863 (Sigma-Aldrich), 4μ8C (EMD Millipore), GSK2606414 (EMD Millipore), tunicamycin (Cayman Chemical), and PNGase F (New England Biolabs).

### 2.4.2 Cell culture and transfection

HEK293, HEK293T, MEF, HeLa, and U2OS cells were cultured in DMEM containing 4.5 g/l glucose and l-glutamine (Corning) supplemented with 10% fetal bovine serum (FBS) (Thermo Fisher Scientific and Gemini Bio Products) at 37°C and 5% CO2. 293T.FluERAD cells stably expressing a split-Venus system for the analysis of the dislocation step of ERAD [154] were kindly provided by Peter Cresswell (Yale University, New Haven, CT). U2OS cells stably expressing Venus-DD [146] and HEK293 cells stably expressing the CHOP::GFP reporter were kindly provided by Ron Kopito (Stanford University, Stanford, CA). DGAT2-/- MEF cells were kindly provided by Robert Farese, Jr. (Harvard University, Cambridge, MA). All plasmid transfections were performed using X-tremeGENE HP (Roche) transfection reagent according to the manufacturer's instructions.

### 2.4.3 Immunoblotting analysis

Cells were washed extensively in phosphate-buffered saline (PBS) and lysed in 1% SDS. Protein amounts were normalized using a bicinchoninic acid (BCA) protein assay (Thermo Fisher Scientific). Proteins were separated on 4–20% polyacrylamide gradient gels (Bio-Rad) and transferred onto low-fluorescence polyvinylidene fluoride or nitrocellulose membranes (Bio-Rad). Large-format gel electrophoresis was performed using 10% acrylamide gels made with acrylamide/bis 19:1. Membranes were incubated in 5% nonfat milk in PBS plus 0.1% Tween-20 (PBST) for 30 min to reduce nonspecific antibody binding. Membranes were then incubated for at least 2 h in PBST containing 5% milk or 1% bovine serum albumin (BSA; Sigma-Aldrich) and primary antibodies, followed by incubation for at least 1 h in PBST containing 1% BSA and fluorescence-conjugated secondary antibodies. Immunoblots were visualized on a LI-COR imager (LI-COR Biosciences), and ImageJ [184] was used for quantification.

### 2.4.4 Immunofluorescence microscopy

HeLa and MEF cells were plated on poly-l-lysine–coated coverslips. Cells were treated the next day, washed with PBS, and fixed at room temperature with 4% paraformaldehyde in PBS for 10 min. Cells were washed three times with PBS and permeabilized with 0.1% Triton X-100 plus 1% BSA in PBS at room temperature for 30 min. Cells were washed three times with 1% BSA in PBS and incubated for 2 h in primary antibodies, washed three times, and incubated for 1 h with Alexa Fluor–conjugated secondary antibodies, BODIPY493/503 (LD staining; Thermo Fisher Scientific), and 4′,6-diamidino-2-phenylindole (DAPI; nuclei staining; Thermo Fisher Scientific). Cells were washed three times and mounted using Fluoromount-G (SouthernBiotech). Cells were visualized using a DeltaVision Elite microscope and acquired images deconvolved and analyzed using SoftWoRx. The abundance of LDs per cell was determined by measuring the area of BODIPY493/503–stained LDs per cell using ImageJ [184].

### 2.4.5 Affinity Purifications

HEK293 cells were harvested, washed with PBS, and lysed in immunoprecipitation (IP) buffer (50 mM Tris-HCl, pH 7.5, 150 mM NaCl, 1% digitonin, and protease inhibitor tablets [Thermo Fisher Scientific]) at 4°C for 30 min. Lysates were clarified by centrifugation at 20,000 × g for 10 min. Protein concentrations were measured using the BCA assay. For the affinity purification of S-tagged protein complexes, lysates were loaded onto S-protein agarose beads (EMD Millipore) at a concentration of 25 µl beads per 1 mg of lysate. For endogenous Hrd1 IPs, 2 mg of lysate was incubated with anti-Hrd1 antibodies for 1 h and then loaded onto 25 µl of protein G agarose beads (EMD Millipore). Lysates were incubated with the beads rotating at 4°C for 2 h, washed three times with lysis buffer containing 0.1% digitonin, and eluted in loading buffer.

### 2.4.6 Radiolabeling and pulse-chase analysis

HEK293 cells plated on poly-l-lysine–coated plates were washed twice with “cold” medium, which lacked l-methionine and l-cysteine and contained 10% dialyzed FBS, and then starved in this medium for 30 min. Cells were radiolabeled in medium containing 125 µCi/ml 35S-labeled cysteine/methionine (Easytag Express Protein Labeling Mix 35S; PerkinElmer) for 30 min, washed twice with Hanks’ buffered saline solution, and then chased in complete medium

containing 75 μM emetine for the indicated times. Cells were harvested, collected by centrifugation, washed in PBS, and lysed in pulse-chase IP buffer (25 mmol/l 4-(2-hydroxyethyl)-1-piperazineethanesulfonic acid buffer, pH 7.4, 150 mmol/l NaCl, 5 mmol/l MgCl2, 1% 3-[(3-cholamidopropyl)dimethylammonio]-1-propanesulfonate detergent, and protease inhibitors). Lysates were cleared by centrifugation at 20,000 × g for 15 min at 4°C and protein concentrations determined using the BCA assay. Lysates were precleared with protein G beads (EMD Millipore). CD147 was immunoprecipitated from lysates by incubation with anti-CD147 antibody (8D6; Santa Cruz biotechnology) for 4 h at 4°C with mixing, followed by incubation with protein G beads (EMD Millipore) for an additional 2 h at 4°C with mixing. Immunoprecipitated proteins were washed thrice with the pulse-chase IP buffer and then separated by SDS–PAGE. Gels were dried and exposed to a Storage Phosphor Screen (GE Healthcare Life Sciences) for 16 h at room temperature. Radioactive signals corresponding to CD147(Mat.) and CD147(CG) were detected using a Typhoon 9400 Molecular Imager (GE Healthcare Life Sciences).

### 2.4.7 SILAC Mass spectrometry

Parental HEK293 cells or HEK293 cells expressing S-tagged Hrd1 were grown in DMEM lacking l-arginine and l-lysine supplemented with 10% dialyzed FBS (Life Technologies) and the appropriate SILAC amino acids: light, l-arginine (Arg0) and l-lysine (Lys0); medium, 13C6-l-arginine (Arg6) and 4,4,5,5-D4-l-lysine (Lys4); and heavy, 13C615N4-l-arginine (Arg10) and 13C615N2-l-lysine (Lys8). Cells were cultured for at least seven cell doublings to allow for complete incorporation of the stable isotope-labeled amino acids (Cambridge Isotope Laboratories). Parental HEK293 control cells were light SILAC labeled, and S-tagged Hrd1 cells were either medium or heavy labeled. At 16 h before harvest, the S-tagged Hrd1 cells were incubated with either vehicle (medium SILAC labeled) or 1 μg/ml triacsin C (heavy SILAC labeled). After several washes in PBS, cells were lysed in IP buffer, and 3 mg of protein lysate was loaded onto 75 μl of S-protein agarose beads (EMD Millipore). Lysates were rotated at 4°C for 2 h and washed three times with IP buffer containing 0.1% digitonin and twice with 50 mM ammonium bicarbonate. Beads were resuspended in 75 μl of 0.2% RapiGest SF (Waters) in 50 mM ammonium bicarbonate for 15 min at 65°C, followed by incubation with 2.5 μg of trypsin (Thermo Fisher Scientific) overnight at 37°C. The affinity purification for each condition was performed separately to prevent exchange of interaction partners during the incubations. After the proteolysis step, equal volumes of digested peptides were combined and acidified with HCl to pH 2.0. Rapigest SF precipitate was removed by centrifugation at 20,000 × g for 30 min and the peptide solution concentrated to 40 μl using a SpeedVac. Digested peptides were analyzed by LC-MS/MS on a Thermo Scientific Q Exactive Orbitrap Mass spectrometer in conjunction with a Proxeon Easy-nLC II HPLC (Thermo Fisher Scientific) and Proxeon nanospray source at the University of California, Davis, Proteomics Core Facility. The digested peptides were loaded onto a 100 μm × 25 mm Magic C18 100-Å 5U reverse-phase trap, where they were desalted online before being separated using a 75 μm × 150 mm Magic C18 200-Å 3U reverse-phase column. Peptides were eluted using a 180-min gradient with a flow rate of 300 nl/min. An MS survey scan was obtained for the m/z range 300–1600, and MS/MS spectra were acquired using a top 15 method, in which the top 15 ions in the MS spectra were subjected to high-energy collisional dissociation. An isolation mass window of 1.6 m/z was used for the precursor ion selection, and a normalized collision energy of 27% was used for fragmentation. A 5-s duration was used for the dynamic exclusion. The acquired MS/MS spectra were searched against a full UniProt database of

human protein sequences, and SILAC ratios were determined using MaxQuant. The mass spectrometry proteomics data have been deposited to the ProteomeXchange Consortium via the PRIDE partner repository with the data set identifier PXD005633.

### 2.4.8 Lipidomic profiling

HEK293 cells were grown to 70% confluence in a 10-cm dish and treated for 16 h with vehicle or 1 μg/ml triacsin C. Cells were washed twice with PBS and harvested, and cell pellets were stored at −80°C. Lipid metabolite extraction and analysis by SRM-based LC-MS/MS was performed as previously described [181,185,186]. Briefly, nonpolar lipid metabolites were extracted in 2:1:1 chloroform/methanol/PBS supplemented with internal standards C12:0 dodecylglycerol (10 nmol) and pentadecanoic acid (10 nmol). The organic and aqueous layers were collected after separation by centrifugation at 1000 × g for 5 min. The aqueous layer was acidified by addition of 0.1% formic acid and subjected to a second chloroform extraction. The resulting organic layers were combined and mixed, dried down under N2, and dissolved in 120 μl of chloroform. A 10-μl aliquot was analyzed by SRM LC-MS/MS. Metabolites were separated using a Luna reverse-phase C5 column (Phenomenex), and MS analysis was performed on an Agilent 6430 QQQ LC-MS/MS. Quantification of metabolites was performed by integrating the area under the peak, normalized to internal standard values, adjusted based on external standard curves, and expressed as relative levels compared with the control sample.

### 2.4.9 XBP1 splicing assay

RNA was isolated using TRIzol Reagent (Life Technologies) and cDNA generated using the High-Capacity cDNA Reverse Transcription Kit (Applied Biosystems) according to the manufacturer's directions. XBP1 was amplified using the primers 5'-AAACAGA¬GT¬AGCAGC-TCAGACTGC-3' and 5'-TCCTTCTGGGTAGACCTCT¬GGGAG-3'. Amplified products were separated on a 2.5% agarose gel at 80 V for 2 h and visualized using a Gel Doc imaging system (Bio-Rad).

### 2.4.10 Cell viability

Cells were trypsinized, pelleted by centrifugation at 500 × g for 5 min, washed in PBS, and resuspended in 100 μl of PBS containing 2.5 μg/ml propidium iodide (BD Biosciences). After a 5-min incubation, cells were diluted with PBS to a final volume of 1 ml and analyzed using a BD Biosciences LSRFortessa. Cell suspensions were stored on ice throughout the procedure. Subsequent data analysis was performed using FlowJo software.

## 2.5 Figures

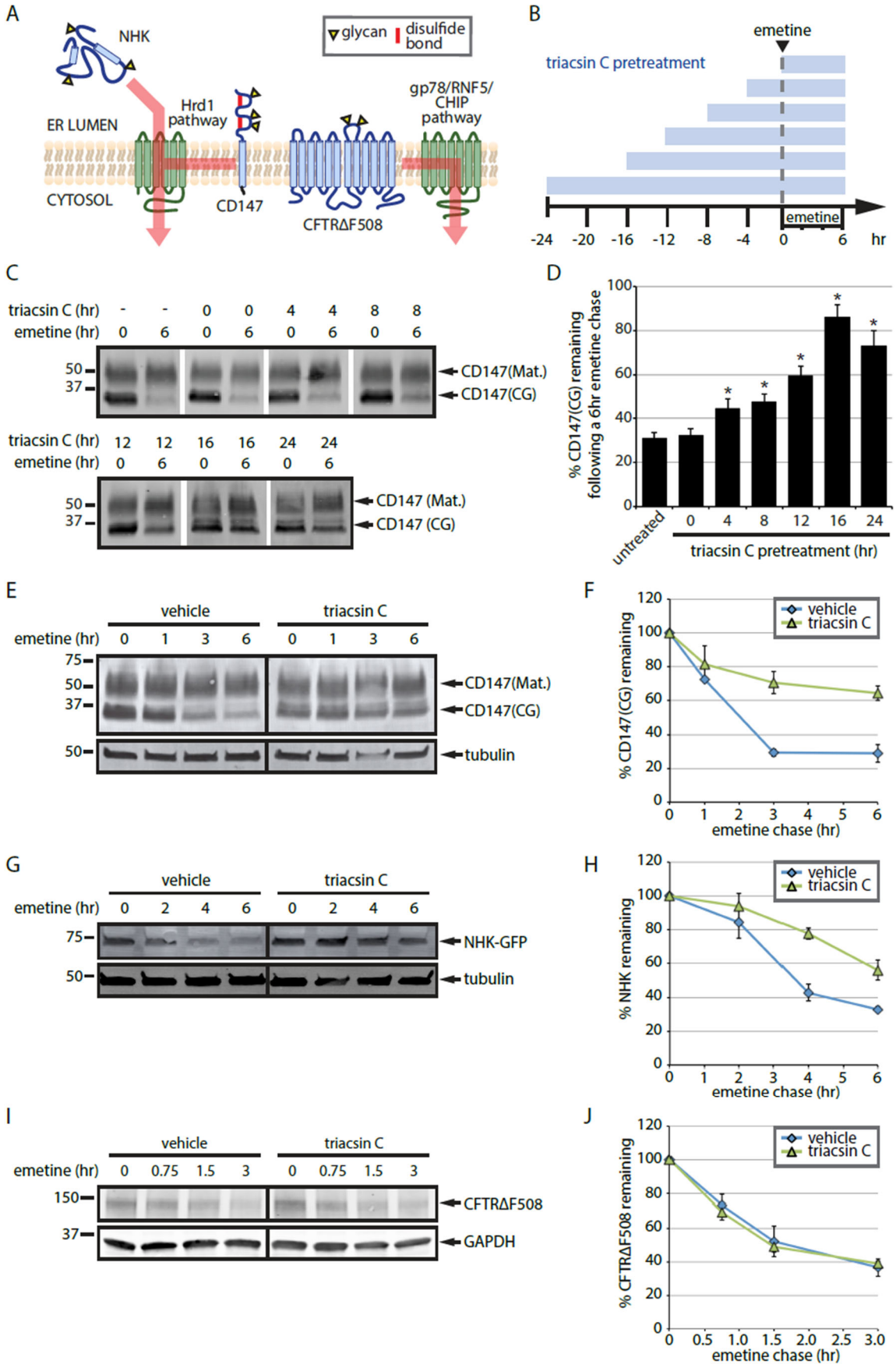
A
NHK
glycan
disulfide bond
ER LUMEN
Hrd1 pathway
gp78/RNF5/ CHIP pathway
CYTOSOL
CD147
CFTRΔF508
B
emetine
triacsin C pretreatment
emetine
-24 -20 -16 -12 -8 -4 0 6 hr
C
triacsin C (hr) - - 0 0 4 4 8 8
emetine (hr) 0 6 0 6 0 6 0 6
50
37
CD147(Mat.)
CD147(CG)
triacsin C (hr) 12 12 16 16 24 24
emetine (hr) 0 6 0 6 0 6
50
37
CD147 (Mat.)
CD147 (CG)
D
% CD147(CG) remaining following a 6hr emetine chase
100
80
60
40
20
0
*
untreated
0 4 8 12 16 24
triacsin C pretreatment (hr)
E
vehicle
triacsin C
emetine (hr) 0 1 3 6 0 1 3 6
75
50
37
CD147(Mat.)
CD147(CG)
50
tubulin
F
vehicle
triacsin C
% CD147(CG) remaining
120
100
80
60
40
20
0
0 1 2 3 4 5 6
emetine chase (hr)
G
vehicle
triacsin C
emetine (hr) 0 2 4 6 0 2 4 6
75
NHK-GFP
50
tubulin
H
vehicle
triacsin C
% NHK remaining
120
100
80
60
40
20
0
0 1 2 3 4 5 6
emetine chase (hr)
I
vehicle
triacsin C
emetine (hr) 0 0.75 1.5 3 0 0.75 1.5 3
150
CFTRΔF508
37
GAPDH
J
vehicle
triacsin C
% CFTRΔF508 remaining
120
100
80
60
40
20
0
0 0.5 1.0 1.5 2.0 2.5 3.0
emetine chase (hr)

Figure 2-1: Triacsin C inhibits a subset of ERAD pathways. (A) ERAD substrate panel, indicating substrate topology and degradation pathway(s). Substrates are indicated in blue and ERAD components in green. Yellow triangles indicate N-linked glycans. (B) Triacsin C treatment time course. Triacsin C was added for the indicated times (blue bars) and maintained in the medium throughout the emetine chase. (C) HEK293 cells were pretreated with 1 μg/ml triacsin C for the indicated times (as depicted in B), followed by addition of 75 μM emetine for 6 h. CD147 levels were assessed by immunoblotting of SDS lysates. (D) The relative CD147(CG) levels in C were quantified and are presented as percentage of the levels at time 0 h (n = 3). Asterisk indicates significant stabilization ($p < 0.05$). (E) HEK293 cells were pretreated with vehicle or 1 μg/ml triacsin C for 16 h, followed by 75 μM emetine for the indicated times. CD147 levels were assessed by immunoblotting of SDS lysates. (F) The relative levels of CD147(CG) in E were quantified and are presented as percentage of the levels at time 0 h (n = 3). (G) HEK293 cells expressing NHK-GFP were pretreated with vehicle or 1 μg/ml triacsin C for 16 h, followed by 75 μM emetine for the indicated times. NHK-GFP levels were assessed by immunoblotting of SDS lysates. (H) The relative levels of NHK-GFP in G were quantified and are presented as percentage of the levels at time 0 h (n = 3). (I) HEK293 cells expressing CFTRΔF508 were pretreated with vehicle or 1 μg/ml triacsin C for 16 h, followed by 75 μM emetine for the indicated times. CFTRΔF508 levels were assessed by immunoblotting of SDS lysates. (J) The relative levels of CFTRΔF508 in I were quantified and are presented as percentage of the levels at time 0 h (n = 4). Mat., mature; CG, core glycosylated. Error bars indicate SEM.

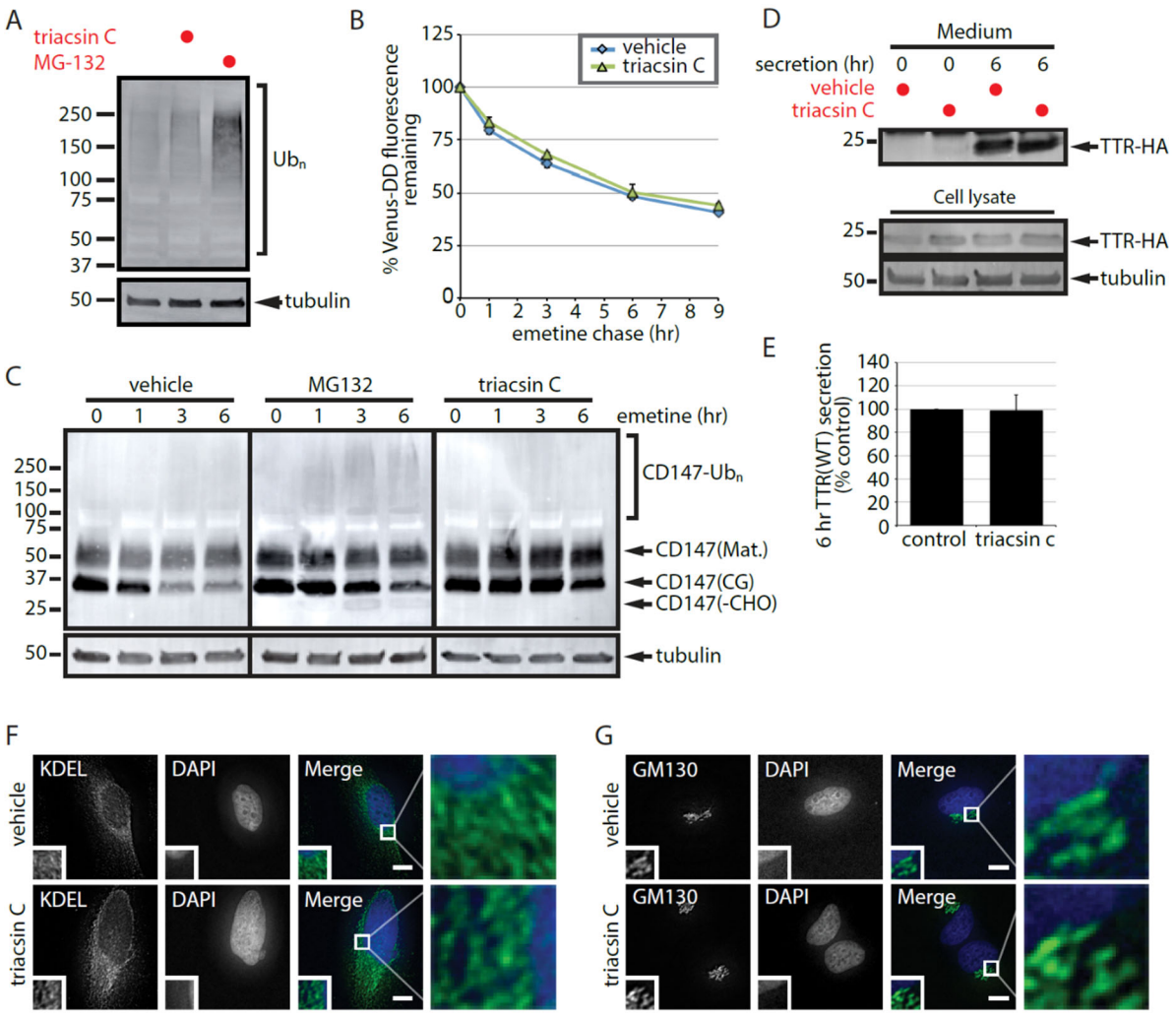


Figure 2-2: Triacsin C does not generally inhibit the ubiquitin-proteasome system or protein secretion. (A) SDS lysates from HEK293 cells incubated with 1 µg/ml triacsin C for 16 h or 10 µM MG-132 for 6 h were analyzed by immunoblotting. (B) U2OS cells stably expressing Venus-DD were incubated with vehicle or 1 µg/ml triacsin C for 16 h, followed by emetine treatments for the indicated times. Venus fluorescence levels were monitored by flow cytometry and quantified as the percentage of the levels at time 0 h (n = 3). (C) HEK293 cells were incubated with vehicle or 1 µg/ml triacsin C for 16 h and then treated with 75 µM emetine for the indicated times. Where indicated, 10 µM MG-132 was added at the beginning of the emetine chase. The levels of the different forms of CD147 were assessed by immunoblotting of SDS lysates. (D) HEK293 cells expressing TTR-HA were treated with vehicle or 1 µg/ml triacsin C for 16 h. Cells were washed with PBS, and the medium was replaced with serum-free OPTI-MEM containing vehicle or 1 µg/ml triacsin C for the remaining 6 h. Lysates and TTR-HA immunoprecipitated from the media were analyzed by immunoblotting. (E) The levels of TTR-HA in the media were quantified from D and are presented as percentage of the levels in the control sample (n = 3). (F, G) The morphology of the ER, anti-KDEL (green) and the Golgi complex, anti-GM130 (green), in HeLa cells treated with vehicle or 1 µg/ml triacsin C for 16 h was analyzed by immunofluorescence microscopy. Nuclei were stained with DAPI (blue). Scale bar, 10 µm. Mat., mature; CG, core glycosylated; -CHO, deglycosylated. Error bars indicate SEM.

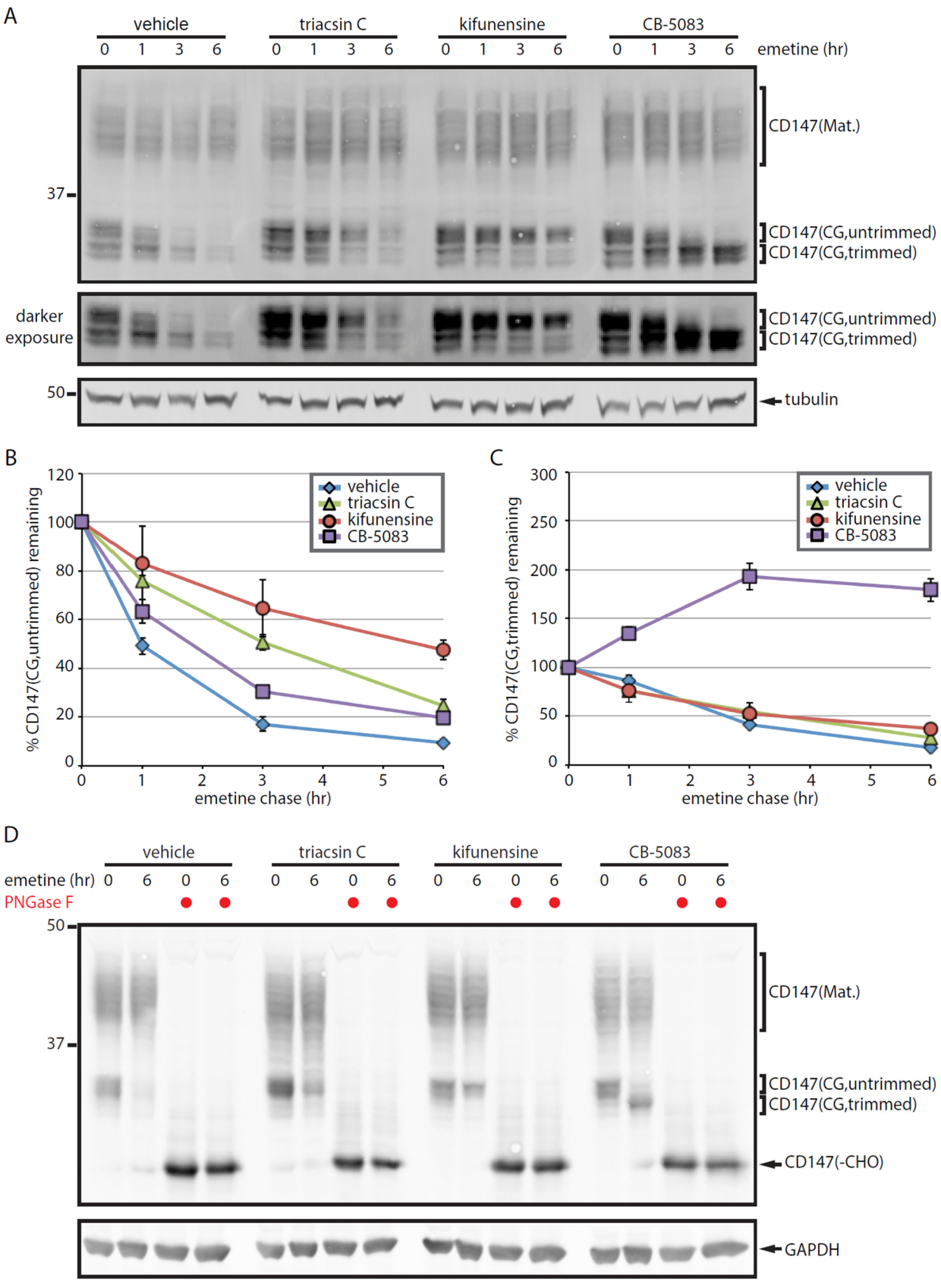
A
vehicle
triacsin C
kifunensine
CB-5083
0 1 3 6
emetine (hr)
37
CD147(Mat.)
CD147(CG,untrimmed)
CD147(CG,trimmed)
darker exposure
50
tubulin
B
% CD147(CG,untrimmed) remaining
emetine chase (hr)
C
% CD147(CG,trimmed) remaining
D
PNGase F
CD147(-CHO)
GAPDH

Figure 2-3: Triacsin C impairs ERAD substrate glycan trimming. (A) HEK293 cells were pretreated with vehicle or 1 μg/ml triacsin C for 16 h, followed by 75 μM emetine for the indicated times. Where indicated, 5 μg/ml kifunensine and 5 μM CB-5083 were added at the beginning of the emetine chase. SDS lysates were separated on large-format SDS–PAGE gels and analyzed by immunoblotting to visualize the different CD147 glycoforms. A darker exposure of the CD147(CG) bands is provided to facilitate visualization of the different trimmed glycoforms. (B, C) The relative levels of untrimmed CD147(CG) (B) and trimmed CD147(CG) (C) were quantified from A and are presented as percentage of the levels at time 0 h (n = 3). (D) Lysates from cells treated as in A were incubated with PNGase F as indicated and analyzed by immunoblotting. Mat., mature; CG, core glycosylated; -CHO, deglycosylated. Error bars indicate SEM.

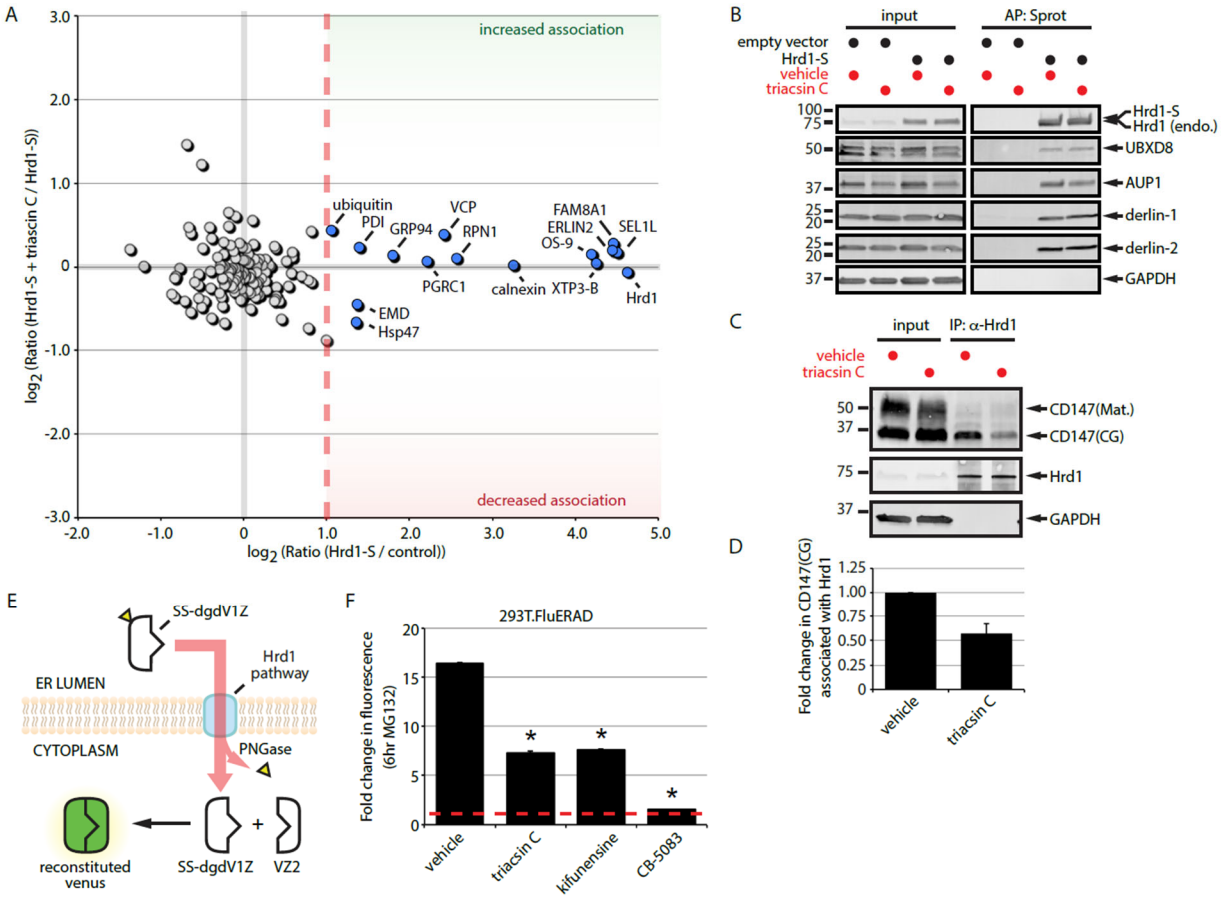


Figure 2-4: Triacsin C impairs substrate delivery to and dislocation from the Hrd1 complex. (A) Two-dimensional plot representing the proteomic analysis of Hrd1-S interactors from a triple SILAC experiment. The ratio of Hrd1-S/control on the x-axis indicates the strength of the interaction under basal conditions. The ratio of Hrd1-S + triacsin C/Hrd1-S on the y-axis indicates the change in the interaction in response to triacsin C treatment. Gray filled circles are nonspecific interactors, and blue filled circles are high-confidence interactors. (B) HEK293 cells expressing an empty vector or S-tagged Hrd1 were pretreated with vehicle or 1 µg/ml triacsin C for 16 h. Affinity-purified complexes were analyzed by immunoblotting with the indicated antibodies. (C) HEK293 cells were pretreated with vehicle or 1 µg/ml triacsin C for 16 h. Endogenous Hrd1 complexes were immunoprecipitated and analyzed by immunoblotting with the indicated antibodies. (D) The fold change in Hrd1-associated CD147(CG) in C was quantified and is presented as a bar graph (n = 3). (E) The split-Venus dislocation assay. See text for description. (F) 293T.FluERAD cells, which stably express the deglycosylation-dependent Venus dislocation system, were pretreated with 1 µg/ml triacsin C for 16 h, followed by a 0- or 6-h treatment with 10 µM MG-132. Where indicated, 5 µg/ml kifunensine or 5 µM CB-5083 was added together with 10 µM MG-132 for 0 or 6 h. Venus fluorescence levels were quantified by flow cytometry and are represented as the fold change relative to the 0 h. Asterisk indicates a significant decrease in the fold change in fluorescence levels ($p < 0.05$). AP, affinity purification; CG, core glycosylated; endo., endogenous; IP, immunoprecipitation; Mat., mature; Sprot, S-protein agarose. Error bars indicate SEM

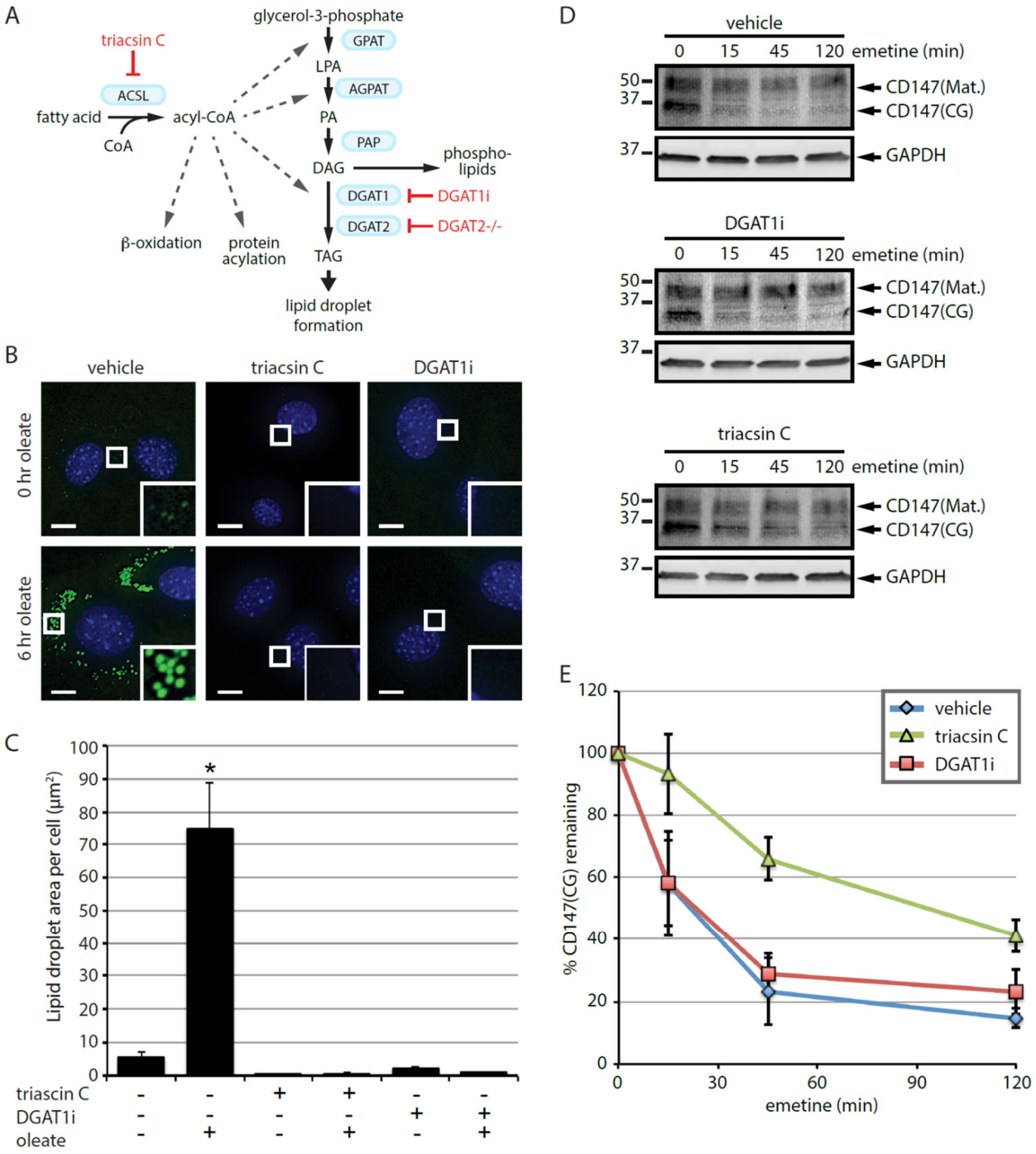


Figure 2-5: Lipid droplet biogenesis is dispensable for CD147 ERAD. (A) The Kennedy pathway of TAG synthesis indicating the enzymes (blue boxes) and metabolites. Select additional pathways that use acyl-CoA are also depicted. Approaches to disrupt LD biogenesis through the inhibition of ACSLs (triacsin C) or the DGAT enzymes (DGAT1i and DGAT2-/-) are indicated in red. (B) DGAT2-/- MEFs were pretreated with 1 μg/ml triacsin C or 20 μM DGAT1i for 3 h and then incubated with 200 μM oleate for 0 or 6 h as indicated. Fluorescence microscopy was employed to visualize LDs (green) and nuclei (blue). Scale bar, 5 μm. (C) The abundance of LDs was quantified from cells treated as shown in B. Asterisk indicates a significant increase in LD amount

relative to untreated cells ($p < 0.05$). (D) DGAT2-/- MEFs were pretreated with vehicle, 1 μg/ml triacsin C, or 20 μM DGAT1i for 16 h, followed by 75 μM emetine for the indicated times. CD147 levels were assessed by immunoblotting of SDS lysates. (E) The relative levels of CD147(CG) in D were quantified and are presented as percentage of the levels at time 0 h ($n = 3$). ACSL, long-chain acyl-CoA synthetase; AGPAT, acylglycerolphosphate acyltransferase; DAG, diacylglycerol; DGAT, diacylglycerol acyltransferase; GPAT, glycerol-phosphate acyltransferase; LPA, lysophosphatidic acid; PA, phosphatidic acid; PAP, phosphatidic acid phosphatase; TAG, triacylglycerol. Error bars indicate SEM.

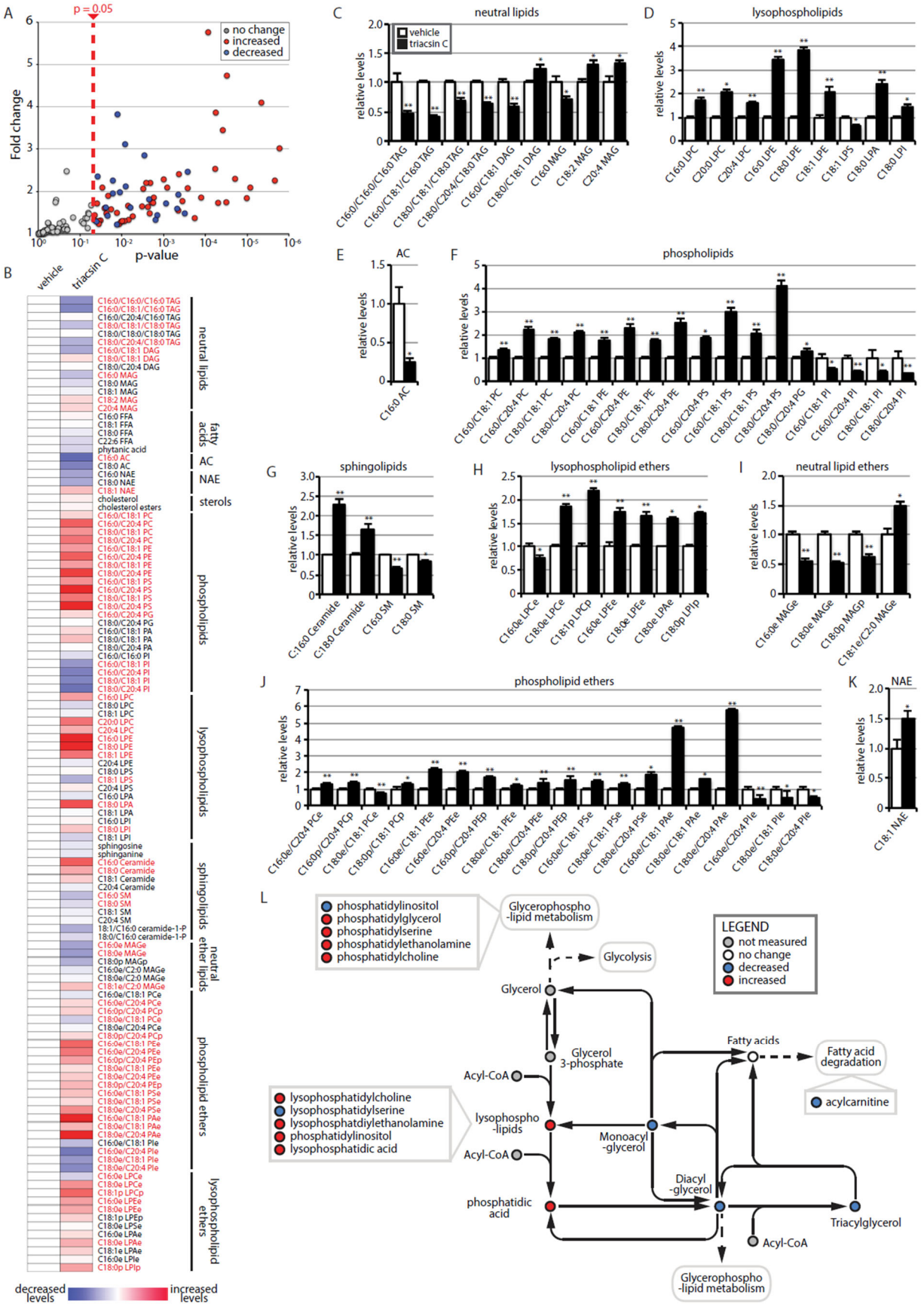
A
p = 0.05
no change
increased
decreased
Fold change
p-value
B
vehicle
triacsin C
neutral lipids
fatty acids
AC
NAE
sterols
phospholipids
lysophospholipids
sphingolipids
neutral ether lipids
phospholipid ethers
lysophospholipid ethers
decreased levels
increased levels
C
neutral lipids
vehicle
triacsin C
relative levels
D
lysophospholipids
E
AC
F
phospholipids
G
sphingolipids
H
lysophospholipid ethers
I
neutral lipid ethers
J
phospholipid ethers
K
NAE
L
phosphatidylinositol
phosphatidylglycerol
phosphatidylserine
phosphatidylethanolamine
phosphatidylcholine
Glycerophospho -lipid metabolism
Glycolysis
Glycerol
Glycerol 3-phosphate
Acyl-CoA
lysophosphatidylcholine
lysophosphatidylserine
lysophosphatdiylethanolamine
phosphatidylinositol
lysophosphatidic acid
lysophospho -lipids
Monoacyl -glycerol
Diacyl -glycerol
phosphatidic acid
Fatty acids
Fatty acid degradation
acylcarnitine
Triacylglycerol
Acyl-CoA
Glycerophospho -lipid metabolism
LEGEND
not measured
no change
decreased
increased

Figure 2-6: Triacsin C alters the cellular lipid landscape. Targeted metabolomic analysis of the nonpolar metabolome of cells treated with 1 μg/ml triacsin C for 16 h revealed alterations in 71 lipid species, illustrated as a volcano plot (A) and a heat map organized by lipid class (B). Red text in B indicates a significant change ($p < 0.05$). (C–K) Quantification showing the relative levels of significantly altered lipids ($n = 4$ or 5). *$p < 0.05$, **$p < 0.01$. White bars, vehicle; black bars, triacsin C. (L) Pathway map depicting the general effects of triacsin C on neutral lipids and phospholipids. DAG, diacylglycerol; FFA, free fatty acid; MAG, monoacylglycerol; NAE, N-acylethanolamine; PA, phosphatidic acid; PC, phosphatidylcholine; PE phosphatidy-lethanolamine; PG, phosphatidy¬lglycerol; PI, phosphatidylinositol; PS, phosphatidylserine; TAG, triacylglycerol. “L” before a lipid phospholipid designation indicates lyso-; “e” after a lipid designation indicates an ether lipid; “p” after a lipid designation designates plasmalogen. Error bars indicate SEM.

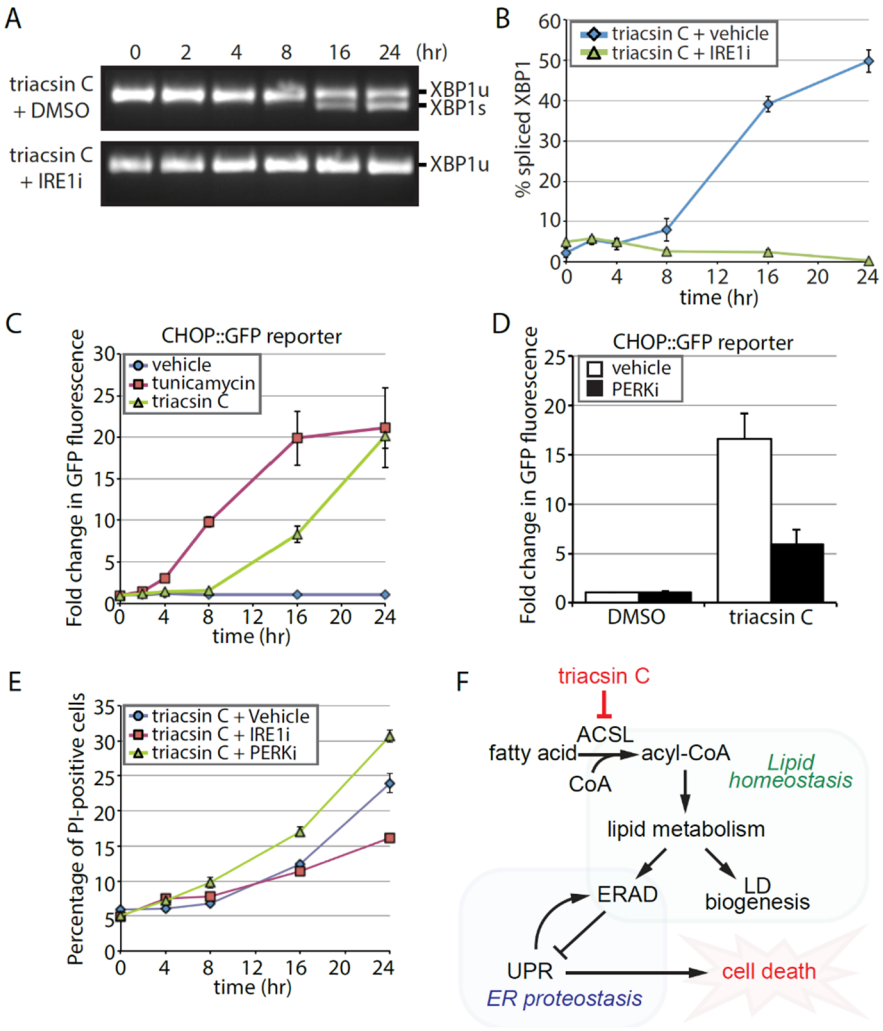


Figure 2-7: Triacsin C activates opposing arms of the UPR. (A) Reverse transcription PCR assay of XBP1 mRNA from HEK293 cells treated with 1 µg/ml triacsin C for the indicated times in the presence and absence of 100 µM IRE1 inhibitor 4µ8c (IRE1i). XBP1 amplicons were separated on an agarose gel and imaged. XBP1u, unspliced XBP1; XBP1s, spliced XBP1. (B) Quantification of the percentage of spliced XBP1 in A (n = 3). (C) HEK293 cells stably expressing a CHOP::GFP construct were treated with vehicle, 1 µg/ml triacsin C, or 5 µg/ml tunicamycin as indicated and GFP levels measured using flow cytometry. The fold change in GFP fluorescence relative to time 0 h is shown (n = 3). (D) HEK293 cells stably expressing a CHOP::GFP construct were treated with vehicle or 1 µg/ml triacsin C for 0 and 16 h in the presence and absence of 1 µM PERK inhibitor GSK2606414 (PERKi). GFP levels were measured using flow cytometry. The fold change in GFP fluorescence relative to time 0 h is shown (n = 3). (E) HEK293 cells were treated with 1 µg/ml triacsin C and vehicle, 100 µM IRE1i, or 1 µM PERKi for the indicated times and stained with propidium iodide to identify apoptotic cells. The percentage of apoptotic cells relative to time 0 h is shown (n = 3). (F) A model depicting the relationship between fatty acid metabolism and ER proteostasis. Disruptions in fatty acid metabolism result in lipid disequilibrium, causing impairments in ER quality control by inhibiting specific steps in ERAD (independent of LDs). The disruption in ER homeostasis activates the UPR, which protects cells via the PERK pathway and eventually kills cells via the IRE1 pathway. Error bars indicate SEM.

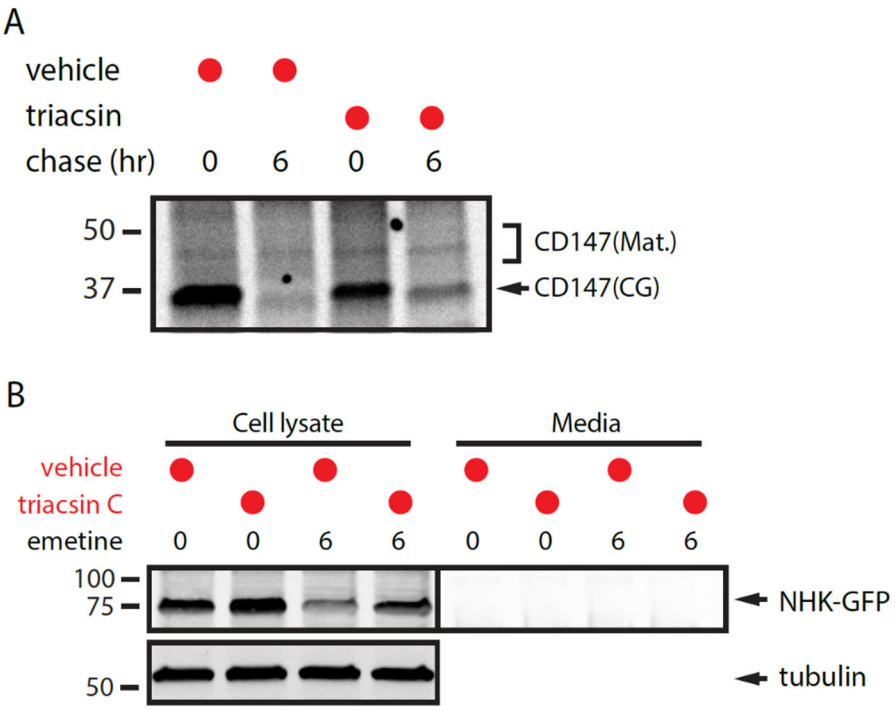


Figure 2-S1. Analysis of CD147 maturation and NHK secretion. (A) HEK293 cells were pretreated with vehicle or 1 µg/mL triacsin C for 16 hr, pulse labeled, and samples collected at 0 hr and 6 hr. CD147 was immunoprecipitated, separated by SDS-PAGE, and radioactivity detected using a Typhoon 9400. (B) HEK293 cells expressing NHK-GFP were treated with vehicle or 1 µg/mL triacsin C for 16 hr. Cells were washed with PBS, and the media was replaced with serum-free OPTI-MEM containing vehicle or 1 µg/mL triacsin C for the remaining 6 hr. Lysates and NHK-GFP immunoprecipitated from the media were analyzed by immunoblotting.

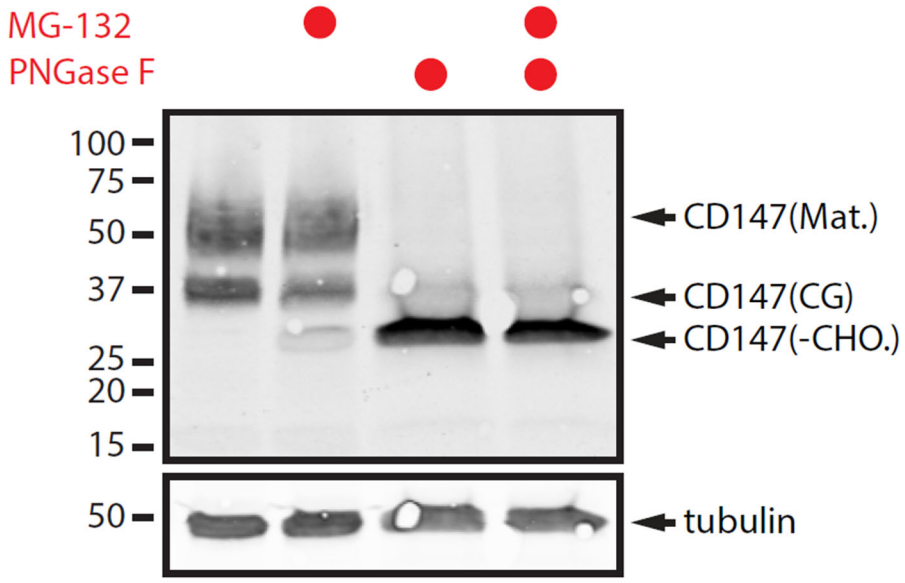


Figure 2-S2. Proteasome inhibition causes accumulation of CD147 in a deglycosylated form. HEK293 cells incubated with vehicle or 10 μM MG-132 for 6 hr were lysed in 1% SDS. Lysates were then incubated in the presence and absence of PNGase F for 30 min at 37o C. Proteins were separated by SDS-PAGE and analyzed by immunoblotting.

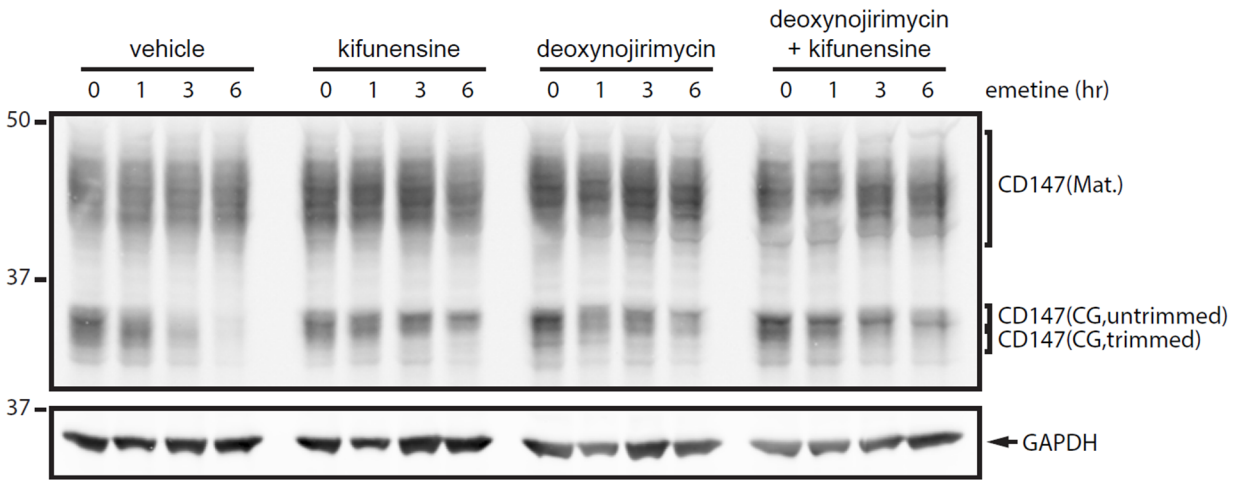


Figure 2-S3. Analysis of glucosidases and mannosidases in CD147 glycan trimming and degradation. HEK293 cells were incubated with 75 μM emetine in the presence and absence of 5 μg/mL kifunensine and 50 μM deoxynojirimycin as indicated. SDS lysates were separated on large format SDS-PAGE gels and analyzed by immunoblotting to visualize the different CD147 glycoforms.

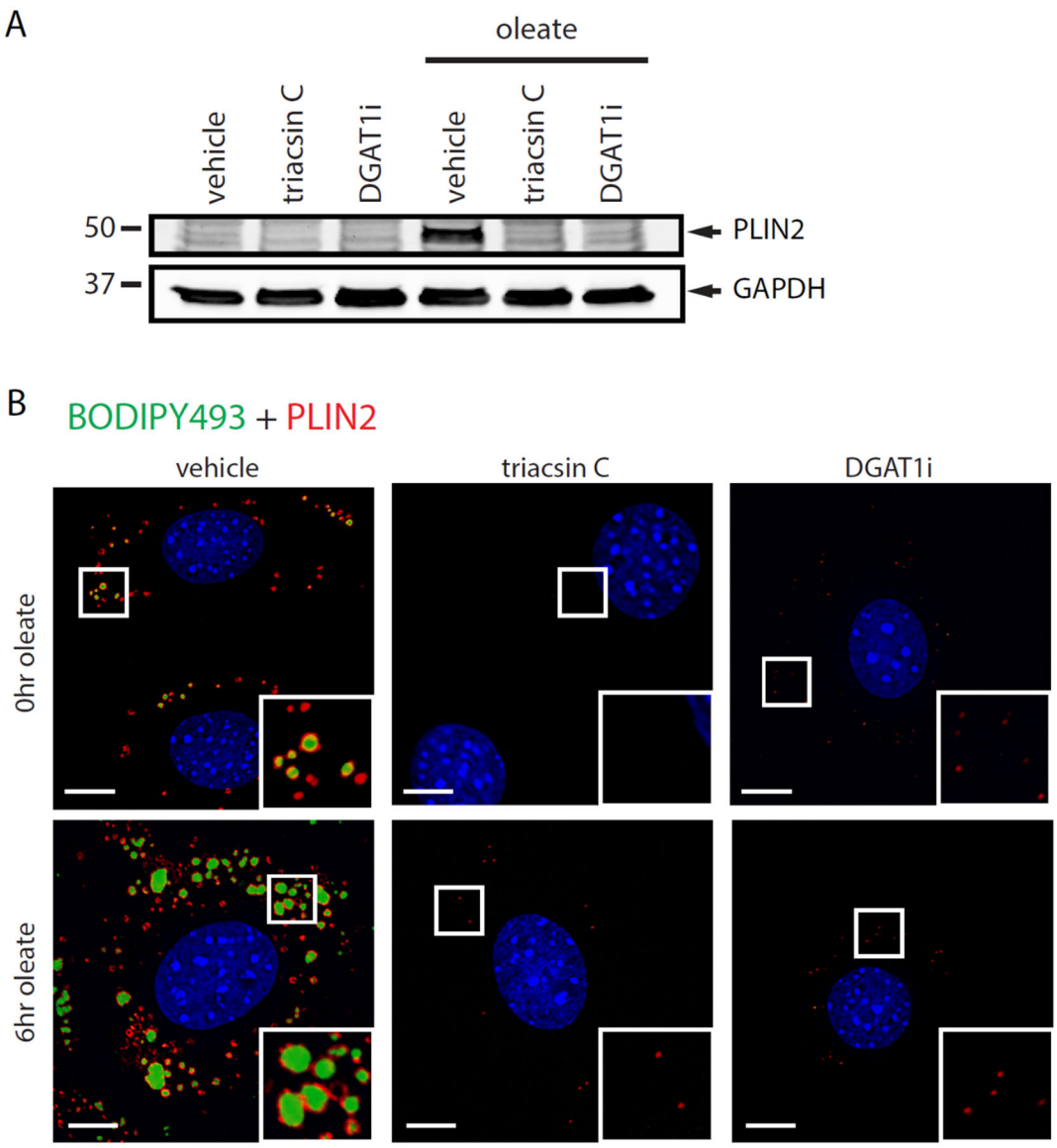


Figure 2-S4. Triacsin C and DGAT1 reduce the amount of PLIN2-positive lipid droplets. (A) DGAT2-/- MEFs were pretreated with 1 µg/mL triacsin C or 20 µM DGAT1i for 3 hr and then incubated with 200 µM oleate for 0 hr or 6 hr as indicated. Cells were lysed in 1% SDS and PLIN2 levels were analyzed by immunoblotting. (B) Cells were treated as in panel A and immunofluorescence microscopy employed to visualize PLIN2 (red), LDs (green), and nuclei (blue). Scale bar = 10 µm.

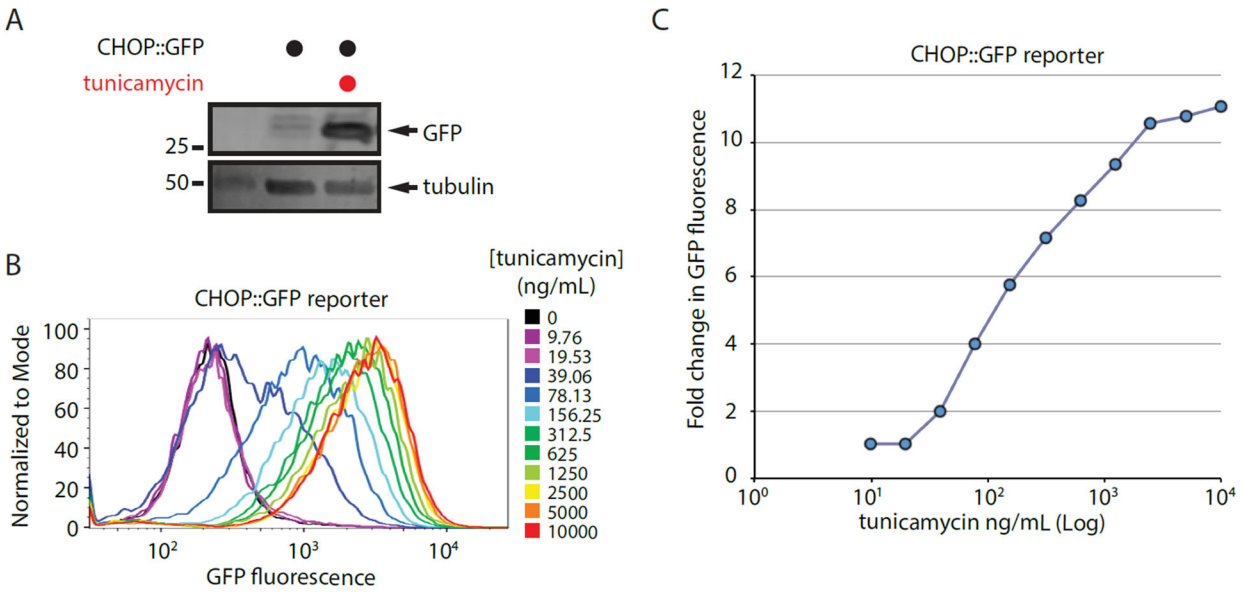


Figure 2-S5. Characterization of a CHOP::GFP reporter cell line. (A) Untransfected HEK293 cells or HEK293 cells stably expressing the CHOP::GFP reporter plasmid were incubated in the presence or absence of 5 µg/mL tunicamycin as indicated. GFP levels were analyzed by immunoblotting. (B) HEK293 cells stably expressing a CHOP::GFP construct were treated with increasing concentrations of tunicamycin. GFP levels were measured using flow cytometry and are represented as a histogram normalized to the mode. (C) The fold change in GFP fluorescence levels relative to time 0 hr from cells treated as in panel B is shown.

# Chapter 3: A VCP inhibitor substrate trapping approach (VISTA) enables proteomic profiling of endogenous ERAD substrates

Contents in this chapter are modified with permission from the previously published research article:

Huang EY*, To M*, Tran E, Dionisio LTA, Cho HJ, Baney KLM, Pataki CI, Olzmann, JA. A VCP inhibitor substrate trapping approach (VISTA) identifies endogenous ERAD substrates. Mol Biol Cell. 2018 May 1;29(9):1021-1030.
*These authors contributed equally

## 3.1 Introduction

The endoplasmic reticulum (ER) mediates the folding, modification, and deployment of one-third of the cellular proteome. Proteins that fail to fold or lack requisite oligomeric binding partners are degraded through ER-associated degradation (ERAD), a ubiquitin-dependent process that targets substrates to the 26S proteasome for proteolysis [6,94,187]. A modular network of ERAD machinery coordinates substrate recognition and dislocation (also known as retrotranslocation) from the ER lumen or membrane into the cytoplasm [17,188]. ER-resident E3 ubiquitin ligases mediate substrate ubiquitination, which serves both as a proteasomal targeting signal and a binding interface that facilitates substrate extraction by the homohexameric AAA ATPase VCP (also known as p97) and its associated ubiquitin-binding cofactors (e.g., UFD1L and NPLOC4[6,189]. VCP-mediated ATP hydrolysis generates the necessary force for the extraction of the ubiquitinated substrate, which is partially unfolded as it is threaded through the VCP central pore [29,190,191].

A canonical role of ERAD is the clearance of misfolded proteins (i.e., quality control), such as the ΔF508 mutant cystic fibrosis transmembrane conductance regulator in cystic fibrosis and the truncated null Hong Kong (NHK) variant of α-1 antitrypsin in α-1 antitrypsin deficiency [93]. The identification of disease-associated mutant proteins as ERAD substrates has provided useful tools to study the mechanisms of ERAD [192]. A less appreciated role of ERAD is in regulating the levels of endogenous proteins (i.e., quantity control) [70,193,194]. For example, ERAD controls the flux through the cholesterol synthesis pathway by facilitating the sterol-regulated degradation of HMG CoA reductase [195] and squalene monooxygenase [196,197]. ERAD quantity control has also been implicated in a wide variety of pathological conditions, such as cancer, hepatic steatosis, obesity, diabetes insipidus, and immune system function, through its ability to degrade ER-resident proteins (e.g., HMG CoA reductase, Insig1/2), secreted proteins (e.g., ApoB100, proAVP), and plasma membrane proteins (e.g., KAI1, CD147, pre–B cell receptor, SLC1A5, SLC38A2) [101,195,198–205]. Thus, by influencing the abundance of ER-resident proteins and secreted proteins, ERAD impacts both cell autonomous and noncell autonomous processes.

Despite the importance of ERAD in protein quantity control, our understanding of the endogenous substrates targeted by ERAD remains limited. This surprising dearth of knowledge is in part due to the lack of generalizable methods to identify endogenous ERAD substrates in human cells. Here, we describe a quantitative ubiquitin proteomics strategy termed VCP inhibitor substrate trapping approach (VISTA) to identify endogenous ERAD substrates.

## 3.2 Results and Discussion

### 3.2.1 VCP Inhibition traps ubiquitinated NHK in complex with the Hrd1 E3 ubiquitin ligase

A principal function of VCP is to extract ubiquitinated ERAD substrates from the ER into the cytosol for proteasomal degradation [189,206]. CB5083 is a small-molecule VCP inhibitor that impairs the degradation of several integral membrane ERAD substrates, including CD147 [200], c18orf32 [207], and overexpressed TCRα-GFP [90]. In addition, incubation with CB5083 results in the accumulation of ubiquitinated proteins [90,208]. We reasoned that acute pharmacological inhibition

of VCP with CB5083 could be exploited to stabilize or "trap" ERAD substrates in a ubiquitinated, membrane-bound form (Figure 3-1A).

As a first test of the utility of CB5083 to trap ERAD substrates, we examined the impact of CB5083 treatment on the well-characterized luminal ERAD substrate NHK. In a translation shut-off assay, the half-life HA-tagged NHK (NHK-HA) was greatly extended in the presence of CB5083 (Figure 3-1, B and C), demonstrating that incubation with CB5083 impairs the degradation of a luminal ERAD substrate. Dislocation and ubiquitination of NHK are mediated by a membrane-embedded, macromolecular complex containing the E3 ubiquitin ligase Hrd1 [99,139]. Thus, we sought to test the hypothesis that VCP inhibition traps polyubiquitinated NHK in complex with Hrd1. CB5083 treatment led to both an increase in ubiquitinated proteins in cell lysates (i.e., Input) as well as an increased association of NHK-HA and ubiquitinated proteins with S-tagged Hrd1 (Hrd1-S), consistent with impaired clearance of ubiquitin-conjugated proteins (Figure 3-1D). A portion of NHK-HA associated with Hrd1-S migrated as a high-¬molecular-weight smear that was sensitive to incubation with the catalytic core of the deubiquitinating enzyme USP2 (USP2cc; Figure 3-1D), indicating that this fraction of NHK-HA in complex with Hrd1-S is ubiquitinated. Furthermore, immunoprecipitations of NHK-HA indicate that CB5083 increases the association of NHK-HA with components of the Hrd1 complex, including Hrd1, SEL1L, OS-9, and XTP3-B (Figure 3-1E). These proof-of-principle experiments demonstrate that CB5083 treatment traps a known ERAD substrate in a ubiquitinated form, in complex with its membrane-embedded degradation apparatus. We also observed that CB5083 treatment resulted in the accumulation of the core glycosylated form of integral membrane protein CD147 (CD147[CG]), an endogenous ERAD substrate [101,200], but it caused only a small increase in the association of CD147(CG) with Hrd1-S (Supplemental Figure 3-S1). This may reflect differences in the mode of interaction between Hrd1 and its luminal and integral membrane substrates. For example, under periods of VCP impairment, an integral membrane substrate may be preferentially released into the surrounding membrane to prevent prolonged occupancy of the Hrd1 ubiquitination complex.

### 3.2.2 Global analysis of trapped, ubiquitinated proteins identifies endogenous ERAD substrates in HepG2 liver cells

To identify endogenous ERAD substrates, VCP inhibition was coupled with quantitative ubiquitin proteomics in a method we refer to as ERAD-VISTA (Figure 3-2A). Cells were labeled by stable isotope labeling with amino acids in cell culture (SILAC) and treated with vehicle (light) or CB5083 (heavy). Beads conjugated with antibodies that recognize peptides bearing diglycine (diGly)-modified lysine residues (i.e., a tryptic ubiquitin remnant) [208,209] ) were used to affinity purify ubiquitin-modified peptides from membrane fractions for proteomic analysis. Consistent with the trapping of ubiquitinated proteins, CB5083 treatment resulted in greater levels of polyubiquitinated proteins in cell lysate and the ER-enriched membrane fraction (Figure 3-2B). Proteomic analysis of diGly-modified peptides purified from membrane fractions identified a total of 5573 diGly-modified peptides across four independent experiments, corresponding to 478 proteins (Supplemental Table S1). There was some variability in the number of unique diGly peptides identified (Figure 3-2C and Supplemental Table 3-S1), which may be due to different batches of diGly beads. Experiments 3 and 4 were performed with the same batch of beads and were very similar with respect to the number of unique diGly peptides identified in each

experiment (Figure 3-2C and Supplemental Table 3-S1). diGly-modified peptides with SILAC ratios greater than 2.0 (123 proteins), indicating an accumulation of the ubiquitinated peptide during VCP inhibition, were considered candidate ERAD substrates (Supplemental Figure 3-S2 and Supplemental Table 3-S1). A single diGly modification was identified for the majority of proteins (68.2% for all proteins, 59.2% for proteins with SILAC ratio > 2), but a fraction of the proteins were also observed that contained two diGly modifications (18.8% for all proteins, 20.8% for proteins with SILAC ratio > 2) or three diGly modifications (9.6% for all proteins, 12.5% for proteins with SILAC ratio > 2; Figure 3-2D). As expected, a large number of ubiquitin diGly peptides were identified, most of which corresponded to K48 and K63 diGly-modified peptides (Figure 3-2E). In all four experiments, K11, K33, and K48 diGly peptides showed a strong increase, consistent with a role in protein degradation (Figure 3-2F). In contrast, the amount of K63 diGly peptide was mostly unchanged and the amount of K27 diGly peptide showed a decrease (Figure 3-2F).

Among the list of candidate substrates (Supplemental Table 3-S1), three bona fide endogenous ERAD substrates were detected: Apolipoprotein B100 (ApoB100) [70,210], 7-dehydrocholesterol reductase (DHCR7) [211], and insulin-induced gene 2 (Insig2) [204]. Following CB5083 treatment, increases in the levels of two diGly peptides in ApoB100 (K196, 13.805-fold increase; K2697, 9.249-fold increase), a cluster of three diGly peptides in DHCR7 (K4, 3.602-fold increase; K11, 3.497-fold increase; K13, 3.861-fold increase), and one diGly peptide in Insig2 (K221, 7.27-fold increase) were detected (Figure 3-2, G–L), suggesting that modification of these lysines by ERAD E3 ligases targets these substrates to the proteasome. Other reported endogenous ERAD substrates may not have been identified due to their low abundance in HepG2 cells or their regulated degradation under specific conditions, such as IP3 receptor degradation following ligand binding [212] or HMG CoA reductase degradation following sterol accumulation in ER membranes [213]. Although it is unlikely to be a comprehensive list, these data demonstrate the ability of ERAD-VISTA to detect known and candidate endogenous ERAD substrates.

Gene ontology (GO) enrichment analysis of candidate ERAD substrates revealed an expected enrichment in proteins that are known to localize to cell membranes (e.g., ER and plasma membrane) as well as complexes associated with various components of the ERAD network (Figure 3-3A and Supplemental Table 3-S2). Indeed, analysis of the annotated localizations revealed that 59.2% of the candidate substrates were predicted to be present in, or transit through, the secretory pathway (Supplemental Table 3-S3). A smaller portion of the candidate substrates are annotated as mitochondrial (8.3%), lysosomal (0.8%), and vesicular (1.7%; Supplemental Table 3-S3), indicating a high degree of enrichment in ubiquitinated secretory proteins. We observed an enrichment in proteins involved amino acid transport, protein catabolism, protein folding, and cholesterol and fatty acid biosynthesis (Figure 3-3B and Supplemental Table 3-S2). This functional diversity reflects the wide array of potential ERAD substrates transiting the early secretory pathway and is consistent with a broad cellular role for ERAD through its regulation of a multitude of targets.

### 3.2.3 Degradation of endogenous SCD1 and RNF5 requires VCP, ubiquitin conjugation, and the proteasome

We next sought to validate select putative ERAD substrates from our candidate list. Two candidate substrates were selected for further analysis. Stearoyl-CoA desaturase (SCD1) is an ER-localized enzyme that catalyzes the production of monounsaturated fatty acids from saturated fatty acids [214]. Levels of a diGly-modified lysine in the cytosolic C-terminus of SCD1 increased in response to CB5083 (K341, 10.621-fold increase; Figure 3-4, A and B). Overexpressed SCD1 in CHO-K1 and HeLa cells as well as endogenous SCD1 in NIH3T3-L1 cells are degraded by the proteasome [215,216]. However, whether VCP is required for SCD1 degradation and whether endogenous SCD1 is degraded in HepG2 cells remains unknown. Consistent with SCD1 being a direct substrate of VCP, CB5083 treatment increased the amount of VCP associated with S-tagged SCD1 (SCD1-S; Figure 3-4C). Moreover, the degradation of SCD1 was impaired by CB5083, the proteasome inhibitor MG132, and an inhibitor of the E1 ubiquitin-activating enzyme MLN7243 (Figure 3-4, D and E). We observed an anti-SCD1 immunoreactive, lower-molecular-weight band that was partially degraded in control cells and exhibited a modest accumulation in the presence of the inhibitors (Figure 3-4D). This band was depleted by multiple small interfering RNAs (siRNAs) targeting SCD1 (Supplemental Figure 3-S3), confirming that it is a fragment of SCD1, but its functional significance is unclear at this time. Our data suggest that SCD1 is constitutively degraded by a VCP-dependent ERAD pathway in HepG2 cells. This is similar to the SCD1 yeast orthologue OLE1, which undergoes degradation through an ERAD pathway that requires the VCP orthologue CDC48 [217]. Future experiments will explore if SCD1 degradation is regulated by the metabolic state of the cell, such as fluctuations in the ratio of unsaturated to saturated fatty acids.

Another candidate ERAD substrate identified using VISTA is RNF5, an ERAD E3 ligase that mediates the clearance of misfolded proteins [141,142,218] and controls the stability of proteins involved in a variety of cellular processes such as autophagy [219], amino acid transport [198], and viral immunity [220]. We identified four diGly-modified lysines that clustered within the cytosolic N-terminus of RNF5 and increased following CB5083 treatment (K68, 4.029-fold increase; K75, 7.038-fold increase; K86, 6.307-fold increase; K93, 8.339-fold increase; Figure 3-4, F and G). Similar to SCD1-S, CB5083 treatment increased the amount of VCP that coprecipitated with S-RNF5 (Figure 3-4H). Translation shut-off experiments indicated that the degradation of endogenous RNF5 was impaired by CB5083, MG132, and MLN7243 (Figure 3-4, I and J). Together, our findings indicate that two of the candidate ERAD substrates in HepG2 cells identified by ERAD-VISTA, SCD1 and RNF5, are constitutively degraded by a VCP- and ubiquitin-dependent ERAD pathway.

### 3.2.4 Autoubiquitination targets RNF5 to the ERAD pathway in HepG2 cells

Maltose-binding protein (MBP)–tagged RNF5 autoubiquitinates in vitro through an intramolecular reaction that requires an intact RING finger domain [221]. However, whether RNF5 autoubiquitinates in cells and whether this activity contributes to its proteasomal clearance has not been examined. We generated an S-tagged RNF5 construct containing a cysteine-to-alanine substitution (C42A), which disrupts the RING finger and abrogates its catalytic activity [221]. When transfected into HepG2 cells, S-RNF5(WT) overexpression was low (Supplemental Figure 3-S4A) and the S-RNF5(C42A) exhibited a threefold increase in protein levels relative to its wild-type counterpart (Figure 3-5, A and B). Inhibitors of ERAD increased the steady-state levels of wild-type RNF5, but not S-RNF5(C42A) (Figure 3-5, A and B), indicating that RNF5 ubiquitination activity is required for its degradation. Affinity purification of S-RNF5(WT) revealed a laddering

of RNF5 bands, with three to four particularly prominent bands that were separated by ~8 kDa (i.e., the size of ubiquitin) and that increased following CB5083 treatment (Figure 3-5, C and D). These bands were greatly reduced by incubation with USP2cc, indicating that these represent ubiquitinated forms of RNF5 (Figure 3-5, C and D). The ubiquitinated RNF5 species were mostly absent in the C42A mutant RNF5 (Figure 3-5, C and D). We considered that the small amount of ubiquitinated S-RNF5(C42A) may be due to ubiquitination S-RNF5(C42A) by endogenous RNF5. Indeed, FLAG-HA-RNF5 coprecipitated with S-RNF5, indicating the presence of RNF5 homo-oligomers (Supplemental Figure 3-S4B). To examine the possibility of trans-molecular RNF5 autoubiquitination, we expressed S-RNF5(C42A) in RNF5 knockout (KO) cells generated using CRISPR/Cas9 (Supplemental Figure 3-S5). Similar to the control cells, S-RNF5(C42A) still exhibited a small amount of laddering in the RNF5 KO cells, indicating that the endogenous RNF5 does not contribute to the ubiquitination of S-RNF5(C42A) (Supplemental Figure 3-S5B). Our data are in very good agreement with previous in vitro studies [221] and suggest RNF5 autoubiquitination is a cis-molecular reaction. The residual ubiquitination of S-RNF5(C42A) must be mediated by an unknown E3 ligase.

Our proteomics results indicate that all four lysines in RNF5 are ubiquitinated and are sensitive to VCP inhibition (Figure 3-4, F and G, and Supplemental Table 3-S1). To explore the contribution of these lysines to RNF5 degradation we generated constructs harboring lysine-to-arginine substitutions. Although there was a small decrease in the ubiquitination of S-RNF5(K75R) and S-RNF(K86R), all S-RNF5 single lysine mutants were still ubiquitinated (Figure 3-5E). Therefore, we generated an S-RNF5 construct in which all four lysines were substituted with arginine (4K-R). The 4K-R mutant exhibited a dramatic reduction in ubiquitination (Figure 3-5, F and G). A very small amount of ubiquitinated S-RNF5(4K-R) was visible, suggesting that RNF5 may either ubiquitinate noncanonical residues (e.g., serine) or one of the lysines in the S-tag. Although the S-tag contains two lysine residues, the ubiquitination of RNF5 was nearly abolished in the 4K-R mutant. This may indicate a structural preference for the cluster of 4-lysine residues over the lysines in the N-terminal S-tag. It is notable that S-RNF5(4K-R), despite being no longer ubiquitinated, still coprecipitated ubiquitinated proteins in the presence of CB5083 (Figure 3-5F). This was in contrast to the inactive S-RNF5(C42A), which did not coprecipitate ubiquitinated proteins (Figure 3-5C). These results suggest that the S-RNF5(4K-R) mutant uncouples RNF5 catalytic activity and autoubiquitination. This uncoupling mutant could be useful for exploring the functional importance of RNF5 degradation.

In summary, we have developed a new global approach for the identification of endogenous ERAD substrates. This approach identified known (ApoB100, DHCR7, and Insig2) and novel (SCD1 and RNF5) substrates. ERAD-VISTA has several important benefits over previous strategies to study ubiquitinated substrates: 1) The method uses endogenous ubiquitin and does not require overexpression of tagged ubiquitin (e.g., his-ubiquitin) [222–224]. 2) The method does not require in-depth knowledge and/or genetic manipulation of the degradation pathway (e.g., proteomic analyses of tagged E3 ligase complexes) [225–228] or tagged substrate delivery factors [101]. 3) The method does not require expression of chimeric proteins that could affect function (e.g., fusions of E3 ligases to tandem ubiquitin-binding domains) [229,230] or to ubiquitin [231]. 4) The method measures changes in substrate ubiquitination rather than steady-state protein levels (e.g., steady-state SILAC) [232] or GFP-based global protein profiling [233,234], thereby facilitating substrate identification even when only a small fraction is ubiquitinated and degraded. A limitation of

ERAD-VISTA is that it relies on diGly ubiquitin proteomics which may impact reproducibility due to stochastic sampling, especially for low-abundance targets [235]. Thus, achieving comprehensive assessments of the ERAD substrate landscape is a challenge. However, depth and coverage may be improved by employing recent improvements in diGly methodologies involving the fractionation of peptides using strong cation exchange chromatography before immunoaffinity purification [236,237]. It is also important to note that because the diGly approach is specific to diGly-modified lysines, it will not identify ubiquitination on nonlysine residues such as serine [238]. An additional limitation of ERAD-VISTA is that some CB5083-sensitive ubiquitination events might not target the modified protein for degradation and may instead reflect regulatory ubiquitination, such as the ubiquitin-dependent regulation of protein complexes [239–241]. Thus, the candidate ERAD substrate must be validated with traditional approaches. ERAD-VISTA expands the available toolbox of strategies for probing the ERAD substrate landscape in different cell types and under different conditions (e.g., ER stress).

## 3.3 Materials and methods

### 3.3.1 Plasmids, antibodies, and reagents

The NHK-HA and Hrd1-S plasmids used were previously described [200]. The S-RNF5 plasmid in a pcDNA3.1(+) backbone was a kind gift from Ron Kopito (Stanford University), and the FLAG-HA-RNF5 plasmid in a pcDNA5/FRT/TO backbone was a kind gift from John Christianson (Ludwig Institute for Cancer Research, University of Oxford). S-RNF5 lysine-to-arginine and cysteine-to-alanine substitutions were generated by site-directed mutagenesis and confirmed by sequencing. To generate the SCD1-S expression plasmid, SCD1 was PCR amplified from pANT7_cGST-SCD1 (DNASU Plasmid Repository, HsCD00631016) and ligated into a pcDNA3.1(–) vector bearing an in frame C-terminal S-tag.

The primary antibodies used for immunoblotting include anti-S peptide (EMD Millipore), anti-HA (Sigma-Aldrich), anti-ubiquitin (FK2; EMD Millipore), anti-tubulin (Abcam), anti-Hrd1 (Bethyl Laboratories), anti-SEL1L (Santa Cruz), anti-CD147 (Santa Cruz), anti-VCP (Novus Biologicals), anti-calnexin (Proteintech Group), anti-UBXD8 (Proteintech Group), anti-AUP1 (Proteintech Group), anti-GAPDH (EMD Millipore), anti-SCD1 (Cell Signaling Technology), and anti-RNF5 (Abcam). Anti-OS-9 and anti-XTP3-B were kind gifts from Ron Kopito (Stanford University). Secondary antibodies used were Alexa Fluor 680 goat anti-mouse (Life Technologies) and IRDye 800 goat anti-rabbit (LI-COR Biosciences).

Chemical reagents used include emetine (Sigma-Aldrich), CB5083 (Cleave Biosciences and Cayman Chemical), MLN7243 (Chemietek), MG132 (Selleck Chemicals), and Bortezomib (Cell Signaling Technologies).

### 3.3.2 Cell culture, transfections, and stable cell line generation

HepG2 cells (American Type Culture Collection) were cultured in Roswell Park Memorial Institute 1640 (RPMI; Thermo Fisher Scientific) or DMEM containing 4.5 g/l glucose and l-glutamine (Corning) supplemented with 10% fetal bovine serum (FBS; Thermo Fisher Scientific

and Gemini Bio Products) at 37°C and 5% CO2. Stable HEK293 cells expressing S-tagged Hrd1 [200] were grown in DMEM supplemented with 10% FBS at 37°C and 5% $CO_2$.

Cells at 60–80% confluence were transfected with the indicated plasmids using XtremeGENE HP DNA transfection reagent (Sigma-Aldrich) following the manufacturer's protocols. Depletion of SCD1 in HepG2 cells was accomplished by transfection of SCD1-targeting siRNAs from Sigma-Aldrich using RNAiMAX Lipofectamine reagent (Thermo Fisher Scientific). siRNA sequences targeting SCD1 include 5′-GAUAUGCUGUGGUGCUUAA-3′ (siRNA1), 5′-GAUAUCGUCCUUAUGACAA-3′ (siRNA2), 5′-GACGAUAUCUCUAGCUCCU-3′ (siRNA3), and 5′-GUGAGUACCGCUGGCACAU-3′ (siRNA4). MISSION siRNA Universal Negative Control #1 (SIC001) was used as the control siRNA.

### 3.3.3 Differential fractionation

Cultured cells were collected, washed with ice-cold phosphate-buffered saline (PBS), and incubated in hypotonic lysis medium (HLM: 20 mM Tris-HCl, pH 7.4, 1 mM EDTA) supplemented with 10 mM N-ethylmaleimide (NEM; Thermo Fisher Scientific) on ice for 10 min. Cells were then transferred to a 7-ml chilled glass dounce homogenizer and dounced using a tight pestle for 40 strokes. Samples were centrifuged (500 × g, 5 min, two times) to remove unbroken cells. The remaining supernatant was then centrifuged (20,000 × g, 30 min at 4°C) to separate heavy membrane and cytosolic fractions. The resulting pellet (membrane) was then reconstituted to its corresponding cytosolic fraction volume using either HLM buffer (for immunoblotting) or 8M urea lysis buffer (for diGly enrichment, details below). For immunoblotting, SDS was then added to achieve a final detergent concentration of 1% and equal volumes were analyzed.

### 3.3.4 Affinity purification

Cells were collected and washed twice using ice-cold PBS. Cells were resuspended in immunoprecipitation (IP) lysis buffer (50 mM Tris-HCl, pH 7.5, 150 mM NaCl, 1% digitonin [EMD Millipore]) containing protease inhibitor tablets (Thermo Fisher Scientific) and gently rotated for 30 min at 4°C. Lysates were centrifuged (20,000 × g, 10 min) and soluble protein (supernatant) transferred to new tubes. Supernatant protein concentration was then determined using the BCA assay (Thermo Fisher Scientific) according to the manufacturer's instructions.

S-protein agarose bead slurry (25 µl bead bed/mg lysate; EMD Millipore) was washed two times with IP lysis buffer followed by one time with IP buffer containing 1% digitonin. Beads were then mixed with equivalent amounts of supernatant (2 h rotating, 4°C), washed three times with IP lysis buffer containing 0.1% digitonin, and proteins eluted with Laemmli buffer for immunoblotting. Where indicated, affinity-purified proteins were treated with 1 µg of USP2cc (Boston Biochem) for 1 h at 37°C before elution from the beads.

### 3.3.5 Immunoblotting

Cells were washed with PBS and lysed in 1% SDS. Protein quantity was determined using a bicinchoninic acid assay (Thermo Fisher Scientific). Normalized cell lysates in Laemmli sample buffer were heated at 65°C for 5 min and resolved on 4–20% SDS–PAGE gradient gels (Bio-Rad

Laboratories). Gels were transferred to nitrocellulose membrane (Bio-Rad Laboratories), blocked in PBS containing 0.1% Tween-20 (PBST) and 5% milk, and then incubated with primary antibody for either 2 h at room temperature or overnight at 4°C. Blots were then washed and incubated with secondary antibodies in PBST. Following washing PBST, blots were visualized using the LI-COR Odyssey Imaging System. Densitometry analyses were performed using the UN-SCAN-IT gel analysis (version 6.1; Silk Scientific) or ImageJ (version 1.49b; National Institutes of Health, Bethesda, MD) software.

### 3.3.6 Enrichment of diGly-modified peptides

Cells were cultured in SILAC DMEM lacking lysine and arginine, supplemented with 10% dialyzed FBS and the appropriate amino acids: light media—l-arginine (Arg0) and l-lysine (Lys0; Sigma-¬Aldrich) or heavy media—l-arginine (Arg0) and 13C615N2-l-lysine (Lys8; Cambridge Isotope Laboratories). Samples were then processed for diGly immunopurification [208,209]. Following a 6 h treatment with DMSO (light) or 5 μM CB5083 (heavy), membrane fractions were collected, solubilized in urea lysis buffer (8 M urea, 50 mM Tris-HCl, pH 8.0, 50 mM NaCl), reduced with 10 mM dithiothreitol (Thermo Fisher Scientific), and alkylated with 25 mM iodoacetamide (Thermo Fisher Scientific). Equal amounts of protein totaling 5–10 mg from the membrane fractions were combined, diluted with 50 mM Tris-HCl, pH 8.0, 4 M urea, and digested overnight with 2 μg/mg LysC (Wako Laboratory Chemicals). Proteins were further diluted to 1.6 M urea and digested for 24 h with 10 μg/mg mass spectrometry grade trypsin (Thermo Fisher Scientific). Digested peptides were desalted via Sep-Pak C18 6-cc cartridges (Waters) and lyophilized. Samples were then immunoprecipitated using a PTMScan Ubiquitin remnant Motif (K-ε-GG) Kit (Cell Signaling Technologies) according to the manufacturer's protocols. Briefly, lyophilized peptides were dissolved in IAP buffer (50 mM MOPS/NaOH, pH 7.2, 10 mM Na2HPO4, and 50 mM NaCl) and cleared by centrifugation at 10,000 × g for 5 min. For each independent experiment, one tube of K-ε-GG antibody bead conjugates were washed four times with PBS, and clarified peptides were incubated with the beads for at least 2 h with gentle agitation. Beads were washed two times with IAP buffer and three times with MilliQ water and eluted twice with 0.15% trifluoroacetic acid. Eluted peptides were desalted using C18 StageTips (Thermo Fisher Scientific), dried using a Speedvac, and resuspended in 0.1% formic acid (Sigma-Aldrich) for analysis by tandem mass spectrometry (LC-MS/MS).

### 3.3.7 LC-MS/MS analysis

Digested peptides were analyzed by LC-MS/MS on a Q Exactive Orbitrap mass spectrometer (Thermo Fisher Scientific) in conjunction with Proxeon Easy-nLC II HPLC (Thermo Fisher Scientific) and a Proxeon nanospray source at the UC Davis Proteomics Core Facility as described [200]. The resulting MS/MS raw spectral data were analyzed using the MaxQuant software platform (version 1.5.1.0) [242], employing the full UniProt human protein sequence database to obtain diGly-modified peptide SILAC ratios. A reversed-protein decoy search strategy was also employed to minimize false discovery rate. All mass spectrometry files are available through the Proteomics Identifications (PRIDE) database (Project accession: PXD008842).

### 3.3.8 Bioinformatic analyses

GO analysis of candidate ERAD substrates was performed using the Database for Annotation, Visualization and Integrated Discovery (DAVID) v6.8 (Supplemental Table 3-S3) [243]. REVIGO [244] was then used to simplify and visualize the GO terms and the Benjamini corrected p values. GO networks were exported from REVIGO and the final networks generated using Cytoscape [245]. Protein localization and topology listed in Supplemental Table 3-S2 were based on UNIPROT annotations.

### 3.3.9 Generation of RNF5 knockout cells

RNF5 knockout lines were generated using the targeting sequence 5′-CGCTCGCGATTTGGCCCTTC-3′ cloned into PX459 (Addgene; plasmid #48139) transfected into HEK293 cells. PX459 without a targeting sequence was transfected as a control. Transfected cells were selected with 1 μg/ml puromycin (Sigma-Aldrich) for at least 1 wk. Clonal cell lines were isolated by limited dilution and screened for knockout by immunoblotting.

## 3.4 Figures

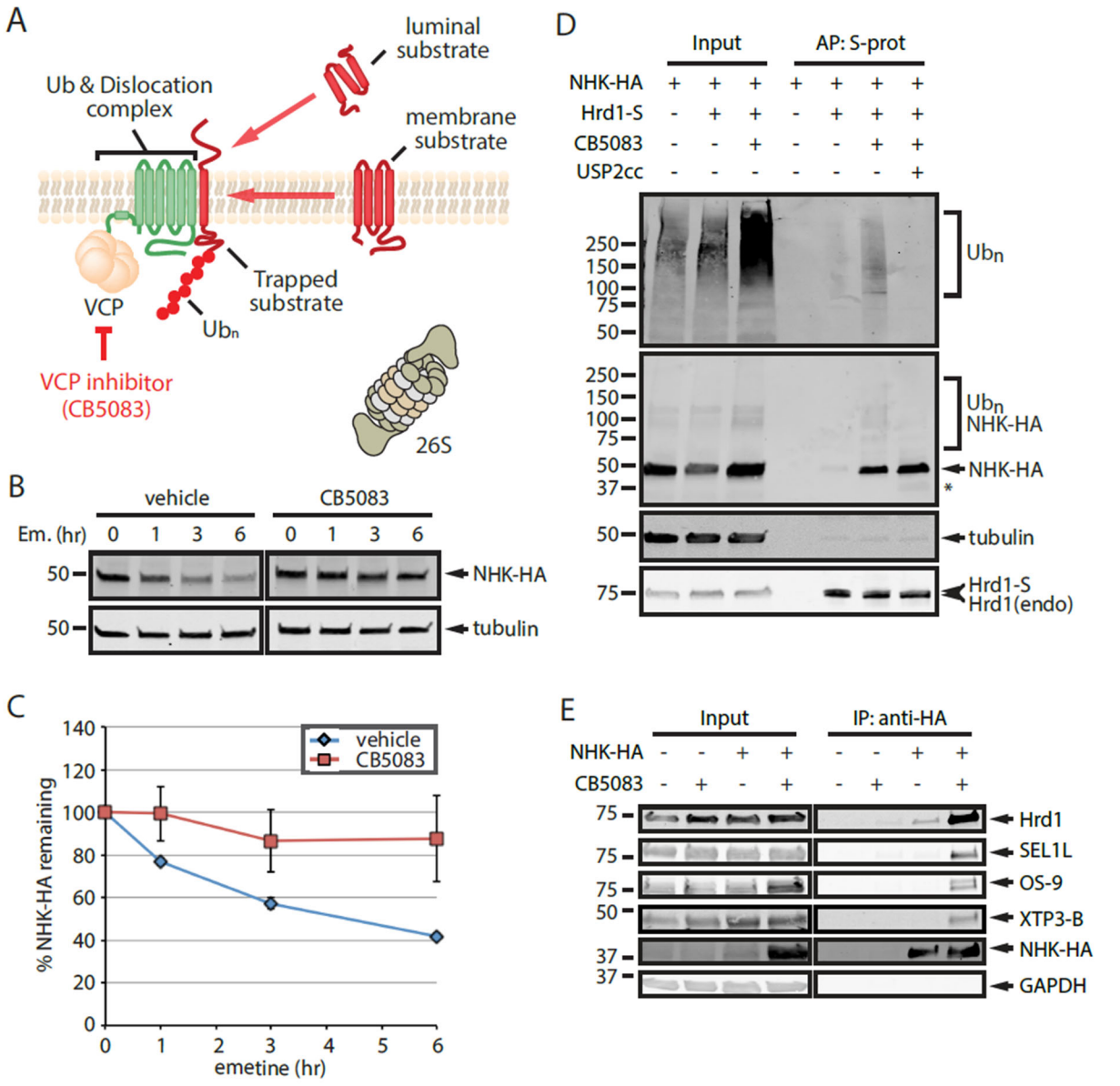


Figure 3-1: VCP inhibition traps the ERAD substrate NHK in complex with the E3 ligase Hrd1. (A) Schematic of VISTA. Pharmacological inhibition of VCP with CB5083 prevents the dislocation of ubiquitinated ERAD substrates. (B) HEK293 cells expressing NHK-HA were incubated with 75 µM emetine and either vehicle or 5 µM CB5083 for the indicated time points. SDS lysates were analyzed by immunoblotting for the indicated targets. (C) The relative levels of NHK-HA (panel B) were quantified and presented as a percentage of the levels at time 0 h ± SEM (n = 3). (D) HEK293 cells stably expressing Hrd1-S were transiently transfected with NHK-HA, treated with vehicle or 5 µM CB5083, subject to affinity purification with S-protein (S-prot) agarose, and SDS lysates analyzed by immunoblotting; n = 3. (E) HEK293 cells stably expressing NHK-HA were treated with vehicle or 5 µM CB5083, subject to affinity purification with anti-HA–conjugated agarose, and SDS lysates analyzed by immunoblotting. Asterisk indicates a USP2cc-reactive band. AP, affinity purification; IP, immunoprecipitation; S-prot, S-protein; Ubn, ubiquitinated; endo, endogenous; Em., emetine.

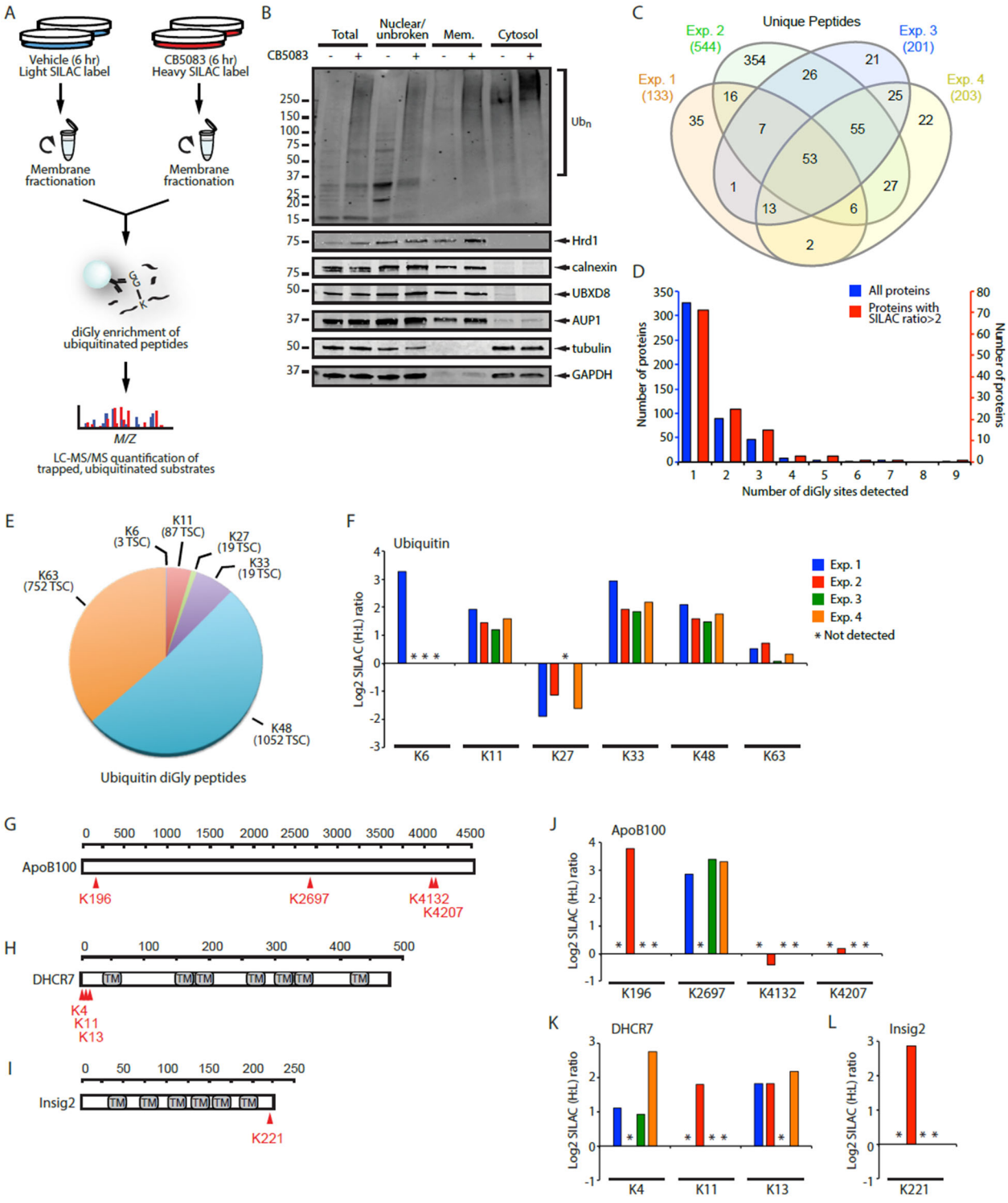


Figure 3-2: Global analysis of trapped, ubiquitinated proteins identifies validated and candidate ERAD substrates in cultured liver cells. (A) Schematic of ERAD-VISTA experimental workflow. (B) HepG2 cells treated with vehicle or 5 μM CB5083 were fractionated by differential centrifugation and equal volumes analyzed by immunoblotting; n = 3. (C) Venn diagram comparing unique diGly-modified peptides identified from the four independent

experiments. (D) Bar graph indicating the number of unique diGly sites identified for all proteins (blue) and for proteins with a SILAC ratio > 2 (red). (E) Pie chart illustrating the relative abundance of diGly-modified ubiquitin peptides, based on total spectral counts. (F) Log2 SILAC peptide ratios for individual diGly-modified peptides from ubiquitin. (G–I) Protein domain structure and the identified diGly-modified lysine residues for three validated endogenous ERAD substrates (ApoB100, DHCR7, and Insig2). TM: transmembrane domain. (J–L) Log2 SILAC peptide ratios for individual diGly-modified peptides from ApoB100 (J), DHCR7 (K), and Insig2 (L). Colors indicate the experiment from which the diGly peptide was identified, as in panel F. Mem., membrane; Ubn, ubiquitinated; Exp., experiment; TSC, total spectral counts. Asterisk indicates that the diGly peptide was not detected in that experiment. See also Supplemental Table 3-S1.

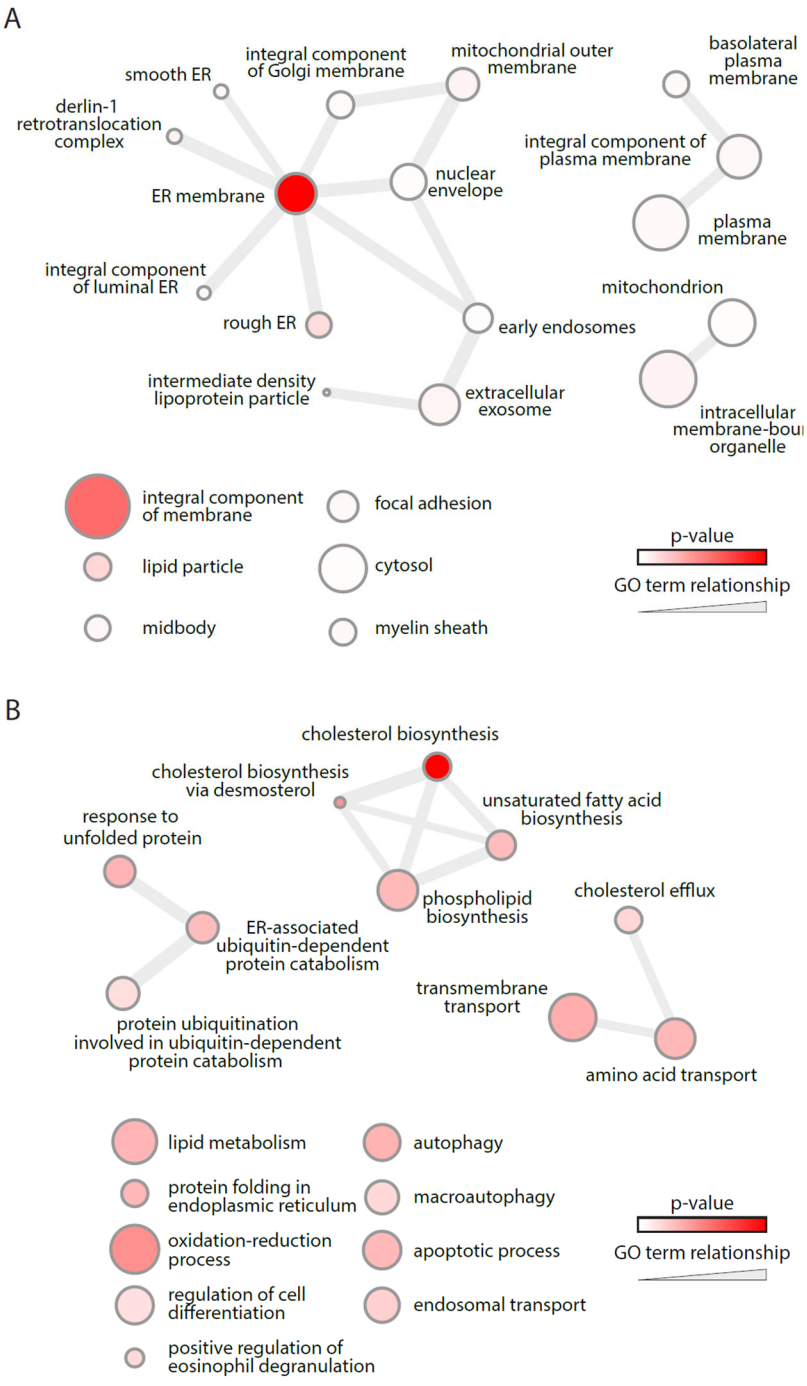


Figure 3-3: Gene ontology analysis of candidate ERAD substrates. (A, B) DAVID and REVIGO were used to identify enriched GO terms, cellular component (A) or biological function (B), within the candidate ERAD substrate list. Cytoscape networks were generated by REVIGO. Circle size indicates the frequency of the GO term in the GO annotation database, edge thickness is proportional to the degree of GO term similarity, and color indicates the p value (red being more significant). See also Supplemental Table S2.

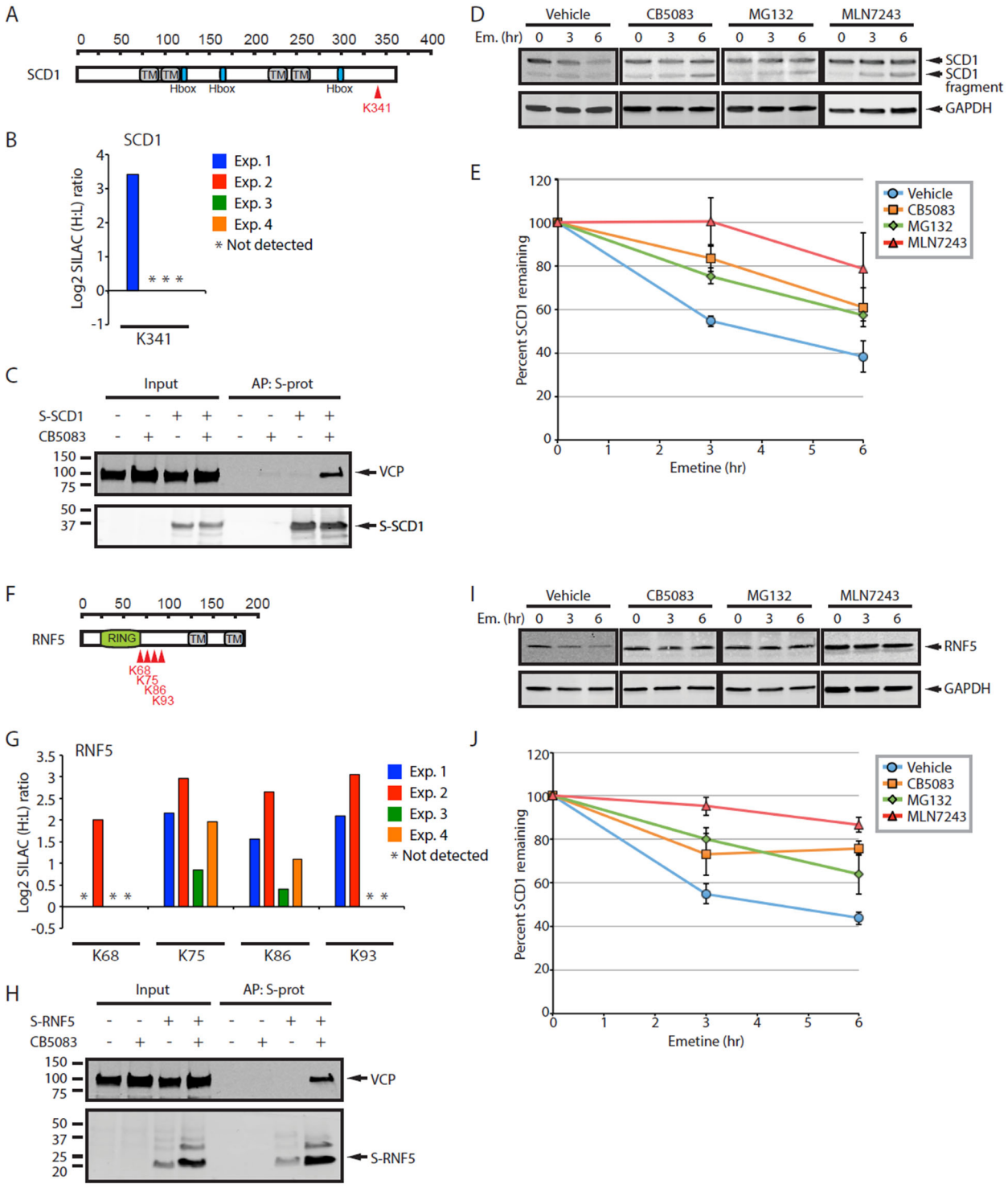


Figure 3-4: Endogenous SCD1 and RNF5 are degraded via a VCP- and ubiquitin-dependent proteasomal pathway. (A) Diagram of SCD1 protein structure, with detected diGly-modified lysine residue indicated. (B) Log2 SILAC peptide ratios for individual diGly-modified peptides from SCD1. (C) HepG2 cells expressing SCD1-S were treated with vehicle or 5 μM CB5083, subject to affinity purification with S-protein (S-prot) agarose, and SDS lysates analyzed by

immunoblotting; n = 3. (D, E) HepG2 cells were treated with 75 μM emetine and 5 μM CB5083, 10 μM MG132, or 10 μM MLN7243 to disrupt various components of ERAD. SCD1 protein stability was assessed via immunoblotting (D) and relative levels quantified (E). Graphical data are expressed as mean ± SEM (n = 3–6 per group). (F) Diagram of RNF5 protein structure, with detected diGly-modified lysine residues indicated. (G) Log2 SILAC peptide ratios for individual diGly-modified peptides from RNF5. (H) HepG2 cells expressing S-RNF5 were treated with vehicle or 5 μM CB5083, subject to affinity purification with S-protein (agarose, and SDS lysates analyzed by immunoblotting) (n = 3). (I, J) HepG2 cells were treated with 75 μM emetine and 5 μM CB5083, 10 μM MG132, or 10 μM MLN7243 to disrupt various components of ERAD. RNF5 protein stability was assessed via immunoblotting (I) and relative levels quantified (J). Graphical data are expressed as mean ± SEM (n = 3–6 per group). TM: transmembrane domain. S-prot, S-protein; Exp., experiment; Em., emetine. Asterisk indicates that the diGly peptide was not detected in that experiment. See also Supplemental Table 3-S1.

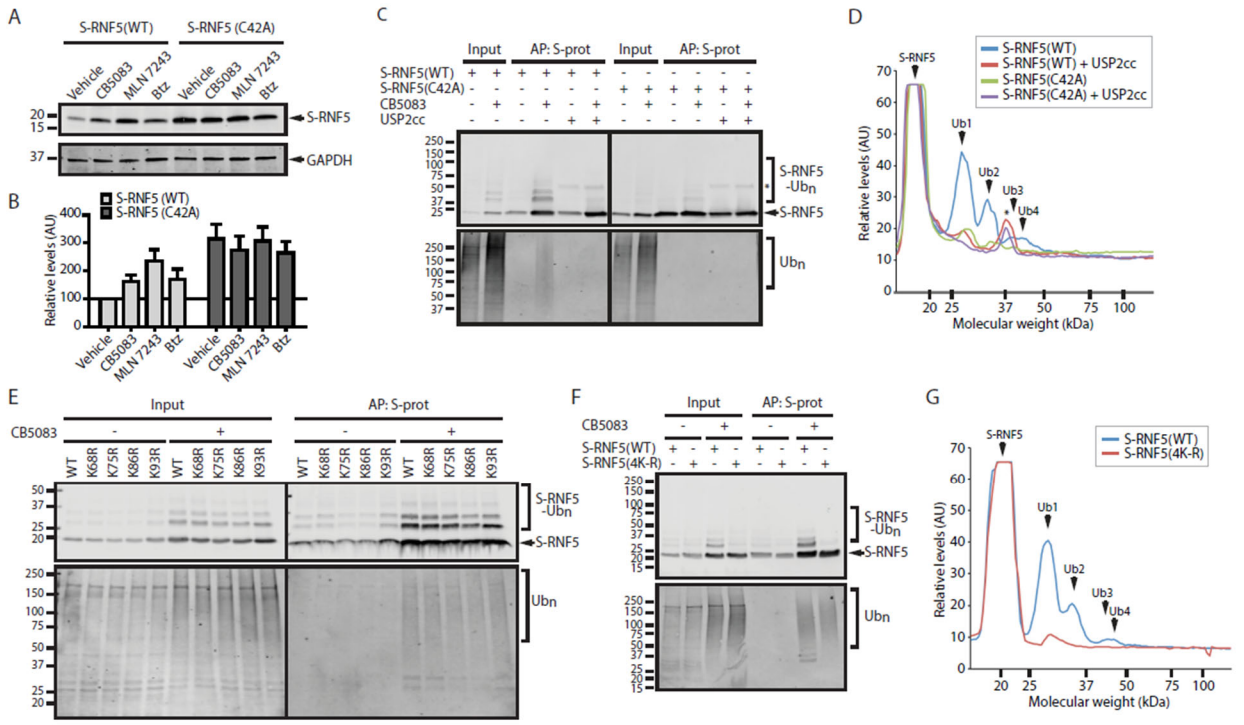


Figure 3-5: RNF5 autoubiquitination targets it for ERAD. (A) HepG2 cells transfected with S-RNF5(WT) and S-RNF5(C42A) were treated as indicated and lysates analyzed by immunoblotting. (B) Densitometric quantification of S-RNF5 (panel A). Data are expressed as mean ± SEM (n = 4 per group). (C) HepG2 cells transfected with S-RNF5(WT) and S-RNF5(C42A) were treated for 6 h with vehicle or 5 µM CB5083. S-tagged proteins were affinity purified, incubated in the presence and absence of USP2cc, and analyzed by immunoblotting. (D) Densitometric quantification of S-RNF5 (panel C). (E) HepG2 cells expressing S-RNF5(WT) or S-RNF5(C42A) were treated for 6 h with vehicle or 5 µM CB5083. S-tagged proteins were affinity purified, incubated in the presence or absence of USP2cc, and analyzed by immunoblotting. (F) HepG2 cells expressing S-RNF5(WT) or S-RNF5(4K-R) were treated for 6 h with vehicle or 5 µM CB5083. S-tagged proteins were affinity purified, incubated in the presence or absence of USP2cc, and analyzed by immunoblotting. (G) Densitometric quantification of S-RNF5 affinity purified from CB5083 treated HepG2 cells (panel F). Btz: bortezomib; Ubn, ubiquitinated; S-prot, S-protein. AU: arbitrary units. Asterisk indicates a USP2cc-reactive band.

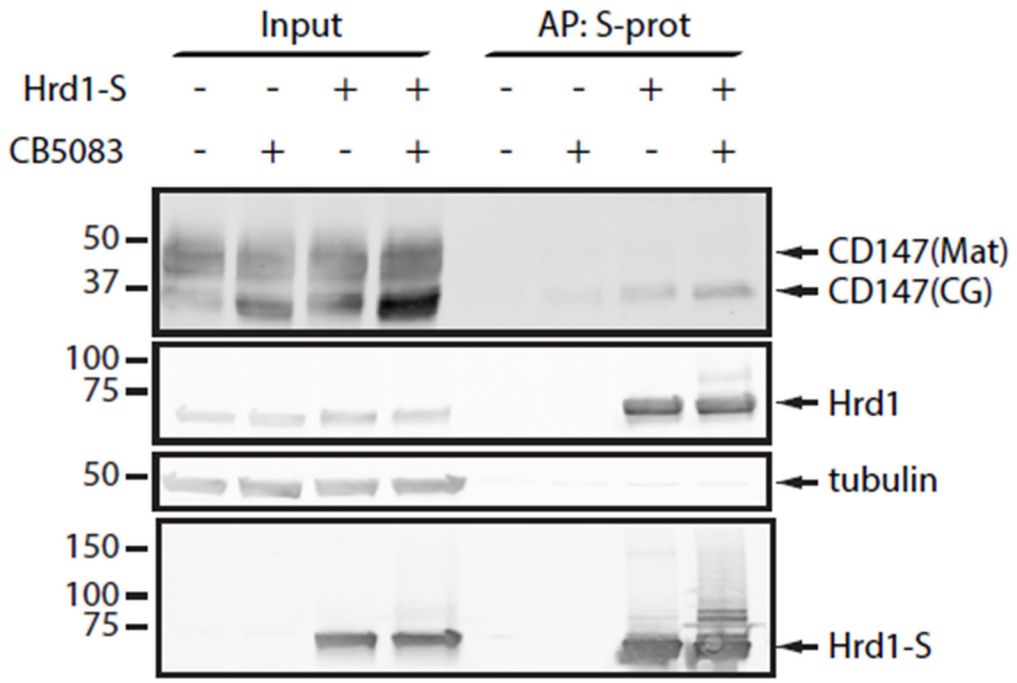


Figure 3-S1. Immunoblot analysis of the Hrd1-CD147 interaction. HEK293 cells stably expressing Hrd1-S were treated with vehicle or 5 μM CB5083, subject to affinity purification with S-protein (S-prot) agarose, and SDS lysates analyzed by immunoblotting. CG, core glycosylated, Mat, mature.

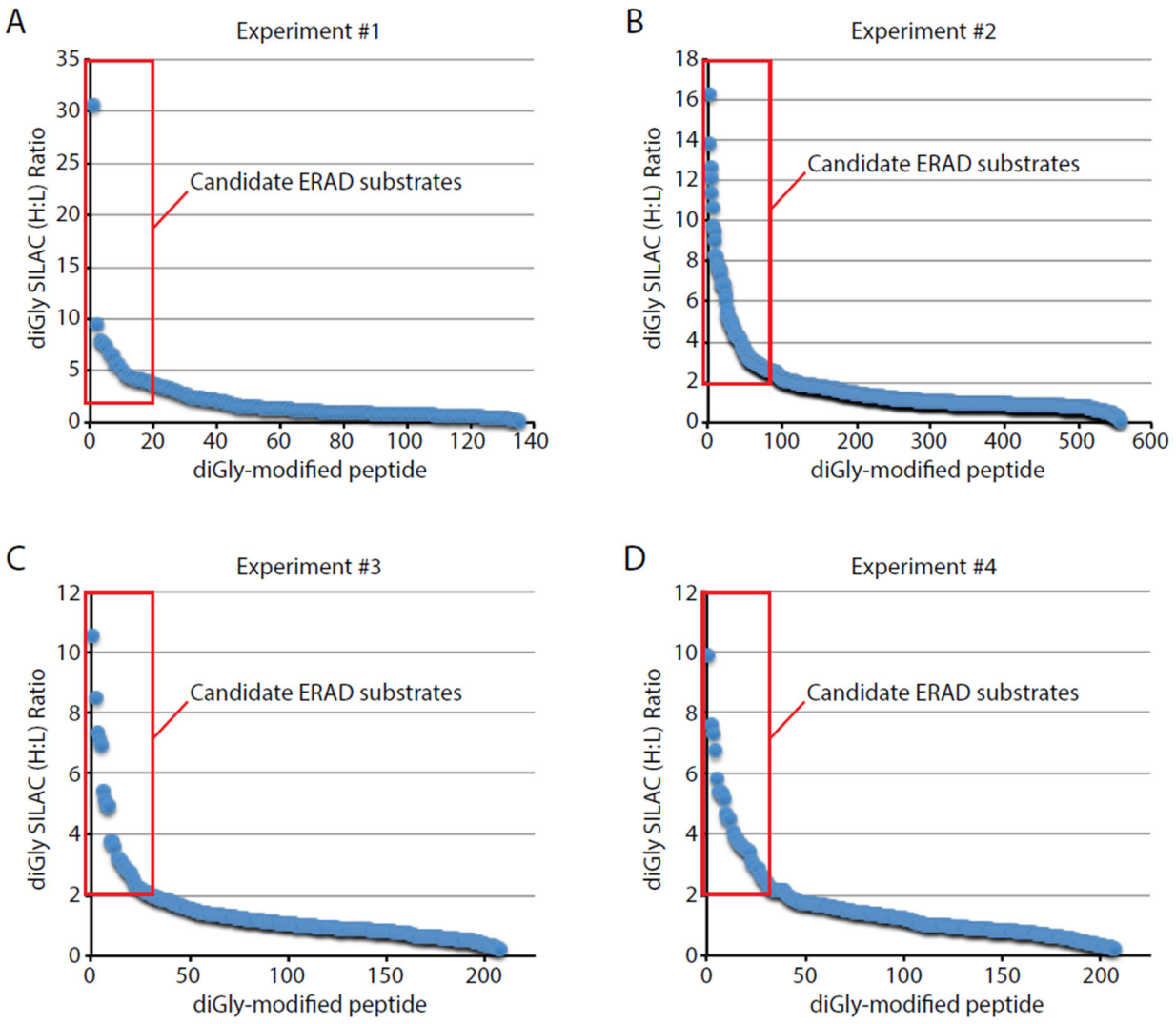


Figure 3-S2. Proteomic analysis of diGly-modified peptides. (A-D) Scatterplot of diGly-modified peptide SILAC H/L (CB5083:vehicle) ratios identified from four independent experiments. Detected diGly-modified peptides with SILAC ratios >2.0 are candidate ERAD substrates of interest (red box)

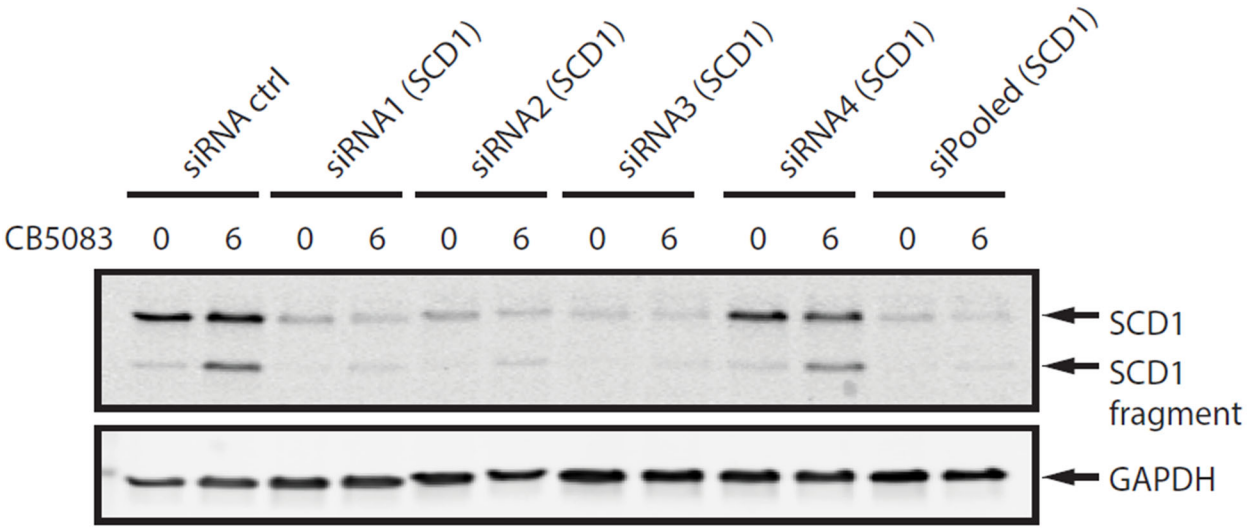


Figure 3-S3. Analysis of a lower molecular anti-SCD1 immunoreactive band. HepG2 cells were transfected with control or SCD1-targeted siRNAs, incubated in the presence or absence of CB5083 for 6 hr, and analyzed by immunoblotting with the indicated antibodies. NT: non-targeting siRNA control.

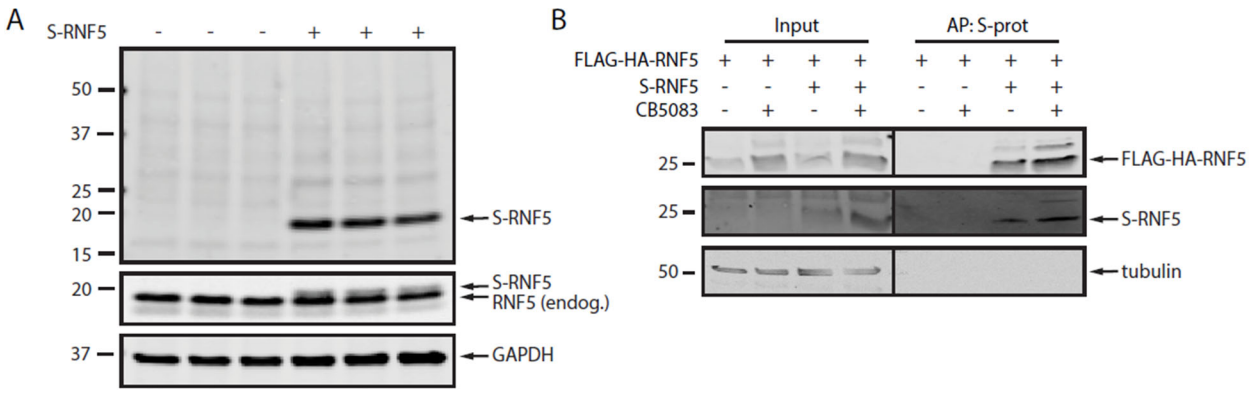


Figure 3-S4. RNF5 forms a homo-oligomer. (A) HepG2 cells were transfected with S-RNF5 in triplicate and analyzed by immunoblotting. (B) HepG2 cells were transfected with FLAG-HA-RNF5 and S-RNF5 and treated for 6 hrwith vehicle or 5 μM CB5083 as indicated. Cells were lysed, subjected to affinity purification with S-protein agarose, and SDS lysates analyzed by immunoblotting. AP, affinity purification; S-prot, S-protein; Endog., endogenous.

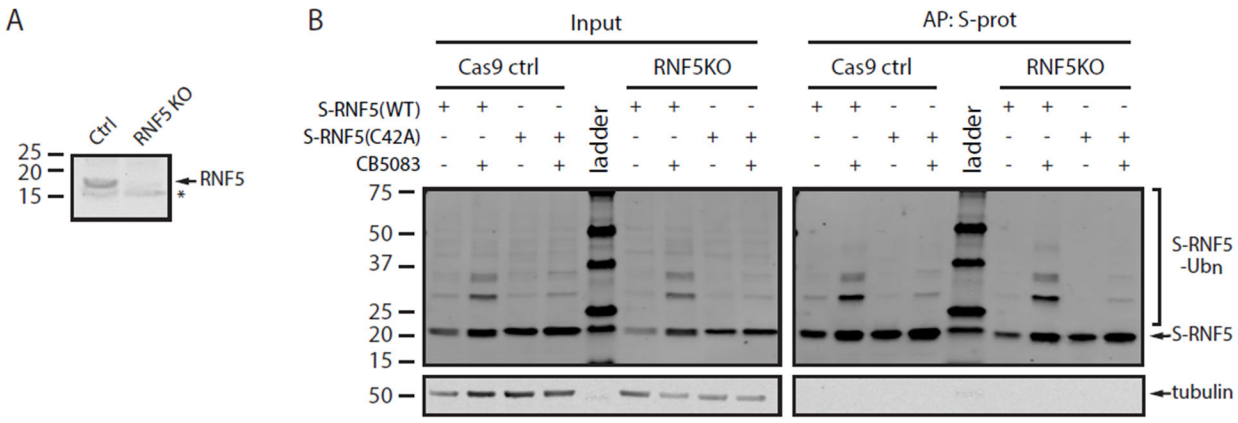


Figure 3-S5. RNF5 undergoes cis-molecular autoubiquitination. (A) SDS lysates from control and RNF5 KO cells were analyzed by immunoblotting. (B) Control and RNF5 KO cells were transiently transfected with the indicated S-RNF5 constructs and incubated in the presence and absence of 5 μM CB5083. Cells were lysed, subjected to affinity purification with S-protein agarose, and SDS lysates analyzed by immunoblotting.AP, affinity purification; S-prot, S-protein; KO, knockout.Ubn, ubiquitinated.

# Conclusions

Endoplasmic reticulum-associated degradation (ERAD) plays a vital role in maintaining cellular homeostasis for proteins as well as lipids. Intricate mechanisms exist for ERAD to control lipid metabolism, yet lipid metabolism can in turn affect ERAD. In Chapter 2, we show that inhibition of long chain acyl CoA synthetases (ACSLs) using the chemical inhibitor triacsin C leads to broad disruptions in lipid homeostasis. Furthermore, these disruptions inhibit ERAD through inhibition of glycan trimming and delivery of CD147 to the Hrd1 dislocon. While treatment with triacsin C inhibits the formation of lipid droplets (LDs), we use genetics and small-molecule inhibition to show that the ERAD of CD147 is not dependent on the formation of LDs. Prolonged exposure to triacsin C results in activation of the unfolded protein response (UPR) to restore cellular homeostasis. However, cells failing to restore triacsin-induced UPR eventually undergo IRE1-dependent cell death.

Recent studies uncoupling lipid bilayer stress from proteotoxic stress in the UPR have found diverging responses [64,246]. Our study has shown that treatment with triacsin C results in broad disruptions in the cellular lipid environment, a defect in ERAD, and activation of the UPR. However, it is not yet clear if activation of the UPR in this case is primarily driven by lipid bilayer stress, proteotoxic stress, or a mix of both. Treatment with tunicamycin results in rapid upregulation of IRE1 and a slower upregulation of PERK, and treatment with triacsin C results in a slow increase in both. Because of this, it is unlikely that the downstream response after treatment with triacsin C is driven by proteotoxic stress alone. However, further studies are needed to determine the factors driving the UPR and how the downstream response may differ from proteotoxic stress and/or lipid bilayer stress alone.

Chapter 2 elucidates a close relationship between lipid metabolism and ERAD. However, the precise mechanisms by which these lipid changes impair glycan trimming are yet to be determined. While our analysis of the Hrd1 dislocation complex shows that its components are not changed following triacsin C treatment, it is possible that lipid composition of the ER bilayer can play a functional role in facilitating protein interactions and delivery. In addition, inhibition of ACSLs may impact protein acylation, the process by which fatty acids are covalently attached to proteins. While the palmitoylation of calnexin assigns the protein to calcium signaling instead of protein quality control, it is unclear how or if other ERAD factors can be regulated by lipidation [173].

Understanding the many different endogenous substrates of ERAD and how they may separate into different pathways remains a fundamental challenge. For example, FSP27, a crucial regulator of lipid droplet fusion and storage, is deacetylated by HDAC6, resulting in rapid degradation [247]. In addition, a mutation of TM6SF2, an ER protein of unknown function, is associated with increased hepatic triglyceride content and expressed as an unstable protein [248]. Currently, little is known about the degradation pathways of FSP27 and TM6SF2. While these kinds of candidate-based approaches can be of use for specific diseases and conditions, there is a lack of tools available to globally profile the ERAD substrate landscape.

In Chapter 3, we develop a method to profile endogenous ERAD substrates. The VCP inhibitor substrate trapping approach (VISTA) allows for proteomic profiling of endogenous ERAD substrates without genetic manipulation. In addition, the modular nature of VISTA allows for enhancements to the technique as technologies develop. For example, advancements in

quantitative multiplexed proteomics allow for much higher multiplexing to compare ERAD pathways across up to 11 conditions in a single mass spectrometry run [249]. The increased number of samples would allow for direct, easy comparisons of VISTA to total protein turnover proteomics for a more targeted approach to ERAD substrate identification [250]. In addition, background can further be decreased by combining VISTA with a UbiSite antibody recognizing the C-terminal 13 amino acids of ubiquitin, removing diglycine remnants from the ubiquitin-like proteins NEDD8 and ISG15 [251]. Although comprehensive identification of ERAD pathways and substrates remains a challenge, VISTA adds to the existing tools with which to study the ERAD substrate landscape.

The work presented in this dissertation provides insight into the intricacies of ERAD and lipid metabolism. While it is clear that ERAD plays a vital role in human health and metabolism, much work remains in understanding the endogenous pathways and how to manipulate them. Furthering this understanding can lead to a more focused effort in developing targeted therapeutics.

## References


1. Amm, I., Sommer, T. & Wolf, D. H. Protein quality control and elimination of protein waste: the role of the ubiquitin–proteasome system. *... et Biophysica Acta (BBA)-Molecular Cell ...* (2014).

2. Kleiger, G. & Mayor, T. Perilous journey: a tour of the ubiquitin-proteasome system. *Trends Cell Biol.* **24,** 352–359 (2014).

3. Ciechanover, A. The ubiquitin-proteasome pathway: on protein death and cell life. *EMBO J.* **17,** 7151–7160 (1998).

4. Chen, B., Retzlaff, M., Roos, T. & Frydman, J. Cellular strategies of protein quality control. *Cold Spring Harb. Perspect. Biol.* **3,** a004374 (2011).

5. Komander, D. & Rape, M. The ubiquitin code. *Annu. Rev. Biochem.* **81,** 203–229 (2012).

6. Olzmann, J. A., Kopito, R. R. & Christianson, J. C. The mammalian endoplasmic reticulum-associated degradation system. *Cold Spring Harb. Perspect. Biol.* **5,** (2013).

7. Helenius, A. & Aebi, M. Roles of N-linked glycans in the endoplasmic reticulum. *Annu. Rev. Biochem.* **73,** 1019–1049 (2004).

8. Adams, B. M., Oster, M. E. & Hebert, D. N. Protein quality control in the endoplasmic reticulum. *Protein J.* **38,** 317–329 (2019).

9. Caramelo, J. J. & Parodi, A. J. Getting in and out from calnexin/calreticulin cycles. *J. Biol. Chem.* **283,** 10221–10225 (2008).

10. Olivari, S. & Molinari, M. Glycoprotein folding and the role of EDEM1, EDEM2 and EDEM3 in degradation of folding-defective glycoproteins. *FEBS Lett.* **581,** 3658–3664 (2007).

11. Lamriben, L., Graham, J. B., Adams, B. M. & Hebert, D. N. N-glycan based ER molecular chaperone and protein quality control system: the calnexin binding cycle. *Traffic* (2015). doi:10.1111/tra.12358

12. Satoh, T. *et al.* Structural basis for oligosaccharide recognition of misfolded glycoproteins by OS-9 in ER-associated degradation. *Mol. Cell* **40,** 905–916 (2010).

13. Ushioda, R., Hoseki, J. & Nagata, K. Glycosylation-independent ERAD pathway serves as a backup system under ER stress. *Mol. Biol. Cell* **24,** 3155–3163 (2013).

14. Tang, H.-Y., Huang, C.-H., Zhuang, Y.-H., Christianson, J. C. & Chen, X. EDEM2 and OS-9 are required for ER-associated degradation of non-glycosylated sonic hedgehog. *PLoS One* **9,** e92164 (2014).

15. Cormier, J. H., Tamura, T., Sunryd, J. C. & Hebert, D. N. EDEM1 recognition and delivery of misfolded proteins to the SEL1L-containing ERAD complex. *Mol. Cell* **34,** 627–633 (2009).

16. Kostova, Z., Tsai, Y. C. & Weissman, A. M. Ubiquitin ligases, critical mediators of endoplasmic reticulum-associated degradation. *Semin. Cell Dev. Biol.* **18,** 770–779 (2007).

17. Christianson, J. C. *et al.* Defining human ERAD networks through an integrative mapping strategy. *Nat. Cell Biol.* **14,** 93–105 (2011).

18. Ploegh, H. L. A lipid-based model for the creation of an escape hatch from the endoplasmic reticulum. *Nature* **448,** 435–438 (2007).

19. Ye, Y., Shibata, Y., Yun, C., Ron, D. & Rapoport, T. A. A membrane protein complex mediates retro-translocation from the ER lumen into the cytosol. *Nature* **429,** 841–847 (2004).

20. Loureiro, J. *et al.* Signal peptide peptidase is required for dislocation from the endoplasmic reticulum. *Nature* **441,** 894–897 (2006).

21. Scott, D. C. & Schekman, R. Role of Sec61p in the ER-associated degradation of short-lived transmembrane proteins. *J. Cell Biol.* **181,** 1095–1105 (2008).

22. Willer, M., Forte, G. M. A. & Stirling, C. J. Sec61p is required for ERAD-L: genetic dissection of the translocation and ERAD-L functions of Sec61P using novel derivatives of CPY. *J. Biol. Chem.* **283,** 33883–33888 (2008).

23. Carvalho, P., Stanley, A. M. & Rapoport, T. A. Retrotranslocation of a misfolded luminal ER protein by the ubiquitin-ligase Hrd1p. *Cell* **143,** 579–591 (2010).

24. Baldridge, R. D. & Rapoport, T. A. Autoubiquitination of the hrd1 ligase triggers protein retrotranslocation in ERAD. *Cell* **166,** 394–407 (2016).

25. Schoebel, S. *et al.* Cryo-EM structure of the protein-conducting ERAD channel Hrd1 in complex with Hrd3. *Nature* **548,** 352–355 (2017).

26. Vasic, V. *et al.* Hrd1 forms the retrotranslocation pore regulated by auto-ubiquitination and binding of misfolded proteins. *Nat. Cell Biol.* **22,** 274–281 (2020).

27. Meyer, H., Bug, M. & Bremer, S. Emerging functions of the VCP/p97 AAA-ATPase in the ubiquitin system. *Nat. Cell Biol.* **14,** 117–123 (2012).

28. Banerjee, S. *et al.* 2.3 Å resolution cryo-EM structure of human p97 and mechanism of allosteric inhibition. *Science* **351,** 871–875 (2016).

29. Bodnar, N. O. & Rapoport, T. A. Molecular mechanism of substrate processing by the cdc48 atpase complex. *Cell* **169,** 722–735.e9 (2017).

30. Twomey, E. C. *et al.* Substrate processing by the Cdc48 ATPase complex is initiated by ubiquitin unfolding. *Science* **365,** (2019).

31. Neutzner, A. *et al.* A systematic search for endoplasmic reticulum (ER) membrane-associated RING finger proteins identifies Nixin/ZNRF4 as a regulator of calnexin stability and ER homeostasis. *J. Biol. Chem.* **286,** 8633–8643 (2011).

32. Jo, Y., Lee, P. C. W., Sguigna, P. V. & DeBose-Boyd, R. A. Sterol-induced degradation of HMG CoA reductase depends on interplay of two Insigs and two ubiquitin ligases, gp78 and Trc8. *Proc. Natl. Acad. Sci. USA* **108,** 20503–20508 (2011).

33. Zhang, T., Xu, Y., Liu, Y. & Ye, Y. gp78 functions downstream of Hrd1 to promote degradation of misfolded proteins of the endoplasmic reticulum. *Mol. Biol. Cell* **26,** 4438–4450 (2015).

34. Leto, D. E. *et al.* Genome-wide CRISPR Analysis Identifies Substrate-Specific Conjugation Modules in ER-Associated Degradation. *Mol. Cell* **73,** 377–389.e11 (2019).

35. Shmueli, A., Tsai, Y. C., Yang, M., Braun, M. A. & Weissman, A. M. Targeting of gp78 for ubiquitin-mediated proteasomal degradation by Hrd1: cross-talk between E3s in the endoplasmic reticulum. *Biochem. Biophys. Res. Commun.* **390,** 758–762 (2009).

36. Huang, E. Y. *et al.* A VCP inhibitor substrate trapping approach (VISTA) enables proteomic profiling of endogenous ERAD substrates. *Mol. Biol. Cell* **29,** 1021–1030 (2018).

37. Komander, D., Clague, M. J. & Urbé, S. Breaking the chains: structure and function of the deubiquitinases. *Nat. Rev. Mol. Cell Biol.* **10,** 550–563 (2009).

38. Peterson, B. G., Glaser, M. L., Rapoport, T. A. & Baldridge, R. D. Cycles of autoubiquitination and deubiquitination regulate the ERAD ubiquitin ligase Hrd1. *Elife* **8,** (2019).

39. Ernst, R., Mueller, B., Ploegh, H. L. & Schlieker, C. The otubain YOD1 is a deubiquitinating enzyme that associates with p97 to facilitate protein dislocation from the ER. *Mol. Cell* **36,** 28–38 (2009).

40. Stein, A., Ruggiano, A., Carvalho, P. & Rapoport, T. A. Key steps in ERAD of luminal ER proteins reconstituted with purified components. *Cell* **158,** 1375–1388 (2014).

41. Bard, J. A. M. *et al.* Structure and function of the 26S proteasome. *Annu. Rev. Biochem.* **87,** 697–724 (2018).

42. Finley, D. Recognition and processing of ubiquitin-protein conjugates by the proteasome. *Annu. Rev. Biochem.* **78,** 477–513 (2009).

43. Ikeda, Y. *et al.* Regulated endoplasmic reticulum-associated degradation of a polytopic protein: p97 recruits proteasomes to Insig-1 before extraction from membranes. *J. Biol. Chem.* **284,** 34889–34900 (2009).

44. Nishikawa, S. I., Fewell, S. W., Kato, Y., Brodsky, J. L. & Endo, T. Molecular chaperones in the yeast endoplasmic reticulum maintain the solubility of proteins for retrotranslocation and degradation. *J. Cell Biol.* **153,** 1061–1070 (2001).

45. Lee, S.-O. *et al.* Protein disulphide isomerase is required for signal peptide peptidase-mediated protein degradation. *EMBO J.* **29,** 363–375 (2010).

46. Wang, Q. *et al.* A ubiquitin ligase-associated chaperone holdase maintains polypeptides in soluble states for proteasome degradation. *Mol. Cell* **42,** 758–770 (2011).

47. Suzuki, M. *et al.* Derlin-1 and UBXD8 are engaged in dislocation and degradation of lipidated ApoB-100 at lipid droplets. *Mol. Biol. Cell* **23,** 800–810 (2012).

48. Nguyen, K. T. *et al.* N-terminal acetylation and the N-end rule pathway control degradation of the lipid droplet protein PLIN2. *J. Biol. Chem.* **294,** 379–388 (2019).

49. Karagöz, G. E., Acosta-Alvear, D. & Walter, P. The Unfolded Protein Response: Detecting and Responding to Fluctuations in the Protein-Folding Capacity of the Endoplasmic Reticulum. *Cold Spring Harb. Perspect. Biol.* **11,** (2019).

50. Hetz, C. The unfolded protein response: controlling cell fate decisions under ER stress and beyond. *Nat. Rev. Mol. Cell Biol.* **13,** 89–102 (2012).

51. Lu, M. *et al.* Opposing unfolded-protein-response signals converge on death receptor 5 to control apoptosis. *Science* **345,** 98–101 (2014).

52. Mori, K. Signalling pathways in the unfolded protein response: development from yeast to mammals. *J. Biochem.* **146,** 743–750 (2009).

53. Harding, H. P., Zhang, Y. & Ron, D. Protein translation and folding are coupled by an endoplasmic-reticulum-resident kinase. *Nature* **397,** 271–274 (1999).

54. Vattem, K. M. & Wek, R. C. Reinitiation involving upstream ORFs regulates ATF4 mRNA translation in mammalian cells. *Proc. Natl. Acad. Sci. USA* **101,** 11269–11274 (2004).

55. Carrara, M., Prischi, F., Nowak, P. R. & Ali, M. M. Crystal structures reveal transient PERK luminal domain tetramerization in endoplasmic reticulum stress signaling. *EMBO J.* **34,** 1589–1600 (2015).

56. Haze, K., Yoshida, H., Yanagi, H., Yura, T. & Mori, K. Mammalian transcription factor ATF6 is synthesized as a transmembrane protein and activated by proteolysis in response to endoplasmic reticulum stress. *Mol. Biol. Cell* **10,** 3787–3799 (1999).

57. Sano, R. & Reed, J. C. ER stress-induced cell death mechanisms. *Biochimica et Biophysica Acta (BBA)-Molecular Cell …* (2013).

58. Adams, C. J., Kopp, M. C., Larburu, N., Nowak, P. R. & Ali, M. M. U. Structure and molecular mechanism of ER stress signaling by the unfolded protein response signal activator IRE1. *Front. Mol. Biosci.* **6,** 11 (2019).

59. Hu, H., Tian, M., Ding, C. & Yu, S. The C/EBP Homologous Protein (CHOP) Transcription Factor Functions in Endoplasmic Reticulum Stress-Induced Apoptosis and Microbial Infection. *Front. Immunol.* **9,** 3083 (2018).

60. Volmer, R., van der Ploeg, K. & Ron, D. Membrane lipid saturation activates endoplasmic reticulum unfolded protein response transducers through their transmembrane domains. *Proc. Natl. Acad. Sci. USA* **110,** 4628–4633 (2013).

61. Promlek, T. *et al.* Membrane aberrancy and unfolded proteins activate the endoplasmic reticulum stress sensor Ire1 in different ways. *Mol. Biol. Cell* **22,** 3520–3532 (2011).

62. Shyu, P. *et al.* Membrane phospholipid alteration causes chronic ER stress through early degradation of homeostatic ER-resident proteins. *Sci. Rep.* **9,** 8637 (2019).

63. Thibault, G. *et al.* The membrane stress response buffers lethal effects of lipid disequilibrium by reprogramming the protein homeostasis network. *Mol. Cell* **48,** 16–27 (2012).

64. Ho, N. *et al.* ER stress sensor Ire1 deploys a divergent transcriptional program in response to lipid bilayer stress. *BioRxiv* (2019). doi:10.1101/774133

65. Sekijima, Y. *et al.* The biological and chemical basis for tissue-selective amyloid disease. *Cell* **121,** 73–85 (2005).

66. Lukacs, G. L. & Verkman, A. S. CFTR: folding, misfolding and correcting the ΔF508 conformational defect. *Trends Mol. Med.* **18,** 81–91 (2012).

67. Pettit, R. S. & Fellner, C. CFTR modulators for the treatment of cystic fibrosis. *Pharmacy and Therapeutics* (2014).

68. Vij, N., Fang, S. & Zeitlin, P. L. Selective Inhibition of Endoplasmic Reticulum-associated Degradation Rescues ΔF508-Cystic Fibrosis Transmembrane Regulator and Suppresses Interleukin-8 …. *J. Bio. Chem.* (2006).

69. Lev, S. Nonvesicular lipid transfer from the endoplasmic reticulum. *Cold Spring Harb. Perspect. Biol.* **4,** (2012).

70. Stevenson, J., Huang, E. Y. & Olzmann, J. A. Endoplasmic Reticulum-Associated Degradation and Lipid Homeostasis. *Annu. Rev. Nutr.* **36,** 511–542 (2016).

71. Maxfield, F. R. & Tabas, I. Role of cholesterol and lipid organization in disease. *Nature* **438,** 612–621 (2005).

72. Luirink, I. K. *et al.* 20-Year Follow-up of Statins in Children with Familial Hypercholesterolemia. *N. Engl. J. Med.* **381,** 1547–1556 (2019).

73. DeBose-Boyd, R. A. Feedback regulation of cholesterol synthesis: sterol-accelerated ubiquitination and degradation of HMG CoA reductase. *Cell Res.* **18,** 609–621 (2008).

74. Sharpe, L. J. & Brown, A. J. Controlling cholesterol synthesis beyond 3-hydroxy-3-methylglutaryl-CoA reductase (HMGCR). *J. Biol. Chem.* **288,** 18707–18715 (2013).

75. Olzmann, J. A., Richter, C. M. & Kopito, R. R. Spatial regulation of UBXD8 and p97/VCP controls ATGL-mediated lipid droplet turnover. *Proc. Natl. Acad. Sci. USA* **110,** 1345–1350 (2013).

76. Wernick, N. L. B., Chinnapen, D. J.-F., Cho, J. A. & Lencer, W. I. Cholera toxin: an intracellular journey into the cytosol by way of the endoplasmic reticulum. *Toxins (Basel)* **2,** 310–325 (2010).

77. Simpson, J. C. *et al.* Ricin A chain utilises the endoplasmic reticulum-associated protein degradation pathway to enter the cytosol of yeast. *FEBS Lett.* **459,** 80–84 (1999).

78. van den Boomen, D. J. H. & Lehner, P. J. Identifying the ERAD ubiquitin E3 ligases for viral and cellular targeting of MHC class I. *Mol. Immunol.* **68,** 106–111 (2015).

79. Stagg, H. R. *et al.* The TRC8 E3 ligase ubiquitinates MHC class I molecules before dislocation from the ER. *J. Cell Biol.* **186,** 685–692 (2009).

80. van de Weijer, M. L. *et al.* A high-coverage shRNA screen identifies TMEM129 as an E3 ligase involved in ER-associated protein degradation. *Nat. Commun.* **5,** 3832 (2014).

81. Amano, T. *et al.* Synoviolin/Hrd1, an E3 ubiquitin ligase, as a novel pathogenic factor for arthropathy. *Genes Dev.* **17,** 2436–2449 (2003).

82. Ye, Y., Baek, S.-H., Ye, Y. & Zhang, T. Proteomic characterization of endogenous substrates of mammalian ubiquitin ligase Hrd1. *Cell Biosci.* **8,** 46 (2018).

83. Lee, K. A. *et al.* Ubiquitin ligase substrate identification through quantitative proteomics at both the protein and peptide levels. *J. Biol. Chem.* **286,** 41530–41538 (2011).

84. Ashktorab, H. *et al.* SEL1L, an UPR response protein, a potential marker of colonic cell transformation. *Dig. Dis. Sci.* **57,** 905–912 (2012).

85. Mellai, M. *et al.* SEL1L plays a major role in human malignant gliomas. *J. Pathol. Clin. Res.* (2019). doi:10.1002/cjp2.134

86. Yanagisawa, K. *et al.* Novel metastasis-related gene CIM functions in the regulation of multiple cellular stress-response pathways. *Cancer Res.* **70,** 9949–9958 (2010).

87. Brockmeier, U. *et al.* The function of hypoxia-inducible factor (HIF) is independent of the endoplasmic reticulum protein OS-9. *PLoS One* **6,** e19151 (2011).

88. Deshaies, R. J. Proteotoxic crisis, the ubiquitin-proteasome system, and cancer therapy. *BMC Biol.* **12,** 94 (2014).

89. Milano, A., Perri, F. & Caponigro, F. The ubiquitin–proteasome system as a molecular target in solid tumors: an update on bortezomib. *Onco. Targets. Ther.* (2009).

90. Anderson, D. J. *et al.* Targeting the AAA ATPase p97 as an Approach to Treat Cancer through Disruption of Protein Homeostasis. *Cancer Cell* **28,** 653–665 (2015).

91. Papadopoulos, K. P. *et al.* A phase I/II study of carfilzomib 2-10-min infusion in patients with advanced solid tumors. *Cancer Chemother. Pharmacol.* **72,** 861–868 (2013).

92. Roeten, M. S. F., Cloos, J. & Jansen, G. Positioning of proteasome inhibitors in therapy of solid malignancies. *Cancer Chemother. Pharmacol.* **81,** 227–243 (2017).

93. Guerriero, C. J. & Brodsky, J. L. The delicate balance between secreted protein folding and endoplasmic reticulum-associated degradation in human physiology. *Physiol. Rev.* **92,** 537–576 (2012).

94. Christianson, J. C. & Ye, Y. Cleaning up in the endoplasmic reticulum: ubiquitin in charge. *Nat. Struct. Mol. Biol.* **21,** 325–335 (2014).

95. Walter, P. & Ron, D. The unfolded protein response: from stress pathway to homeostatic regulation. *Science* **334,** 1081–1086 (2011).

96. Wang, M. & Kaufman, R. J. Protein misfolding in the endoplasmic reticulum as a conduit to human disease. *Nature* **529,** 326–335 (2016).

97. Xu, C. & Ng, D. T. Glycosylation-directed quality control of protein folding. *Nat. Rev. Mol. Cell Biol.* (2015). doi:10.1038/nrm4073

98. Cherepanova, N., Shrimal, S. & Gilmore, R. N-linked glycosylation and homeostasis of the endoplasmic reticulum. *Curr. Opin. Cell Biol.* **41,** 57–65 (2016).

99. Christianson, J. C., Shaler, T. A., Tyler, R. E. & Kopito, R. R. OS-9 and GRP94 deliver mutant alpha1-antitrypsin to the Hrd1-SEL1L ubiquitin ligase complex for ERAD. *Nat. Cell Biol.* **10,** 272–282 (2008).

100. Mueller, B., Klemm, E. J., Spooner, E., Claessen, J. H. & Ploegh, H. L. SEL1L nucleates a protein complex required for dislocation of misfolded glycoproteins. *Proc. Natl. Acad. Sci. USA* **105,** 12325–12330 (2008).

101. Tyler, R. E. *et al.* Unassembled CD147 is an endogenous endoplasmic reticulum-associated degradation substrate. *Mol. Biol. Cell* **23,** 4668–4678 (2012).

102. Lilley, B. N. & Ploegh, H. L. A membrane protein required for dislocation of misfolded proteins from the ER. *Nature* **429,** 834–840 (2004).

103. Mehnert, M., Sommer, T. & Jarosch, E. Der1 promotes movement of misfolded proteins through the endoplasmic reticulum membrane. *Nat. Cell Biol.* **16,** 77–86 (2014).

104. Greenblatt, E. J., Olzmann, J. A. & Kopito, R. R. Derlin-1 is a rhomboid pseudoprotease required for the dislocation of mutant α-1 antitrypsin from the endoplasmic reticulum. *Nat. Struct. Mol. Biol.* **18,** 1147–1152 (2011).

105. Plemper, R. K., Böhmler, S., Bordallo, J., Sommer, T. & Wolf, D. H. Mutant analysis links the translocon and BiP to retrograde protein transport for ER degradation. *Nature* **388,** 891–895 (1997).

106. Walther, T. C. & Farese, R. V. Lipid droplets and cellular lipid metabolism. *Annu. Rev. Biochem.* **81,** 687–714 (2012).

107. Pol, A., Gross, S. P. & Parton, R. G. Review: biogenesis of the multifunctional lipid droplet: lipids, proteins, and sites. *J. Cell Biol.* **204,** 635–646 (2014).

108. Hashemi, H. F. & Goodman, J. M. The life cycle of lipid droplets. *Curr. Opin. Cell Biol.* **33,** 119–124 (2015).

109. Listenberger, L. L. *et al.* Triglyceride accumulation protects against fatty acid-induced lipotoxicity. *Proc. Natl. Acad. Sci. USA* **100,** 3077–3082 (2003).

110. Kurat, C. F. *et al.* Cdk1/Cdc28-dependent activation of the major triacylglycerol lipase Tgl4 in yeast links lipolysis to cell-cycle progression. *Mol. Cell* **33,** 53–63 (2009).

111. Rambold, A. S., Cohen, S. & Lippincott-Schwartz, J. Fatty acid trafficking in starved cells: regulation by lipid droplet lipolysis, autophagy, and mitochondrial fusion dynamics. *Dev. Cell* **32,** 678–692 (2015).

112. Tang, T. *et al.* Desnutrin/ATGL activates PPARδ to promote mitochondrial function for insulin secretion in islet β cells. *Cell Metab.* **18,** 883–895 (2013).

113. Haemmerle, G. *et al.* ATGL-mediated fat catabolism regulates cardiac mitochondrial function via PPAR-α and PGC-1. *Nat. Med.* **17,** 1076–1085 (2011).

114. Herker, E. *et al.* Efficient hepatitis C virus particle formation requires diacylglycerol acyltransferase-1. *Nat. Med.* **16,** 1295–1298 (2010).

115. Miyanari, Y. *et al.* The lipid droplet is an important organelle for hepatitis C virus production. *Nat. Cell Biol.* **9,** 1089–1097 (2007).

116. Anand, P. *et al.* A novel role for lipid droplets in the organismal antibacterial response. *Elife* **1,** e00003 (2012).

117. Cermelli, S., Guo, Y., Gross, S. P. & Welte, M. A. The lipid-droplet proteome reveals that droplets are a protein-storage depot. *Curr. Biol.* **16,** 1783–1795 (2006).

118. Moldavski, O. *et al.* Lipid Droplets Are Essential for Efficient Clearance of Cytosolic Inclusion Bodies. *Dev. Cell* **33,** 603–610 (2015).

119. Hodges, B. D. M. & Wu, C. C. Proteomic insights into an expanded cellular role for cytoplasmic lipid droplets. *J. Lipid Res.* **51,** 262–273 (2010).

120. Brasaemle, D. L., Dolios, G., Shapiro, L. & Wang, R. Proteomic analysis of proteins associated with lipid droplets of basal and lipolytically stimulated 3T3-L1 adipocytes. *J. Biol. Chem.* **279,** 46835–46842 (2004).

121. Liu, P. *et al.* Chinese hamster ovary K2 cell lipid droplets appear to be metabolic organelles involved in membrane traffic. *J. Biol. Chem.* **279,** 3787–3792 (2004).

122. Zehmer, J. K. *et al.* Targeting sequences of UBXD8 and AAM-B reveal that the ER has a direct role in the emergence and regression of lipid droplets. *J. Cell Sci.* **122,** 3694–3702 (2009).

123. Spandl, J., Lohmann, D., Kuerschner, L., Moessinger, C. & Thiele, C. Ancient ubiquitous protein 1 (AUP1) localizes to lipid droplets and binds the E2 ubiquitin conjugase G2 (Ube2g2) via its G2 binding region. *J. Biol. Chem.* **286,** 5599–5606 (2011).

124. Jo, Y., Hartman, I. Z. & DeBose-Boyd, R. A. Ancient ubiquitous protein-1 mediates sterol-induced ubiquitination of 3-hydroxy-3-methylglutaryl CoA reductase in lipid droplet-associated endoplasmic reticulum membranes. *Mol. Biol. Cell* **24,** 169–183 (2013).

125. Klemm, E. J., Spooner, E. & Ploegh, H. L. Dual role of ancient ubiquitous protein 1 (AUP1) in lipid droplet accumulation and endoplasmic reticulum (ER) protein quality control. *J. Biol. Chem.* **286,** 37602–37614 (2011).

126. Ohsaki, Y., Cheng, J., Fujita, A., Tokumoto, T. & Fujimoto, T. Cytoplasmic lipid droplets are sites of convergence of proteasomal and autophagic degradation of apolipoprotein B. *Mol. Biol. Cell* **17,** 2674–2683 (2006).

127. Hartman, I. Z. *et al.* Sterol-induced dislocation of 3-hydroxy-3-methylglutaryl coenzyme A reductase from endoplasmic reticulum membranes into the cytosol through a subcellular compartment resembling lipid droplets. *J. Biol. Chem.* **285,** 19288–19298 (2010).

128. Fei, W., Wang, H., Fu, X., Bielby, C. & Yang, H. Conditions of endoplasmic reticulum stress stimulate lipid droplet formation in Saccharomyces cerevisiae. *Biochem. J.* **424,** 61–67 (2009).

129. Vevea, J. D. *et al.* Role for lipid droplet biogenesis and microlipophagy in adaptation to lipid imbalance in yeast. *Dev. Cell* **35,** 584–599 (2015).

130. Olzmann, J. A. & Kopito, R. R. Lipid droplet formation is dispensable for endoplasmic reticulum-associated degradation. *J. Biol. Chem.* **286,** 27872–27874 (2011).

131. Velázquez, A. P., Tatsuta, T., Ghillebert, R., Drescher, I. & Graef, M. Lipid droplet-mediated ER homeostasis regulates autophagy and cell survival during starvation. *J. Cell Biol.* **212,** 621–631 (2016).

132. Petschnigg, J. *et al.* Good fat, essential cellular requirements for triacylglycerol synthesis to maintain membrane homeostasis in yeast. *J. Biol. Chem.* **284,** 30981–30993 (2009).

133. Garbarino, J. *et al.* Sterol and diacylglycerol acyltransferase deficiency triggers fatty acid-mediated cell death. *J. Biol. Chem.* **284,** 30994–31005 (2009).

134. Igal, R. A., Wang, P. & Coleman, R. A. Triacsin C blocks de novo synthesis of glycerolipids and cholesterol esters but not recycling of fatty acid into phospholipid:

evidence for functionally separate pools of acyl-CoA. *Biochem. J.* **324 ( Pt 2),** 529–534 (1997).

135. Tomoda, H., Igarashi, K. & omura, S. Inhibition of acyi-CoA synthetase by triacsins.

136. Fujimoto, Y. *et al.* Involvement of ACSL in local synthesis of neutral lipids in cytoplasmic lipid droplets in human hepatocyte HuH7. *J. Lipid Res.* **48,** 1280–1292 (2007).

137. Kassan, A. *et al.* Acyl-CoA synthetase 3 promotes lipid droplet biogenesis in ER microdomains. *J. Cell Biol.* **203,** 985–1001 (2013).

138. Nakatsukasa, K. & Kamura, T. Subcellular Fractionation Analysis of the Extraction of Ubiquitinated Polytopic Membrane Substrate during ER-Associated Degradation. *PLoS One* **11,** e0148327 (2016).

139. Hosokawa, N. *et al.* Human XTP3-B forms an endoplasmic reticulum quality control scaffold with the HRD1-SEL1L ubiquitin ligase complex and BiP. *J. Biol. Chem.* **283,** 20914–20924 (2008).

140. Meacham, G. C., Patterson, C., Zhang, W., Younger, J. M. & Cyr, D. M. The Hsc70 co-chaperone CHIP targets immature CFTR for proteasomal degradation. *Nat. Cell Biol.* **3,** 100–105 (2001).

141. Younger, J. M. *et al.* Sequential quality-control checkpoints triage misfolded cystic fibrosis transmembrane conductance regulator. *Cell* **126,** 571–582 (2006).

142. Morito, D. *et al.* Gp78 cooperates with RMA1 in endoplasmic reticulum-associated degradation of CFTRDeltaF508. *Mol. Biol. Cell* **19,** 1328–1336 (2008).

143. Tang, W., Chang, S. B. & Hemler, M. E. Links between CD147 function, glycosylation, and caveolin-1. *Mol. Biol. Cell* **15,** 4043–4050 (2004).

144. Banaszynski, L. A., Chen, L.-C., Maynard-Smith, L. A., Ooi, A. G. L. & Wandless, T. J. A rapid, reversible, and tunable method to regulate protein function in living cells using synthetic small molecules. *Cell* **126,** 995–1004 (2006).

145. Egeler, E. L., Urner, L. M., Rakhit, R., Liu, C. W. & Wandless, T. J. Ligand-switchable substrates for a ubiquitin-proteasome system. *J. Biol. Chem.* **286,** 31328–31336 (2011).

146. Bersuker, K., Brandeis, M. & Kopito, R. R. Protein misfolding specifies recruitment to cytoplasmic inclusion bodies. *J. Cell Biol.* **213,** 229–241 (2016).

147. Han, G.-S., O'Hara, L., Carman, G. M. & Siniossoglou, S. An unconventional diacylglycerol kinase that regulates phospholipid synthesis and nuclear membrane growth. *J. Biol. Chem.* **283,** 20433–20442 (2008).

148. Adeyo, O. *et al.* The yeast lipin orthologue Pah1p is important for biogenesis of lipid droplets. *J. Cell Biol.* **192,** 1043–1055 (2011).

149. Caldwell, S. R., Hill, K. J. & Cooper, A. A. Degradation of endoplasmic reticulum (ER) quality control substrates requires transport between the ER and Golgi. *J. Biol. Chem.* **276,** 23296–23303 (2001).

150. Taxis, C., Vogel, F. & Wolf, D. H. ER-golgi traffic is a prerequisite for efficient ER degradation. *Mol. Biol. Cell* **13,** 1806–1818 (2002).

151. Vashist, S. *et al.* Distinct retrieval and retention mechanisms are required for the quality control of endoplasmic reticulum protein folding. *J. Cell Biol.* **155,** 355–368 (2001).

152. Bogdanov, M., Mileykovskaya, E. & Dowhan, W. Lipids in the assembly of membrane proteins and organization of protein supercomplexes: implications for lipid-linked disorders. *Subcell. Biochem.* **49,** 197–239 (2008).

153. Contreras, F.-X., Ernst, A. M., Wieland, F. & Brügger, B. Specificity of intramembrane protein-lipid interactions. *Cold Spring Harb. Perspect. Biol.* **3,** (2011).

154. Grotzke, J. E., Lu, Q. & Cresswell, P. Deglycosylation-dependent fluorescent proteins provide unique tools for the study of ER-associated degradation. *Proc. Natl. Acad. Sci. USA* **110,** 3393–3398 (2013).

155. Harris, C. A. *et al.* DGAT enzymes are required for triacylglycerol synthesis and lipid droplets in adipocytes. *J. Lipid Res.* **52,** 657–667 (2011).

156. Cao, J. *et al.* Targeting Acyl-CoA:diacylglycerol acyltransferase 1 (DGAT1) with small molecule inhibitors for the treatment of metabolic diseases. *J. Biol. Chem.* **286,** 41838–41851 (2011).

157. Stone, S. J. *et al.* Lipopenia and skin barrier abnormalities in DGAT2-deficient mice. *J. Biol. Chem.* **279,** 11767–11776 (2004).

158. Masuda, Y. *et al.* ADRP/adipophilin is degraded through the proteasome-dependent pathway during regression of lipid-storing cells. *J. Lipid Res.* **47,** 87–98 (2006).

159. Xu, G. *et al.* Post-translational regulation of adipose differentiation-related protein by the ubiquitin/proteasome pathway. *J. Biol. Chem.* **280,** 42841–42847 (2005).

160. Takahashi, Y. *et al.* Perilipin2 plays a positive role in adipocytes during lipolysis by escaping proteasomal degradation. *Sci. Rep.* **6,** 20975 (2016).

161. Fu, S. *et al.* Aberrant lipid metabolism disrupts calcium homeostasis causing liver endoplasmic reticulum stress in obesity. *Nature* **473,** 528–531 (2011).

162. Li, Z. *et al.* The ratio of phosphatidylcholine to phosphatidylethanolamine influences membrane integrity and steatohepatitis. *Cell Metab.* **3,** 321–331 (2006).

163. Volmer, R. & Ron, D. Lipid-dependent regulation of the unfolded protein response. *Curr. Opin. Cell Biol.* **33,** 67–73 (2015).

164. Jonikas, M. C. *et al.* Comprehensive characterization of genes required for protein folding in the endoplasmic reticulum. *Science* **323,** 1693–1697 (2009).

165. Hiramatsu, N., Chiang, W.-C., Kurt, T. D., Sigurdson, C. J. & Lin, J. H. Multiple Mechanisms of Unfolded Protein Response-Induced Cell Death. *Am. J. Pathol.* **185,** 1800–1808 (2015).

166. Novoa, I., Zeng, H., Harding, H. P. & Ron, D. Feedback inhibition of the unfolded protein response by GADD34-mediated dephosphorylation of eIF2alpha. *J. Cell Biol.* **153,** 1011–1022 (2001).

167. Wang, X. Z. *et al.* Cloning of mammalian Ire1 reveals diversity in the ER stress responses. *EMBO J.* **17,** 5708–5717 (1998).

168. Lin, J. H. *et al.* IRE1 signaling affects cell fate during the unfolded protein response. *Science* **318,** 944–949 (2007).

169. Han, D. *et al.* IRE1alpha kinase activation modes control alternate endoribonuclease outputs to determine divergent cell fates. *Cell* **138,** 562–575 (2009).

170. Yen, C. L., Stone, S. J., Koliwad, S., Harris, C. & Farese, R. V. Thematic review series: glycerolipids. DGAT enzymes and triacylglycerol biosynthesis. *J. Lipid Res.* **49,** 2283–2301 (2008).

171. Benyair, R., Ogen-Shtern, N. & Lederkremer, G. Z. Glycan regulation of ER-associated degradation through compartmentalization. *Semin. Cell Dev. Biol.* **41,** 99–109 (2015).

172. Tamura, T., Cormier, J. H. & Hebert, D. N. Characterization of early EDEM1 protein maturation events and their functional implications. *J. Biol. Chem.* **286,** 24906–24915 (2011).

173. Lynes, E. M. *et al.* Palmitoylation is the switch that assigns calnexin to quality control or ER Ca2+ signaling. *J. Cell Sci.* **126,** 3893–3903 (2013).

174. Lakkaraju, A. K. *et al.* Palmitoylated calnexin is a key component of the ribosome-translocon complex. *EMBO J.* **31,** 1823–1835 (2012).

175. Lynes, E. M. *et al.* Palmitoylated TMX and calnexin target to the mitochondria-associated membrane. *EMBO J.* **31,** 457–470 (2012).

176. Fairbank, M., Huang, K., El-Husseini, A. & Nabi, I. R. RING finger palmitoylation of the endoplasmic reticulum Gp78 E3 ubiquitin ligase. *FEBS Lett.* **586,** 2488–2493 (2012).

177. Lin, J. H., Li, H., Zhang, Y., Ron, D. & Walter, P. Divergent effects of PERK and IRE1 signaling on cell viability. *PLoS One* **4,** e4170 (2009).

178. Han, J. *et al.* ER-stress-induced transcriptional regulation increases protein synthesis leading to cell death. *Nat. Cell Biol.* **15,** 481–490 (2013).

179. Urano, F. *et al.* Coupling of stress in the ER to activation of JNK protein kinases by transmembrane protein kinase IRE1. *Science* **287,** 664–666 (2000).

180. Hetz, C., Chevet, E. & Harding, H. P. Targeting the unfolded protein response in disease. *Nat. Rev. Drug Discov.* **12,** 703–719 (2013).

181. Benjamin, D. I. *et al.* Diacylglycerol Metabolism and Signaling Is a Driving Force Underlying FASN Inhibitor Sensitivity in Cancer Cells. *ACS Chem. Biol.* **10,** 1616–1623 (2015).

182. Menendez, J. A. & Lupu, R. Fatty acid synthase and the lipogenic phenotype in cancer pathogenesis. *Nat. Rev. Cancer* **7,** 763–777 (2007).

183. Currie, E., Schulze, A., Zechner, R., Walther, T. C. & Farese, R. V. Cellular fatty acid metabolism and cancer. *Cell Metab.* **18,** 153–161 (2013).

184. Schneider, C. A., Rasband, W. S. & Eliceiri, K. W. NIH Image to ImageJ: 25 years of image analysis. *Nat. Methods* **9,** 671–675 (2012).

185. Mulvihill, M. M. *et al.* Metabolic profiling reveals PAFAH1B3 as a critical driver of breast cancer pathogenicity. *Chem. Biol.* **21,** 831–840 (2014).

186. Benjamin, D. I. *et al.* Ether lipid generating enzyme AGPS alters the balance of structural and signaling lipids to fuel cancer pathogenicity. *Proc. Natl. Acad. Sci. USA* **110,** 14912–14917 (2013).

187. Ruggiano, A., Foresti, O. & Carvalho, P. Quality control: ER-associated degradation: protein quality control and beyond. *J. Cell Biol.* **204,** 869–879 (2014).

188. Carvalho, P., Goder, V. & Rapoport, T. A. Distinct ubiquitin-ligase complexes define convergent pathways for the degradation of ER proteins. *Cell* **126,** 361–373 (2006).

189. Ye, Y., Tang, W. K., Zhang, T. & Xia, D. A Mighty "Protein Extractor" of the Cell: Structure and Function of the p97/CDC48 ATPase. *Front Mol Biosci* **4,** 39 (2017).

190. Ernst, R. *et al.* Enzymatic blockade of the ubiquitin-proteasome pathway. *PLoS Biol.* **8,** e1000605 (2011).

191. Blythe, E. E., Olson, K. C., Chau, V. & Deshaies, R. J. Ubiquitin- and ATP-dependent unfoldase activity of P97/VCP•NPLOC4•UFD1L is enhanced by a mutation that causes multisystem proteinopathy. *Proc. Natl. Acad. Sci. USA* **114,** E4380–E4388 (2017).

192. Needham, P. G. & Brodsky, J. L. How early studies on secreted and membrane protein quality control gave rise to the ER associated degradation (ERAD) pathway: the early history of ERAD. *Biochim. Biophys. Acta* **1833,** 2447–2457 (2013).

193. Qi, L., Tsai, B. & Arvan, P. New Insights into the Physiological Role of Endoplasmic Reticulum-Associated Degradation. *Trends Cell Biol.* **27,** 430–440 (2017).

194. Hegde, R. S. & Ploegh, H. L. Quality and quantity control at the endoplasmic reticulum. *Curr. Opin. Cell Biol.* **22,** 437–446 (2010).

195. Song, B.-L., Sever, N. & DeBose-Boyd, R. A. Gp78, a membrane-anchored ubiquitin ligase, associates with Insig-1 and couples sterol-regulated ubiquitination to degradation of HMG CoA reductase. *Mol. Cell* **19,** 829–840 (2005).

196. Gill, S., Stevenson, J., Kristiana, I. & Brown, A. J. Cholesterol-dependent degradation of squalene monooxygenase, a control point in cholesterol synthesis beyond HMG-CoA reductase. *Cell Metab.* **13,** 260–273 (2011).

197. Foresti, O., Ruggiano, A., Hannibal-Bach, H. K., Ejsing, C. S. & Carvalho, P. Sterol homeostasis requires regulated degradation of squalene monooxygenase by the ubiquitin ligase Doa10/Teb4. *Elife* **2,** e00953 (2013).

198. Jeon, Y. J. *et al.* Regulation of glutamine carrier proteins by RNF5 determines breast cancer response to ER stress-inducing chemotherapies. *Cancer Cell* **27,** 354–369 (2015).

199. Ji, Y. *et al.* The Sel1L-Hrd1 Endoplasmic Reticulum-Associated Degradation Complex Manages a Key Checkpoint in B Cell Development. *Cell Rep.* **16,** 2630–2640 (2016).

200. To, M. *et al.* Lipid disequilibrium disrupts ER proteostasis by impairing ERAD substrate glycan trimming and dislocation. *Mol. Biol. Cell* **28,** 270–284 (2017).

201. Tsai, Y. C. *et al.* The ubiquitin ligase gp78 promotes sarcoma metastasis by targeting KAI1 for degradation. *Nat. Med.* **13,** 1504–1509 (2007).

202. Fisher, E., Lake, E. & McLeod, R. S. Apolipoprotein B100 quality control and the regulation of hepatic very low density lipoprotein secretion. *J Biomed Res* **28,** 178–193 (2014).

203. Lee, J. N., Gong, Y., Zhang, X. & Ye, J. Proteasomal degradation of ubiquitinated Insig proteins is determined by serine residues flanking ubiquitinated lysines. *Proc. Natl. Acad. Sci. USA* **103,** 4958–4963 (2006).

204. Liu, T.-F. *et al.* Ablation of gp78 in liver improves hyperlipidemia and insulin resistance by inhibiting SREBP to decrease lipid biosynthesis. *Cell Metab.* **16,** 213–225 (2012).

205. Shi, G. *et al.* ER-associated degradation is required for vasopressin prohormone processing and systemic water homeostasis. *J. Clin. Invest.* **127,** 3897–3912 (2017).

206. Bagola, K., Mehnert, M., Jarosch, E. & Sommer, T. Protein dislocation from the ER. *Biochim. Biophys. Acta* **1808,** 925–936 (2011).

207. Bersuker, K. *et al.* A Proximity Labeling Strategy Provides Insights into the Composition and Dynamics of Lipid Droplet Proteomes. *Dev. Cell* **44,** 97–112.e7 (2018).

208. Gendron, J. M. *et al.* Using the Ubiquitin-modified Proteome to Monitor Distinct and Spatially Restricted Protein Homeostasis Dysfunction. *Mol. Cell Proteomics* **15,** 2576–2593 (2016).

209. Kim, W. *et al.* Systematic and quantitative assessment of the ubiquitin-modified proteome. *Mol. Cell* **44,** 325–340 (2011).

210. Ginsberg, H. N. & Fisher, E. A. The ever-expanding role of degradation in the regulation of apolipoprotein B metabolism. *J. Lipid Res.* **50 Suppl,** S162–6 (2009).

211. Prabhu, A. V., Luu, W., Sharpe, L. J. & Brown, A. J. Cholesterol-mediated Degradation of 7-Dehydrocholesterol Reductase Switches the Balance from Cholesterol to Vitamin D Synthesis. *J. Biol. Chem.* **291,** 8363–8373 (2016).

212. Wojcikiewicz, R. J. H., Pearce, M. M. P., Sliter, D. A. & Wang, Y. When worlds collide: IP(3) receptors and the ERAD pathway. *Cell Calcium* **46,** 147–153 (2009).

213. Jo, Y. & Debose-Boyd, R. A. Control of cholesterol synthesis through regulated ER-associated degradation of HMG CoA reductase. *Crit Rev Biochem Mol Biol* **45,** 185–198 (2010).

214. Ntambi, J. M. & Miyazaki, M. Recent insights into stearoyl-CoA desaturase-1. *Curr Opin Lipidol* **14,** 255–261 (2003).

215. Kato, H., Sakaki, K. & Mihara, K. Ubiquitin-proteasome-dependent degradation of mammalian ER stearoyl-CoA desaturase. *J. Cell Sci.* **119,** 2342–2353 (2006).

216. Mziaut, H., Korza, G. & Ozols, J. The N terminus of microsomal Δ9 stearoyl-CoA desaturase contains the sequence determinant for its rapid degradation. *Proc. Natl. Acad. Sci. USA* **97,** 8883–8888 (2000).

217. Braun, S., Matuschewski, K., Rape, M., Thoms, S. & Jentsch, S. Role of the ubiquitin-selective CDC48(UFD1/NPL4 )chaperone (segregase) in ERAD of OLE1 and other substrates. *EMBO J.* **21,** 615–621 (2002).

218. Grove, D. E., Fan, C.-Y., Ren, H. Y. & Cyr, D. M. The endoplasmic reticulum-associated Hsp40 DNAJB12 and Hsc70 cooperate to facilitate RMA1 E3-dependent degradation of nascent CFTRDeltaF508. *Mol. Biol. Cell* **22,** 301–314 (2011).

219. Kuang, E. *et al.* Regulation of ATG4B stability by RNF5 limits basal levels of autophagy and influences susceptibility to bacterial infection. *PLoS Genet.* **8,** e1003007 (2012).

220. Zhong, B. *et al.* The E3 ubiquitin ligase RNF5 targets virus-induced signaling adaptor for ubiquitination and degradation. *J. Immunol.* **184,** 6249–6255 (2010).

221. Matsuda, N., Suzuki, T., Tanaka, K. & Nakano, A. Rma1, a novel type of RING finger protein conserved from Arabidopsis to human, is a membrane-bound ubiquitin ligase. *J. Cell Sci.* **114,** 1949–1957 (2001).

222. Kirkpatrick, D. S., Weldon, S. F., Tsaprailis, G., Liebler, D. C. & Gandolfi, A. J. Proteomic identification of ubiquitinated proteins from human cells expressing His-tagged ubiquitin. *Proteomics* **5,** 2104–2111 (2005).

223. Peng, J. *et al.* A proteomics approach to understanding protein ubiquitination. *Nat. Biotechnol.* **21,** 921–926 (2003).

224. Hitchcock, A. L., Auld, K., Gygi, S. P. & Silver, P. A. A subset of membrane-associated proteins is ubiquitinated in response to mutations in the endoplasmic reticulum degradation machinery. *Proc. Natl. Acad. Sci. USA* **100,** 12735–12740 (2003).

225. Tan, M. K., Lim, H. J. & Harper, J. W. SCF(FBXO22) regulates histone H3 lysine 9 and 36 methylation levels by targeting histone demethylase KDM4A for ubiquitin-mediated proteasomal degradation. *Mol. Cell. Biol.* **31,** 3687–3699 (2011).

226. Gao, D. *et al.* mTOR drives its own activation via SCF(βTrCP)-dependent degradation of the mTOR inhibitor DEPTOR. *Mol. Cell* **44,** 290–303 (2011).

227. Harper, J. W. & Tan, M. K. Understanding cullin-RING E3 biology through proteomics-based substrate identification. *Mol. Cell Proteomics* **11,** 1541–1550 (2012).

228. Tan, M. K., Lim, H. J., Bennett, E. J., Shi, Y. & Harper, J. W. Parallel SCF adaptor capture proteomics reveals a role for SCFFBXL17 in NRF2 activation via BACH1 repressor turnover. *Mol. Cell* **52,** 9–24 (2013).

229. Mark, K. G., Loveless, T. B. & Toczyski, D. P. Isolation of ubiquitinated substrates by tandem affinity purification of E3 ligase-polyubiquitin-binding domain fusions (ligase traps). *Nat. Protoc.* **11,** 291–301 (2016).

230. Mark, K. G., Simonetta, M., Maiolica, A., Seller, C. A. & Toczyski, D. P. Ubiquitin ligase trapping identifies an SCF(Saf1) pathway targeting unprocessed vacuolar/lysosomal proteins. *Mol. Cell* **53,** 148–161 (2014).

231. O'Connor, H. F. *et al.* Ubiquitin-Activated Interaction Traps (UBAITs) identify E3 ligase binding partners. *EMBO Rep.* (2015). doi:10.15252/embr.201540620

232. Foresti, O., Rodriguez-Vaello, V., Funaya, C. & Carvalho, P. Quality control of inner nuclear membrane proteins by the Asi complex. *Science* **346,** 751–755 (2014).

233. Yen, H. C. & Elledge, S. J. Identification of SCF ubiquitin ligase substrates by global protein stability profiling. *Science* **322,** 923–929 (2008).

234. Yen, H. C., Xu, Q., Chou, D. M., Zhao, Z. & Elledge, S. J. Global protein stability profiling in mammalian cells. *Science* **322,** 918–923 (2008).

235. Ordureau, A., Münch, C. & Harper, J. W. Quantifying ubiquitin signaling. *Mol. Cell* **58,** 660–676 (2015).

236. Na, C. H. *et al.* Synaptic protein ubiquitination in rat brain revealed by antibody-based ubiquitome analysis. *J. Proteome Res.* **11,** 4722–4732 (2012).

237. Udeshi, N. D. *et al.* Methods for quantification of in vivo changes in protein ubiquitination following proteasome and deubiquitinase inhibition. *Mol. Cell Proteomics* **11,** 148–159 (2012).

238. Shimizu, Y., Okuda-Shimizu, Y. & Hendershot, L. M. Ubiquitylation of an ERAD substrate occurs on multiple types of amino acids. *Mol. Cell* **40,** 917–926 (2010).

239. Rape, M. *et al.* Mobilization of processed, membrane-tethered SPT23 transcription factor by CDC48(UFD1/NPL4), a ubiquitin-selective chaperone. *Cell* **107,** 667–677 (2001).

240. Hoppe, T. *et al.* Activation of a membrane-bound transcription factor by regulated ubiquitin/proteasome-dependent processing. *Cell* **102,** 577–586 (2000).

241. Ramanathan, H. N. & Ye, Y. The p97 ATPase associates with EEA1 to regulate the size of early endosomes. *Cell Res.* **22,** 346–359 (2012).

242. Cox, J. & Mann, M. MaxQuant enables high peptide identification rates, individualized p.p.b.-range mass accuracies and proteome-wide protein quantification. *Nat. Biotechnol.* **26,** 1367–1372 (2008).

243. Huang, D. W., Sherman, B. T. & Lempicki, R. A. Systematic and integrative analysis of large gene lists using DAVID bioinformatics resources. *Nat. Protoc.* **4,** 44–57 (2009).

244. Supek, F., Bošnjak, M., Škunca, N. & Šmuc, T. REVIGO summarizes and visualizes long lists of gene ontology terms. *PLoS One* **6,** e21800 (2011).

245. Shannon, P. *et al.* Cytoscape: a software environment for integrated models of biomolecular interaction networks. *Genome Res.* **13,** 2498–2504 (2003).

246. Fun, X. H. & Thibault, G. Lipid bilayer stress and proteotoxic stress-induced unfolded protein response deploy divergent transcriptional and non-transcriptional programmes. *Biochimica et Biophysica Acta (BBA)-Molecular and …* (2020).

247. Qian, H. *et al.* HDAC6-mediated acetylation of lipid droplet-binding protein CIDEC regulates fat-induced lipid storage. *J. Clin. Invest.* **127,** 1353–1369 (2017).

248. Kozlitina, J. *et al.* Exome-wide association study identifies a TM6SF2 variant that confers susceptibility to nonalcoholic fatty liver disease. *Nat. Genet.* **46,** 352–356 (2014).

249. Pappireddi, N., Martin, L. & Wühr, M. A review on quantitative multiplexed proteomics. *Chembiochem* **20,** 1210–1224 (2019).

250. Christiano, R., Kabatnik, S., Mejhert, N., Farese, R. V. & Walther, T. C. A systematic protein turnover map for decoding protein degradation. *BioRxiv* (2020). doi:10.1101/2020.03.09.983734

251. Akimov, V. *et al.* UbiSite approach for comprehensive mapping of lysine and N-terminal ubiquitination sites. *Nat. Struct. Mol. Biol.* **25,** 631–640 (2018).

## Appendix

Supplemental Table 2-S1. High confidence Hrd1 interacting proteins.

Supplemental Table 2-S2. SILAC proteomic analysis of Hrd1 interacting proteins.

Supplemental Table 2-S3. Metabolomic profiling of triacsin C treated cells.

Supplemental Table 3-S1. SILAC ratio of diGly peptides.

Supplemental Table 3-S2. GO analysis of cellular component (CC) and biological process (BP).

Supplemental Table 3-S3. Predicted subcellular localizations of candidate ERAD substrates.

**Supplemental Table 2-S1. High confidence Hrd1 interacting proteins.**

| UniProt Protein Name | Uniprot ID | Ratio M/L (Log2) | Ratio H/M (Log2) | Ratio H/L (Log2) | Localization | Predicted Topology | Domains | Brief protein description |
|---|---|---|---|---|---|---|---|---|
| E3 ubiquitin-protein ligase synoviolin | Q86TM6 | 4.629 | -0.060 | 4.554 | ER | Polytopic TM | RING | E3 ligase involved in ERAD |
| Protein sel-1 homolog 1 | Q9UBV2 | 4.505 | 0.171 | 4.447 | ER | Single-pass TM | TPR repeats | Luminal adaptor for the ERAD E3 ligase Hrd1 |
| Protein FAM8A1 | Q9UBU6 | 4.460 | 0.277 | 4.677 | ER | Polytopic TM | | Regulator of the ERAD E3 ligase Hrd1 |
| Erlin-2 | O94905 | 4.448 | 0.195 | 4.637 | ER | Polytopic TM | SPFH-like | ERAD substrate-specific recognition factor |
| Protein OS-9 | Q13438 | 4.254 | 0.044 | 4.284 | ER | Luminal, soluble | MRH | Lectin involved in substrate recognition and delivery to the Hrd1 dislocation complex |
| Endoplasmic reticulum lectin 1 | Q96DZ1 | 4.200 | 0.154 | 4.277 | ER | Luminal, soluble | MRH | Lectin involved in substrate recognition and delivery to the Hrd1 dislocation complex |
| Calnexin | P27824 | 3.254 | 0.019 | 3.316 | ER | Single-pass TM | | Chaperone involved in the folding of glycosylated secretory proteins |
| Dolichyl-diphosphooligosaccharide--protein glycosyltransferase subunit 1 | P04843 | 2.569 | 0.104 | 2.755 | ER | | | Subunit of the N-oligosaccharyl transferase (OST) complex, which mediates the transfer of a high mannose oligosaccharide to nascent secretory proteins |
| Transitional endoplasmic reticulum ATPase | P55072 | 2.417 | 0.385 | 2.778 | ER, Cyto, Nuc | Cyto, soluble | AAA+ ATPase | ATPase involved in the ubiquitin-dependent extraction of proteins for degradation and ubiquitin-dependent dissociation of protein complexes |

| | | | | | | | | |
|---|---|---|---|---|---|---|---|---|
| Membrane-associated progesterone receptor component 1 | O00264 | 2.215 | 0.069 | 2.504 | ER | | | Putatitive receptor for progesterone |
| Endoplasmin | P14625 | 1.799 | 0.132 | 1.937 | ER | Luminal, soluble | | Chaperone involved in the folding of a specific set of secretory proteins |
| Protein disulfide-isomerase | P07237 | 1.397 | 0.235 | 1.495 | ER | Luminal, soluble | | Disulfide isomerase involved in secretory protein folding and maturation |
| Emerin | P50402 | 1.371 | -0.452 | 0.855 | Nuc | | | |
| Serpin H1 | P50454 | 1.359 | -0.667 | 1.090 | ER | Luminal, soluble | | Chaperone involved in collagen folding and maturation |
| Ubiquitin-60S ribosomal protein L40 | P62987 | 1.063 | 0.441 | 1.275 | ER, Cyto, Nuc | Cyto, soluble | | Posttranslational modification implicated in protein degradation and regulation |

**Supplemental Table 2-S2. SILAC proteomic analysis of Hrd1 interacting proteins.**

| Uniprot ID | Gene Symbol | Ratio M/L (Log2) | Ratio H/M (Log2) | Ratio H/L (Log2) |
|---|---|---|---|---|
| Q86TM6 | SYVN1 | 4.63 | -0.06 | 4.55 |
| Q9UBV2 | SE1L1 | 4.50 | 0.17 | 4.45 |
| Q9UBU6 | FA8A1 | 4.46 | 0.28 | 4.68 |
| O94905 | ERLN2 | 4.45 | 0.19 | 4.64 |
| Q13438 | OS9 | 4.25 | 0.04 | 4.28 |
| Q96DZ1 | ERLEC | 4.20 | 0.15 | 4.28 |
| P27824 | CALX | 3.25 | 0.02 | 3.32 |
| P04843 | RPN1 | 2.57 | 0.10 | 2.75 |
| P55072 | TERA | 2.42 | 0.39 | 2.78 |
| O00264 | PGRC1 | 2.22 | 0.07 | 2.50 |
| P14625 | ENPL | 1.80 | 0.13 | 1.94 |
| P07237 | PDIA1 | 1.40 | 0.23 | 1.49 |
| P50402 | EMD | 1.37 | -0.45 | 0.86 |
| P50454 | SERPH | 1.36 | -0.67 | 1.09 |
| P62987 | RL40 | 1.06 | 0.44 | 1.28 |
| P05141 | ADT2 | 1.00 | -0.87 | 0.23 |
| P15924 | DESP | 0.82 | 0.42 | 1.15 |
| P25705 | ATPA | 0.81 | -0.18 | 0.52 |
| P09874 | PARP1 | 0.78 | -0.74 | 0.15 |
| P23284 | PPIB | 0.78 | -0.17 | 0.57 |
| P11021 | GRP78 | 0.69 | -0.11 | 0.50 |
| Q5T0Z8 | CF132 | 0.59 | 0.11 | 0.73 |
| P62826 | RAN | 0.59 | 0.17 | 0.84 |
| P07900 | HS90A | 0.58 | -0.08 | 0.21 |
| P14618 | KPYM | 0.54 | -0.23 | 0.51 |
| P06733 | ENOA | 0.52 | 0.07 | 0.71 |
| Q92616 | GCN1L | 0.46 | -0.63 | -0.05 |
| P60842 | IF4A1 | 0.43 | -0.41 | 0.07 |
| Q8NC51 | SERBP1 | 0.39 | -0.25 | 0.09 |
| P62258 | 1433E | 0.39 | -0.35 | 0.25 |
| P19105 | ML12A | 0.39 | -0.39 | -0.02 |
| P13489 | RINI | 0.39 | 0.22 | 0.67 |
| P78371 | TCPB | 0.38 | -0.41 | -0.12 |
| P62847 | RS24 | 0.37 | 0.25 | 0.60 |
| Q06830 | PRDX1 | 0.32 | 0.00 | 0.21 |
| P08107 | HSP71 | 0.31 | 0.02 | 0.29 |

| | | | | |
|---|---|---|---|---|
| P39019 | RS19 | 0.28 | -0.27 | -0.10 |
| P08238 | HS90B | 0.27 | -0.17 | -0.17 |
| P42766 | RL35 | 0.27 | -0.07 | 0.08 |
| P50914 | RL14 | 0.26 | 0.09 | 0.24 |
| P63261 | ACTG | 0.22 | 0.02 | 0.15 |
| P36578 | RL4 | 0.22 | -0.13 | -0.18 |
| P62753 | RS6 | 0.19 | -0.34 | -0.22 |
| P62158 | CALM | 0.19 | 0.09 | 0.15 |
| P61513 | RL37A | 0.18 | -0.18 | -0.11 |
| P62280 | RS11 | 0.17 | 0.05 | 0.19 |
| P61978 | HNRPK | 0.17 | -0.22 | 0.16 |
| P29692 | EF1D | 0.16 | -0.33 | -0.05 |
| P46776 | RL27A | 0.16 | 0.01 | -0.04 |
| P08670 | VIME | 0.16 | -0.07 | 0.01 |
| P46783 | RS10 | 0.15 | -0.20 | -0.05 |
| P50990 | TCPQ | 0.14 | -0.36 | -0.03 |
| O43175 | SERA | 0.14 | -0.28 | -0.17 |
| P38646 | GRP75 | 0.13 | 0.09 | 0.35 |
| P32969 | RL9 | 0.12 | 0.27 | 0.39 |
| P84098 | RL19 | 0.12 | -0.21 | -0.08 |
| P48643 | TCPE | 0.12 | -0.20 | -0.08 |
| Q86V81 | THOC4 | 0.10 | 0.55 | 0.69 |
| P18124 | RL7 | 0.09 | -0.14 | -0.12 |
| Q9NVI7 | ATD3A | 0.09 | -0.31 | -0.34 |
| P26641 | EF1G | 0.09 | -0.51 | -0.31 |
| P18077 | RL35A | 0.08 | -0.09 | -0.08 |
| P40429 | RL13A | 0.07 | 0.05 | 0.24 |
| P62081 | RS7 | 0.07 | -0.12 | 0.03 |
| P67936 | TPM4 | 0.06 | 0.15 | 0.22 |
| Q9BQE3 | TBA1C | 0.06 | -0.29 | -0.34 |
| P46778 | RL21 | 0.05 | 0.04 | -0.08 |
| P23528 | COF1 | 0.04 | 0.22 | 0.47 |
| P26373 | RL13 | 0.03 | -0.10 | -0.06 |
| P39023 | RL3 | 0.03 | -0.12 | -0.06 |
| P62701 | RS4X | 0.02 | 0.07 | 0.01 |
| P62277 | RS13 | 0.01 | -0.14 | -0.07 |
| P61247 | RS3A | 0.00 | -0.06 | 0.05 |
| P22061 | PIMT | 0.00 | 0.08 | 0.10 |
| P0CW22 | RS17L | -0.01 | -0.35 | -0.17 |

| | | | | |
|---|---|---|---|---|
| Q14498 | RBM39 | -0.01 | 0.24 | 0.27 |
| P16949 | STMN1 | -0.02 | -0.35 | -0.20 |
| P06748 | NPM | -0.02 | -0.10 | -0.06 |
| Q00839 | HNRPU | -0.02 | -0.27 | -0.31 |
| P18621 | RL17 | -0.04 | -0.39 | -0.26 |
| P62269 | RS18 | -0.05 | 0.28 | 0.34 |
| P62249 | RS16 | -0.05 | -0.17 | -0.10 |
| P21796 | VDAC1 | -0.06 | -0.03 | 0.15 |
| P23396 | RS3 | -0.06 | -0.10 | -0.27 |
| P62917 | RL8 | -0.07 | -0.12 | 0.08 |
| Q02543 | RL18A | -0.07 | -0.22 | -0.18 |
| Q02878 | RL6 | -0.08 | -0.09 | -0.16 |
| P45880 | VDAC2 | -0.09 | -0.02 | -0.10 |
| P62241 | RS8 | -0.09 | -0.16 | -0.04 |
| P61313 | RL15 | -0.09 | 0.11 | 0.14 |
| P62937 | PPIA | -0.10 | 0.60 | 0.47 |
| P62266 | RS23 | -0.11 | -0.31 | -0.32 |
| P11142 | HSP7C | -0.12 | 0.18 | -0.11 |
| P61254 | RL26 | -0.12 | -0.26 | -0.64 |
| Q07020 | RL18 | -0.12 | -0.18 | -0.28 |
| Q5VTE0 | EF1A3 | -0.14 | -0.02 | -0.38 |
| O43390 | HNRPR | -0.15 | -0.23 | -0.46 |
| Q9Y5A9 | YTHD2 | -0.15 | 0.26 | -0.15 |
| P49915 | GUAA | -0.16 | -0.06 | -0.10 |
| P62899 | RL31 | -0.16 | -0.04 | -0.04 |
| P60660 | MYL6 | -0.18 | 0.48 | 0.09 |
| P61353 | RL27 | -0.18 | -0.05 | -0.45 |
| P35580 | MYH10 | -0.18 | 0.65 | 0.47 |
| P09651 | ROA1 | -0.19 | -0.12 | -0.46 |
| P55060 | XPO2 | -0.21 | -0.19 | -0.49 |
| P60866 | RS20 | -0.22 | -0.21 | -0.42 |
| P07437 | TBB5 | -0.23 | -0.22 | -0.44 |
| P26583 | HMGB2 | -0.23 | 0.00 | -0.40 |
| P25398 | RS12 | -0.23 | -0.67 | -0.77 |
| Q8NHW5 | RLA0L | -0.24 | 0.29 | 0.11 |
| P62906 | RL10A | -0.24 | 0.15 | -0.21 |
| P30050 | RL12 | -0.25 | -0.47 | -0.36 |
| P62424 | RL7A | -0.25 | -0.14 | -0.34 |
| P19338 | NUCL | -0.26 | 0.00 | -0.30 |

| | | | | |
|---|---|---|---|---|
| P23246 | SFPQ | -0.26 | -0.36 | -0.63 |
| P46781 | RS9 | -0.27 | 0.01 | -0.08 |
| P11940 | PABP1 | -0.29 | -0.31 | -0.59 |
| P62854 | RS26 | -0.29 | -0.03 | -0.29 |
| Q14103 | HNRPD | -0.32 | 0.11 | -0.25 |
| Q92522 | H1X | -0.38 | -0.61 | -1.01 |
| Q99880 | H2B1L | -0.39 | 0.34 | -0.12 |
| P16403 | H12 | -0.39 | -0.26 | -0.80 |
| P35579 | MYH9 | -0.41 | 0.47 | -0.01 |
| Q15233 | NONO | -0.47 | -0.42 | -1.09 |
| Q14257 | RCN2 | -0.49 | 0.22 | -0.39 |
| P52272 | HNRPM | -0.51 | 1.22 | 0.66 |
| P11586 | C1TC | -0.51 | -0.48 | -1.02 |
| P49411 | EFTU | -0.54 | -0.22 | -0.68 |
| P62750 | RL23A | -0.54 | -0.08 | -0.75 |
| P17844 | DDX5 | -0.54 | -0.38 | -0.89 |
| Q96AE4 | FUBP1 | -0.59 | -0.19 | -0.86 |
| Q92841 | DDX17 | -0.63 | -0.55 | -1.08 |
| P35232 | PHB | -0.64 | 0.40 | -0.34 |
| Q99623 | PHB2 | -0.67 | 0.47 | -0.27 |
| Q9BUJ2 | HNRL1 | -0.68 | 1.46 | 0.88 |
| P22626 | ROA2 | -0.71 | -0.41 | -0.78 |
| P10809 | CH60 | -0.76 | -0.02 | -0.81 |
| P20073 | ANXA7 | -0.81 | -0.11 | -0.80 |
| P52597 | HNRPF | -0.83 | -0.14 | -1.01 |
| Q15365 | PCBP1 | -0.86 | -0.32 | -1.09 |
| P31943 | HNRH1 | -1.21 | 0.00 | -1.24 |
| Q92945 | FUBP2 | -1.37 | 0.21 | -1.02 |

**Supplemental Table 2-S3. Metabolomic profiling of triacsin C treated cells.**

| Metabolite | DMSO average | DMSO SEM | triacsin C average | triacsin C SEM | p-value against DMSO |
|---|---|---|---|---|---|
| C16:0 NAE | 4.26 | 1.35 | 2.36 | 1.42 | 0.37 |
| sphingosine | 0.72 | 0.05 | 0.64 | 0.06 | 0.32 |
| sphinganine | 0.76 | 0.05 | 0.69 | 0.02 | 0.20 |
| C16:0e MAGe | 0.89 | 0.07 | 0.49 | 0.05 | 0.00 |
| C18:1 NAE | 1.27 | 0.14 | 1.91 | 0.13 | 0.01 |
| C18:0 NAE | 4.27 | 1.18 | 2.45 | 1.61 | 0.38 |
| C16:0 MAG | 1.24 | 0.10 | 0.87 | 0.07 | 0.02 |
| C18:0p MAGp | 0.91 | 0.07 | 0.56 | 0.06 | 0.01 |
| C18:0e MAGe | 0.89 | 0.05 | 0.46 | 0.04 | 0.00 |
| C18:2 MAG | 0.83 | 0.07 | 1.08 | 0.06 | 0.03 |
| C18:1 MAG | 1.07 | 0.07 | 1.01 | 0.06 | 0.51 |
| C16:0e/C2:0 MAGe | 1.24 | 0.08 | 1.08 | 0.20 | 0.47 |
| C18:0 MAG | 1.16 | 0.08 | 0.95 | 0.16 | 0.27 |
| C20:4 MAG | 0.91 | 0.10 | 1.21 | 0.05 | 0.05 |
| C18:1e/C2:0 MAGe | 0.85 | 0.11 | 1.26 | 0.08 | 0.02 |
| C18:0e/C2:0 MAGe | 0.80 | 0.08 | 0.77 | 0.04 | 0.77 |
| C16:0 AC | 1.15 | 0.22 | 0.30 | 0.04 | 0.01 |
| Pregninolone sulfate | 0.89 | 0.04 | 0.95 | 0.06 | 0.41 |
| C18:0 AC | 1.58 | 0.59 | 0.64 | 0.14 | 0.21 |
| C16:0e LPEe | 1.22 | 0.08 | 2.11 | 0.18 | 0.00 |
| C16:0 LPE | 1.50 | 0.07 | 5.18 | 0.45 | 0.00 |
| C18:0p LPEp | 1.28 | 0.10 | 1.75 | 0.22 | 0.07 |
| C18:0e LPEe | 1.30 | 0.08 | 2.16 | 0.24 | 0.01 |
| C18:1 LPE | 1.45 | 0.07 | 3.03 | 0.31 | 0.00 |
| C18:0 LPE | 1.36 | 0.08 | 5.26 | 0.50 | 0.00 |
| C16:0e LPCe | 1.38 | 0.08 | 1.07 | 0.10 | 0.04 |
| C16:0 LPC | 1.48 | 0.11 | 2.58 | 0.22 | 0.00 |
| C20:4 LPE | 1.39 | 0.08 | 1.25 | 0.06 | 0.24 |
| C18:0e LPCe | 1.40 | 0.12 | 2.61 | 0.23 | 0.00 |
| C18:0e LPSe | 0.96 | 0.06 | 0.99 | 0.09 | 0.75 |
| C18:1 LPC | 1.20 | 0.07 | 1.11 | 0.11 | 0.50 |
| C18:0 LPC | 1.28 | 0.06 | 1.04 | 0.12 | 0.08 |
| C18:1 LPS | 1.54 | 0.17 | 0.95 | 0.09 | 0.02 |
| C18:0 LPS | 1.42 | 0.09 | 1.48 | 0.21 | 0.77 |

| | | | | | |
|---|---|---|---|---|---|
| C16:0 Ceramide | 0.89 | 0.02 | 2.04 | 0.13 | 0.00 |
| C20:4 LPC | 1.46 | 0.06 | 2.38 | 0.21 | 0.00 |
| C20:4 LPS | 0.89 | 0.13 | 1.02 | 0.14 | 0.53 |
| C18:1p LPCp | 1.33 | 0.11 | 2.93 | 0.37 | 0.00 |
| C20:0 LPC | 1.14 | 0.39 | 2.38 | 0.11 | 0.03 |
| C18:1 Ceramide | 0.85 | 0.07 | 1.18 | 0.21 | 0.15 |
| C18:0 Ceramide | 1.00 | 0.04 | 1.65 | 0.16 | 0.00 |
| C20:4 Ceramide | 1.09 | 0.12 | 0.99 | 0.11 | 0.60 |
| C16:0/C18:1 DAG | 0.98 | 0.05 | 0.57 | 0.05 | 0.00 |
| C18:0/C18:1 DAG | 1.05 | 0.04 | 1.30 | 0.06 | 0.01 |
| C18:0/C20:4 DAG | 0.84 | 0.06 | 0.86 | 0.09 | 0.86 |
| C16:0e/C18:1 PEe | 0.76 | 0.05 | 1.66 | 0.21 | 0.00 |
| C16:0 SM | 0.91 | 0.03 | 0.61 | 0.04 | 0.00 |
| C16:0/C18:1 PE | 0.85 | 0.05 | 1.51 | 0.10 | 0.00 |
| C16:0p/C20:4 PEp | 0.84 | 0.04 | 1.45 | 0.06 | 0.00 |
| C16:0e/C20:4 PEe | 0.83 | 0.06 | 1.70 | 0.21 | 0.00 |
| C18:1 SM | 0.83 | 0.03 | 0.77 | 0.04 | 0.20 |
| C18:0 SM | 0.87 | 0.03 | 0.72 | 0.04 | 0.01 |
| C18:0e/C18:1 PEe | 0.82 | 0.02 | 1.00 | 0.08 | 0.04 |
| C16:0/C20:4 PE | 0.73 | 0.06 | 1.66 | 0.18 | 0.00 |
| C18:0/C18:1 PE | 0.96 | 0.04 | 1.68 | 0.07 | 0.00 |
| C16:0e/C18:1 PCe | 0.91 | 0.03 | 0.80 | 0.04 | 0.07 |
| C16:0e/C18:1 PSe | 0.88 | 0.06 | 1.30 | 0.07 | 0.00 |
| C18:0p/C20:4 PEp | 0.91 | 0.04 | 1.41 | 0.08 | 0.00 |
| C18:0e/C20:4 PEe | 0.94 | 0.03 | 1.32 | 0.10 | 0.01 |
| C20:4 SM | 0.89 | 0.03 | 0.85 | 0.04 | 0.43 |
| C16:0/C18:1 PC | 0.91 | 0.04 | 1.20 | 0.07 | 0.01 |
| C16:0/C18:1 PS | 0.89 | 0.03 | 1.65 | 0.11 | 0.00 |
| C16:0p/C20:4 PCp | 0.79 | 0.03 | 1.08 | 0.03 | 0.00 |
| C18:0/C20:4 PE | 0.80 | 0.05 | 2.03 | 0.15 | 0.00 |
| C16:0e/C20:4 PCe | 0.92 | 0.04 | 1.20 | 0.07 | 0.01 |
| C16:0/C20:4 PG | 0.84 | 0.07 | 1.10 | 0.07 | 0.04 |
| C18:0e/C18:1 PCe | 0.92 | 0.03 | 0.69 | 0.03 | 0.00 |
| C18:0e/C18:1 PSe | 0.97 | 0.05 | 1.26 | 0.07 | 0.01 |
| C16:0/C20:4 PC | 0.92 | 0.03 | 2.09 | 0.08 | 0.00 |
| C16:0/C20:4 PS | 0.99 | 0.04 | 2.98 | 0.15 | 0.00 |
| C18:0/C18:1 PC | 0.94 | 0.04 | 1.73 | 0.06 | 0.00 |
| C18:0/C18:1 PS | 0.93 | 0.05 | 1.92 | 0.15 | 0.00 |

| | | | | | |
|---|---|---|---|---|---|
| C18:0p/C20:4 PCp | 0.92 | 0.04 | 1.18 | 0.07 | 0.01 |
| C18:0e/C20:4 PCe | 0.92 | 0.02 | 0.87 | 0.04 | 0.35 |
| C18:0e/C20:4 PSe | 1.06 | 0.14 | 2.01 | 0.31 | 0.02 |
| C18:0/C20:4 PG | 1.07 | 0.07 | 1.08 | 0.09 | 0.96 |
| C18:0/C20:4 PC | 0.95 | 0.04 | 2.00 | 0.09 | 0.00 |
| C18:0/C20:4 PS | 0.99 | 0.05 | 4.06 | 0.27 | 0.00 |
| C16:0/C16:0/C16:0 TAG | 1.20 | 0.15 | 0.57 | 0.04 | 0.01 |
| C16:0/C18:1/C16:0 TAG | 0.94 | 0.03 | 0.40 | 0.02 | 0.00 |
| C16:0/C20:4/C16:0 TAG | 0.81 | 0.06 | 0.85 | 0.04 | 0.63 |
| C18:0/C18:1/C18:0 TAG | 0.96 | 0.04 | 0.67 | 0.05 | 0.00 |
| C18:0/C18:0/C18:0 TAG | 1.57 | 0.20 | 1.58 | 0.24 | 0.96 |
| C18:0/C20:4/C18:0 TAG | 0.86 | 0.04 | 0.54 | 0.03 | 0.00 |
| cholesterol | 0.69 | 0.08 | 0.78 | 0.09 | 0.43 |
| cholesteryl esters | 0.83 | 0.04 | 0.91 | 0.06 | 0.32 |
| C16:0 FFA | 1.04 | 0.05 | 1.13 | 0.05 | 0.26 |
| C18:1 FFA | 1.00 | 0.02 | 1.03 | 0.07 | 0.72 |
| C18:0 FFA | 1.03 | 0.04 | 0.93 | 0.08 | 0.34 |
| phytanic acid | 1.32 | 0.33 | 1.04 | 0.33 | 0.58 |
| C22:6 FFA | 1.29 | 0.30 | 1.04 | 0.29 | 0.57 |
| C16:0e LPAe | 0.88 | 0.14 | 1.10 | 0.12 | 0.28 |
| C16:0 LPA | 0.99 | 0.04 | 0.87 | 0.09 | 0.32 |
| C18:1e LPAe | 0.94 | 0.11 | 1.29 | 0.11 | 0.07 |
| C18:0e LPAe | 0.91 | 0.13 | 1.47 | 0.14 | 0.03 |
| C18:1 LPA | 0.99 | 0.04 | 0.96 | 0.08 | 0.78 |
| C18:0 LPA | 1.00 | 0.14 | 2.41 | 0.17 | 0.00 |
| C16:0e LPIe | 0.87 | 0.17 | 0.96 | 0.07 | 0.62 |
| C16:0 LPI | 1.02 | 0.17 | 1.11 | 0.15 | 0.72 |
| C18:0p LPIp | 0.91 | 0.18 | 1.56 | 0.18 | 0.04 |
| C18:1 LPI | 0.99 | 0.16 | 0.77 | 0.09 | 0.25 |
| C18:0 LPI | 1.00 | 0.05 | 1.45 | 0.15 | 0.04 |
| 18:1/C16:0 ceramide-1-phosphate | 1.23 | 0.24 | 0.74 | 0.02 | 0.05 |
| 18:0/C16:0 ceramide-1-phosphate | 0.89 | 0.16 | 0.71 | 0.06 | 0.31 |
| C16:0e/18:1 PAe | 1.11 | 0.13 | 5.26 | 0.37 | 0.00 |
| C16:0/C18:1 PA | 0.93 | 0.12 | 1.20 | 0.07 | 0.09 |
| C18:0e/C18:1 PAe | 0.91 | 0.12 | 1.43 | 0.12 | 0.02 |
| C18:0/C18:1 PA | 0.93 | 0.18 | 1.39 | 0.12 | 0.06 |
| C18:0e/C20:4 PAe | 1.00 | 0.08 | 5.76 | 0.52 | 0.00 |
| C18:0/C20:4 PA | 0.92 | 0.13 | 0.94 | 0.11 | 0.89 |

| | | | | | |
|---|---|---|---|---|---|
| C16:0/C16:0 PI | 1.04 | 0.09 | 0.88 | 0.08 | 0.22 |
| C16:0e/18:1 PIe | 1.18 | 0.19 | 0.80 | 0.03 | 0.06 |
| C16:0/C18:1 PI | 1.15 | 0.17 | 0.58 | 0.07 | 0.01 |
| C16:0e/20:4 PIe | 1.18 | 0.19 | 0.41 | 0.02 | 0.00 |
| C18:0e/C18:1 PIe | 1.18 | 0.20 | 0.61 | 0.04 | 0.02 |
| C16:0/C20:4 PI | 1.05 | 0.08 | 0.43 | 0.05 | 0.00 |
| C18:0/C18:1 PI | 1.33 | 0.34 | 0.57 | 0.02 | 0.04 |
| C18:0e/C20:4 PIe | 1.25 | 0.25 | 0.55 | 0.03 | 0.02 |
| C18:0/C20:4 PI | 1.25 | 0.26 | 0.40 | 0.03 | 0.01 |

**Supplemental Table 3-S1. SILAC ratio of diGly peptides.**

| Uniprot ID | Gene name | Fasta headers | GlyGly (K) Probabilities | MS/MS count | Average ratio (when detected) |
|---|---|---|---|---|---|
| Q15041 | AR6P1 | >sp\|Q15041\|AR6P1_HUMAN ADP-ribosylation factor-like protein 6-interacting protein 1 OS=Homo sapiens GN=ARL6IP1 PE=1 SV=2 | IFGSNK(1)WTTEQQQR | 10 | 17.92 |
| Q92979 | NEP1 | >sp\|Q92979\|NEP1_HUMAN Ribosomal RNA small subunit methyltransferase NEP1 OS=Homo sapiens GN=EMG1 PE=1 SV=4 | LGAGNK(1)IGGR | 1 | 16.32 |
| P04114 | APOB | >sp\|P04114\|APOB_HUMAN Apolipoprotein B-100 OS=Homo sapiens GN=APOB PE=1 SV=2 | K(1)GNVATEISTER | 1 | 13.81 |
| Q9UP95 | S12A4 | >sp\|Q9UP95\|S12A4_HUMAN Solute carrier family 12 member 4 OS=Homo sapiens GN=SLC12A4 PE=1 SV=2;>sp\|Q9UHW9\|S12A6_HUMAN Solute carrier family 12 member 6 OS=Homo sapiens GN=SLC12A6 PE=1 SV=2 | LLQAIAK(1)DNIIPFLR | 1 | 12.64 |
| Q8WWT9 | S13A3 | >sp\|Q8WWT9\|S13A3_HUMAN Solute carrier family 13 member 3 OS=Homo sapiens GN=SLC13A3 PE=1 SV=1 | SLFGQK(1)EVR | 1 | 12.14 |
| Q9H3H5 | GPT | >sp\|Q9H3H5\|GPT_HUMAN UDP-N-acetylglucosamine--dolichyl-phosphate N-acetylglucosaminephosphotransferase OS=Homo sapiens GN=DPAGT1 PE=1 SV=2 | LCGQDLNK(1)TSR | 2 | 11.39 |
| O00767 | ACOD | >sp\|O00767\|ACOD_HUMAN Acyl-CoA desaturase OS=Homo sapiens GN=SCD PE=1 SV=2 | VSK(1)AAILAR | 2 | 10.62 |
| Q9NZS9 | BFAR | >sp\|Q9NZS9\|BFAR_HUMAN Bifunctional apoptosis regulator OS=Homo sapiens GN=BFAR PE=1 SV=1 | SELK(1)TVPQR | 2 | 9.75 |

| | | | | | |
|---|---|---|---|---|---|
| Q9NXW2 | DJB12 | >sp\|Q9NXW2\|DJB12_HUMAN DnaJ homolog subfamily B member 12 OS=Homo sapiens GN=DNAJB12 PE=1 SV=4 | AIGTAYAVLSNPEK(1)R | 2 | 9.47 |
| P04114 | APOB | >sp\|P04114\|APOB_HUMAN Apolipoprotein B-100 OS=Homo sapiens GN=APOB PE=1 SV=2 | DLK(1)VEDIPLAR | 25 | 9.25 |
| Q96BD0 | SO4A1 | >sp\|Q96BD0\|SO4A1_HUMAN Solute carrier organic anion transporter family member 4A1 OS=Homo sapiens GN=SLCO4A1 PE=1 SV=2 | GEASNPDFGK(1)TIR | 1 | 8.49 |
| Q9UPY5 | XCT | >sp\|Q9UPY5\|XCT_HUMAN Cystine/glutamate transporter OS=Homo sapiens GN=SLC7A11 PE=1 SV=1 | IMSEK(1)ITR | 1 | 8.18 |
| Q96QK8 | SIM14 | >sp\|Q96QK8\|SIM14_HUMAN Small integral membrane protein 14 OS=Homo sapiens GN=SMIM14 PE=1 SV=1 | GSSLPGK(1)PTSPHNGQDPPAPPVD | 4 | 8.07 |
| Q70UQ0 | IKIP | >sp\|Q70UQ0\|IKIP_HUMAN Inhibitor of nuclear factor kappa-B kinase-interacting protein OS=Homo sapiens GN=IKBIP PE=1 SV=1 | GAPAAEPGK(1)R | 1 | 7.81 |
| O75915 | PRAF3 | >sp\|O75915\|PRAF3_HUMAN PRA1 family protein 3 OS=Homo sapiens GN=ARL6IP5 PE=1 SV=1 | LTDYISK(0.976)VK(0.024) | 1 | 7.66 |
| O60427 | FADS1 | >sp\|O60427\|FADS1_HUMAN Fatty acid desaturase 1 OS=Homo sapiens GN=FADS1 PE=1 SV=3 | ILSVELGK(0.824)QK(0.176) | 2 | 7.58 |
| P04920 | B3A2 | >sp\|P04920\|B3A2_HUMAN Anion exchange protein 2 OS=Homo sapiens GN=SLC4A2 PE=1 SV=4 | SLAGQSGQGK(1)PR | 1 | 7.53 |
| Q9P0S3 | ORML1 | >sp\|Q9P0S3\|ORML1_HUMAN ORM1-like protein 1 OS=Homo sapiens GN=ORMDL1 PE=1 SV=1;>sp\|Q8N138\|ORML3_HUMAN ORM1-like protein 3 OS=Homo sapiens GN=ORMDL3 PE=1 SV=1 | IFGINK(1)Y | 2 | 7.37 |
| P51572 | BAP31 | >sp\|P51572\|BAP31_HUMAN B-cell receptor-associated protein 31 OS=Homo sapiens GN=BCAP31 PE=1 SV=3 | GAAVDGGK(1)LDVGNAEVK | 1 | 7.34 |

| | | | | | |
|---|---|---|---|---|---|
| Q9Y5U4 | INSI2 | >sp\|Q9Y5U4\|INSI2_HUMAN Insulin-induced gene 2 protein OS=Homo sapiens GN=INSIG2 PE=1 SV=2 | VIAEK(1)SHQE | 4 | 7.27 |
| P0CK96 | S352B | >sp\|P0CK96\|S352B_HUMAN Solute carrier family 35 member E2B OS=Homo sapiens GN=SLC35E2B PE=2 SV=1 | LLSGDK(1)YR | 1 | 6.87 |
| Q6ZVX9 | PAQR9 | >sp\|Q6ZVX9\|PAQR9_HUMAN Progestin and adipoQ receptor family member 9 OS=Homo sapiens GN=PAQR9 PE=2 SV=1 | DPPASAK(1)PLLR | 3 | 6.86 |
| P51572 | BAP31 | >sp\|P51572\|BAP31_HUMAN B-cell receptor-associated protein 31 OS=Homo sapiens GN=BCAP31 PE=1 SV=3 | QSEGLTK(1)EYDR | 1 | 6.76 |
| P50454 | SERPH | >sp\|P50454\|SERPH_HUMAN Serpin H1 OS=Homo sapiens GN=SERPINH1 PE=1 SV=2 | LSPK(1)AATLAER | 1 | 6.38 |
| P04844 | RPN2 | >sp\|P04844\|RPN2_HUMAN Dolichyl-diphosphooligosaccharide--protein glycosyltransferase subunit 2 OS=Homo sapiens GN=RPN2 PE=1 SV=3 | MLAQQAVK(1)R | 3 | 6.33 |
| Q99942 | RNF5 | >sp\|Q99942\|RNF5_HUMAN E3 ubiquitin-protein ligase RNF5 OS=Homo sapiens GN=RNF5 PE=1 SV=1 | LK(1)TPPRPQGQRPAPESR | 2 | 6.32 |
| Q96GF1 | RN185 | >sp\|Q96GF1\|RN185_HUMAN E3 ubiquitin-protein ligase RNF185 OS=Homo sapiens GN=RNF185 PE=1 SV=1 | QVCPVCK(1)AGISR | 2 | 6.01 |
| P0CG47 | UBB | >sp\|P0CG47\|UBB_HUMAN Polyubiquitin-B OS=Homo sapiens GN=UBB PE=1 SV=1;>sp\|P0CG48\|UBC_HUMAN Polyubiquitin-C OS=Homo sapiens GN=UBC PE=1 SV=3;>sp\|P62979\|RS27A_HUMAN Ubiquitin-40S ribosomal protein S27a OS=Homo sapiens GN=RPS27A PE=1 SV=2;>sp\|P62987\|RL40_HUMA | MQIFVK(1)TLTGK | 8 | 6.01 |

| | | | | | |
|---|---|---|---|---|---|
| O75845 | SC5D | >sp\|O75845\|SC5D_HUMAN Lathosterol oxidase OS=Homo sapiens GN=SC5D PE=1 SV=2 | IGGSFK(1)NPSSFEGK | 1 | 5.40 |
| P49768 | PSN1 | >sp\|P49768\|PSN1_HUMAN Presenilin-1 OS=Homo sapiens GN=PSEN1 PE=1 SV=1 | NSK(1)YNAESTER | 1 | 5.32 |
| Q13501 | SQSTM | >sp\|Q13501\|SQSTM_HUMAN Sequestosome-1 OS=Homo sapiens GN=SQSTM1 PE=1 SV=1 | NYDIGAALDTIQYSK(1)HPPPL | 18 | 5.27 |
| Q16850 | CP51A | >sp\|Q16850\|CP51A_HUMAN Lanosterol 14-alpha demethylase OS=Homo sapiens GN=CYP51A1 PE=1 SV=3 | DIFYK(0.994)AIQK(0.006) | 1 | 5.18 |
| Q8NDN9 | RCBT1 | >sp\|Q8NDN9\|RCBT1_HUMAN RCC1 and BTB domain-containing protein 1 OS=Homo sapiens GN=RCBTB1 PE=2 SV=1 | EFIAK(0.945)ASK(0.055) | 1 | 5.15 |
| Q53GQ0 | DHB12 | >sp\|Q53GQ0\|DHB12_HUMAN Very-long-chain 3-oxoacyl-CoA reductase OS=Homo sapiens GN=HSD17B12 PE=1 SV=2 | SK(0.948)DK(0.052)LDQVSSEIK | 1 | 5.11 |
| P55061 | BI1 | >sp\|P55061\|BI1_HUMAN Bax inhibitor 1 OS=Homo sapiens GN=TMBIM6 PE=1 SV=2 | K(1)INFDALLK | 3 | 4.96 |
| P0CG47 | UBB | >sp\|P0CG47\|UBB_HUMAN Polyubiquitin-B OS=Homo sapiens GN=UBB PE=1 SV=1;>sp\|P0CG48\|UBC_HUMAN Polyubiquitin-C OS=Homo sapiens GN=UBC PE=1 SV=3;>sp\|P62979\|RS27A_HUMAN Ubiquitin-40S ribosomal protein S27a OS=Homo sapiens GN=RPS27A PE=1 SV=2;>sp\|P62987\|RL40_HUMA | IQDK(1)EGIPPDQQR | 139 | 4.89 |
| P61619 | S61A1 | >sp\|P61619\|S61A1_HUMAN Protein transport protein Sec61 subunit alpha isoform 1 OS=Homo sapiens GN=SEC61A1 PE=1 SV=2;>sp\|Q9H9S3\|S61A2_HUMAN Protein transport | DVAK(1)QLK | 1 | 4.83 |

| | | | | | |
|---|---|---|---|---|---|
| | | protein Sec61 subunit alpha isoform 2 OS=Homo sapiens GN=SEC61A2 PE=2 SV=3 | | | |
| Q7Z3D4 | LYSM3 | >sp\|Q7Z3D4\|LYSM3_HUMAN LysM and putative peptidoglycan-binding domain-containing protein 3 OS=Homo sapiens GN=LYSMD3 PE=1 SV=2 | FEPDNK(1)NTQR | 2 | 4.81 |
| Q15800 | MSMO1 | >sp\|Q15800\|MSMO1_HUMAN Methylsterol monooxygenase 1 OS=Homo sapiens GN=MSMO1 PE=1 SV=1 | IFGTDSQYNAYNEK(1)R | 7 | 4.81 |
| Q9Y282 | ERGIC3 | >sp\|Q9Y282\|ERGI3_HUMAN Endoplasmic reticulum-Golgi intermediate compartment protein 3 OS=Homo sapiens GN=ERGIC3 PE=1 SV=1 | MEALGK(0.832)LK(0.168) | 3 | 4.74 |
| O15173 | PGRC2 | >sp\|O15173\|PGRC2_HUMAN Membrane-associated progesterone receptor component 2 OS=Homo sapiens GN=PGRMC2 PE=1 SV=1 | EK(1)YDYVGR | 2 | 4.60 |
| Q99942 | RNF5 | >sp\|Q99942\|RNF5_HUMAN E3 ubiquitin-protein ligase RNF5 OS=Homo sapiens GN=RNF5 PE=1 SV=1 | EK(1)VVPLYGR | 18 | 4.48 |
| P67775 | PP2AA | >sp\|P67775\|PP2AA_HUMAN Serine/threonine-protein phosphatase 2A catalytic subunit alpha isoform OS=Homo sapiens GN=PPP2CA PE=1 SV=1;>sp\|P62714\|PP2AB_HUMAN Serine/threonine-protein phosphatase 2A catalytic subunit beta isoform OS=Homo sapiens GN=PPP2CB PE=1 | EILTK(1)ESNVQEVR | 2 | 4.43 |
| P51572 | BAP31 | >sp\|P51572\|BAP31_HUMAN B-cell receptor-associated protein 31 OS=Homo sapiens GN=BCAP31 PE=1 SV=3 | LDVGNAEVK(1)LEEENR | 5 | 4.36 |
| O95816 | BAG2 | >sp\|O95816\|BAG2_HUMAN BAG family molecular chaperone regulator 2 OS=Homo sapiens GN=BAG2 PE=1 SV=1 | LLEHSK(0.792)GAGSK(0.208) | 2 | 4.28 |

| | | | | | |
|---|---|---|---|---|---|
| Q9UNL2 | SSRG | >sp\|Q9UNL2\|SSRG_HUMAN Translocon-associated protein subunit gamma OS=Homo sapiens GN=SSR3 PE=1 SV=1 | REDAVSK(1)EVTR | 1 | 4.22 |
| Q14677 | EPN4 | >sp\|Q14677\|EPN4_HUMAN Clathrin interactor 1 OS=Homo sapiens GN=CLINT1 PE=1 SV=1 | LGELSDK(1)IGSTIDDTISK | 1 | 4.21 |
| P49326 | FMO5 | >sp\|P49326\|FMO5_HUMAN Dimethylaniline monooxygenase [N-oxide-forming] 5 OS=Homo sapiens GN=FMO5 PE=1 SV=2 | VQGPGK(1)WDGAR | 1 | 4.10 |
| Q99942 | RNF5 | >sp\|Q99942\|RNF5_HUMAN E3 ubiquitin-protein ligase RNF5 OS=Homo sapiens GN=RNF5 PE=1 SV=1 | QECPVCK(1)AGISR | 1 | 4.03 |
| P84090 | ERH | >sp\|P84090\|ERH_HUMAN Enhancer of rudimentary homolog OS=Homo sapiens GN=ERH PE=1 SV=1 | SHTILLVQPTK(1)RPEGR | 13 | 3.92 |
| Q9UBM7 | DHCR7 | >sp\|Q9UBM7\|DHCR7_HUMAN 7-dehydrocholesterol reductase OS=Homo sapiens GN=DHCR7 PE=1 SV=1 | AK(1)SLDGVTNDR | 7 | 3.86 |
| O95864 | FADS2 | >sp\|O95864\|FADS2_HUMAN Fatty acid desaturase 2 OS=Homo sapiens GN=FADS2 PE=1 SV=1 | NSK(1)ITEDFR | 10 | 3.79 |
| Q00765 | REEP5 | >sp\|Q00765\|REEP5_HUMAN Receptor expression-enhancing protein 5 OS=Homo sapiens GN=REEP5 PE=1 SV=3 | ETADAITK(0.998)EAK(0.002) | 6 | 3.76 |
| P61619 | S61A1 | >sp\|P61619\|S61A1_HUMAN Protein transport protein Sec61 subunit alpha isoform 1 OS=Homo sapiens GN=SEC61A1 PE=1 SV=2;>sp\|Q9H9S3\|S61A2_HUMAN Protein transport protein Sec61 subunit alpha isoform 2 OS=Homo sapiens GN=SEC61A2 PE=2 SV=3 | QLK(1)EQQMVMR | 5 | 3.75 |
| P46977 | STT3A | >sp\|P46977\|STT3A_HUMAN Dolichyl-diphosphooligosaccharide--protein glycosyltransferase subunit STT3A OS=Homo | NLDISRPDK(0.448)K(0.552) | 1 | 3.72 |

| | | | | | |
|---|---|---|---|---|---|
| | | sapiens GN=STT3A PE=1 SV=2 | | | |
| Q9Y5Z9 | UBIA1 | >sp\|Q9Y5Z9\|UBIA1_HUMAN UbiA prenyltransferase domain-containing protein 1 OS=Homo sapiens GN=UBIAD1 PE=1 SV=1 | AASQVLGEK(1)INILSGETVK | 11 | 3.60 |
| Q9UBM7 | DHCR7 | >sp\|Q9UBM7\|DHCR7_HUMAN 7-dehydrocholesterol reductase OS=Homo sapiens GN=DHCR7 PE=1 SV=1 | AAK(1)SQPNIPK | 3 | 3.60 |
| Q96HR9 | REEP6 | >sp\|Q96HR9\|REEP6_HUMAN Receptor expression-enhancing protein 6 OS=Homo sapiens GN=REEP6 PE=1 SV=1 | NVK(1)PSQTPQPK | 6 | 3.52 |
| P02649 | APOE | >sp\|P02649\|APOE_HUMAN Apolipoprotein E OS=Homo sapiens GN=APOE PE=1 SV=1 | AK(1)LEEQAQQIR | 4 | 3.50 |
| P61956 | SUMO2 | >sp\|P61956\|SUMO2_HUMAN Small ubiquitin-related modifier 2 OS=Homo sapiens GN=SUMO2 PE=1 SV=3 | ADEK(0.009)PK(0.941)EGVK(0.05) | 2 | 3.49 |
| Q8TB61 | S35B2 | >sp\|Q8TB61\|S35B2_HUMAN Adenosine 3'-phospho 5'-phosphosulfate transporter 1 OS=Homo sapiens GN=SLC35B2 PE=1 SV=1 | AVPVESPVQK(1)V | 9 | 3.48 |
| Q86UQ4 | ABCAD | >sp\|Q86UQ4\|ABCAD_HUMAN ATP-binding cassette sub-family A member 13 OS=Homo sapiens GN=ABCA13 PE=2 SV=3 | LLEFGNEVIWK(1) | 1 | 3.48 |
| Q9P0S3 | ORML1 | >sp\|Q9P0S3\|ORML1_HUMAN ORM1-like protein 1 OS=Homo sapiens GN=ORMDL1 PE=1 SV=1;>sp\|Q8N138\|ORML3_HUMAN ORM1-like protein 3 OS=Homo sapiens GN=ORMDL3 PE=1 SV=1;>sp\|Q53FV1\|ORML2_HUMAN ORM1-like protein 2 OS=Homo sapiens GN=ORMDL2 PE=1 SV=2 | GTPFETPDQGK(1)AR | 5 | 3.40 |
| Q9UNL2 | SSRG | >sp\|Q9UNL2\|SSRG_HUMAN Translocon-associated protein subunit gamma OS=Homo sapiens GN=SSR3 PE=1 SV=1 | GSSK(1)QQSEEDLLLQDFSR | 2 | 3.39 |

| | | | | | |
|---|---|---|---|---|---|
| P0CG47 | UBB | >sp\|P0CG47\|UBB_HUMAN Polyubiquitin-B OS=Homo sapiens GN=UBB PE=1 SV=1;>sp\|P0CG48\|UBC_HUMAN Polyubiquitin-C OS=Homo sapiens GN=UBC PE=1 SV=3;>sp\|P62979\|RS27A_HUMAN Ubiquitin-40S ribosomal protein S27a OS=Homo sapiens GN=RPS27A PE=1 SV=2;>sp\|P62987\|RL40_HUMA | LIFAGK(1)QLEDGRTLSDYNIQK | 6 | 3.36 |
| P61978 | HNRPK | >sp\|P61978\|HNRPK_HUMAN Heterogeneous nuclear ribonucleoprotein K OS=Homo sapiens GN=HNRNPK PE=1 SV=1 | GAK(1)IK(1)ELR | 1 | 3.33 |
| P61978 | HNRPK | >sp\|P61978\|HNRPK_HUMAN Heterogeneous nuclear ribonucleoprotein K OS=Homo sapiens GN=HNRNPK PE=1 SV=1 | GAK(1)IK(1)ELR | 1 | 3.33 |
| Q8TC12 | RDH11 | >sp\|Q8TC12\|RDH11_HUMAN Retinol dehydrogenase 11 OS=Homo sapiens GN=RDH11 PE=1 SV=2 | AFAK(1)GFLAEEK | 22 | 3.30 |
| Q9NXW2 | DJB12 | >sp\|Q9NXW2\|DJB12_HUMAN DnaJ homolog subfamily B member 12 OS=Homo sapiens GN=DNAJB12 PE=1 SV=4 | QYDQFGDDK(1)SQAAR | 2 | 3.25 |
| Q9BV81 | EMC6 | >sp\|Q9BV81\|EMC6_HUMAN ER membrane protein complex subunit 6 OS=Homo sapiens GN=EMC6 PE=1 SV=1 | AAVVAK(1)R | 3 | 3.25 |
| Q9Y679 | AUP1 | >sp\|Q9Y679\|AUP1_HUMAN Ancient ubiquitous protein 1 OS=Homo sapiens GN=AUP1 PE=1 SV=1 | GELVESLK(1)R | 8 | 3.21 |
| Q15392 | DHC24 | >sp\|Q15392\|DHC24_HUMAN Delta(24)-sterol reductase OS=Homo sapiens GN=DHCR24 PE=1 SV=2 | HVENYLK(1)TNR | 2 | 3.19 |
| Q99942 | RNF5 | >sp\|Q99942\|RNF5_HUMAN E3 ubiquitin-protein ligase RNF5 OS=Homo sapiens GN=RNF5 PE=1 SV=1 | GSQK(1)PQDPR | 20 | 3.17 |
| P11021 | GRP78 | >sp\|P11021\|GRP78_HUMAN 78 kDa glucose- | VLEDSDLK(0.44)K(0.56) | 1 | 3.16 |

| | | | | | |
|---|---|---|---|---|---|
| | | regulated protein OS=Homo sapiens GN=HSPA5 PE=1 SV=2 | | | |
| P63261 | ACTG | >sp\|P63261\|ACTG_HUMAN Actin, cytoplasmic 2 OS=Homo sapiens GN=ACTG1 PE=1 SV=1;>sp\|P60709\|ACTB_HUMAN Actin, cytoplasmic 1 OS=Homo sapiens GN=ACTB PE=1 SV=1;>sp\|P68133\|ACTS_HUMAN Actin, alpha skeletal muscle OS=Homo sapiens GN=ACTA1 PE=1 SV=1;>sp\|P68032\|ACTC | DSYVGDEAQSK(1)R | 7 | 3.15 |
| Q8TCT9 | HM13 | >sp\|Q8TCT9\|HM13_HUMAN Minor histocompatibility antigen H13 OS=Homo sapiens GN=HM13 PE=1 SV=1 | EGTEASASK(0.998)GLEK(0.002) | 4 | 3.14 |
| Q9Y679 | AUP1 | >sp\|Q9Y679\|AUP1_HUMAN Ancient ubiquitous protein 1 OS=Homo sapiens GN=AUP1 PE=1 SV=1 | VQQLVAK(1)ELGQTGTR | 24 | 3.13 |
| Q7L5N7 | PCAT2 | >sp\|Q7L5N7\|PCAT2_HUMAN Lysophosphatidylcholine acyltransferase 2 OS=Homo sapiens GN=LPCAT2 PE=1 SV=1 | K(1)ITQTALK | 2 | 3.13 |
| Q14254 | FLOT2 | >sp\|Q14254\|FLOT2_HUMAN Flotillin-2 OS=Homo sapiens GN=FLOT2 PE=1 SV=2 | AEAYQK(1)YGDAAK | 2 | 3.08 |
| Q70UQ0 | IKIP | >sp\|Q70UQ0\|IKIP_HUMAN Inhibitor of nuclear factor kappa-B kinase-interacting protein OS=Homo sapiens GN=IKBIP PE=1 SV=1 | SEGGK(1)TPVAR | 1 | 3.07 |
| Q00765 | REEP5 | >sp\|Q00765\|REEP5_HUMAN Receptor expression-enhancing protein 5 OS=Homo sapiens GN=REEP5 PE=1 SV=3 | AK(1)ETADAITK | 6 | 3.03 |
| Q8WUY1 | THEM6 | >sp\|Q8WUY1\|THEM6_HUMAN Protein THEM6 OS=Homo sapiens GN=THEM6 PE=1 SV=2 | MESGLSDVTK(1)DQ | 3 | 3.01 |
| Q14677 | EPN4 | >sp\|Q14677\|EPN4_HUMAN Clathrin interactor 1 OS=Homo sapiens GN=CLINT1 PE=1 SV=1 | SQNTDMVQK(0.996)SVSK(0.004) | 3 | 2.92 |
| O95816 | BAG2 | >sp\|O95816\|BAG2_HUMAN BAG family molecular | GAGSK(1)TLQQNAESR | 17 | 2.89 |

| | | | | | |
|---|---|---|---|---|---|
| | | chaperone regulator 2 OS=Homo sapiens GN=BAG2 PE=1 SV=1 | | | |
| Q96CS7 | PKHB2 | >sp\|Q96CS7\|PKHB2_HUMAN Pleckstrin homology domain-containing family B member 2 OS=Homo sapiens GN=PLEKHB2 PE=1 SV=1 | DTQPPDGK(0.837)SK(0.163) | 4 | 2.88 |
| Q8NCU8 | YB039 | >sp\|Q8NCU8\|YB039_HUMAN Uncharacterized protein encoded by LINC00116 OS=Homo sapiens GN=LINC00116 PE=1 SV=1 | LQDK(1)LAATQK | 1 | 2.87 |
| Q15392 | DHC24 | >sp\|Q15392\|DHC24_HUMAN Delta(24)-sterol reductase OS=Homo sapiens GN=DHCR24 PE=1 SV=2 | DIQK(1)QVR | 4 | 2.83 |
| P61956 | SUMO2 | >sp\|P61956\|SUMO2_HUMAN Small ubiquitin-related modifier 2 OS=Homo sapiens GN=SUMO2 PE=1 SV=3;>sp\|Q6EEV6\|SUMO4_HUMAN Small ubiquitin-related modifier 4 OS=Homo sapiens GN=SUMO4 PE=1 SV=2;>sp\|P55854\|SUMO3_HUMAN Small ubiquitin-related modifier 3 OS=Homo sapi | VAGQDGSVVQFK(0.382)IK(0.618) | 1 | 2.83 |
| Q99541 | PLIN2 | >sp\|Q99541\|PLIN2_HUMAN Perilipin-2 OS=Homo sapiens GN=PLIN2 PE=1 SV=2 | GAVTGSVEK(0.832)TK(0.168) | 14 | 2.81 |
| P0CG47 | UBB | >sp\|P0CG47\|UBB_HUMAN Polyubiquitin-B OS=Homo sapiens GN=UBB PE=1 SV=1;>sp\|P0CG48\|UBC_HUMAN Polyubiquitin-C OS=Homo sapiens GN=UBC PE=1 SV=3;>sp\|P62979\|RS27A_HUMAN Ubiquitin-40S ribosomal protein S27a OS=Homo sapiens GN=RPS27A PE=1 SV=2;>sp\|P62987\|RL40_HUMA | TLTGK(1)TITLEVEPSDTIENVKAK | 7 | 2.78 |
| Q9NZ01 | TECR | >sp\|Q9NZ01\|TECR_HUMAN Very-long-chain enoyl-CoA reductase OS=Homo | DLRPAGSK(1)TR | 1 | 2.77 |

| | | | | | |
|---|---|---|---|---|---|
| | | sapiens GN=TECR PE=1 SV=1 | | | |
| P05023 | AT1A1 | >sp\|P05023\|AT1A1_HUMAN Sodium/potassium-transporting ATPase subunit alpha-1 OS=Homo sapiens GN=ATP1A1 PE=1 SV=1;>sp\|P13637\|AT1A3_HUMAN Sodium/potassium-transporting ATPase subunit alpha-3 OS=Homo sapiens GN=ATP1A3 PE=1 SV=3;>sp\|P50993\|AT1A2_HUMAN Sodium/po | TDK(1)LVNER | 2 | 2.77 |
| Q9NZ01 | TECR | >sp\|Q9NZ01\|TECR_HUMAN Very-long-chain enoyl-CoA reductase OS=Homo sapiens GN=TECR PE=1 SV=1 | SYLK(1)EFR | 6 | 2.76 |
| Q9C0D9 | EPT1 | >sp\|Q9C0D9\|EPT1_HUMAN Ethanolaminephosphotransferase 1 OS=Homo sapiens GN=EPT1 PE=1 SV=3 | AGYEYVSPEQLAGFDK(0.468)YK(0.532) | 2 | 2.76 |
| Q9C0D9 | EPT1 | >sp\|Q9C0D9\|EPT1_HUMAN Ethanolaminephosphotransferase 1 OS=Homo sapiens GN=EPT1 PE=1 SV=3 | AGYEYVSPEQLAGFDK(0.5)YK(0.5) | 2 | 2.75 |
| P31641 | SC6A6 | >sp\|P31641\|SC6A6_HUMAN Sodium- and chloride-dependent taurine transporter OS=Homo sapiens GN=SLC6A6 PE=1 SV=2 | DILK(1)PSPGK | 2 | 2.74 |
| Q9BQA9 | CQ062 | >sp\|Q9BQA9\|CQ062_HUMAN Uncharacterized protein C17orf62 OS=Homo sapiens GN=C17orf62 PE=1 SV=1 | STGK(1)VVLK | 3 | 2.67 |
| P05023 | AT1A1 | >sp\|P05023\|AT1A1_HUMAN Sodium/potassium-transporting ATPase subunit alpha-1 OS=Homo sapiens GN=ATP1A1 PE=1 SV=1;>sp\|P13637\|AT1A3_HUMAN Sodium/potassium-transporting ATPase subunit alpha-3 OS=Homo sapiens GN=ATP1A3 PE=1 SV=3;>sp\|P50993\|AT1A2_HUMAN Sodium/po | NSVFQQGMK(0.702)NK(0.298) | 1 | 2.65 |

| | | | | | |
|---|---|---|---|---|---|
| Q16850 | CP51A | >sp\|Q16850\|CP51A_HUMAN Lanosterol 14-alpha demethylase OS=Homo sapiens GN=CYP51A1 PE=1 SV=3 | GVAYDVPNPVFLEQK(0.451)K(0.549) | 4 | 2.65 |
| Q96LD4 | TRI47 | >sp\|Q96LD4\|TRI47_HUMAN Tripartite motif-containing protein 47 OS=Homo sapiens GN=TRIM47 PE=1 SV=2 | TVALIK(1)SAAVAER | 7 | 2.65 |
| Q96B21 | TM45B | >sp\|Q96B21\|TM45B_HUMAN Transmembrane protein 45B OS=Homo sapiens GN=TMEM45B PE=1 SV=1 | K(1)NSPLHYYQR | 1 | 2.63 |
| Q13114 | TRAF3 | >sp\|Q13114\|TRAF3_HUMAN TNF receptor-associated factor 3 OS=Homo sapiens GN=TRAF3 PE=1 SV=2 | VTELESVDK(1)SAGQVAR | 1 | 2.62 |
| Q16850 | CP51A | >sp\|Q16850\|CP51A_HUMAN Lanosterol 14-alpha demethylase OS=Homo sapiens GN=CYP51A1 PE=1 SV=3 | YLQDNPASGEK(1)FAYVPFGAGR | 8 | 2.61 |
| Q9Y5Z9 | UBIA1 | >sp\|Q9Y5Z9\|UBIA1_HUMAN UbiA prenyltransferase domain-containing protein 1 OS=Homo sapiens GN=UBIAD1 PE=1 SV=1 | SQAFNK(1)LPQR | 1 | 2.59 |
| Q8TCT9 | HM13 | >sp\|Q8TCT9\|HM13_HUMAN Minor histocompatibility antigen H13 OS=Homo sapiens GN=HM13 PE=1 SV=1 | DPAAVTESK(0.996)EGTEASASK(0.004) | 2 | 2.59 |
| Q9NUQ2 | PLCE | >sp\|Q9NUQ2\|PLCE_HUMAN 1-acyl-sn-glycerol-3-phosphate acyltransferase epsilon OS=Homo sapiens GN=AGPAT5 PE=1 SV=3 | YNPEQTK(1)VLSASQAFAAQR | 2 | 2.59 |
| Q8NBX0 | SCPDL | >sp\|Q8NBX0\|SCPDL_HUMAN Saccharopine dehydrogenase-like oxidoreductase OS=Homo sapiens GN=SCCPDH PE=1 SV=1 | NVSNLK(1)PVPLIGPK | 2 | 2.58 |
| P08034 | CXB1 | >sp\|P08034\|CXB1_HUMAN Gap junction beta-1 protein OS=Homo sapiens GN=GJB1 PE=1 SV=1 | LEGHGDPLHLEEVK(1)R | 2 | 2.58 |
| Q9Y3E5 | PTH2 | >sp\|Q9Y3E5\|PTH2_HUMAN Peptidyl-tRNA hydrolase 2, mitochondrial OS=Homo sapiens GN=PTRH2 PE=1 SV=1 | TSK(1)THTDTESEASILGDSGEYK | 3 | 2.55 |

| | | | | | |
|---|---|---|---|---|---|
| Q15843 | NEDD8 | >sp\|Q15843\|NEDD8_HUMAN NEDD8 OS=Homo sapiens GN=NEDD8 PE=1 SV=1 | TLTGK(1)EIEIDIEPTDK | 4 | 2.50 |
| P38435 | VKGC | >sp\|P38435\|VKGC_HUMAN Vitamin K-dependent gamma-carboxylase OS=Homo sapiens GN=GGCX PE=1 SV=2 | TSPSSDK(0.999)VQK(0.001) | 2 | 2.50 |
| Q9BWH2 | FUND2 | >sp\|Q9BWH2\|FUND2_HUMAN FUN14 domain-containing protein 2 OS=Homo sapiens GN=FUNDC2 PE=1 SV=2 | K(1)SNQIPTEVR | 10 | 2.49 |
| P55085 | PAR2 | >sp\|P55085\|PAR2_HUMAN Proteinase-activated receptor 2 OS=Homo sapiens GN=F2RL1 PE=1 SV=1 | TVK(1)QMQVSLTSK | 1 | 2.48 |
| Q5I7T1 | AG10B | >sp\|Q5I7T1\|AG10B_HUMAN Putative Dol-P-Glc:Glc(2)Man(9)GlcNAc(2)-PP-Dol alpha-1,2-glucosyltransferase OS=Homo sapiens GN=ALG10B PE=1 SV=2;>sp\|Q5BKT4\|AG10A_HUMAN Dol-P-Glc:Glc(2)Man(9)GlcNAc(2)-PP-Dol alpha-1,2-glucosyltransferase OS=Homo sapiens GN=ALG10 PE | NK(1)AASSIQR | 1 | 2.47 |
| P27824 | CALX | >sp\|P27824\|CALX_HUMAN Calnexin OS=Homo sapiens GN=CANX PE=1 SV=2 | DKGDEEEEGEEK(1)LEEK | 5 | 2.35 |
| Q15843 | NEDD8 | >sp\|Q15843\|NEDD8_HUMAN NEDD8 OS=Homo sapiens GN=NEDD8 PE=1 SV=1 | LIYSGK(1)QMNDEK | 3 | 2.35 |
| P62745 | RHOB | >sp\|P62745\|RHOB_HUMAN Rho-related GTP-binding protein RhoB OS=Homo sapiens GN=RHOB PE=1 SV=1 | MK(1)QEPVRTDDGR | 2 | 2.35 |
| O95816 | BAG2 | >sp\|O95816\|BAG2_HUMAN BAG family molecular chaperone regulator 2 OS=Homo sapiens GN=BAG2 PE=1 SV=1 | AQAK(0.999)INAK(0.001) | 18 | 2.34 |
| O75844 | FACE1 | >sp\|O75844\|FACE1_HUMAN CAAX prenyl protease 1 homolog OS=Homo | NEEEGNSEEIK(0.976)AK(0.024) | 4 | 2.32 |

| | | | | | |
|---|---|---|---|---|---|
| | | sapiens GN=ZMPSTE24 PE=1 SV=2 | | | |
| Q96B96 | TM159 | >sp\|Q96B96\|TM159_HUMAN Promethin OS=Homo sapiens GN=TMEM159 PE=1 SV=2 | AK(1)EEPQSISR | 3 | 2.32 |
| O95197 | RTN3 | >sp\|O95197\|RTN3_HUMAN Reticulon-3 OS=Homo sapiens GN=RTN3 PE=1 SV=2 | SIVEK(0.911)IQAK(0.089) | 1 | 2.31 |
| O95140 | MFN2 | >sp\|O95140\|MFN2_HUMAN Mitofusin-2 OS=Homo sapiens GN=MFN2 PE=1 SV=3 | IK(1)QITEEVER | 7 | 2.31 |
| Q53GQ0 | DHB12 | >sp\|Q53GQ0\|DHB12_HUMAN Very-long-chain 3-oxoacyl-CoA reductase OS=Homo sapiens GN=HSD17B12 PE=1 SV=2 | SK(1)GVFVQSVLPYFVATK | 1 | 2.30 |
| Q8TCT9 | HM13 | >sp\|Q8TCT9\|HM13_HUMAN Minor histocompatibility antigen H13 OS=Homo sapiens GN=HM13 PE=1 SV=1 | GK(1)NASDMPETITSR | 1 | 2.30 |
| Q8N2H4 | SYS1 | >sp\|Q8N2H4\|SYS1_HUMAN Protein SYS1 homolog OS=Homo sapiens GN=SYS1 PE=1 SV=1 | EIPLNSAPK(1)SNV | 7 | 2.29 |
| Q9H0E2 | TOLIP | >sp\|Q9H0E2\|TOLIP_HUMAN Toll-interacting protein OS=Homo sapiens GN=TOLLIP PE=1 SV=1 | LNITVVQAK(0.995)LAK(0.005) | 9 | 2.28 |
| P48066 | S6A11 | >sp\|P48066\|S6A11_HUMAN Sodium- and chloride-dependent GABA transporter 3 OS=Homo sapiens GN=SLC6A11 PE=2 SV=1 | ALPLGNGK(1)AAEEAR | 5 | 2.24 |
| P33527 | MRP1 | >sp\|P33527\|MRP1_HUMAN Multidrug resistance-associated protein 1 OS=Homo sapiens GN=ABCC1 PE=1 SV=3 | VDANEEVEALIVK(0.959)SPQK(0.041) | 2 | 2.22 |
| Q9BUV8 | CT024 | >sp\|Q9BUV8\|CT024_HUMAN Uncharacterized protein C20orf24 OS=Homo sapiens GN=C20orf24 PE=2 SV=1 | RK(1)EEPPQPQLANGALK | 3 | 2.21 |
| O14964 | HGS | >sp\|O14964\|HGS_HUMAN Hepatocyte growth factor-regulated tyrosine kinase substrate OS=Homo sapiens GN=HGS PE=1 SV=1 | FGIEK(1)EVR | 1 | 2.20 |

| | | | | | |
|---|---|---|---|---|---|
| Q99755 | PI51A | >sp\|Q99755\|PI51A_HUMAN Phosphatidylinositol 4-phosphate 5-kinase type-1 alpha OS=Homo sapiens GN=PIP5K1A PE=1 SV=1 | GAIQLGITHTVGSLSTK(1)PER | 3 | 2.18 |
| Q8TC12 | RDH11 | >sp\|Q8TC12\|RDH11_HUMAN Retinol dehydrogenase 11 OS=Homo sapiens GN=RDH11 PE=1 SV=2 | GELVAK(1)EIQTTTGNQQVLVR | 1 | 2.17 |
| Q07820 | MCL1 | >sp\|Q07820\|MCL1_HUMAN Induced myeloid leukemia cell differentiation protein Mcl-1 OS=Homo sapiens GN=MCL1 PE=1 SV=3 | LLATEK(1)EASAR | 2 | 2.17 |
| Q53GQ0 | DHB12 | >sp\|Q53GQ0\|DHB12_HUMAN Very-long-chain 3-oxoacyl-CoA reductase OS=Homo sapiens GN=HSD17B12 PE=1 SV=2 | DKLDQVSSEIK(0.985)EK(0.015) | 1 | 2.17 |
| Q8N0X7 | SPG20 | >sp\|Q8N0X7\|SPG20_HUMAN Spartin OS=Homo sapiens GN=SPG20 PE=1 SV=1 | IQPEEK(0.999)PVEVSPAVTK(0.001) | 1 | 2.14 |
| Q15392 | DHC24 | >sp\|Q15392\|DHC24_HUMAN Delta(24)-sterol reductase OS=Homo sapiens GN=DHCR24 PE=1 SV=2 | EK(1)LGCQDAFPEVYDK | 1 | 2.13 |
| Q6UX53 | MET7B | >sp\|Q6UX53\|MET7B_HUMAN Methyltransferase-like protein 7B OS=Homo sapiens GN=METTL7B PE=1 SV=2 | ELFSQIK(0.993)GLTGASGK(0.007) | 1 | 2.13 |
| P48066 | S6A11 | >sp\|P48066\|S6A11_HUMAN Sodium- and chloride-dependent GABA transporter 3 OS=Homo sapiens GN=SLC6A11 PE=2 SV=1 | LTTPSTDLK(1)MR | 1 | 2.12 |
| Q16850 | CP51A | >sp\|Q16850\|CP51A_HUMAN Lanosterol 14-alpha demethylase OS=Homo sapiens GN=CYP51A1 PE=1 SV=3 | LK(1)DSWVER | 1 | 2.12 |
| O75387 | LAT3 | >sp\|O75387\|LAT3_HUMAN Large neutral amino acids transporter small subunit 3 OS=Homo sapiens GN=SLC43A1 PE=1 SV=1 | DGVATK(1)SIRPR | 9 | 2.12 |
| P0CG47 | UBB | >sp\|P0CG47\|UBB_HUMAN Polyubiquitin-B OS=Homo sapiens GN=UBB PE=1 | AK(1)IQDKEGIPPDQQR | 26 | 2.10 |

| | | | | | |
|---|---|---|---|---|---|
| | | SV=1;>sp\|P0CG48\|UBC_HUMAN Polyubiquitin-C OS=Homo sapiens GN=UBC PE=1 SV=3;>sp\|P62979\|RS27A_HUMAN Ubiquitin-40S ribosomal protein S27a OS=Homo sapiens GN=RPS27A PE=1 SV=2;>sp\|P62987\|RL40_HUMA | | | |
| Q96CS3 | FAF2 | >sp\|Q96CS3\|FAF2_HUMAN FAS-associated factor 2 OS=Homo sapiens GN=FAF2 PE=1 SV=2 | EEEVQQQK(1)LAEER | 4 | 2.09 |
| Q9H6A9 | PCX3 | >sp\|Q9H6A9\|PCX3_HUMAN Pecanex-like protein 3 OS=Homo sapiens GN=PCNXL3 PE=1 SV=2;>sp\|Q96RV3\|PCX1_HUMAN Pecanex-like protein 1 OS=Homo sapiens GN=PCNX PE=1 SV=2 | GSIQNAK(1)QALR | 1 | 2.08 |
| Q15155 | NOMO1 | >sp\|Q15155\|NOMO1_HUMAN Nodal modulator 1 OS=Homo sapiens GN=NOMO1 PE=1 SV=5 | ALGQAASDNSGPEDAK(1)R | 2 | 2.07 |
| Q9H2H9 | S38A1 | >sp\|Q9H2H9\|S38A1_HUMAN Sodium-coupled neutral amino acid transporter 1 OS=Homo sapiens GN=SLC38A1 PE=1 SV=1 | SLTNSHLEK(0.435)K(0.565) | 3 | 2.04 |
| P69849 | NOMO3 | >sp\|P69849\|NOMO3_HUMAN Nodal modulator 3 OS=Homo sapiens GN=NOMO3 PE=3 SV=2;>sp\|Q5JPE7\|NOMO2_HUMAN Nodal modulator 2 OS=Homo sapiens GN=NOMO2 PE=1 SV=1 | LQGVGALGQAASDNSGPEDAK(1)R | 3 | 2.03 |
| P08134 | RHOC | >sp\|P08134\|RHOC_HUMAN Rho-related GTP-binding protein RhoC OS=Homo sapiens GN=RHOC PE=1 SV=1 | MK(1)QEPVR | 2 | 2.02 |
| P48449 | ERG7 | >sp\|P48449\|ERG7_HUMAN Lanosterol synthase OS=Homo sapiens GN=LSS PE=1 SV=1 | LSQVPDNPPDYQK(1)YYR | 1 | 2.02 |
| P21796 | VDAC1 | >sp\|P21796\|VDAC1_HUMAN Voltage-dependent anion-selective channel protein 1 OS=Homo sapiens GN=VDAC1 PE=1 SV=2 | LTFDSSFSPNTGK(0.828)K(0.172) | 5 | 2.02 |

| | | | | | |
|---|---|---|---|---|---|
| Q9H3N1 | TMX1 | >sp\|Q9H3N1\|TMX1_HUMAN Thioredoxin-related transmembrane protein 1 OS=Homo sapiens GN=TMX1 PE=1 SV=1 | LLSESAQPLK(0.864)K(0.136) | 4 | 1.99 |
| P38435 | VKGC | >sp\|P38435\|VKGC_HUMAN Vitamin K-dependent gamma-carboxylase OS=Homo sapiens GN=GGCX PE=1 SV=2 | DK(1)AELISGPR | 2 | 1.99 |
| Q96A29 | FUCT1 | >sp\|Q96A29\|FUCT1_HUMAN GDP-fucose transporter 1 OS=Homo sapiens GN=SLC35C1 PE=1 SV=1 | DSEK(1)SAMGV | 3 | 1.99 |
| P33897 | ABCD1 | >sp\|P33897\|ABCD1_HUMAN ATP-binding cassette sub-family D member 1 OS=Homo sapiens GN=ABCD1 PE=1 SV=2;>sp\|Q9UBJ2\|ABCD2_HUMAN ATP-binding cassette sub-family D member 2 OS=Homo sapiens GN=ABCD2 PE=1 SV=1 | DVLSGGEK(1)QR | 5 | 1.97 |
| Q9NY64 | GTR8 | >sp\|Q9NY64\|GTR8_HUMAN Solute carrier family 2, facilitated glucose transporter member 8 OS=Homo sapiens GN=SLC2A8 PE=1 SV=3 | GK(1)TLEQITAHFEGR | 1 | 1.97 |
| Q9H8H3 | METT7A | >sp\|Q9H8H3\|MET7A_HUMAN Methyltransferase-like protein 7A OS=Homo sapiens GN=METTL7A PE=1 SV=1 | ASFSK(0.965)LK(0.035) | 1 | 1.96 |
| O95573 | ACSL3 | >sp\|O95573\|ACSL3_HUMAN Long-chain-fatty-acid--CoA ligase 3 OS=Homo sapiens GN=ACSL3 PE=1 SV=3 | TK(1)ADFFEDENGQR | 1 | 1.93 |
| Q9H3N1 | TMX1 | >sp\|Q9H3N1\|TMX1_HUMAN Thioredoxin-related transmembrane protein 1 OS=Homo sapiens GN=TMX1 PE=1 SV=1 | K(1)LLSESAQPLK | 1 | 1.92 |
| O95573 | ACSL3 | >sp\|O95573\|ACSL3_HUMAN Long-chain-fatty-acid--CoA ligase 3 OS=Homo sapiens GN=ACSL3 PE=1 SV=3 | VFTYAK(0.413)NK(0.587) | 2 | 1.92 |
| P07437 | TBB5 | >sp\|P07437\|TBB5_HUMAN Tubulin beta chain OS=Homo sapiens GN=TUBB PE=1 | K(1)LAVNMVPFPR | 3 | 1.91 |

| | | | | | |
|---|---|---|---|---|---|
| | | SV=2;>sp\|P68371\|TBB4B_HUMAN Tubulin beta-4B chain OS=Homo sapiens GN=TUBB4B PE=1 SV=1;>sp\|P04350\|TBB4A_HUMAN Tubulin beta-4A chain OS=Homo sapiens GN=TUBB4A PE=1 SV=2;>sp\|Q3ZCM7\|TBB8_HUM | | | |
| P21796 | VDAC1 | >sp\|P21796\|VDAC1_HUMAN Voltage-dependent anion-selective channel protein 1 OS=Homo sapiens GN=VDAC1 PE=1 SV=2 | LTFDSSFSPNTGK(0.424)K(0.576) | 5 | 1.90 |
| Q9NPA0 | EMC7 | >sp\|Q9NPA0\|EMC7_HUMAN ER membrane protein complex subunit 7 OS=Homo sapiens GN=EMC7 PE=1 SV=1 | LFSSK(0.068)SSGK(0.932) | 5 | 1.89 |
| O75387 | LAT3 | >sp\|O75387\|LAT3_HUMAN Large neutral amino acids transporter small subunit 3 OS=Homo sapiens GN=SLC43A1 PE=1 SV=1 | LSQK(1)APSLEDGSDAFMSPQDVR | 7 | 1.89 |
| O95140 | MFN2 | >sp\|O95140\|MFN2_HUMAN Mitofusin-2 OS=Homo sapiens GN=MFN2 PE=1 SV=3 | FLGPK(1)NSR | 1 | 1.89 |
| P05023 | AT1A1 | >sp\|P05023\|AT1A1_HUMAN Sodium/potassium-transporting ATPase subunit alpha-1 OS=Homo sapiens GN=ATP1A1 PE=1 SV=1 | CSSILLHGK(0.999)EQPLDEELK(0.001) | 1 | 1.89 |
| Q9BUV8 | CT024 | >sp\|Q9BUV8\|CT024_HUMAN Uncharacterized protein C20orf24 OS=Homo sapiens GN=C20orf24 PE=2 SV=1 | VSVWSK(1)VLR | 3 | 1.88 |
| Q8NE00 | TM104 | >sp\|Q8NE00\|TM104_HUMAN Transmembrane protein 104 OS=Homo sapiens GN=TMEM104 PE=1 SV=2 | AEK(1)RPILSVQR | 7 | 1.88 |
| Q6UWP7 | LCLT1 | >sp\|Q6UWP7\|LCLT1_HUMAN Lysocardiolipin acyltransferase 1 OS=Homo sapiens GN=LCLAT1 PE=1 SV=1 | SNAFAEK(0.999)NGLQK(0.001) | 2 | 1.87 |
| Q9BSR8 | YIPF4 | >sp\|Q9BSR8\|YIPF4_HUMAN Protein YIPF4 OS=Homo sapiens GN=YIPF4 PE=1 SV=1 | LNLGGDFIK(1)ESTATTFLR | 2 | 1.86 |

| | | | | | |
|---|---|---|---|---|---|
| Q9H3N1 | TMX1 | >sp\|Q9H3N1\|TMX1_HUMAN Thioredoxin-related transmembrane protein 1 OS=Homo sapiens GN=TMX1 PE=1 SV=1 | LLSESAQPLK(0.412)K(0.588) | 4 | 1.86 |
| P04843 | RPN1 | >sp\|P04843\|RPN1_HUMAN Dolichyl-diphosphooligosaccharide--protein glycosyltransferase subunit 1 OS=Homo sapiens GN=RPN1 PE=1 SV=1 | LK(1)TEGSDLCDR | 2 | 1.85 |
| Q9NXF8 | ZDHC7 | >sp\|Q9NXF8\|ZDHC7_HUMAN Palmitoyltransferase ZDHHC7 OS=Homo sapiens GN=ZDHHC7 PE=1 SV=2 | SEK(1)PTWER | 1 | 1.84 |
| O00264 | PGRC1 | >sp\|O00264\|PGRC1_HUMAN Membrane-associated progesterone receptor component 1 OS=Homo sapiens GN=PGRMC1 PE=1 SV=3 | K(1)FYGPEGPYGVFAGR | 1 | 1.84 |
| Q15758 | AAAT | >sp\|Q15758\|AAAT_HUMAN Neutral amino acid transporter B(0) OS=Homo sapiens GN=SLC1A5 PE=1 SV=2 | CVEENNGVAK(1)HISR | 1 | 1.83 |
| Q14152 | EIF3A | >sp\|Q14152\|EIF3A_HUMAN Eukaryotic translation initiation factor 3 subunit A OS=Homo sapiens GN=EIF3A PE=1 SV=1 | LK(1)QFEER | 1 | 1.82 |
| Q9Y5Y0 | FLVCR1 | >sp\|Q9Y5Y0\|FLVC1_HUMAN Feline leukemia virus subgroup C receptor-related protein 1 OS=Homo sapiens GN=FLVCR1 PE=1 SV=1 | TVMLSK(1)QSESAI | 1 | 1.82 |
| Q9Y397 | ZDHC9 | >sp\|Q9Y397\|ZDHC9_HUMAN Palmitoyltransferase ZDHHC9 OS=Homo sapiens GN=ZDHHC9 PE=1 SV=2 | IK(1)NFQINNQIVK | 2 | 1.81 |
| P78382 | S35A1 | >sp\|P78382\|S35A1_HUMAN CMP-sialic acid transporter OS=Homo sapiens GN=SLC35A1 PE=2 SV=1 | QDTTSIQQGETASK(1)ER | 1 | 1.81 |
| O75955 | FLOT1 | >sp\|O75955\|FLOT1_HUMAN Flotillin-1 OS=Homo sapiens GN=FLOT1 PE=1 SV=3 | LTGVSISQVNHK(1)PLR | 1 | 1.80 |
| Q14677 | EPN4 | >sp\|Q14677\|EPN4_HUMAN Clathrin interactor 1 | QDAFANFANFSK(1) | 1 | 1.80 |

| | | | | | |
|---|---|---|---|---|---|
| | | OS=Homo sapiens GN=CLINT1 PE=1 SV=1 | | | |
| P05787 | K2C8 | >sp\|P05787\|K2C8_HUMAN Keratin, type II cytoskeletal 8 OS=Homo sapiens GN=KRT8 PE=1 SV=7;>P05787 SWISS-PROT:P05787 Tax_Id=9606 Gene_Symbol=KRT8 Keratin, type II cytoskeletal 8;>H-INV:HIT000292931 Tax_Id=9606 Gene_Symbol=- Similar to Keratin, type II cytoske | LQAEIEGLK(1)GQR | 12 | 1.80 |
| P00387 | NB5R3 | >sp\|P00387\|NB5R3_HUMAN NADH-cytochrome b5 reductase 3 OS=Homo sapiens GN=CYB5R3 PE=1 SV=3 | TVK(1)SVGMIAGGTGITPMLQVIR | 1 | 1.79 |
| Q9Y6K9 | NEMO | >sp\|Q9Y6K9\|NEMO_HUMAN NF-kappa-B essential modulator OS=Homo sapiens GN=IKBKG PE=1 SV=2 | LK(1)EEAEQHK | 3 | 1.79 |
| P08183 | MDR1 | >sp\|P08183\|MDR1_HUMAN Multidrug resistance protein 1 OS=Homo sapiens GN=ABCB1 PE=1 SV=3 | ELLAYAK(1)AGAVAEEVLAAIR | 1 | 1.79 |
| Q16850 | CP51A | >sp\|Q16850\|CP51A_HUMAN Lanosterol 14-alpha demethylase OS=Homo sapiens GN=CYP51A1 PE=1 SV=3 | QHVSIIEK(1)ETK | 3 | 1.78 |
| Q9HD45 | TM9S3 | >sp\|Q9HD45\|TM9S3_HUMAN Transmembrane 9 superfamily member 3 OS=Homo sapiens GN=TM9SF3 PE=1 SV=2 | IYTNVK(1)ID | 5 | 1.77 |
| P49585 | PCY1A | >sp\|P49585\|PCY1A_HUMAN Choline-phosphate cytidylyltransferase A OS=Homo sapiens GN=PCYT1A PE=1 SV=2 | VEEK(1)SIDLIQK | 2 | 1.77 |
| Q9NPA0 | EMC7 | >sp\|Q9NPA0\|EMC7_HUMAN ER membrane protein complex subunit 7 OS=Homo sapiens GN=EMC7 PE=1 SV=1 | LFSSK(0.999)SSGK(0.001) | 5 | 1.76 |
| P08183 | MDR1 | >sp\|P08183\|MDR1_HUMAN Multidrug resistance protein 1 OS=Homo sapiens GN=ABCB1 PE=1 SV=3;>sp\|P21439\|MDR3_HUMAN | GTQLSGGQK(1)QR | 2 | 1.74 |

| | | | | | |
|---|---|---|---|---|---|
| | | Phosphatidylcholine translocator ABCB4 OS=Homo sapiens GN=ABCB4 PE=1 SV=2 | | | |
| Q9UPY5 | XCT | >sp\|Q9UPY5\|XCT_HUMAN Cystine/glutamate transporter OS=Homo sapiens GN=SLC7A11 PE=1 SV=1 | K(1)PVVSTISK | 1 | 1.74 |
| P56937 | DHB7 | >sp\|P56937\|DHB7_HUMAN 3-keto-steroid reductase OS=Homo sapiens GN=HSD17B7 PE=1 SV=1 | VTIQK(1)TDNQAR | 3 | 1.73 |
| Q15843 | NEDD8 | >sp\|Q15843\|NEDD8_HUMAN NEDD8 OS=Homo sapiens GN=NEDD8 PE=1 SV=1 | QMNDEK(0.995)TAADYK(0.005) | 1 | 1.73 |
| Q03519 | TAP2 | >sp\|Q03519\|TAP2_HUMAN Antigen peptide transporter 2 OS=Homo sapiens GN=TAP2 PE=1 SV=1 | QDLGFFQETK(1)TGELNSR | 3 | 1.73 |
| Q8NBQ5 | DHB11 | >sp\|Q8NBQ5\|DHB11_HUMAN Estradiol 17-beta-dehydrogenase 11 OS=Homo sapiens GN=HSD17B11 PE=1 SV=3 | LTAYEFAK(0.941)LK(0.059) | 1 | 1.71 |
| Q99569 | PKP4 | >sp\|Q99569\|PKP4_HUMAN Plakophilin-4 OS=Homo sapiens GN=PKP4 PE=1 SV=2;>sp\|Q9UQB3\|CTND2_HUMAN Catenin delta-2 OS=Homo sapiens GN=CTNND2 PE=1 SV=3 | SPSIDSIQK(1)DPR | 2 | 1.70 |
| Q12846 | STX4 | >sp\|Q12846\|STX4_HUMAN Syntaxin-4 OS=Homo sapiens GN=STX4 PE=1 SV=2 | LGNK(1)VQELEK | 9 | 1.70 |
| Q99541 | PLIN2 | >sp\|Q99541\|PLIN2_HUMAN Perilipin-2 OS=Homo sapiens GN=PLIN2 PE=1 SV=2 | TK(1)SVVSGSINTVLGSR | 22 | 1.69 |
| Q8WUM9 | S20A1 | >sp\|Q8WUM9\|S20A1_HUMAN Sodium-dependent phosphate transporter 1 OS=Homo sapiens GN=SLC20A1 PE=1 SV=1 | DSGLYK(1)ELLHK | 7 | 1.69 |
| P53985 | MOT1 | >sp\|P53985\|MOT1_HUMAN Monocarboxylate transporter 1 OS=Homo sapiens GN=SLC16A1 PE=1 SV=3 | ESK(1)EEETSIDVAGKPNEVTK | 10 | 1.69 |
| Q9NRX5 | SERC1 | >sp\|Q9NRX5\|SERC1_HUMAN Serine incorporator 1 | TSNNSQVNK(1)LTLTSDESTLIEDGGAR | 1 | 1.69 |

| | | | | | |
|---|---|---|---|---|---|
| | | OS=Homo sapiens GN=SERINC1 PE=1 SV=1 | | | |
| O9599 9 | BCL1 0 | >sp\|O95999\|BCL10_HUM AN B-cell lymphoma/leukemia 10 OS=Homo sapiens GN=BCL10 PE=1 SV=1 | SNSDESNFSEK(1)LR | 1 | 1.69 |
| P05023 | AT1A 1 | >sp\|P05023\|AT1A1_HUM AN Sodium/potassium-transporting ATPase subunit alpha-1 OS=Homo sapiens GN=ATP1A1 PE=1 SV=1;>sp\|P13637\|AT1A3_ HUMAN Sodium/potassium-transporting ATPase subunit alpha-3 OS=Homo sapiens GN=ATP1A3 PE=1 SV=3;>sp\|P50993\|AT1A2_ HUMAN Sodium/po | QGAIVAVTGDGVNDSPALK(0.786)K(0.2 14) | 2 | 1.68 |
| Q9303 4 | CUL5 | >sp\|Q93034\|CUL5_HUMA N Cullin-5 OS=Homo sapiens GN=CUL5 PE=1 SV=4 | TQEAIIQIMK(1)MR | 6 | 1.68 |
| Q3SX M5 | HSD L1 | >sp\|Q3SXM5\|HSDL1_HU MAN Inactive hydroxysteroid dehydrogenase-like protein 1 OS=Homo sapiens GN=HSDL1 PE=1 SV=3 | LQVVAK(1)DIADTYK | 1 | 1.68 |
| Q6ZT2 1 | TMP PE | >sp\|Q6ZT21\|TMPPE_HUM AN Transmembrane protein with metallophosphoesterase domain OS=Homo sapiens GN=TMPPE PE=2 SV=2 | VVGSLEK(1)TR | 5 | 1.66 |
| P23634 | AT2B 4 | >sp\|P23634\|AT2B4_HUM AN Plasma membrane calcium-transporting ATPase 4 OS=Homo sapiens GN=ATP2B4 PE=1 SV=2 | NEK(1)GEVEQEK | 3 | 1.66 |
| O1525 8 | RER1 | >sp\|O15258\|RER1_HUMA N Protein RER1 OS=Homo sapiens GN=RER1 PE=1 SV=1 | SEGDSVGESVHGK(1)PSVVYR | 1 | 1.65 |
| Q8N1F 7 | NUP9 3 | >sp\|Q8N1F7\|NUP93_HUM AN Nuclear pore complex protein Nup93 OS=Homo sapiens GN=NUP93 PE=1 SV=2 | LSPATENK(1)LR | 2 | 1.65 |
| Q9H44 4 | CHM 4B | >sp\|Q9H444\|CHM4B_HU MAN Charged multivesicular body protein | AGK(1)GGPTPQEAIQR | 8 | 1.65 |

| | | | | | |
|---|---|---|---|---|---|
| | | 4b OS=Homo sapiens GN=CHMP4B PE=1 SV=1 | | | |
| O14495 | PLPP3 | >sp\|O14495\|PLPP3_HUMAN Phospholipid phosphatase 3 OS=Homo sapiens GN=PLPP3 PE=1 SV=1 | AIVPESK(1)NGGSPALNNNPR | 11 | 1.64 |
| O15258 | RER1 | >sp\|O15258\|RER1_HUMAN Protein RER1 OS=Homo sapiens GN=RER1 PE=1 SV=1 | EDAGK(1)AFAS | 2 | 1.63 |
| Q9Y3P4 | RHBD3 | >sp\|Q9Y3P4\|RHBD3_HUMAN Rhomboid domain-containing protein 3 OS=Homo sapiens GN=RHBDD3 PE=2 SV=1 | VEGAVSLLVGGQVGTETLVTHGK(1)GGPAHSEGPGPP | 1 | 1.62 |
| O75396 | SC22B | >sp\|O75396\|SC22B_HUMAN Vesicle-trafficking protein SEC22b OS=Homo sapiens GN=SEC22B PE=1 SV=4 | K(1)LNEQSPTR | 1 | 1.61 |
| Q9HC07 | TM165 | >sp\|Q9HC07\|TM165_HUMAN Transmembrane protein 165 OS=Homo sapiens GN=TMEM165 PE=1 SV=1 | TK(1)LLNGPGDVETGTSITVPQK | 6 | 1.61 |
| Q9UFH2 | DYH17 | >sp\|Q9UFH2\|DYH17_HUMAN Dynein heavy chain 17, axonemal OS=Homo sapiens GN=DNAH17 PE=1 SV=2 | NVTEK(0.5)QK(0.5) | 5 | 1.61 |
| Q9H6H4 | REEP4 | >sp\|Q9H6H4\|REEP4_HUMAN Receptor expression-enhancing protein 4 OS=Homo sapiens GN=REEP4 PE=1 SV=1 | SYETVLSFGK(1)R | 2 | 1.60 |
| Q9NUJ7 | PLCX1 | >sp\|Q9NUJ7\|PLCX1_HUMAN PI-PLC X domain-containing protein 1 OS=Homo sapiens GN=PLCXD1 PE=2 SV=1 | VK(1)TEALIR | 11 | 1.59 |
| P55085 | PAR2 | >sp\|P55085\|PAR2_HUMAN Proteinase-activated receptor 2 OS=Homo sapiens GN=F2RL1 PE=1 SV=1 | K(1)SSSYSSSSTTVK | 2 | 1.58 |
| Q9UFH2 | DYH17 | >sp\|Q9UFH2\|DYH17_HUMAN Dynein heavy chain 17, axonemal OS=Homo sapiens GN=DNAH17 PE=1 SV=2 | NVTEK(0.981)QK(0.019) | 5 | 1.56 |
| Q9HC07 | TM165 | >sp\|Q9HC07\|TM165_HUMAN Transmembrane protein 165 OS=Homo sapiens | K(0.984)K(0.016)DEEFQR | 1 | 1.56 |

| | | | | | |
|---|---|---|---|---|---|
| | | GN=TMEM165 PE=1 SV=1 | | | |
| O15260 | SURF4 | >sp\|O15260\|SURF4_HUMAN Surfeit locus protein 4 OS=Homo sapiens GN=SURF4 PE=1 SV=3 | SEGK(1)SMFAGVPTMR | 1 | 1.55 |
| Q8NBQ5 | DHB11 | >sp\|Q8NBQ5\|DHB11_HUMAN Estradiol 17-beta-dehydrogenase 11 OS=Homo sapiens GN=HSD17B11 PE=1 SV=3 | EDIYSSAK(0.862)K(0.138) | 1 | 1.55 |
| P24001 | IL32 | >sp\|P24001\|IL32_HUMAN Interleukin-32 OS=Homo sapiens GN=IL32 PE=1 SV=3 | FYDK(1)MQNAESGR | 5 | 1.55 |
| Q99650 | OSMR | >sp\|Q99650\|OSMR_HUMAN Oncostatin-M-specific receptor subunit beta OS=Homo sapiens GN=OSMR PE=1 SV=1 | SLTETELTK(1)PNYLYLLPTEK | 2 | 1.54 |
| P56747 | CLD6 | >sp\|P56747\|CLD6_HUMAN Claudin-6 OS=Homo sapiens GN=CLDN6 PE=1 SV=2 | GPSEYPTK(1)NYV | 2 | 1.53 |
| P13639 | EF2 | >sp\|P13639\|EF2_HUMAN Elongation factor 2 OS=Homo sapiens GN=EEF2 PE=1 SV=4 | YFDPANGK(0.978)FSK(0.022) | 1 | 1.53 |
| O14495 | PLPP3 | >sp\|O14495\|PLPP3_HUMAN Phospholipid phosphatase 3 OS=Homo sapiens GN=PLPP3 PE=1 SV=1 | MQNYK(0.996)YDK(0.004) | 5 | 1.52 |
| P08034 | CXB1 | >sp\|P08034\|CXB1_HUMAN Gap junction beta-1 protein OS=Homo sapiens GN=GJB1 PE=1 SV=1 | LSPEYK(1)QNEINK | 10 | 1.52 |
| Q15738 | NSDHL | >sp\|Q15738\|NSDHL_HUMAN Sterol-4-alpha-carboxylate 3-dehydrogenase, decarboxylating OS=Homo sapiens GN=NSDHL PE=1 SV=2 | VNADIEK(0.992)VNQNQAK(0.008) | 2 | 1.51 |
| Q8TCJ2 | STT3B | >sp\|Q8TCJ2\|STT3B_HUMAN Dolichyl-diphosphooligosaccharide--protein glycosyltransferase subunit STT3B OS=Homo sapiens GN=STT3B PE=1 SV=1 | AEPSAPESK(0.4)HK(0.6) | 1 | 1.50 |
| O95573 | ACSL3 | >sp\|O95573\|ACSL3_HUMAN Long-chain-fatty-acid--CoA ligase 3 OS=Homo | EVLNEEDEVQPNGK(0.787)IFK(0.213) | 1 | 1.49 |

| | | | | | |
|---|---|---|---|---|---|
| | | sapiens GN=ACSL3 PE=1 SV=3 | | | |
| Q6NUQ4 | TM214 | >sp\|Q6NUQ4\|TM214_HUMAN Transmembrane protein 214 OS=Homo sapiens GN=TMEM214 PE=1 SV=2 | ATK(1)TAGVGR | 1 | 1.49 |
| Q6NUK4 | REEP3 | >sp\|Q6NUK4\|REEP3_HUMAN Receptor expression-enhancing protein 3 OS=Homo sapiens GN=REEP3 PE=1 SV=1 | FLHPLLSSK(1)ER | 3 | 1.49 |
| O75396 | SC22B | >sp\|O75396\|SC22B_HUMAN Vesicle-trafficking protein SEC22b OS=Homo sapiens GN=SEC22B PE=1 SV=4 | GEALSALDSK(1)ANNLSSLSK | 3 | 1.48 |
| Q9Y3E5 | PTH2 | >sp\|Q9Y3E5\|PTH2_HUMAN Peptidyl-tRNA hydrolase 2, mitochondrial OS=Homo sapiens GN=PTRH2 PE=1 SV=1 | NDLK(0.985)MGK(0.015) | 3 | 1.48 |
| Q99735 | MGST2 | >sp\|Q99735\|MGST2_HUMAN Microsomal glutathione S-transferase 2 OS=Homo sapiens GN=MGST2 PE=1 SV=1 | YK(1)VTPPAVTGSPEFER | 3 | 1.47 |
| Q15758 | AAAT | >sp\|Q15758\|AAAT_HUMAN Neutral amino acid transporter B(0) OS=Homo sapiens GN=SLC1A5 PE=1 SV=2 | GPAGDATVASEK(1)ESVM | 2 | 1.47 |
| Q9Y653 | GPR56 | >sp\|Q9Y653\|GPR56_HUMAN G-protein coupled receptor 56 OS=Homo sapiens GN=GPR56 PE=1 SV=2 | GGPSPLK(1)SNSDSAR | 2 | 1.46 |
| P37173 | TGFR2 | >sp\|P37173\|TGFR2_HUMAN TGF-beta receptor type-2 OS=Homo sapiens GN=TGFBR2 PE=1 SV=2 | FAEVYK(0.964)AK(0.036) | 4 | 1.46 |
| P08183 | MDR1 | >sp\|P08183\|MDR1_HUMAN Multidrug resistance protein 1 OS=Homo sapiens GN=ABCB1 PE=1 SV=3 | FYDPLAGK(0.999)VLLDGK(0.001) | 1 | 1.46 |
| Q9P2E9 | RRBP1 | >sp\|Q9P2E9\|RRBP1_HUMAN Ribosome-binding protein 1 OS=Homo sapiens GN=RRBP1 PE=1 SV=4 | GNTPATGTTQGK(0.449)K(0.551) | 1 | 1.45 |
| P68363 | TBA1B | >sp\|P68363\|TBA1B_HUMAN Tubulin alpha-1B chain OS=Homo sapiens GN=TUBA1B PE=1 SV=1;>sp\|Q71U36\|TBA1A_HUMAN Tubulin alpha- | DVNAAIATIK(0.14)TK(0.86) | 9 | 1.45 |

| | | | | | |
|---|---|---|---|---|---|
| | | 1A chain OS=Homo sapiens GN=TUBA1A PE=1 SV=1;>sp\|Q13748\|TBA3C_HUMAN Tubulin alpha-3C/D chain OS=Homo sapiens GN=TUBA3C PE=1 SV=3;>sp\|Q6PE | | | |
| Q99541 | PLIN2 | >sp\|Q99541\|PLIN2_HUMAN Perilipin-2 OS=Homo sapiens GN=PLIN2 PE=1 SV=2 | DSVASTITGVMDK(0.323)TK(0.677) | 5 | 1.45 |
| Q99624 | S38A3 | >sp\|Q99624\|S38A3_HUMAN Sodium-coupled neutral amino acid transporter 3 OS=Homo sapiens GN=SLC38A3 PE=1 SV=1 | SCMEGK(0.999)SFLQK(0.001) | 1 | 1.45 |
| P05023 | AT1A1 | >sp\|P05023\|AT1A1_HUMAN Sodium/potassium-transporting ATPase subunit alpha-1 OS=Homo sapiens GN=ATP1A1 PE=1 SV=1;>sp\|P13637\|AT1A3_HUMAN Sodium/potassium-transporting ATPase subunit alpha-3 OS=Homo sapiens GN=ATP1A3 PE=1 SV=3;>sp\|P50993\|AT1A2_HUMAN Sodium/po | AIAK(1)GVGIISEGNETVEDIAAR | 3 | 1.45 |
| O15427 | MOT4 | >sp\|O15427\|MOT4_HUMAN Monocarboxylate transporter 4 OS=Homo sapiens GN=SLC16A3 PE=1 SV=1 | LHK(1)PPADSGVDLR | 12 | 1.43 |
| O14495 | PLPP3 | >sp\|O14495\|PLPP3_HUMAN Phospholipid phosphatase 3 OS=Homo sapiens GN=PLPP3 PE=1 SV=1 | YDK(1)AIVPESK | 8 | 1.42 |
| P54727 | RD23B | >sp\|P54727\|RD23B_HUMAN UV excision repair protein RAD23 homolog B OS=Homo sapiens GN=RAD23B PE=1 SV=1 | LIYAGK(0.999)ILNDDTALK(0.001) | 4 | 1.42 |
| P62834 | RAP1A | >sp\|P62834\|RAP1A_HUMAN Ras-related protein Rap-1A OS=Homo sapiens GN=RAP1A PE=1 SV=1;>sp\|P61224\|RAP1B_HUMAN Ras-related protein Rap-1b OS=Homo sapiens GN=RAP1B PE=1 SV=1;>sp\|A6NIZ1\|RP1BL_HUMAN Ras-related | VVGK(1)EQGQNLAR | 2 | 1.42 |

| | | | | | |
|---|---|---|---|---|---|
| | | protein Rap-1b-like protein OS=Homo sapiens PE=2 SV | | | |
| Q08357 | S20A2 | >sp\|Q08357\|S20A2_HUMAN Sodium-dependent phosphate transporter 2 OS=Homo sapiens GN=SLC20A2 PE=1 SV=1 | LVGDTVSYSK(0.5)K(0.5) | 1 | 1.41 |
| Q08357 | S20A2 | >sp\|Q08357\|S20A2_HUMAN Sodium-dependent phosphate transporter 2 OS=Homo sapiens GN=SLC20A2 PE=1 SV=1 | LVGDTVSYSK(0.5)K(0.5) | 1 | 1.41 |
| Q9NV96 | CC50A | >sp\|Q9NV96\|CC50A_HUMAN Cell cycle control protein 50A OS=Homo sapiens GN=TMEM30A PE=1 SV=1 | DEVDGGPPCAPGGTAK(1)TR | 2 | 1.41 |
| P0DMV9 | HS71B | >sp\|P0DMV9\|HS71B_HUMAN Heat shock 70 kDa protein 1B OS=Homo sapiens GN=HSPA1B PE=1 SV=1;>sp\|P0DMV8\|HS71A_HUMAN Heat shock 70 kDa protein 1A OS=Homo sapiens GN=HSPA1A PE=1 SV=1;>sp\|P11142\|HSP7C_HUMAN Heat shock cognate 71 kDa protein OS=Homo sapiens GN=HSPA | ITITNDK(1)GR | 36 | 1.40 |
| Q9H3P7 | GCP60 | >sp\|Q9H3P7\|GCP60_HUMAN Golgi resident protein GCP60 OS=Homo sapiens GN=ACBD3 PE=1 SV=4 | EK(1)IQQDADSVITVGR | 1 | 1.40 |
| Q96A57 | TM230 | >sp\|Q96A57\|TM230_HUMAN Transmembrane protein 230 OS=Homo sapiens GN=TMEM230 PE=1 SV=1 | TNLATGIPSSK(0.962)VK(0.038) | 8 | 1.39 |
| P07910 | HNRPC | >sp\|P07910\|HNRPC_HUMAN Heterogeneous nuclear ribonucleoproteins C1/C2 OS=Homo sapiens GN=HNRNPC PE=1 SV=4 | ASNVTNK(1)TDPR | 3 | 1.39 |
| Q96JJ7 | TMX3 | >sp\|Q96JJ7\|TMX3_HUMAN Protein disulfide-isomerase TMX3 OS=Homo sapiens GN=TMX3 PE=1 SV=2 | YEVSK(1)SENENQEQIEESK | 1 | 1.38 |
| Q9H8H3 | METT7A | >sp\|Q9H8H3\|MET7A_HUMAN Methyltransferase-like protein 7A OS=Homo | VTCIDPNPNFEK(0.996)FLIK(0.004) | 4 | 1.38 |

| | | | | | |
|---|---|---|---|---|---|
| | | sapiens GN=METTL7A PE=1 SV=1 | | | |
| P78536 | ADA 17 | >sp\|P78536\|ADA17_HUMAN Disintegrin and metalloproteinase domain-containing protein 17 OS=Homo sapiens GN=ADAM17 PE=1 SV=1 | IIK(1)PFPAPQTPGR | 1 | 1.37 |
| Q9NU 53 | GIN M1 | >sp\|Q9NU53\|GINM1_HUMAN Glycoprotein integral membrane protein 1 OS=Homo sapiens GN=GINM1 PE=2 SV=1 | VDVIPVTAINLYPDGPEK(1)R | 6 | 1.37 |
| Q9HC 07 | TM16 5 | >sp\|Q9HC07\|TM165_HUMAN Transmembrane protein 165 OS=Homo sapiens GN=TMEM165 PE=1 SV=1 | MSPDEGQEELEEVQAELK(0.5)K(0.5) | 3 | 1.37 |
| Q9C0 H2 | TTY H3 | >sp\|Q9C0H2\|TTYH3_HUMAN Protein tweety homolog 3 OS=Homo sapiens GN=TTYH3 PE=1 SV=3 | AK(1)YLATSQPRPDSSGSH | 11 | 1.37 |
| Q96LD 4 | TRI4 7 | >sp\|Q96LD4\|TRI47_HUMAN Tripartite motif-containing protein 47 OS=Homo sapiens GN=TRIM47 PE=1 SV=2 | ALQEAEQSK(1)VLSAVEDR | 2 | 1.37 |
| P27105 | STO M | >sp\|P27105\|STOM_HUMAN Erythrocyte band 7 integral membrane protein OS=Homo sapiens GN=STOM PE=1 SV=3 | LPDSFK(0.999)DSPSK(0.001) | 1 | 1.36 |
| Q9HD B5 | NRX 3B | >sp\|Q9HDB5\|NRX3B_HUMAN Neurexin-3-beta OS=Homo sapiens GN=NRXN3 PE=1 SV=4;>sp\|Q9Y4C0\|NRX3A_HUMAN Neurexin-3 OS=Homo sapiens GN=NRXN3 PE=1 SV=4 | LAVGFSTTVK(1) | 2 | 1.36 |
| P08183 | MDR 1 | >sp\|P08183\|MDR1_HUMAN Multidrug resistance protein 1 OS=Homo sapiens GN=ABCB1 PE=1 SV=3;>sp\|P21439\|MDR3_HUMAN Phosphatidylcholine translocator ABCB4 OS=Homo sapiens GN=ABCB4 PE=1 SV=2 | VVQEALDK(1)AR | 3 | 1.36 |
| P62820 | RAB1 A | >sp\|P62820\|RAB1A_HUMAN Ras-related protein Rab-1A OS=Homo sapiens GN=RAB1A PE=1 | YASENVNK(0.998)LLVGNK(0.002) | 1 | 1.36 |

| | | | | | |
|---|---|---|---|---|---|
| | | SV=3;>sp\|Q9H0U4\|RAB1B_HUMAN Ras-related protein Rab-1B OS=Homo sapiens GN=RAB1B PE=1 SV=1 | | | |
| Q8IYS2 | K2013 | >sp\|Q8IYS2\|K2013_HUMAN Uncharacterized protein KIAA2013 OS=Homo sapiens GN=KIAA2013 PE=2 SV=1 | SK(1)EDPSV | 2 | 1.36 |
| P53985 | MOT1 | >sp\|P53985\|MOT1_HUMAN Monocarboxylate transporter 1 OS=Homo sapiens GN=SLC16A1 PE=1 SV=3 | K(1)DLHDANTDLIGR | 3 | 1.36 |
| Q86TG7 | PEG10 | >sp\|Q86TG7\|PEG10_HUMAN Retrotransposon-derived protein PEG10 OS=Homo sapiens GN=PEG10 PE=1 SV=2 | NVK(1)DGLITPTIAPNGAQVLQVK | 7 | 1.35 |
| Q99541 | PLIN2 | >sp\|Q99541\|PLIN2_HUMAN Perilipin-2 OS=Homo sapiens GN=PLIN2 PE=1 SV=2 | GAVTGAK(1)DAVTTTVTGAK | 1 | 1.35 |
| Q96GF1 | RN185 | >sp\|Q96GF1\|RN185_HUMAN E3 ubiquitin-protein ligase RNF185 OS=Homo sapiens GN=RNF185 PE=1 SV=1 | DK(1)VIPLYGR | 1 | 1.35 |
| Q8NC54 | KCT2 | >sp\|Q8NC54\|KCT2_HUMAN Keratinocyte-associated transmembrane protein 2 OS=Homo sapiens GN=KCT2 PE=2 SV=2 | LDQNVNEAMPSLK(1)ITNDYIF | 5 | 1.35 |
| P23458 | JAK1 | >sp\|P23458\|JAK1_HUMAN Tyrosine-protein kinase JAK1 OS=Homo sapiens GN=JAK1 PE=1 SV=2 | DFLK(1)EFNNK | 54 | 1.35 |
| Q8TAV3 | CP2W1 | >sp\|Q8TAV3\|CP2W1_HUMAN Cytochrome P450 2W1 OS=Homo sapiens GN=CYP2W1 PE=1 SV=2 | QK(1)TVVLTGFEAVK | 3 | 1.34 |
| P0CG47 | UBB | >sp\|P0CG47\|UBB_HUMAN Polyubiquitin-B OS=Homo sapiens GN=UBB PE=1 SV=1;>sp\|P0CG48\|UBC_HUMAN Polyubiquitin-C OS=Homo sapiens GN=UBC PE=1 SV=3;>sp\|P62979\|RS27A_HUMAN Ubiquitin-40S ribosomal protein S27a OS=Homo sapiens GN=RPS27A PE=1 | TLSDYNIQK(1)ESTLHLVLR | 752 | 1.34 |

| | | | | | |
|---|---|---|---|---|---|
| | | SV=2;>sp\|P62987\|RL40_HUMA | | | |
| Q12893 | TM115 | >sp\|Q12893\|TM115_HUMAN Transmembrane protein 115 OS=Homo sapiens GN=TMEM115 PE=1 SV=1 | QLALK(1)ALNER | 7 | 1.33 |
| Q8TC12 | RDH11 | >sp\|Q8TC12\|RDH11_HUMAN Retinol dehydrogenase 11 OS=Homo sapiens GN=RDH11 PE=1 SV=2;>sp\|Q96NR8\|RDH12_HUMAN Retinol dehydrogenase 12 OS=Homo sapiens GN=RDH12 PE=1 SV=3 | LDLSDTK(1)SIR | 3 | 1.33 |
| Q9H8H3 | METT7A | >sp\|Q9H8H3\|MET7A_HUMAN Methyltransferase-like protein 7A OS=Homo sapiens GN=METTL7A PE=1 SV=1 | FLIK(1)SIAENR | 2 | 1.33 |
| Q96CV9 | OPTN | >sp\|Q96CV9\|OPTN_HUMAN Optineurin OS=Homo sapiens GN=OPTN PE=1 SV=2 | QLQMDEMK(1)QTIAK | 1 | 1.32 |
| Q9GZM5 | YIPF3 | >sp\|Q9GZM5\|YIPF3_HUMAN Protein YIPF3 OS=Homo sapiens GN=YIPF3 PE=1 SV=1 | QVADQMWQAGK(1)R | 2 | 1.31 |
| P48029 | SC6A8 | >sp\|P48029\|SC6A8_HUMAN Sodium- and chloride-dependent creatine transporter 1 OS=Homo sapiens GN=SLC6A8 PE=1 SV=1 | SAENGIYSVSGDEK(0.462)K(0.538) | 3 | 1.31 |
| P15260 | INGR1 | >sp\|P15260\|INGR1_HUMAN Interferon gamma receptor 1 OS=Homo sapiens GN=IFNGR1 PE=1 SV=1 | SIILPK(1)SLISVVR | 8 | 1.30 |
| P48065 | S6A12 | >sp\|P48065\|S6A12_HUMAN Sodium- and chloride-dependent betaine transporter OS=Homo sapiens GN=SLC6A12 PE=1 SV=2 | EGLIAGEK(1)ETHL | 9 | 1.30 |
| Q99541 | PLIN2 | >sp\|Q99541\|PLIN2_HUMAN Perilipin-2 OS=Homo sapiens GN=PLIN2 PE=1 SV=2 | DSVASTITGVMDK(0.977)TK(0.023) | 5 | 1.30 |
| Q86YT5 | S13A5 | >sp\|Q86YT5\|S13A5_HUMAN Solute carrier family 13 member 5 OS=Homo sapiens GN=SLC13A5 PE=1 SV=1 | AK(1)ELPGSQVIFEGPTLGQQEDQER | 1 | 1.30 |

| | | | | | |
|---|---|---|---|---|---|
| Q01650 | LAT1 | >sp\|Q01650\|LAT1_HUMAN Large neutral amino acids transporter small subunit 1 OS=Homo sapiens GN=SLC7A5 PE=1 SV=2 | MLAAK(1)SADGSAPAGEGEGVTLQR | 6 | 1.30 |
| P10586 | PTPRF | >sp\|P10586\|PTPRF_HUMAN Receptor-type tyrosine-protein phosphatase F OS=Homo sapiens GN=PTPRF PE=1 SV=2 | TFALHK(0.995)SGSSEK(0.005) | 1 | 1.29 |
| P20020 | AT2B1 | >sp\|P20020\|AT2B1_HUMAN Plasma membrane calcium-transporting ATPase 1 OS=Homo sapiens GN=ATP2B1 PE=1 SV=3;>sp\|Q16720\|AT2B3_HUMAN Plasma membrane calcium-transporting ATPase 3 OS=Homo sapiens GN=ATP2B3 PE=1 SV=3;>sp\|Q01814\|AT2B2_HUMAN Plasma membrane calcium | NEK(1)GEIEQER | 5 | 1.29 |
| Q9BY71 | LRRC3 | >sp\|Q9BY71\|LRRC3_HUMAN Leucine-rich repeat-containing protein 3 OS=Homo sapiens GN=LRRC3 PE=1 SV=1 | SLPSAPASK(1)DPIGPGP | 3 | 1.29 |
| P53985 | MOT1 | >sp\|P53985\|MOT1_HUMAN Monocarboxylate transporter 1 OS=Homo sapiens GN=SLC16A1 PE=1 SV=3 | EEETSIDVAGK(0.003)PNEVTK(0.996)AAESPDQK | 1 | 1.29 |
| P48066 | S6A11 | >sp\|P48066\|S6A11_HUMAN Sodium- and chloride-dependent GABA transporter 3 OS=Homo sapiens GN=SLC6A11 PE=2 SV=1 | LK(1)SDGTIAAITEK | 3 | 1.29 |
| P06213 | INSR | >sp\|P06213\|INSR_HUMAN Insulin receptor OS=Homo sapiens GN=INSR PE=1 SV=4 | DIIK(1)GEAETR | 4 | 1.28 |
| Q92783 | STAM1 | >sp\|Q92783\|STAM1_HUMAN Signal transducing adapter molecule 1 OS=Homo sapiens GN=STAM PE=1 SV=3 | ASPALVAK(1)DPGTVANK | 2 | 1.28 |
| Q13501 | SQSTM | >sp\|Q13501\|SQSTM_HUMAN Sequestosome-1 OS=Homo sapiens GN=SQSTM1 PE=1 SV=1 | AYLLGK(1)EDAAR | 4 | 1.28 |
| Q8IY22 | CMIP | >sp\|Q8IY22\|CMIP_HUMAN C-Maf-inducing protein | ILTSK(1)FLR | 10 | 1.27 |

| | | | | | |
|---|---|---|---|---|---|
| | | OS=Homo sapiens GN=CMIP PE=1 SV=3 | | | |
| Q8IY22 | CMIP | >sp\|Q8IY22\|CMIP_HUMAN C-Maf-inducing protein OS=Homo sapiens GN=CMIP PE=1 SV=3 | TFLSK(1)ILTSK | 12 | 1.27 |
| Q99808 | S29A1 | >sp\|Q99808\|S29A1_HUMAN Equilibrative nucleoside transporter 1 OS=Homo sapiens GN=SLC29A1 PE=1 SV=3 | AGK(1)EESGVSVSNSQPTNESHSIK | 5 | 1.27 |
| Q13501 | SQSTM | >sp\|Q13501\|SQSTM_HUMAN Sequestosome-1 OS=Homo sapiens GN=SQSTM1 PE=1 SV=1 | CSVCPDYDLCSVCEGK(1)GLHR | 2 | 1.26 |
| Q9BXS4 | TMM59 | >sp\|Q9BXS4\|TMM59_HUMAN Transmembrane protein 59 OS=Homo sapiens GN=TMEM59 PE=1 SV=1 | SK(1)TEDHEEAGPLPTK(1)VNLAHSEI | 1 | 1.26 |
| O75396 | SC22B | >sp\|O75396\|SC22B_HUMAN Vesicle-trafficking protein SEC22b OS=Homo sapiens GN=SEC22B PE=1 SV=4 | DLQQYQSQAK(1)QLFR | 2 | 1.26 |
| P07437 | TBB5 | >sp\|P07437\|TBB5_HUMAN Tubulin beta chain OS=Homo sapiens GN=TUBB PE=1 SV=2 | ISVYYNEATGGK(1)YVPR | 1 | 1.26 |
| P55085 | PAR2 | >sp\|P55085\|PAR2_HUMAN Proteinase-activated receptor 2 OS=Homo sapiens GN=F2RL1 PE=1 SV=1 | SSSYSSSSTTVK(1)TSY | 8 | 1.26 |
| P05026 | AT1B1 | >sp\|P05026\|AT1B1_HUMAN Sodium/potassium-transporting ATPase subunit beta-1 OS=Homo sapiens GN=ATP1B1 PE=1 SV=1 | FIWNSEK(0.661)K(0.339) | 1 | 1.25 |
| Q9C0B5 | ZDHC5 | >sp\|Q9C0B5\|ZDHC5_HUMAN Palmitoyltransferase ZDHHC5 OS=Homo sapiens GN=ZDHHC5 PE=1 SV=2;>sp\|Q9ULC8\|ZDHC8_HUMAN Probable palmitoyltransferase ZDHHC8 OS=Homo sapiens GN=ZDHHC8 PE=1 SV=3 | TTNEQVTGK(1)FR | 5 | 1.25 |
| Q9UPY5 | XCT | >sp\|Q9UPY5\|XCT_HUMAN Cystine/glutamate transporter OS=Homo | LPSLGNK(1)EPPGQEK | 3 | 1.25 |

| | | | | | |
|---|---|---|---|---|---|
| | | sapiens GN=SLC7A11 PE=1 SV=1 | | | |
| P53985 | MOT1 | >sp\|P53985\|MOT1_HUMAN Monocarboxylate transporter 1 OS=Homo sapiens GN=SLC16A1 PE=1 SV=3 | ESKEEETSIDVAGK(1)PNEVTK | 10 | 1.25 |
| Q16625 | OCLN | >sp\|Q16625\|OCLN_HUMAN Occludin OS=Homo sapiens GN=OCLN PE=1 SV=1 | YDK(1)SNILWDK | 2 | 1.24 |
| Q9ULC5 | ACSL5 | >sp\|Q9ULC5\|ACSL5_HUMAN Long-chain-fatty-acid--CoA ligase 5 OS=Homo sapiens GN=ACSL5 PE=1 SV=1 | LGVK(1)GSFEELCQNQVVR | 1 | 1.24 |
| Q9Y508 | RN114 | >sp\|Q9Y508\|RN114_HUMAN E3 ubiquitin-protein ligase RNF114 OS=Homo sapiens GN=RNF114 PE=1 SV=1 | ATIK(1)DASLQPR | 3 | 1.23 |
| Q8TB61 | S35B2 | >sp\|Q8TB61\|S35B2_HUMAN Adenosine 3'-phospho 5'-phosphosulfate transporter 1 OS=Homo sapiens GN=SLC35B2 PE=1 SV=1 | ACVFGNEPK(1)ASDEVPLAPR | 4 | 1.23 |
| Q9NZI8 | IF2B1 | >sp\|Q9NZI8\|IF2B1_HUMAN Insulin-like growth factor 2 mRNA-binding protein 1 OS=Homo sapiens GN=IGF2BP1 PE=1 SV=2 | IAPPETPDSK(1)VR | 10 | 1.22 |
| Q8NC54 | KCT2 | >sp\|Q8NC54\|KCT2_HUMAN Keratinocyte-associated transmembrane protein 2 OS=Homo sapiens GN=KCT2 PE=2 SV=2 | DGLCSK(1)TVEYHR | 5 | 1.22 |
| Q9UKJ5 | CHIC2 | >sp\|Q9UKJ5\|CHIC2_HUMAN Cysteine-rich hydrophobic domain-containing protein 2 OS=Homo sapiens GN=CHIC2 PE=1 SV=1 | SIEK(1)LLEWENNR | 10 | 1.21 |
| P08183 | MDR1 | >sp\|P08183\|MDR1_HUMAN Multidrug resistance protein 1 OS=Homo sapiens GN=ABCB1 PE=1 SV=3 | YNK(1)NLEEAK | 11 | 1.21 |
| Q9H8M9 | EVA1A | >sp\|Q9H8M9\|EVA1A_HUMAN Protein eva-1 homolog A OS=Homo sapiens GN=EVA1A PE=1 SV=1 | TLNK(1)NVFTSAEELER | 12 | 1.21 |
| P48066 | S6A11 | >sp\|P48066\|S6A11_HUMAN Sodium- and chloride-dependent GABA | SDGTIAAITEK(1)ETHF | 6 | 1.21 |

| | | | | | |
|---|---|---|---|---|---|
| | | transporter 3 OS=Homo sapiens GN=SLC6A11 PE=2 SV=1 | | | |
| Q9BT67 | NFIP1 | >sp\|Q9BT67\|NFIP1_HUMAN NEDD4 family-interacting protein 1 OS=Homo sapiens GN=NDFIP1 PE=1 SV=1 | TK(1)AEATIPLVPGR | 10 | 1.21 |
| Q9NP58 | ABCB6 | >sp\|Q9NP58\|ABCB6_HUMAN ATP-binding cassette sub-family B member 6, mitochondrial OS=Homo sapiens GN=ABCB6 PE=1 SV=1 | EAIIK(1)YQGLEWK | 9 | 1.20 |
| Q9NU53 | GINM1 | >sp\|Q9NU53\|GINM1_HUMAN Glycoprotein integral membrane protein 1 OS=Homo sapiens GN=GINM1 PE=2 SV=1 | AENLEDK(1)TCI | 3 | 1.20 |
| Q14596 | NBR1 | >sp\|Q14596\|NBR1_HUMAN Next to BRCA1 gene 1 protein OS=Homo sapiens GN=NBR1 PE=1 SV=3 | TDDLTCQQEETFLLAK(1)EER | 2 | 1.19 |
| O14672 | ADA10 | >sp\|O14672\|ADA10_HUMAN Disintegrin and metalloproteinase domain-containing protein 10 OS=Homo sapiens GN=ADAM10 PE=1 SV=1 | LPPPK(0.999)PLPGTLK(0.001) | 2 | 1.19 |
| P31946 | 1433B | >sp\|P31946\|1433B_HUMAN 14-3-3 protein beta/alpha OS=Homo sapiens GN=YWHAB PE=1 SV=3 | SELVQK(0.319)AK(0.681) | 8 | 1.19 |
| Q9Y2G8 | DJC16 | >sp\|Q9Y2G8\|DJC16_HUMAN DnaJ homolog subfamily C member 16 OS=Homo sapiens GN=DNAJC16 PE=2 SV=3 | TGK(1)TEPSFTK | 1 | 1.19 |
| Q9GZM5 | YIPF3 | >sp\|Q9GZM5\|YIPF3_HUMAN Protein YIPF3 OS=Homo sapiens GN=YIPF3 PE=1 SV=1 | GFK(1)GQLSR | 5 | 1.18 |
| Q96J02 | ITCH | >sp\|Q96J02\|ITCH_HUMAN E3 ubiquitin-protein ligase Itchy homolog OS=Homo sapiens GN=ITCH PE=1 SV=2 | TGK(1)SALDNGPQIAYVR | 1 | 1.18 |
| O00161 | SNP23 | >sp\|O00161\|SNP23_HUMAN Synaptosomal-associated protein 23 OS=Homo sapiens GN=SNAP23 PE=1 SV=1 | TITMLDEQK(1)EQLNR | 3 | 1.18 |
| P07737 | PROF1 | >sp\|P07737\|PROF1_HUMAN Profilin-1 OS=Homo | STGGAPTFNVTVTK(0.371)TDK(0.629) | 1 | 1.18 |

| | | | | | |
|---|---|---|---|---|---|
| | | sapiens GN=PFN1 PE=1 SV=2 | | | |
| Q99541 | PLIN2 | >sp\|Q99541\|PLIN2_HUMAN Perilipin-2 OS=Homo sapiens GN=PLIN2 PE=1 SV=2 | NVYSANQK(1)IQDAQDK | 8 | 1.17 |
| Q99541 | PLIN2 | >sp\|Q99541\|PLIN2_HUMAN Perilipin-2 OS=Homo sapiens GN=PLIN2 PE=1 SV=2 | EVSDSLLTSSK(1)GQLQK | 13 | 1.17 |
| Q9H444 | CHM4B | >sp\|Q9H444\|CHM4B_HUMAN Charged multivesicular body protein 4b OS=Homo sapiens GN=CHMP4B PE=1 SV=1 | SVFGK(1)LFGAGGGK | 10 | 1.17 |
| Q92887 | MRP2 | >sp\|Q92887\|MRP2_HUMAN Canalicular multispecific organic anion transporter 1 OS=Homo sapiens GN=ABCC2 PE=1 SV=3 | FLK(1)HNEVR | 4 | 1.17 |
| Q92887 | MRP2 | >sp\|Q92887\|MRP2_HUMAN Canalicular multispecific organic anion transporter 1 OS=Homo sapiens GN=ABCC2 PE=1 SV=3 | NLK(1)TFLR | 1 | 1.16 |
| Q96J02 | ITCH | >sp\|Q96J02\|ITCH_HUMAN E3 ubiquitin-protein ligase Itchy homolog OS=Homo sapiens GN=ITCH PE=1 SV=2 | FIYGNQDLFATSQSK(0.999)EFDPLGPLPPGWEK(0.001) | 2 | 1.16 |
| Q86YT5 | S13A5 | >sp\|Q86YT5\|S13A5_HUMAN Solute carrier family 13 member 5 OS=Homo sapiens GN=SLC13A5 PE=1 SV=1 | AALK(1)VLQEEYR | 1 | 1.16 |
| P52895 | AK1C2 | >sp\|P52895\|AK1C2_HUMAN Aldo-keto reductase family 1 member C2 OS=Homo sapiens GN=AKR1C2 PE=1 SV=3;>sp\|Q04828\|AK1C1_HUMAN Aldo-keto reductase family 1 member C1 OS=Homo sapiens GN=AKR1C1 PE=1 SV=1;>sp\|P42330\|AK1C3_HUMAN Aldo-keto reductase family 1 member C | GVVVLAK(1)SYNEQR | 4 | 1.16 |
| Q9NPF0 | CD320 | >sp\|Q9NPF0\|CD320_HUMAN CD320 antigen OS=Homo sapiens GN=CD320 PE=1 SV=1 | ESLLLSEQK(1)TSLP | 19 | 1.16 |
| P52895 | AK1C2 | >sp\|P52895\|AK1C2_HUMAN Aldo-keto reductase | MDSK(1)YQCVK | 7 | 1.15 |

| | | | | | |
|---|---|---|---|---|---|
| | | family 1 member C2 OS=Homo sapiens GN=AKR1C2 PE=1 SV=3;>sp\|Q04828\|AK1C1_HUMAN Aldo-keto reductase family 1 member C1 OS=Homo sapiens GN=AKR1C1 PE=1 SV=1 | | | |
| P08195 | 4F2 | >sp\|P08195\|4F2_HUMAN 4F2 cell-surface antigen heavy chain OS=Homo sapiens GN=SLC3A2 PE=1 SV=3 | VAEDEAEAAAAAK(0.997)FTGLSK(0.003) | 11 | 1.15 |
| Q15185 | TEBP | >sp\|Q15185\|TEBP_HUMAN Prostaglandin E synthase 3 OS=Homo sapiens GN=PTGES3 PE=1 SV=1 | DVNVNFEK(0.846)SK(0.154) | 1 | 1.15 |
| P58335 | ANTR2 | >sp\|P58335\|ANTR2_HUMAN Anthrax toxin receptor 2 OS=Homo sapiens GN=ANTXR2 PE=1 SV=5 | EEEEEPLPTK(0.419)K(0.581) | 13 | 1.15 |
| P22455 | FGFR4 | >sp\|P22455\|FGFR4_HUMAN Fibroblast growth factor receptor 4 OS=Homo sapiens GN=FGFR4 PE=1 SV=2 | LVLGK(1)PLGEGCFGQVVR | 7 | 1.15 |
| O15427 | MOT4 | >sp\|O15427\|MOT4_HUMAN Monocarboxylate transporter 4 OS=Homo sapiens GN=SLC16A3 PE=1 SV=1 | EVEHFLK(1)AEPEK | 4 | 1.14 |
| P37173 | TGFR2 | >sp\|P37173\|TGFR2_HUMAN TGF-beta receptor type-2 OS=Homo sapiens GN=TGFBR2 PE=1 SV=2 | DYEPPFGSK(1)VR | 1 | 1.14 |
| P04114 | APOB | >sp\|P04114\|APOB_HUMAN Apolipoprotein B-100 OS=Homo sapiens GN=APOB PE=1 SV=2 | FQFPGK(1)PGIYTR | 2 | 1.14 |
| P62937 | PPIA | >sp\|P62937\|PPIA_HUMAN Peptidyl-prolyl cis-trans isomerase A OS=Homo sapiens GN=PPIA PE=1 SV=2 | ALSTGEK(0.93)GFGYK(0.07) | 1 | 1.13 |
| Q96CV9 | OPTN | >sp\|Q96CV9\|OPTN_HUMAN Optineurin OS=Homo sapiens GN=OPTN PE=1 SV=2 | AVLK(0.989)ELSEK(0.011) | 1 | 1.13 |
| P05023 | AT1A1 | >sp\|P05023\|AT1A1_HUMAN Sodium/potassium-transporting ATPase subunit alpha-1 OS=Homo sapiens GN=ATP1A1 PE=1 SV=1 | AVFQANQENLPILK(1)R | 5 | 1.13 |

| | | | | | |
|---|---|---|---|---|---|
| Q04828 | AK1C1 | >sp\|Q04828\|AK1C1_HUMAN Aldo-keto reductase family 1 member C1 OS=Homo sapiens GN=AKR1C1 PE=1 SV=1;>sp\|P42330\|AK1C3_HUMAN Aldo-keto reductase family 1 member C3 OS=Homo sapiens GN=AKR1C3 PE=1 SV=4 | DAGLAK(1)SIGVSNFNRR | 2 | 1.13 |
| Q01650 | LAT1 | >sp\|Q01650\|LAT1_HUMAN Large neutral amino acids transporter small subunit 1 OS=Homo sapiens GN=SLC7A5 PE=1 SV=2 | ALAAPAAEEK(1)EEAR | 16 | 1.13 |
| P15260 | INGR1 | >sp\|P15260\|INGR1_HUMAN Interferon gamma receptor 1 OS=Homo sapiens GN=IFNGR1 PE=1 SV=1 | SATLETK(1)PESK | 16 | 1.13 |
| O15269 | SPTC1 | >sp\|O15269\|SPTC1_HUMAN Serine palmitoyltransferase 1 OS=Homo sapiens GN=SPTLC1 PE=1 SV=1 | EQEIEDQK(1)NPR | 4 | 1.13 |
| Q14596 | NBR1 | >sp\|Q14596\|NBR1_HUMAN Next to BRCA1 gene 1 protein OS=Homo sapiens GN=NBR1 PE=1 SV=3 | GAEGK(1)PGVEAGQEPAEAGER | 2 | 1.12 |
| Q13501 | SQSTM | >sp\|Q13501\|SQSTM_HUMAN Sequestosome-1 OS=Homo sapiens GN=SQSTM1 PE=1 SV=1 | YK(1)CSVCPDYDLCSVCEGK | 2 | 1.11 |
| P16435 | NCPR | >sp\|P16435\|NCPR_HUMAN NADPH--cytochrome P450 reductase OS=Homo sapiens GN=POR PE=1 SV=2 | INK(1)GVATNWLR | 1 | 1.11 |
| P05023 | AT1A1 | >sp\|P05023\|AT1A1_HUMAN Sodium/potassium-transporting ATPase subunit alpha-1 OS=Homo sapiens GN=ATP1A1 PE=1 SV=1 | DK(1)YEPAAVSEQGDK | 2 | 1.11 |
| Q8TBY8 | PMFBP | >sp\|Q8TBY8\|PMFBP_HUMAN Polyamine-modulated factor 1-binding protein 1 OS=Homo sapiens GN=PMFBP1 PE=2 SV=1 | TVAEQDMK(1)MNDMLDR | 5 | 1.11 |
| P63261 | ACTG | >sp\|P63261\|ACTG_HUMAN Actin, cytoplasmic 2 OS=Homo sapiens GN=ACTG1 PE=1 SV=1;>sp\|P60709\|ACTB_HUMAN Actin, | EITALAPSTMK(0.796)IK(0.204) | 3 | 1.11 |

| | | | | | |
|---|---|---|---|---|---|
| | | cytoplasmic 1 OS=Homo sapiens GN=ACTB PE=1 SV=1;>sp\|P68133\|ACTS_HUMAN Actin, alpha skeletal muscle OS=Homo sapiens GN=ACTA1 PE=1 SV=1;>sp\|P68032\|ACTC | | | |
| Q13137 | CACO2 | >sp\|Q13137\|CACO2_HUMAN Calcium-binding and coiled-coil domain-containing protein 2 OS=Homo sapiens GN=CALCOCO2 PE=1 SV=1 | K(1)QQELMDENFDLSK | 2 | 1.11 |
| Q96J02 | ITCH | >sp\|Q96J02\|ITCH_HUMAN E3 ubiquitin-protein ligase Itchy homolog OS=Homo sapiens GN=ITCH PE=1 SV=2 | SQGQLNEK(1)PLPEGWEMR | 3 | 1.11 |
| O60716 | CTND1 | >sp\|O60716\|CTND1_HUMAN Catenin delta-1 OS=Homo sapiens GN=CTNND1 PE=1 SV=1 | K(1)GGPPPPNWR | 3 | 1.10 |
| Q99808 | S29A1 | >sp\|Q99808\|S29A1_HUMAN Equilibrative nucleoside transporter 1 OS=Homo sapiens GN=SLC29A1 PE=1 SV=3 | LDLISK(1)GEEPR | 8 | 1.10 |
| Q9BTU6 | P4K2A | >sp\|Q9BTU6\|P4K2A_HUMAN Phosphatidylinositol 4-kinase type 2-alpha OS=Homo sapiens GN=PI4K2A PE=1 SV=1 | RLALEK(0.998)VPK(0.002) | 1 | 1.10 |
| Q9Y289 | SC5A6 | >sp\|Q9Y289\|SC5A6_HUMAN Sodium-dependent multivitamin transporter OS=Homo sapiens GN=SLC5A6 PE=2 SV=2 | LLSLLPLSCQK(1)R | 3 | 1.09 |
| P08195 | 4F2 | >sp\|P08195\|4F2_HUMAN 4F2 cell-surface antigen heavy chain OS=Homo sapiens GN=SLC3A2 PE=1 SV=3 | FTGLSK(1)EELLK | 8 | 1.09 |
| Q15012 | LAP4A | >sp\|Q15012\|LAP4A_HUMAN Lysosomal-associated transmembrane protein 4A OS=Homo sapiens GN=LAPTM4A PE=1 SV=1 | VSMSFK(1)R | 2 | 1.09 |
| Q8WWI5 | CTL1 | >sp\|Q8WWI5\|CTL1_HUMAN Choline transporter-like protein 1 OS=Homo sapiens GN=SLC44A1 PE=1 SV=1 | ELK(1)PMASGASSA | 1 | 1.08 |
| O43493 | TGON2 | >sp\|O43493\|TGON2_HUMAN Trans-Golgi network | IIAFVLEGK(1)R | 4 | 1.08 |

| | | | | | |
|---|---|---|---|---|---|
| | | integral membrane protein 2 OS=Homo sapiens GN=TGOLN2 PE=1 SV=2 | | | |
| Q9BT67 | NFIP1 | >sp\|Q9BT67\|NFIP1_HUMAN NEDD4 family-interacting protein 1 OS=Homo sapiens GN=NDFIP1 PE=1 SV=1 | K(1)MPETFSNLPR | 1 | 1.08 |
| O60488 | ACSL4 | >sp\|O60488\|ACSL4_HUMAN Long-chain-fatty-acid--CoA ligase 4 OS=Homo sapiens GN=ACSL4 PE=1 SV=2 | TLFK(1)IGYDYK | 9 | 1.08 |
| P68363 | TBA1B | >sp\|P68363\|TBA1B_HUMAN Tubulin alpha-1B chain OS=Homo sapiens GN=TUBA1B PE=1 SV=1;>sp\|Q71U36\|TBA1A_HUMAN Tubulin alpha-1A chain OS=Homo sapiens GN=TUBA1A PE=1 SV=1;>sp\|Q13748\|TBA3C_HUMAN Tubulin alpha-3C/D chain OS=Homo sapiens GN=TUBA3C PE=1 SV=3;>sp\|Q6PE | DVNAAIATIK(0.956)TK(0.044) | 9 | 1.07 |
| Q13393 | PLD1 | >sp\|Q13393\|PLD1_HUMAN Phospholipase D1 OS=Homo sapiens GN=PLD1 PE=1 SV=1 | VVFNK(1)IGDAIAQR | 3 | 1.07 |
| Q9UP95 | S12A4 | >sp\|Q9UP95\|S12A4_HUMAN Solute carrier family 12 member 4 OS=Homo sapiens GN=SLC12A4 PE=1 SV=2 | ELVHIK(1)PDQSNVR | 3 | 1.06 |
| Q8WUM9 | S20A1 | >sp\|Q8WUM9\|S20A1_HUMAN Sodium-dependent phosphate transporter 1 OS=Homo sapiens GN=SLC20A1 PE=1 SV=1 | EGEQK(1)GEEMEK | 1 | 1.06 |
| Q8N0X7 | SPG20 | >sp\|Q8N0X7\|SPG20_HUMAN Spartin OS=Homo sapiens GN=SPG20 PE=1 SV=1 | TRPSSDQLK(1)EASGTDVK | 8 | 1.06 |
| Q92887 | MRP2 | >sp\|Q92887\|MRP2_HUMAN Canalicular multispecific organic anion transporter 1 OS=Homo sapiens GN=ABCC2 PE=1 SV=3 | ITEYTK(1)VENEAPWVTDK | 4 | 1.06 |
| O15438 | MRP3 | >sp\|O15438\|MRP3_HUMAN Canalicular multispecific organic anion transporter 2 OS=Homo sapiens GN=ABCC3 PE=1 SV=3 | LYAWEPSFLK(1)QVEGIR | 4 | 1.06 |

| | | | | | |
|---|---|---|---|---|---|
| P08195 | 4F2 | >sp\|P08195\|4F2_HUMAN 4F2 cell-surface antigen heavy chain OS=Homo sapiens GN=SLC3A2 PE=1 SV=3 | IK(1)VAEDEAEAAAAAK | 27 | 1.06 |
| O15320 | CTGE5 | >sp\|O15320\|CTGE5_HUMAN cTAGE family member 5 OS=Homo sapiens GN=CTAGE5 PE=1 SV=4;>sp\|Q96RT6\|CTGE2_HUMAN cTAGE family member 2 OS=Homo sapiens GN=CTAGE1 PE=1 SV=2 | LLEK(1)FSLVQK | 7 | 1.06 |
| O15162 | PLS1 | >sp\|O15162\|PLS1_HUMAN Phospholipid scramblase 1 OS=Homo sapiens GN=PLSCR1 PE=1 SV=1 | YEIK(1)NSFGQR | 5 | 1.05 |
| Q86SQ4 | GP126 | >sp\|Q86SQ4\|GP126_HUMAN G-protein coupled receptor 126 OS=Homo sapiens GN=GPR126 PE=1 SV=3 | SSDNLGK(1)SLSSSSIGSNSTYLTSK | 4 | 1.05 |
| O95183 | VAMP5 | >sp\|O95183\|VAMP5_HUMAN Vesicle-associated membrane protein 5 OS=Homo sapiens GN=VAMP5 PE=1 SV=1 | GVK(1)LAELQQR | 2 | 1.05 |
| P08183 | MDR1 | >sp\|P08183\|MDR1_HUMAN Multidrug resistance protein 1 OS=Homo sapiens GN=ABCB1 PE=1 SV=3 | TVIAFGGQK(0.387)K(0.613) | 7 | 1.04 |
| Q96K49 | TM87B | >sp\|Q96K49\|TM87B_HUMAN Transmembrane protein 87B OS=Homo sapiens GN=TMEM87B PE=1 SV=1 | SEMAEK(1)MFSSEK | 3 | 1.04 |
| Q99624 | S38A3 | >sp\|Q99624\|S38A3_HUMAN Sodium-coupled neutral amino acid transporter 3 OS=Homo sapiens GN=SLC38A3 PE=1 SV=1 | SFLQK(0.989)SPSK(0.011) | 2 | 1.04 |
| P36894 | BMR1A | >sp\|P36894\|BMR1A_HUMAN Bone morphogenetic protein receptor type-1A OS=Homo sapiens GN=BMPR1A PE=1 SV=2 | TIAK(1)QIQMVR | 4 | 1.04 |
| Q86XX4 | FRAS1 | >sp\|Q86XX4\|FRAS1_HUMAN Extracellular matrix protein FRAS1 OS=Homo sapiens GN=FRAS1 PE=1 SV=2 | NVNILSEPEAAYTFK(0.393)GAK(0.607) | 2 | 1.04 |
| P07148 | FABPL | >sp\|P07148\|FABPL_HUMAN Fatty acid-binding protein, liver OS=Homo | AIGLPEELIQK(0.087)GK(0.913) | 2 | 1.03 |

| | | | | | |
|---|---|---|---|---|---|
| | | sapiens GN=FABP1 PE=1 SV=1 | | | |
| Q9P2R3 | ANFY1 | >sp\|Q9P2R3\|ANFY1_HUMAN Rabankyrin-5 OS=Homo sapiens GN=ANKFY1 PE=1 SV=2 | NNK(1)SAEAILK | 5 | 1.03 |
| O15269 | SPTC1 | >sp\|O15269\|SPTC1_HUMAN Serine palmitoyltransferase 1 OS=Homo sapiens GN=SPTLC1 PE=1 SV=1 | SDLTVK(0.99)EK(0.01) | 6 | 1.03 |
| Q86SQ4 | GP126 | >sp\|Q86SQ4\|GP126_HUMAN G-protein coupled receptor 126 OS=Homo sapiens GN=GPR126 PE=1 SV=3 | SLSSSSIGSNSTYLTSK(0.764)SK(0.236) | 4 | 1.03 |
| Q8NEQ6 | CA064 | >sp\|Q8NEQ6\|CA064_HUMAN Uncharacterized protein C1orf64 OS=Homo sapiens GN=C1orf64 PE=2 SV=1 | SSTWGTVK(0.997)DSLK(0.003) | 3 | 1.03 |
| P0DMV9 | HS71B | >sp\|P0DMV9\|HS71B_HUMAN Heat shock 70 kDa protein 1B OS=Homo sapiens GN=HSPA1B PE=1 SV=1;>sp\|P0DMV8\|HS71A_HUMAN Heat shock 70 kDa protein 1A OS=Homo sapiens GN=HSPA1A PE=1 SV=1 | MVQEAEK(0.983)YK(0.017) | 10 | 1.03 |
| Q9BXS4 | TMM59 | >sp\|Q9BXS4\|TMM59_HUMAN Transmembrane protein 59 OS=Homo sapiens GN=TMEM59 PE=1 SV=1 | TEDHEEAGPLPTK(1)VNLAHSEI | 29 | 1.03 |
| Q86TG7 | PEG10 | >sp\|Q86TG7\|PEG10_HUMAN Retrotransposon-derived protein PEG10 OS=Homo sapiens GN=PEG10 PE=1 SV=2 | DGLITPTIAPNGAQVLQVK(1)R | 1 | 1.03 |
| Q9BY67 | CADM1 | >sp\|Q9BY67\|CADM1_HUMAN Cell adhesion molecule 1 OS=Homo sapiens GN=CADM1 PE=1 SV=2 | GADDAADADTAIINAEGGQNNSEEK(0.217)K(0.783)EYFI | 1 | 1.02 |
| P27105 | STOM | >sp\|P27105\|STOM_HUMAN Erythrocyte band 7 integral membrane protein OS=Homo sapiens GN=STOM PE=1 SV=3 | ALK(1)EASMVITESPAALQLR | 1 | 1.02 |
| O95297 | MPZL1 | >sp\|O95297\|MPZL1_HUMAN Myelin protein zero-like protein 1 OS=Homo sapiens GN=MPZL1 PE=1 SV=1 | DYTGCSTSESLSPVK(1)QAPR | 3 | 1.02 |

| | | | | | |
|---|---|---|---|---|---|
| P11166 | GTR1 | >sp\|P11166\|GTR1_HUMAN Solute carrier family 2, facilitated glucose transporter member 1 OS=Homo sapiens GN=SLC2A1 PE=1 SV=2 | GTADVTHDLQEMK(1)EESR | 1 | 1.02 |
| Q9NV92 | NFIP2 | >sp\|Q9NV92\|NFIP2_HUMAN NEDD4 family-interacting protein 2 OS=Homo sapiens GN=NDFIP2 PE=1 SV=2 | AK(1)AAAMAAAAAETSQR | 1 | 1.02 |
| Q12974 | TP4A2 | >sp\|Q12974\|TP4A2_HUMAN Protein tyrosine phosphatase type IVA 2 OS=Homo sapiens GN=PTP4A2 PE=1 SV=1 | K(1)YGVTTLVR | 1 | 1.02 |
| Q9BY67 | CADM1 | >sp\|Q9BY67\|CADM1_HUMAN Cell adhesion molecule 1 OS=Homo sapiens GN=CADM1 PE=1 SV=2 | GADDAADADTAIINAEGGQNNSEEK(0.5)K(0.5) | 18 | 1.01 |
| P08034 | CXB1 | >sp\|P08034\|CXB1_HUMAN Gap junction beta-1 protein OS=Homo sapiens GN=GJB1 PE=1 SV=1 | RSPGTGAGLAEK(1)SDR | 6 | 1.01 |
| Q12866 | MERTK | >sp\|Q12866\|MERTK_HUMAN Tyrosine-protein kinase Mer OS=Homo sapiens GN=MERTK PE=1 SV=2 | TMK(1)LDNSSQR | 1 | 1.01 |
| Q9H0M0 | WWP1 | >sp\|Q9H0M0\|WWP1_HUMAN NEDD4-like E3 ubiquitin-protein ligase WWP1 OS=Homo sapiens GN=WWP1 PE=1 SV=1 | SSSAFEAAK(1)SR | 4 | 1.01 |
| Q99808 | S29A1 | >sp\|Q99808\|S29A1_HUMAN Equilibrative nucleoside transporter 1 OS=Homo sapiens GN=SLC29A1 PE=1 SV=3 | LEGPGEQETK(1)LDLISK | 11 | 1.01 |
| P63218 | GBG5 | >sp\|P63218\|GBG5_HUMAN Guanine nucleotide-binding protein G(I)/G(S)/G(O) subunit gamma-5 OS=Homo sapiens GN=GNG5 PE=1 SV=3 | SGSSSVAAMK(0.857)K(0.143) | 2 | 1.00 |
| Q8WUX1 | S38A5 | >sp\|Q8WUX1\|S38A5_HUMAN Sodium-coupled neutral amino acid transporter 5 OS=Homo sapiens GN=SLC38A5 PE=1 SV=1 | GPAPGSK(1)PVQFMDFEGK | 1 | 1.00 |
| P29992 | GNA11 | >sp\|P29992\|GNA11_HUMAN Guanine nucleotide-binding protein subunit | ILYK(1)YEQNK | 13 | 1.00 |

| | | | | | |
|---|---|---|---|---|---|
| | | alpha-11 OS=Homo sapiens GN=GNA11 PE=1 SV=2 | | | |
| P05556 | ITB1 | >sp\|P05556\|ITB1_HUMAN Integrin beta-1 OS=Homo sapiens GN=ITGB1 PE=1 SV=2 | MNAK(1)WDTGENPIYK | 6 | 1.00 |
| O75509 | TNR21 | >sp\|O75509\|TNR21_HUMAN Tumor necrosis factor receptor superfamily member 21 OS=Homo sapiens GN=TNFRSF21 PE=1 SV=1 | NK(1)GFFVDESEPLLR | 1 | 1.00 |
| Q13263 | TIF1B | >sp\|Q13263\|TIF1B_HUMAN Transcription intermediary factor 1-beta OS=Homo sapiens GN=TRIM28 PE=1 SV=5 | VLVNDAQK(1)VTEGQQER | 2 | 0.99 |
| Q15758 | AAAT | >sp\|Q15758\|AAAT_HUMAN Neutral amino acid transporter B(0) OS=Homo sapiens GN=SLC1A5 PE=1 SV=2 | SELPLDPLPVPTEEGNPLLK(1)HYR | 10 | 0.99 |
| P27105 | STOM | >sp\|P27105\|STOM_HUMAN Erythrocyte band 7 integral membrane protein OS=Homo sapiens GN=STOM PE=1 SV=3 | DVK(1)LPVQLQR | 1 | 0.99 |
| P11142 | HSP7C | >sp\|P11142\|HSP7C_HUMAN Heat shock cognate 71 kDa protein OS=Homo sapiens GN=HSPA8 PE=1 SV=1 | MVQEAEK(0.983)YK(0.017) | 10 | 0.99 |
| Q9Y2G8 | DJC16 | >sp\|Q9Y2G8\|DJC16_HUMAN DnaJ homolog subfamily C member 16 OS=Homo sapiens GN=DNAJC16 PE=2 SV=3 | TEPSFTK(0.924)ENSSK(0.076) | 1 | 0.99 |
| Q8N2R8 | FA43A | >sp\|Q8N2R8\|FA43A_HUMAN Protein FAM43A OS=Homo sapiens GN=FAM43A PE=2 SV=2 | VGSMFRSK(1) | 3 | 0.99 |
| P05787 | K2C8 | >sp\|P05787\|K2C8_HUMAN Keratin, type II cytoskeletal 8 OS=Homo sapiens GN=KRT8 PE=1 SV=7;>P05787 SWISS-PROT:P05787 Tax_Id=9606 Gene_Symbol=KRT8 Keratin, type II cytoskeletal 8;>Q9H552 TREMBL:Q9H552 Tax_Id=9606 Gene_Symbol=- Keratin-8-like protein 1;>Q8BGZ7 | TLNNK(1)FASFIDK | 1 | 0.99 |

| | | | | | |
|---|---|---|---|---|---|
| Q7Z5G4 | GOGA7 | >sp\|Q7Z5G4\|GOGA7_HUMAN Golgin subfamily A member 7 OS=Homo sapiens GN=GOLGA7 PE=1 SV=2 | VSK(1)YIQEQNEK | 9 | 0.99 |
| P98196 | AT11A | >sp\|P98196\|AT11A_HUMAN Probable phospholipid-transporting ATPase IH OS=Homo sapiens GN=ATP11A PE=1 SV=3 | AADTIEALQK(0.988)AGIK(0.012) | 5 | 0.99 |
| Q9BVT8 | TMUB1 | >sp\|Q9BVT8\|TMUB1_HUMAN Transmembrane and ubiquitin-like domain-containing protein 1 OS=Homo sapiens GN=TMUB1 PE=1 SV=1 | LK(1)FLNDSEQVAR | 2 | 0.99 |
| Q969G9 | NKD1 | >sp\|Q969G9\|NKD1_HUMAN Protein naked cuticle homolog 1 OS=Homo sapiens GN=NKD1 PE=1 SV=1 | LTVAPDGSQSK(1)R | 1 | 0.99 |
| Q9Y6M5 | ZNT1 | >sp\|Q9Y6M5\|ZNT1_HUMAN Zinc transporter 1 OS=Homo sapiens GN=SLC30A1 PE=1 SV=3 | NLIK(1)ELR | 3 | 0.98 |
| Q96QD8 | S38A2 | >sp\|Q96QD8\|S38A2_HUMAN Sodium-coupled neutral amino acid transporter 2 OS=Homo sapiens GN=SLC38A2 PE=1 SV=2 | QAALK(1)SHYADVDPENQNFLLESNLGK | 3 | 0.98 |
| P01892 | 1A02 | >sp\|P01892\|1A02_HUMAN HLA class I histocompatibility antigen, A-2 alpha chain OS=Homo sapiens GN=HLA-A PE=1 SV=1;>sp\|P10316\|1A69_HUMAN HLA class I histocompatibility antigen, A-69 alpha chain OS=Homo sapiens GN=HLA-A PE=1 SV=2;>sp\|P01891\|1A68_HUMAN HLA cla | K(1)GGSYSQAASSDSAQGSDVSLTACK | 2 | 0.98 |
| P05023 | AT1A1 | >sp\|P05023\|AT1A1_HUMAN Sodium/potassium-transporting ATPase subunit alpha-1 OS=Homo sapiens GN=ATP1A1 PE=1 SV=1 | DKYEPAAVSEQGDK(0.422)K(0.578) | 4 | 0.98 |
| P63000 | RAC1 | >sp\|P63000\|RAC1_HUMAN Ras-related C3 botulinum toxin substrate 1 OS=Homo sapiens GN=RAC1 PE=1 SV=1 | EIGAVK(1)YLECSALTQR | 1 | 0.98 |

| | | | | | |
|---|---|---|---|---|---|
| P55082 | MFAP3 | >sp\|P55082\|MFAP3_HUMAN Microfibril-associated glycoprotein 3 OS=Homo sapiens GN=MFAP3 PE=2 SV=1;>sp\|O75121\|MFA3L_HUMAN Microfibrillar-associated protein 3-like OS=Homo sapiens GN=MFAP3L PE=2 SV=3 | LQK(1)AFEIAK | 5 | 0.98 |
| P80370 | DLK1 | >sp\|P80370\|DLK1_HUMAN Protein delta homolog 1 OS=Homo sapiens GN=DLK1 PE=1 SV=3 | IDMTTFSK(1)EAGDEEI | 7 | 0.98 |
| Q86SQ4 | GP126 | >sp\|Q86SQ4\|GP126_HUMAN G-protein coupled receptor 126 OS=Homo sapiens GN=GPR126 PE=1 SV=3 | TATNIIK(0.381)K(0.619) | 1 | 0.98 |
| P02654 | APOC1 | >sp\|P02654\|APOC1_HUMAN Apolipoprotein C-I OS=Homo sapiens GN=APOC1 PE=1 SV=1 | EFGNTLEDK(1)AR | 2 | 0.98 |
| Q9NQX7 | ITM2C | >sp\|Q9NQX7\|ITM2C_HUMAN Integral membrane protein 2C OS=Homo sapiens GN=ITM2C PE=1 SV=1 | ISFQPAVAGIK(0.996)GDK(0.82)ADK(0.184) | 3 | 0.97 |
| Q92783 | STAM1 | >sp\|Q92783\|STAM1_HUMAN Signal transducing adapter molecule 1 OS=Homo sapiens GN=STAM PE=1 SV=3 | AIELSLK(1)EQR | 1 | 0.97 |
| P68363 | TBA1B | >sp\|P68363\|TBA1B_HUMAN Tubulin alpha-1B chain OS=Homo sapiens GN=TUBA1B PE=1 SV=1;>sp\|P68366\|TBA4A_HUMAN Tubulin alpha-4A chain OS=Homo sapiens GN=TUBA4A PE=1 SV=1;>sp\|Q71U36\|TBA1A_HUMAN Tubulin alpha-1A chain OS=Homo sapiens GN=TUBA1A PE=1 SV=1;>sp\|Q13748 | VGINYQPPTVVPGGDLAK(1)VQR | 16 | 0.97 |
| P08581 | MET | >sp\|P08581\|MET_HUMAN Hepatocyte growth factor receptor OS=Homo sapiens GN=MET PE=1 SV=4 | DLIGFGLQVAK(0.5)GMK(0.5) | 1 | 0.97 |
| P08581 | MET | >sp\|P08581\|MET_HUMAN Hepatocyte growth factor receptor OS=Homo sapiens GN=MET PE=1 SV=4 | DLIGFGLQVAK(0.5)GMK(0.5) | 1 | 0.97 |
| P31431 | SDC4 | >sp\|P31431\|SDC4_HUMAN Syndecan-4 OS=Homo | K(1)APTNEFYA | 4 | 0.97 |

| | | | | | |
|---|---|---|---|---|---|
| | | sapiens GN=SDC4 PE=1 SV=2 | | | |
| Q13884 | SNTB1 | >sp\|Q13884\|SNTB1_HUMAN Beta-1-syntrophin OS=Homo sapiens GN=SNTB1 PE=1 SV=3 | EQLGK(1)TGIAGSR | 13 | 0.97 |
| P62979 | RS27A | >sp\|P62979\|RS27A_HUMAN Ubiquitin-40S ribosomal protein S27a OS=Homo sapiens GN=RPS27A PE=1 SV=2 | VDENGK(1)ISR | 43 | 0.97 |
| P0DMV9 | HS71B | >sp\|P0DMV9\|HS71B_HUMAN Heat shock 70 kDa protein 1B OS=Homo sapiens GN=HSPA1B PE=1 SV=1;>sp\|P0DMV8\|HS71A_HUMAN Heat shock 70 kDa protein 1A OS=Homo sapiens GN=HSPA1A PE=1 SV=1 | MVQEAEK(0.5)YK(0.5) | 10 | 0.97 |
| P11142 | HSP7C | >sp\|P11142\|HSP7C_HUMAN Heat shock cognate 71 kDa protein OS=Homo sapiens GN=HSPA8 PE=1 SV=1 | MVQEAEK(0.5)YK(0.5) | 10 | 0.97 |
| Q96K49 | TM87B | >sp\|Q96K49\|TM87B_HUMAN Transmembrane protein 87B OS=Homo sapiens GN=TMEM87B PE=1 SV=1 | SVSNGTAK(1)PATSENFDEDLK | 2 | 0.97 |
| P53801 | PTTG | >sp\|P53801\|PTTG_HUMAN Pituitary tumor-transforming gene 1 protein-interacting protein OS=Homo sapiens GN=PTTG1IP PE=1 SV=1 | YGLFK(1)EENPYAR | 6 | 0.97 |
| Q16625 | OCLN | >sp\|Q16625\|OCLN_HUMAN Occludin OS=Homo sapiens GN=OCLN PE=1 SV=1 | VDSPMAYSSNGK(0.386)VNDK(0.614) | 2 | 0.96 |
| Q9H3Z4 | DNJC5 | >sp\|Q9H3Z4\|DNJC5_HUMAN DnaJ homolog subfamily C member 5 OS=Homo sapiens GN=DNAJC5 PE=1 SV=1 | EINNAHAILTDATK(1)R | 2 | 0.96 |
| Q96AJ9 | VTI1A | >sp\|Q96AJ9\|VTI1A_HUMAN Vesicle transport through interaction with t-SNAREs homolog 1A OS=Homo sapiens GN=VTI1A PE=1 SV=2 | ETDANLGK(1)SSR | 1 | 0.96 |
| Q9Y287 | ITM2B | >sp\|Q9Y287\|ITM2B_HUMAN Integral membrane protein 2B OS=Homo | VTFNSALAQK(1)EAK | 43 | 0.96 |

| | | | | | |
|---|---|---|---|---|---|
| | | sapiens GN=ITM2B PE=1 SV=1 | | | |
| Q14126 | DSG2 | >sp\|Q14126\|DSG2_HUMAN Desmoglein-2 OS=Homo sapiens GN=DSG2 PE=1 SV=2 | ATQFTGATGAIMTTETTK(1)TAR | 3 | 0.96 |
| P21580 | TNAP3 | >sp\|P21580\|TNAP3_HUMAN Tumor necrosis factor alpha-induced protein 3 OS=Homo sapiens GN=TNFAIP3 PE=1 SV=1 | NIQATLESQK(0.875)K(0.125) | 1 | 0.96 |
| Q9BRK3 | MXRA8 | >sp\|Q9BRK3\|MXRA8_HUMAN Matrix-remodeling-associated protein 8 OS=Homo sapiens GN=MXRA8 PE=1 SV=1 | NNILK(1)ER | 4 | 0.96 |
| Q12866 | MERTK | >sp\|Q12866\|MERTK_HUMAN Tyrosine-protein kinase Mer OS=Homo sapiens GN=MERTK PE=1 SV=2 | LQLEK(1)LLESLPDVR | 5 | 0.96 |
| P0DMV9 | HS71B | >sp\|P0DMV9\|HS71B_HUMAN Heat shock 70 kDa protein 1B OS=Homo sapiens GN=HSPA1B PE=1 SV=1;>sp\|P0DMV8\|HS71A_HUMAN Heat shock 70 kDa protein 1A OS=Homo sapiens GN=HSPA1A PE=1 SV=1 | LSK(1)EEIER | 1 | 0.96 |
| Q9Y624 | JAM1 | >sp\|Q9Y624\|JAM1_HUMAN Junctional adhesion molecule A OS=Homo sapiens GN=F11R PE=1 SV=1 | SEGEFK(1)QTSSFLV | 6 | 0.96 |
| P11717 | MPRI | >sp\|P11717\|MPRI_HUMAN Cation-independent mannose-6-phosphate receptor OS=Homo sapiens GN=IGF2R PE=1 SV=3 | SSSAQQK(1)TVSSTK | 3 | 0.96 |
| O15269 | SPTC1 | >sp\|O15269\|SPTC1_HUMAN Serine palmitoyltransferase 1 OS=Homo sapiens GN=SPTLC1 PE=1 SV=1 | EK(1)EELIEEWQPEPLVPPVPK | 2 | 0.96 |
| P29317 | EPHA2 | >sp\|P29317\|EPHA2_HUMAN Ephrin type-A receptor 2 OS=Homo sapiens GN=EPHA2 PE=1 SV=2 | QK(1)VIGAGEFGEVYK | 1 | 0.95 |
| Q86SQ4 | GP126 | >sp\|Q86SQ4\|GP126_HUMAN G-protein coupled receptor 126 OS=Homo sapiens GN=GPR126 PE=1 SV=3 | SK(1)SSSTTYFK | 1 | 0.95 |
| Q15043 | S39AE | >sp\|Q15043\|S39AE_HUMAN Zinc transporter ZIP14 | K(1)DQEEGVMEK | 8 | 0.95 |

| | | | | | |
|---|---|---|---|---|---|
| | | OS=Homo sapiens GN=SLC39A14 PE=1 SV=3 | | | |
| Q14118 | DAG1 | >sp\|Q14118\|DAG1_HUMAN Dystroglycan OS=Homo sapiens GN=DAG1 PE=1 SV=2 | LTLEDQATFIK(0.879)K(0.121) | 8 | 0.95 |
| Q9Y624 | JAM1 | >sp\|Q9Y624\|JAM1_HUMAN Junctional adhesion molecule A OS=Homo sapiens GN=F11R PE=1 SV=1 | K(1)VIYSQPSAR | 5 | 0.95 |
| P51148 | RAB5C | >sp\|P51148\|RAB5C_HUMAN Ras-related protein Rab-5C OS=Homo sapiens GN=RAB5C PE=1 SV=2;>sp\|P20339\|RAB5A_HUMAN Ras-related protein Rab-5A OS=Homo sapiens GN=RAB5A PE=1 SV=2 | NWVK(1)ELQR | 10 | 0.95 |
| P08183 | MDR1 | >sp\|P08183\|MDR1_HUMAN Multidrug resistance protein 1 OS=Homo sapiens GN=ABCB1 PE=1 SV=3;>sp\|P21439\|MDR3_HUMAN Phosphatidylcholine translocator ABCB4 OS=Homo sapiens GN=ABCB4 PE=1 SV=2 | VGDK(1)GTQLSGGQK | 1 | 0.95 |
| Q9UH65 | SWP70 | >sp\|Q9UH65\|SWP70_HUMAN Switch-associated protein 70 OS=Homo sapiens GN=SWAP70 PE=1 SV=1 | GSLK(1)EELLK | 5 | 0.95 |
| O95297 | MPZL1 | >sp\|O95297\|MPZL1_HUMAN Myelin protein zero-like protein 1 OS=Homo sapiens GN=MPZL1 PE=1 SV=1 | INK(1)SESVVYADIR | 1 | 0.94 |
| P21796 | VDAC1 | >sp\|P21796\|VDAC1_HUMAN Voltage-dependent anion-selective channel protein 1 OS=Homo sapiens GN=VDAC1 PE=1 SV=2 | DVFTK(0.999)GYGFGLIK(0.001) | 1 | 0.94 |
| O00308 | WWP2 | >sp\|O00308\|WWP2_HUMAN NEDD4-like E3 ubiquitin-protein ligase WWP2 OS=Homo sapiens GN=WWP2 PE=1 SV=2 | TTTFK(1)DPRPGFESGTK | 3 | 0.94 |
| P07307 | ASGR2 | >sp\|P07307\|ASGR2_HUMAN Asialoglycoprotein receptor 2 OS=Homo | AK(1)DFQDIQQLSSEENDHPFHQGEGPGTR | 3 | 0.94 |

| | | | | | |
|---|---|---|---|---|---|
| | | sapiens GN=ASGR2 PE=1 SV=2 | | | |
| Q86VP1 | TAXB1 | >sp\|Q86VP1\|TAXB1_HUMAN Tax1-binding protein 1 OS=Homo sapiens GN=TAX1BP1 PE=1 SV=2 | EQVK(1)IAENVK | 4 | 0.94 |
| Q9P265 | DIP2B | >sp\|Q9P265\|DIP2B_HUMAN Disco-interacting protein 2 homolog B OS=Homo sapiens GN=DIP2B PE=1 SV=3 | SK(1)LLSPYSPQTQETDSAVQK | 5 | 0.94 |
| Q86UD5 | SL9B2 | >sp\|Q86UD5\|SL9B2_HUMAN Mitochondrial sodium/hydrogen exchanger 9B2 OS=Homo sapiens GN=SLC9B2 PE=1 SV=2 | LK(1)GIDANEPTEGSILLK | 1 | 0.94 |
| Q9NPR9 | GP108 | >sp\|Q9NPR9\|GP108_HUMAN Protein GPR108 OS=Homo sapiens GN=GPR108 PE=2 SV=3 | HLQDASGTDGK(0.999)VAVNLAK(0.001) | 1 | 0.94 |
| Q9H8Y8 | GORS2 | >sp\|Q9H8Y8\|GORS2_HUMAN Golgi reassembly-stacking protein 2 OS=Homo sapiens GN=GORASP2 PE=1 SV=3 | K(1)ISLPGQMAGTPITPLK | 1 | 0.94 |
| Q12893 | TM115 | >sp\|Q12893\|TM115_HUMAN Transmembrane protein 115 OS=Homo sapiens GN=TMEM115 PE=1 SV=1 | VDSPLPSDK(1)APTPPGK | 3 | 0.94 |
| Q96QD8 | S38A2 | >sp\|Q96QD8\|S38A2_HUMAN Sodium-coupled neutral amino acid transporter 2 OS=Homo sapiens GN=SLC38A2 PE=1 SV=2 | FSISPDEDSSSYSSNSDFNYSYPTK(0.999)QAALK(0.001) | 5 | 0.93 |
| Q9NU53 | GINM1 | >sp\|Q9NU53\|GINM1_HUMAN Glycoprotein integral membrane protein 1 OS=Homo sapiens GN=GINM1 PE=2 SV=1 | GILQLDK(1)VDVIPVTAINLYPDGPEK | 1 | 0.93 |
| P07148 | FABPL | >sp\|P07148\|FABPL_HUMAN Fatty acid-binding protein, liver OS=Homo sapiens GN=FABP1 PE=1 SV=1 | VK(1)TVVQLEGDNK | 2 | 0.93 |
| P06733 | ENOA | >sp\|P06733\|ENOA_HUMAN Alpha-enolase OS=Homo sapiens GN=ENO1 PE=1 SV=2 | SILK(1)IHAR | 1 | 0.93 |
| O75436 | VP26A | >sp\|O75436\|VP26A_HUMAN Vacuolar protein sorting-associated protein 26A OS=Homo sapiens GN=VPS26A PE=1 SV=2 | VNLAFK(0.999)QPGK(0.001) | 1 | 0.93 |

| | | | | | |
|---|---|---|---|---|---|
| Q96NT5 | PCFT | >sp\|Q96NT5\|PCFT_HUMAN Proton-coupled folate transporter OS=Homo sapiens GN=SLC46A1 PE=1 SV=1 | MEGSASPPEK(1)PR | 13 | 0.93 |
| P98196 | AT11A | >sp\|P98196\|AT11A_HUMAN Probable phospholipid-transporting ATPase IH OS=Homo sapiens GN=ATP11A PE=1 SV=3 | VIEGK(1)VDQIR | 9 | 0.93 |
| O75694 | NU155 | >sp\|O75694\|NU155_HUMAN Nuclear pore complex protein Nup155 OS=Homo sapiens GN=NUP155 PE=1 SV=1 | NSQFAGGPLGNPNTTAK(1)VQQR | 3 | 0.93 |
| Q9UHN6 | TMEM2 | >sp\|Q9UHN6\|TMEM2_HUMAN Transmembrane protein 2 OS=Homo sapiens GN=TMEM2 PE=1 SV=1 | SQASAK(1)FTSIR | 5 | 0.93 |
| P78552 | I13R1 | >sp\|P78552\|I13R1_HUMAN Interleukin-13 receptor subunit alpha-1 OS=Homo sapiens GN=IL13RA1 PE=1 SV=1 | KYDIYEK(1)QTK | 2 | 0.93 |
| P35670 | ATP7B | >sp\|P35670\|ATP7B_HUMAN Copper-transporting ATPase 2 OS=Homo sapiens GN=ATP7B PE=1 SV=4 | GDIVK(1)VVPGGK | 4 | 0.92 |
| P05362 | ICAM1 | >sp\|P05362\|ICAM1_HUMAN Intercellular adhesion molecule 1 OS=Homo sapiens GN=ICAM1 PE=1 SV=2 | GTPMK(1)PNTQATPP | 14 | 0.92 |
| Q92887 | MRP2 | >sp\|Q92887\|MRP2_HUMAN Canalicular multispecific organic anion transporter 1 OS=Homo sapiens GN=ABCC2 PE=1 SV=3 | NVNSLK(1)EDEELVK | 4 | 0.92 |
| P52569 | CTR2 | >sp\|P52569\|CTR2_HUMAN Cationic amino acid transporter 2 OS=Homo sapiens GN=SLC7A2 PE=1 SV=2 | VTSK(1)SESQVTMLQR | 6 | 0.92 |
| P78552 | I13R1 | >sp\|P78552\|I13R1_HUMAN Interleukin-13 receptor subunit alpha-1 OS=Homo sapiens GN=IL13RA1 PE=1 SV=1 | EETDSVVLIENLK(0.809)K(0.191) | 2 | 0.92 |
| Q8NBN3 | TM87A | >sp\|Q8NBN3\|TM87A_HUMAN Transmembrane protein 87A OS=Homo sapiens GN=TMEM87A PE=1 SV=3 | FAFSPLSEEEEEDEQK(0.946)EPMLK(0.054) | 1 | 0.92 |

| | | | | | |
|---|---|---|---|---|---|
| Q96QD8 | S38A2 | >sp\|Q96QD8\|S38A2_HUMAN Sodium-coupled neutral amino acid transporter 2 OS=Homo sapiens GN=SLC38A2 PE=1 SV=2 | SHYADVDPENQNFLLESNLGK(0.5)K(0.5) | 24 | 0.92 |
| Q9Y287 | ITM2B | >sp\|Q9Y287\|ITM2B_HUMAN Integral membrane protein 2B OS=Homo sapiens GN=ITM2B PE=1 SV=1 | VK(1)VTFNSALAQK | 4 | 0.91 |
| P58335 | ANTR2 | >sp\|P58335\|ANTR2_HUMAN Anthrax toxin receptor 2 OS=Homo sapiens GN=ANTXR2 PE=1 SV=5 | EEEEEPLPTK(0.899)K(0.101) | 13 | 0.91 |
| Q14409 | GLPK3 | >sp\|Q14409\|GLPK3_HUMAN Putative glycerol kinase 3 OS=Homo sapiens GN=GK3P PE=5 SV=2;>sp\|P32189\|GLPK_HUMAN Glycerol kinase OS=Homo sapiens GN=GK PE=1 SV=3 | TSEEIEK(0.994)LAK(0.006) | 3 | 0.91 |
| Q9H305 | CDIP1 | >sp\|Q9H305\|CDIP1_HUMAN Cell death-inducing p53-target protein 1 OS=Homo sapiens GN=CDIP1 PE=1 SV=1 | SSEPPPPYPGGPTAPLLEEK(1)SGAPPTPGR | 24 | 0.91 |
| P55082 | MFAP3 | >sp\|P55082\|MFAP3_HUMAN Microfibril-associated glycoprotein 3 OS=Homo sapiens GN=MFAP3 PE=2 SV=1;>sp\|O75121\|MFA3L_HUMAN Microfibrillar-associated protein 3-like OS=Homo sapiens GN=MFAP3L PE=2 SV=3 | TLELAK(1)VTQFK | 2 | 0.91 |
| Q13501 | SQSTM | >sp\|Q13501\|SQSTM_HUMAN Sequestosome-1 OS=Homo sapiens GN=SQSTM1 PE=1 SV=1 | LLQTK(1)NYDIGAALDTIQYSK | 1 | 0.91 |
| Q969E2 | SCAM4 | >sp\|Q969E2\|SCAM4_HUMAN Secretory carrier-associated membrane protein 4 OS=Homo sapiens GN=SCAMP4 PE=2 SV=1 | SEK(1)ENNFPPLPK | 12 | 0.91 |
| P07306 | ASGR1 | >sp\|P07306\|ASGR1_HUMAN Asialoglycoprotein receptor 1 OS=Homo sapiens GN=ASGR1 PE=1 SV=2 | K(1)GPPPPQPLLQR | 8 | 0.91 |
| Q969G9 | NKD1 | >sp\|Q969G9\|NKD1_HUMAN Protein naked cuticle homolog 1 OS=Homo sapiens GN=NKD1 PE=1 SV=1 | AETK(1)PTEDLR | 1 | 0.91 |

| | | | | | |
|---|---|---|---|---|---|
| Q15025 | TNIP1 | >sp\|Q15025\|TNIP1_HUMAN TNFAIP3-interacting protein 1 OS=Homo sapiens GN=TNIP1 PE=1 SV=2 | EQLTAEAK(1)ELR | 1 | 0.91 |
| Q13443 | ADAM9 | >sp\|Q13443\|ADAM9_HUMAN Disintegrin and metalloproteinase domain-containing protein 9 OS=Homo sapiens GN=ADAM9 PE=1 SV=1 | SQTYESDGK(1)NQANPSR | 9 | 0.91 |
| O15440 | MRP5 | >sp\|O15440\|MRP5_HUMAN Multidrug resistance-associated protein 5 OS=Homo sapiens GN=ABCC5 PE=1 SV=2 | AFSQSVQK(1)IR | 6 | 0.90 |
| P37173 | TGFR2 | >sp\|P37173\|TGFR2_HUMAN TGF-beta receptor type-2 OS=Homo sapiens GN=TGFBR2 PE=1 SV=2 | LSSTWETGK(1)TR | 7 | 0.90 |
| P52569 | CTR2 | >sp\|P52569\|CTR2_HUMAN Cationic amino acid transporter 2 OS=Homo sapiens GN=SLC7A2 PE=1 SV=2 | NLSSPFIFHEK(1)TSEF | 13 | 0.90 |
| Q9C037 | TRIM4 | >sp\|Q9C037\|TRIM4_HUMAN E3 ubiquitin-protein ligase TRIM4 OS=Homo sapiens GN=TRIM4 PE=1 SV=2 | LNQTIASLK(0.837)K(0.163) | 2 | 0.90 |
| Q99650 | OSMR | >sp\|Q99650\|OSMR_HUMAN Oncostatin-M-specific receptor subunit beta OS=Homo sapiens GN=OSMR PE=1 SV=1 | SSILSLIK(0.98)FK(0.02) | 6 | 0.90 |
| Q9ULT6 | ZNRF3 | >sp\|Q9ULT6\|ZNRF3_HUMAN E3 ubiquitin-protein ligase ZNRF3 OS=Homo sapiens GN=ZNRF3 PE=1 SV=3 | HNIIEQK(1)GNPSAVCVETSNLSR | 1 | 0.90 |
| P33527 | MRP1 | >sp\|P33527\|MRP1_HUMAN Multidrug resistance-associated protein 1 OS=Homo sapiens GN=ABCC1 PE=1 SV=3 | TYQVAHMK(0.372)SK(0.628) | 1 | 0.90 |
| Q16186 | ADRM1 | >sp\|Q16186\|ADRM1_HUMAN Proteasomal ubiquitin receptor ADRM1 OS=Homo sapiens GN=ADRM1 PE=1 SV=2 | MSLK(1)GTTVTPDK | 1 | 0.90 |
| Q9HCM4 | E41L5 | >sp\|Q9HCM4\|E41L5_HUMAN Band 4.1-like protein 5 OS=Homo sapiens GN=EPB41L5 PE=1 SV=3 | GQTPAQAETNYLNK(0.386)AK(0.614) | 2 | 0.89 |
| P52895 | AK1C2 | >sp\|P52895\|AK1C2_HUMAN Aldo-keto reductase | SK(1)IADGSVK | 3 | 0.89 |

| | | | | | |
|---|---|---|---|---|---|
| | | family 1 member C2 OS=Homo sapiens GN=AKR1C2 PE=1 SV=3;>sp\|Q04828\|AK1C1_HUMAN Aldo-keto reductase family 1 member C1 OS=Homo sapiens GN=AKR1C1 PE=1 SV=1;>sp\|P42330\|AK1C3_HUMAN Aldo-keto reductase family 1 member C | | | |
| P60866 | RS20 | >sp\|P60866\|RS20_HUMAN 40S ribosomal protein S20 OS=Homo sapiens GN=RPS20 PE=1 SV=1 | DTGK(1)TPVEPEVAIHR | 11 | 0.89 |
| Q969G9 | NKD1 | >sp\|Q969G9\|NKD1_HUMAN Protein naked cuticle homolog 1 OS=Homo sapiens GN=NKD1 PE=1 SV=1 | VK(1)LTVAPDGSQSK | 1 | 0.89 |
| P15260 | INGR1 | >sp\|P15260\|INGR1_HUMAN Interferon gamma receptor 1 OS=Homo sapiens GN=IFNGR1 PE=1 SV=1 | EK(1)SIILPK | 1 | 0.89 |
| Q9NQX7 | ITM2C | >sp\|Q9NQX7\|ITM2C_HUMAN Integral membrane protein 2C OS=Homo sapiens GN=ITM2C PE=1 SV=1 | ADK(1)ASASAPAPASATEILLTPAR | 5 | 0.89 |
| Q9Y342 | PLLP | >sp\|Q9Y342\|PLLP_HUMAN Plasmolipin OS=Homo sapiens GN=PLLP PE=1 SV=1 | AEFPSK(1)VSTR | 22 | 0.89 |
| P20020 | AT2B1 | >sp\|P20020\|AT2B1_HUMAN Plasma membrane calcium-transporting ATPase 1 OS=Homo sapiens GN=ATP2B1 PE=1 SV=3 | IQESYGDVYGICTK(0.949)LK(0.051) | 2 | 0.89 |
| O60487 | MPZL2 | >sp\|O60487\|MPZL2_HUMAN Myelin protein zero-like protein 2 OS=Homo sapiens GN=MPZL2 PE=1 SV=1 | VVEIK(0.377)SK(0.623) | 1 | 0.89 |
| P24001 | IL32 | >sp\|P24001\|IL32_HUMAN Interleukin-32 OS=Homo sapiens GN=IL32 PE=1 SV=3 | VLSDDMK(0.426)K(0.574) | 1 | 0.89 |
| Q8NBQ5 | DHB11 | >sp\|Q8NBQ5\|DHB11_HUMAN Estradiol 17-beta-dehydrogenase 11 OS=Homo sapiens | LVLWDINK(0.991)HGLEETAAK(0.009) | 1 | 0.88 |

| | | | | | |
|---|---|---|---|---|---|
| | | GN=HSD17B11 PE=1 SV=3 | | | |
| Q9973 2 | LITA F | >sp\|Q99732\|LITAF_HUM AN Lipopolysaccharide-induced tumor necrosis factor-alpha factor OS=Homo sapiens GN=LITAF PE=1 SV=2 | ALLGTYK(1)R | 2 | 0.88 |
| P05787 | K2C8 | >sp\|P05787\|K2C8_HUMA N Keratin, type II cytoskeletal 8 OS=Homo sapiens GN=KRT8 PE=1 SV=7;>P05787 SWISS-PROT:P05787 Tax_Id=9606 Gene_Symbol=KRT8 Keratin, type II cytoskeletal 8 | DGK(1)LVSESSDVLPK | 2 | 0.88 |
| P01892 | 1A02 | >sp\|P01892\|1A02_HUMAN HLA class I histocompatibility antigen, A-2 alpha chain OS=Homo sapiens GN=HLA-A PE=1 SV=1;>sp\|P10316\|1A69_H UMAN HLA class I histocompatibility antigen, A-69 alpha chain OS=Homo sapiens GN=HLA-A PE=1 SV=2;>sp\|P01891\|1A68_H UMAN HLA cla | KGGSYSQAASSDSAQGSDVSLTACK(1) V | 6 | 0.88 |
| Q86W 74 | ANR 46 | >sp\|Q86W74\|ANR46_HU MAN Ankyrin repeat domain-containing protein 46 OS=Homo sapiens GN=ANKRD46 PE=1 SV=1 | LLESLEEQEVK(1)GFNR | 1 | 0.88 |
| O0047 1 | EXO C5 | >sp\|O00471\|EXOC5_HUM AN Exocyst complex component 5 OS=Homo sapiens GN=EXOC5 PE=1 SV=1 | K(1)VQELQK(1) | 3 | 0.88 |
| O0047 1 | EXO C5 | >sp\|O00471\|EXOC5_HUM AN Exocyst complex component 5 OS=Homo sapiens GN=EXOC5 PE=1 SV=1 | K(1)VQELQK(1) | 3 | 0.88 |
| Q0482 8 | AK1 C1 | >sp\|Q04828\|AK1C1_HUM AN Aldo-keto reductase family 1 member C1 OS=Homo sapiens GN=AKR1C1 PE=1 SV=1;>sp\|P42330\|AK1C3_ HUMAN Aldo-keto reductase family 1 member | QLEMILNK(0.949)PGLK(0.051) | 1 | 0.88 |

| | | | | | |
|---|---|---|---|---|---|
| | | C3 OS=Homo sapiens GN=AKR1C3 PE=1 SV=4;>sp\|P17516\|AK1C4_HUMAN Aldo-keto reductase family 1 member C | | | |
| Q9Y6N7 | ROBO1 | >sp\|Q9Y6N7\|ROBO1_HUMAN Roundabout homolog 1 OS=Homo sapiens GN=ROBO1 PE=1 SV=1 | TFNSPNLK(1)DGR | 2 | 0.88 |
| O60488 | ACSL4 | >sp\|O60488\|ACSL4_HUMAN Long-chain-fatty-acid--CoA ligase 4 OS=Homo sapiens GN=ACSL4 PE=1 SV=2 | NEEK(1)TAEDYSVDENGQR | 2 | 0.88 |
| Q9H444 | CHM4B | >sp\|Q9H444\|CHM4B_HUMAN Charged multivesicular body protein 4b OS=Homo sapiens GN=CHMP4B PE=1 SV=1 | LFGAGGGK(0.947)AGK(0.053) | 2 | 0.87 |
| P41440 | S19A1 | >sp\|P41440\|S19A1_HUMAN Folate transporter 1 OS=Homo sapiens GN=SLC19A1 PE=1 SV=3 | SAAEEK(1)AAQALSVQDK | 11 | 0.87 |
| P33527 | MRP1 | >sp\|P33527\|MRP1_HUMAN Multidrug resistance-associated protein 1 OS=Homo sapiens GN=ABCC1 PE=1 SV=3 | TYQVAHMK(0.5)SK(0.5) | 1 | 0.87 |
| O15320 | CTGE5 | >sp\|O15320\|CTGE5_HUMAN cTAGE family member 5 OS=Homo sapiens GN=CTAGE5 PE=1 SV=4;>sp\|Q8IX95\|CTGE3_HUMAN Putative cTAGE family member 3 OS=Homo sapiens GN=CTAGE3P PE=5 SV=1 | EQVSELNK(0.969)QK(0.031) | 1 | 0.87 |
| P16422 | EPCAM | >sp\|P16422\|EPCAM_HUMAN Epithelial cell adhesion molecule OS=Homo sapiens GN=EPCAM PE=1 SV=2 | AEIK(1)EMGEMHR | 5 | 0.86 |
| P43007 | SATT | >sp\|P43007\|SATT_HUMAN Neutral amino acid transporter A OS=Homo sapiens GN=SLC1A4 PE=1 SV=1 | SEEETSPLVTHQNPAGPVASAPELESK(1)ESVL | 4 | 0.86 |
| Q15075 | EEA1 | >sp\|Q15075\|EEA1_HUMAN Early endosome antigen 1 OS=Homo sapiens GN=EEA1 PE=1 SV=2 | IQNLEALLQK(1) | 8 | 0.86 |
| O15320 | CTGE5 | >sp\|O15320\|CTGE5_HUMAN cTAGE family member | EYEGYEVESSLK(0.98)DASFEK(0.02) | 2 | 0.86 |

| | | | | | |
|---|---|---|---|---|---|
| | | 5 OS=Homo sapiens GN=CTAGE5 PE=1 SV=4 | | | |
| Q15836 | VAMP3 | >sp\|Q15836\|VAMP3_HUMAN Vesicle-associated membrane protein 3 OS=Homo sapiens GN=VAMP3 PE=1 SV=3;>sp\|P63027\|VAMP2_HUMAN Vesicle-associated membrane protein 2 OS=Homo sapiens GN=VAMP2 PE=1 SV=3;>sp\|P23763\|VAMP1_HUMAN Vesicle-associated membrane protein 1 OS= | VNVDK(1)VLER | 21 | 0.86 |
| P45974 | UBP5 | >sp\|P45974\|UBP5_HUMAN Ubiquitin carboxyl-terminal hydrolase 5 OS=Homo sapiens GN=USP5 PE=1 SV=2 | LEK(1)IFQNAPTDPTQDFSTQVAK | 1 | 0.86 |
| Q13393 | PLD1 | >sp\|Q13393\|PLD1_HUMAN Phospholipase D1 OS=Homo sapiens GN=PLD1 PE=1 SV=1 | ETETK(1)YGIR | 6 | 0.86 |
| Q92887 | MRP2 | >sp\|Q92887\|MRP2_HUMAN Canalicular multispecific organic anion transporter 1 OS=Homo sapiens GN=ABCC2 PE=1 SV=3 | DNILFGTEFNEK(1)R | 11 | 0.86 |
| Q8NBN3 | TM87A | >sp\|Q8NBN3\|TM87A_HUMAN Transmembrane protein 87A OS=Homo sapiens GN=TMEM87A PE=1 SV=3 | VNK(1)AQEDDLK | 1 | 0.85 |
| P08034 | CXB1 | >sp\|P08034\|CXB1_HUMAN Gap junction beta-1 protein OS=Homo sapiens GN=GJB1 PE=1 SV=1 | LLSEQDGSLK(1)DILR | 1 | 0.85 |
| P00441 | SODC | >sp\|P00441\|SODC_HUMAN Superoxide dismutase [Cu-Zn] OS=Homo sapiens GN=SOD1 PE=1 SV=2 | TLVVHEK(0.978)ADDLGK(0.022) | 1 | 0.85 |
| P62820 | RAB1A | >sp\|P62820\|RAB1A_HUMAN Ras-related protein Rab-1A OS=Homo sapiens GN=RAB1A PE=1 SV=3 | MGPGATAGGAEK(0.987)SNVK(0.013) | 1 | 0.85 |
| P61981 | 1433G | >sp\|P61981\|1433G_HUMAN 14-3-3 protein gamma OS=Homo sapiens GN=YWHAG PE=1 SV=2 | VDREQLVQK(1)AR | 1 | 0.85 |
| P21860 | ERBB3 | >sp\|P21860\|ERBB3_HUMAN Receptor tyrosine-protein kinase erbB-3 | GESIEPLDPSEK(0.454)ANK(0.546) | 4 | 0.85 |

| | | | | | |
|---|---|---|---|---|---|
| | | OS=Homo sapiens GN=ERBB3 PE=1 SV=1 | | | |
| Q9Y287 | ITM2B | >sp\|Q9Y287\|ITM2B_HUMAN Integral membrane protein 2B OS=Homo sapiens GN=ITM2B PE=1 SV=1 | VTFNSALAQK(0.983)EAK(0.811)K(0.205) | 1 | 0.85 |
| Q9UBB4 | ATX10 | >sp\|Q9UBB4\|ATX10_HUMAN Ataxin-10 OS=Homo sapiens GN=ATXN10 PE=1 SV=1 | ITSDEPLTK(1)DDIPVFLR | 4 | 0.85 |
| P05362 | ICAM1 | >sp\|P05362\|ICAM1_HUMAN Intercellular adhesion molecule 1 OS=Homo sapiens GN=ICAM1 PE=1 SV=2 | LQQAQK(0.995)GTPMK(0.005)PNTQATPP | 3 | 0.85 |
| P27348 | 1433T | >sp\|P27348\|1433T_HUMAN 14-3-3 protein theta OS=Homo sapiens GN=YWHAQ PE=1 SV=1 | TELIQK(0.5)AK(0.5) | 1 | 0.84 |
| P27348 | 1433T | >sp\|P27348\|1433T_HUMAN 14-3-3 protein theta OS=Homo sapiens GN=YWHAQ PE=1 SV=1 | TELIQK(0.5)AK(0.5) | 1 | 0.84 |
| Q92887 | MRP2 | >sp\|Q92887\|MRP2_HUMAN Canalicular multispecific organic anion transporter 1 OS=Homo sapiens GN=ABCC2 PE=1 SV=3 | TK(1)TLVSK | 3 | 0.84 |
| Q9NQX7 | ITM2C | >sp\|Q9NQX7\|ITM2C_HUMAN Integral membrane protein 2C OS=Homo sapiens GN=ITM2C PE=1 SV=1 | VK(1)ISFQPAVAGIK | 5 | 0.84 |
| P23229 | ITA6 | >sp\|P23229\|ITA6_HUMAN Integrin alpha-6 OS=Homo sapiens GN=ITGA6 PE=1 SV=5 | YIDNLEK(0.413)K(0.587) | 2 | 0.84 |
| P29317 | EPHA2 | >sp\|P29317\|EPHA2_HUMAN Ephrin type-A receptor 2 OS=Homo sapiens GN=EPHA2 PE=1 SV=2 | SEQLK(0.998)PLK(0.002) | 5 | 0.83 |
| Q6EMK4 | VASN | >sp\|Q6EMK4\|VASN_HUMAN Vasorin OS=Homo sapiens GN=VASN PE=1 SV=1 | GQVGPGAGPLELEGVK(0.999)VPLEPGPK(0.001) | 4 | 0.83 |
| Q06481 | APLP2 | >sp\|Q06481\|APLP2_HUMAN Amyloid-like protein 2 OS=Homo sapiens GN=APLP2 PE=1 SV=2 | HLNK(1)MQNHGYENPTYK | 2 | 0.83 |
| P31946 | 1433B | >sp\|P31946\|1433B_HUMAN 14-3-3 protein beta/alpha OS=Homo sapiens GN=YWHAB PE=1 SV=3 | SELVQK(0.993)AK(0.007) | 8 | 0.83 |

| | | | | | |
|---|---|---|---|---|---|
| Q15758 | AAAT | >sp\|Q15758\|AAAT_HUMAN Neutral amino acid transporter B(0) OS=Homo sapiens GN=SLC1A5 PE=1 SV=2 | STEPELIQVK(1)SELPLDPLPVPTEEGNPLLK | 8 | 0.83 |
| P35241 | RADI | >sp\|P35241\|RADI_HUMAN Radixin OS=Homo sapiens GN=RDX PE=1 SV=1 | VLEQHK(0.986)LTK(0.014) | 3 | 0.82 |
| P31946 | 1433B | >sp\|P31946\|1433B_HUMAN 14-3-3 protein beta/alpha OS=Homo sapiens GN=YWHAB PE=1 SV=3;>sp\|Q04917\|1433F_HUMAN 14-3-3 protein eta OS=Homo sapiens GN=YWHAH PE=1 SV=4;>sp\|P61981\|1433G_HUMAN 14-3-3 protein gamma OS=Homo sapiens GN=YWHAG PE=1 SV=2;>sp\|P63104\|1433Z | NLLSVAYK(1)NVVGAR | 2 | 0.82 |
| P17752 | TPH1 | >sp\|P17752\|TPH1_HUMAN Tryptophan 5-hydroxylase 1 OS=Homo sapiens GN=TPH1 PE=1 SV=4 | ENK(1)DHSLER | 2 | 0.82 |
| O00560 | SDCB1 | >sp\|O00560\|SDCB1_HUMAN Syntenin-1 OS=Homo sapiens GN=SDCBP PE=1 SV=1 | SLYPSLEDLK(0.942)VDK(0.058) | 4 | 0.82 |
| P78504 | JAG1 | >sp\|P78504\|JAG1_HUMAN Protein jagged-1 OS=Homo sapiens GN=JAG1 PE=1 SV=3 | EQLNQIK(0.999)NPIEK(0.001) | 11 | 0.82 |
| O15126 | SCAM1 | >sp\|O15126\|SCAM1_HUMAN Secretory carrier-associated membrane protein 1 OS=Homo sapiens GN=SCAMP1 PE=1 SV=2 | EHALAQAELLK(1)R | 6 | 0.82 |
| P78310 | CXAR | >sp\|P78310\|CXAR_HUMAN Coxsackievirus and adenovirus receptor OS=Homo sapiens GN=CXADR PE=1 SV=1 | MGAIPVMIPAQSK(1)DGSIV | 1 | 0.81 |
| Q96QD8 | S38A2 | >sp\|Q96QD8\|S38A2_HUMAN Sodium-coupled neutral amino acid transporter 2 OS=Homo sapiens GN=SLC38A2 PE=1 SV=2 | SHYADVDPENQNFLLESNLGK(0.606)K(0.394) | 24 | 0.81 |
| Q8N4S9 | MALD2 | >sp\|Q8N4S9\|MALD2_HUMAN MARVEL domain-containing protein 2 OS=Homo sapiens | TYSEK(1)VEEYNLR | 1 | 0.81 |

| | | | | | |
|---|---|---|---|---|---|
| | | GN=MARVELD2 PE=1 SV=2 | | | |
| P22455 | FGFR4 | >sp\|P22455\|FGFR4_HUMAN Fibroblast growth factor receptor 4 OS=Homo sapiens GN=FGFR4 PE=1 SV=2 | QFSLESGSSGK(1)SSSSLVR | 3 | 0.81 |
| Q06481 | APLP2 | >sp\|Q06481\|APLP2_HUMAN Amyloid-like protein 2 OS=Homo sapiens GN=APLP2 PE=1 SV=2 | MQNHGYENPTYK(1)YLEQMQI | 1 | 0.81 |
| O95477 | ABCA1 | >sp\|O95477\|ABCA1_HUMAN ATP-binding cassette sub-family A member 1 OS=Homo sapiens GN=ABCA1 PE=1 SV=3 | YGEK(1)YAGNYSGGNK | 1 | 0.80 |
| P05556 | ITB1 | >sp\|P05556\|ITB1_HUMAN Integrin beta-1 OS=Homo sapiens GN=ITGB1 PE=1 SV=2 | WDTGENPIYK(1)SAVTTVVNPK | 10 | 0.80 |
| P34741 | SDC2 | >sp\|P34741\|SDC2_HUMAN Syndecan-2 OS=Homo sapiens GN=SDC2 PE=1 SV=2 | APTK(1)EFYA | 2 | 0.80 |
| Q04828 | AK1C1 | >sp\|Q04828\|AK1C1_HUMAN Aldo-keto reductase family 1 member C1 OS=Homo sapiens GN=AKR1C1 PE=1 SV=1 | SK(1)ALEATK | 1 | 0.80 |
| Q9UEU0 | VTI1B | >sp\|Q9UEU0\|VTI1B_HUMAN Vesicle transport through interaction with t-SNAREs homolog 1B OS=Homo sapiens GN=VTI1B PE=1 SV=3 | LVNTSENLSK(1)SR | 1 | 0.80 |
| Q9BRK3 | MXRA8 | >sp\|Q9BRK3\|MXRA8_HUMAN Matrix-remodeling-associated protein 8 OS=Homo sapiens GN=MXRA8 PE=1 SV=1 | AELAHSPLPAK(0.999)YIDLDK(0.001) | 1 | 0.80 |
| P31431 | SDC4 | >sp\|P31431\|SDC4_HUMAN Syndecan-4 OS=Homo sapiens GN=SDC4 PE=1 SV=2 | DEGSYDLGK(0.435)K(0.56)PIYK(0.005) | 2 | 0.80 |
| P68363 | TBA1B | >sp\|P68363\|TBA1B_HUMAN Tubulin alpha-1B chain OS=Homo sapiens GN=TUBA1B PE=1 SV=1;>sp\|Q71U36\|TBA1A_HUMAN Tubulin alpha-1A chain OS=Homo sapiens GN=TUBA1A PE=1 SV=1;>sp\|Q13748\|TBA3C_HUMAN Tubulin alpha- | GDVVPK(1)DVNAAIATIK | 2 | 0.80 |

| | | | | | |
|---|---|---|---|---|---|
| | | 3C/D chain OS=Homo sapiens GN=TUBA3C PE=1 SV=3;>sp\|Q6PE | | | |
| P01009 | A1AT | >sp\|P01009\|A1AT_HUMAN Alpha-1-antitrypsin OS=Homo sapiens GN=SERPINA1 PE=1 SV=3;>sp\|P20848\|A1ATR_HUMAN Putative alpha-1-antitrypsin-related protein OS=Homo sapiens GN=SERPINA2 PE=1 SV=1 | VVNPTQK(1) | 1 | 0.79 |
| P08727 | K1C19 | >sp\|P08727\|K1C19_HUMAN Keratin, type I cytoskeletal 19 OS=Homo sapiens GN=KRT19 PE=1 SV=4;>P08727 SWISS-PROT:P08727 Tax_Id=9606 Gene_Symbol=KRT19 Keratin, type I cytoskeletal 19;>sp\|Q04695\|K1C17_HUMAN Keratin, type I cytoskeletal 17 OS=Homo sapiens GN=KRT1 | TK(1)FETEQALR | 3 | 0.79 |
| Q16625 | OCLN | >sp\|Q16625\|OCLN_HUMAN Occludin OS=Homo sapiens GN=OCLN PE=1 SV=1 | EHIYDEQPPNVEEWVK(1)NVSAGTQDVPSPPSDYVER | 3 | 0.78 |
| P54252 | ATX3 | >sp\|P54252\|ATX3_HUMAN Ataxin-3 OS=Homo sapiens GN=ATXN3 PE=1 SV=4 | VHK(1)TDLER | 1 | 0.78 |
| Q9NQ84 | GPC5C | >sp\|Q9NQ84\|GPC5C_HUMAN G-protein coupled receptor family C group 5 member C OS=Homo sapiens GN=GPRC5C PE=1 SV=2 | DGK(1)NSQVFR | 6 | 0.78 |
| P30825 | CTR1 | >sp\|P30825\|CTR1_HUMAN High affinity cationic amino acid transporter 1 OS=Homo sapiens GN=SLC7A1 PE=1 SV=1 | TPDGNLDQCK(1) | 3 | 0.78 |
| P11532 | DMD | >sp\|P11532\|DMD_HUMAN Dystrophin OS=Homo sapiens GN=DMD PE=1 SV=3;>sp\|P46939\|UTRO_HUMAN Utrophin OS=Homo sapiens GN=UTRN PE=1 SV=2 | VAAAETAK(0.854)HQAK(0.146) | 1 | 0.77 |
| Q86WA9 | S2611 | >sp\|Q86WA9\|S2611_HUMAN Sodium-independent sulfate anion transporter | EDSILDQK(1)VALLK | 8 | 0.77 |

| | | | | | |
|---|---|---|---|---|---|
| | | OS=Homo sapiens GN=SLC26A11 PE=2 SV=2 | | | |
| P05067 | A4 | >sp\|P05067\|A4_HUMAN Amyloid beta A4 protein OS=Homo sapiens GN=APP PE=1 SV=3 | HLSK(1)MQQNGYENPTYK | 2 | 0.77 |
| P05556 | ITB1 | >sp\|P05556\|ITB1_HUMAN Integrin beta-1 OS=Homo sapiens GN=ITGB1 PE=1 SV=2 | SAVTTVVNPK(1)YEGK | 26 | 0.77 |
| P63104 | 1433Z | >sp\|P63104\|1433Z_HUMAN 14-3-3 protein zeta/delta OS=Homo sapiens GN=YWHAZ PE=1 SV=1 | NELVQK(0.947)AK(0.053) | 1 | 0.77 |
| P14625 | ENPL | >sp\|P14625\|ENPL_HUMAN Endoplasmin OS=Homo sapiens GN=HSP90B1 PE=1 SV=1;>sp\|Q58FF3\|ENPLL_HUMAN Putative endoplasmin-like protein OS=Homo sapiens GN=HSP90B2P PE=5 SV=1 | K(1)TFEINPR | 1 | 0.77 |
| Q5W0Z9 | ZDH20 | >sp\|Q5W0Z9\|ZDH20_HUMAN Probable palmitoyltransferase ZDHHC20 OS=Homo sapiens GN=ZDHHC20 PE=1 SV=1 | SSGSNQPFPIK(0.931)PLSESK(0.069) | 1 | 0.76 |
| Q13286 | CLN3 | >sp\|Q13286\|CLN3_HUMAN Battenin OS=Homo sapiens GN=CLN3 PE=1 SV=1 | TEAPESK(1)PGSSSSLSLR | 9 | 0.76 |
| P04114 | APOB | >sp\|P04114\|APOB_HUMAN Apolipoprotein B-100 OS=Homo sapiens GN=APOB PE=1 SV=2 | FQK(1)AASGTTGTYQEWK | 2 | 0.76 |
| Q93050 | VPP1 | >sp\|Q93050\|VPP1_HUMAN V-type proton ATPase 116 kDa subunit a isoform 1 OS=Homo sapiens GN=ATP6V0A1 PE=1 SV=3 | K(1)EMASGVNTR | 1 | 0.76 |
| Q15836 | VAMP3 | >sp\|Q15836\|VAMP3_HUMAN Vesicle-associated membrane protein 3 OS=Homo sapiens GN=VAMP3 PE=1 SV=3;>sp\|P63027\|VAMP2_HUMAN Vesicle-associated membrane protein 2 OS=Homo sapiens GN=VAMP2 PE=1 | DQK(1)LSELDDRADALQAGASQFETSAAK | 2 | 0.75 |

| | | | | | |
|---|---|---|---|---|---|
| | | SV=3;>sp\|P23763\|VAMP1_HUMAN Vesicle-associated membrane protein 1 OS= | | | |
| Q9NQX7 | ITM2C | >sp\|Q9NQX7\|ITM2C_HUMAN Integral membrane protein 2C OS=Homo sapiens GN=ITM2C PE=1 SV=1 | ISFQPAVAGIK(0.996)GDK(0.82)ADK(0.184) | 3 | 0.75 |
| P02786 | TFR1 | >sp\|P02786\|TFR1_HUMAN Transferrin receptor protein 1 OS=Homo sapiens GN=TFRC PE=1 SV=2 | LAVDEEENADNNTK(0.984)ANVTK(0.013)PK(0.003) | 4 | 0.75 |
| P12004 | PCNA | >sp\|P12004\|PCNA_HUMAN Proliferating cell nuclear antigen OS=Homo sapiens GN=PCNA PE=1 SV=1 | DLSHIGDAVVISCAK(0.804)DGVK(0.196) | 1 | 0.75 |
| Q92887 | MRP2 | >sp\|Q92887\|MRP2_HUMAN Canalicular multispecific organic anion transporter 1 OS=Homo sapiens GN=ABCC2 PE=1 SV=3 | EDEELVK(0.97)GQK(0.03) | 1 | 0.75 |
| P34741 | SDC2 | >sp\|P34741\|SDC2_HUMAN Syndecan-2 OS=Homo sapiens GN=SDC2 PE=1 SV=2 | KPSSAAYQK(1)APTK | 3 | 0.74 |
| P21359 | NF1 | >sp\|P21359\|NF1_HUMAN Neurofibromin OS=Homo sapiens GN=NF1 PE=1 SV=2 | NLLFNPSK(1)PFSR | 3 | 0.74 |
| Q99878 | H2A1J | >sp\|Q99878\|H2A1J_HUMAN Histone H2A type 1-J OS=Homo sapiens GN=HIST1H2AJ PE=1 SV=3;>sp\|Q96KK5\|H2A1H_HUMAN Histone H2A type 1-H OS=Homo sapiens GN=HIST1H2AH PE=1 SV=3;>sp\|Q9BTM1\|H2AJ_HUMAN Histone H2A.J OS=Homo sapiens GN=H2AFJ PE=1 SV=1;>sp\|Q93077\|H2A1C_HU | VTIAQGGVLPNIQAVLLPK(1) | 3 | 0.74 |
| P30825 | CTR1 | >sp\|P30825\|CTR1_HUMAN High affinity cationic amino acid transporter 1 OS=Homo sapiens GN=SLC7A1 PE=1 SV=1 | TILSPK(0.979)NMEPSK(0.021) | 1 | 0.74 |
| O14828 | SCAM3 | >sp\|O14828\|SCAM3_HUMAN Secretory carrier-associated membrane protein 3 OS=Homo sapiens GN=SCAMP3 PE=1 SV=3 | NYGSYSTQASAAAATAELLK(0.5)K(0.5) | 16 | 0.74 |

| | | | | | |
|---|---|---|---|---|---|
| O14828 | SCAM3 | >sp\|O14828\|SCAM3_HUMAN Secretory carrier-associated membrane protein 3 OS=Homo sapiens GN=SCAMP3 PE=1 SV=3 | NYGSYSTQASAAAATAELLK(0.5)K(0.5) | 16 | 0.74 |
| P62820 | RAB1A | >sp\|P62820\|RAB1A_HUMAN Ras-related protein Rab-1A OS=Homo sapiens GN=RAB1A PE=1 SV=3 | SNVK(1)IQSTPVK | 6 | 0.73 |
| O43491 | E41L2 | >sp\|O43491\|E41L2_HUMAN Band 4.1-like protein 2 OS=Homo sapiens GN=EPB41L2 PE=1 SV=1 | TTEVGSVSEVK(0.881)K(0.119) | 4 | 0.73 |
| Q9BV40 | VAMP8 | >sp\|Q9BV40\|VAMP8_HUMAN Vesicle-associated membrane protein 8 OS=Homo sapiens GN=VAMP8 PE=1 SV=1 | NLQSEVEGVK(1)NIMTQNVER | 5 | 0.73 |
| P01111 | RASN | >sp\|P01111\|RASN_HUMAN GTPase NRas OS=Homo sapiens GN=NRAS PE=1 SV=1 | TVDTK(1)QAHELAK | 6 | 0.73 |
| P24001 | IL32 | >sp\|P24001\|IL32_HUMAN Interleukin-32 OS=Homo sapiens GN=IL32 PE=1 SV=3 | GDK(1)EELTPQK | 5 | 0.73 |
| Q9H7X2 | CA115 | >sp\|Q9H7X2\|CA115_HUMAN Uncharacterized protein C1orf115 OS=Homo sapiens GN=C1orf115 PE=2 SV=1 | SK(1)AESSLLR | 8 | 0.72 |
| P61088 | UBE2N | >sp\|P61088\|UBE2N_HUMAN Ubiquitin-conjugating enzyme E2 N OS=Homo sapiens GN=UBE2N PE=1 SV=1 | ICLDILK(0.961)DK(0.039) | 9 | 0.72 |
| Q9H1Z9 | TSN10 | >sp\|Q9H1Z9\|TSN10_HUMAN Tetraspanin-10 OS=Homo sapiens GN=TSPAN10 PE=2 SV=1 | AGPQSPSPGAPPAAK(1)PARG | 1 | 0.72 |
| Q14534 | ERG1 | >sp\|Q14534\|ERG1_HUMAN Squalene monooxygenase OS=Homo sapiens GN=SQLE PE=1 SV=3 | SPPESENK(1)EQLEAR | 5 | 0.71 |
| P11166 | GTR1 | >sp\|P11166\|GTR1_HUMAN Solute carrier family 2, facilitated glucose transporter member 1 OS=Homo sapiens GN=SLC2A1 PE=1 SV=2 | QGGASQSDK(1)TPEELFHPLGADSQV | 14 | 0.71 |
| Q15012 | LAP4A | >sp\|Q15012\|LAP4A_HUMAN Lysosomal-associated transmembrane protein 4A OS=Homo sapiens | MPEK(1)EPPPPYLPA | 1 | 0.71 |

| | | | | | |
|---|---|---|---|---|---|
| | | GN=LAPTM4A PE=1 SV=1 | | | |
| Q9H3M7 | TXNIP | >sp\|Q9H3M7\|TXNIP_HUMAN Thioredoxin-interacting protein OS=Homo sapiens GN=TXNIP PE=1 SV=1 | VYGSGEK(1)VAGR | 7 | 0.70 |
| O43491 | E41L2 | >sp\|O43491\|E41L2_HUMAN Band 4.1-like protein 2 OS=Homo sapiens GN=EPB41L2 PE=1 SV=1 | TTEVGSVSEVK(0.455)K(0.545) | 4 | 0.70 |
| Q86Y82 | STX12 | >sp\|Q86Y82\|STX12_HUMAN Syntaxin-12 OS=Homo sapiens GN=STX12 PE=1 SV=1 | NLMSQLGTK(0.931)QDSSK(0.069) | 1 | 0.70 |
| P62269 | RS18 | >sp\|P62269\|RS18_HUMAN 40S ribosomal protein S18 OS=Homo sapiens GN=RPS18 PE=1 SV=3 | SLVIPEK(1)FQHILR | 1 | 0.69 |
| Q96GS6 | AB17A | >sp\|Q96GS6\|AB17A_HUMAN Alpha/beta hydrolase domain-containing protein 17A OS=Homo sapiens GN=ABHD17A PE=1 SV=1 | ELDTIEVFPTK(1)SAR | 1 | 0.69 |
| P18669 | PGAM1 | >sp\|P18669\|PGAM1_HUMAN Phosphoglycerate mutase 1 OS=Homo sapiens GN=PGAM1 PE=1 SV=2;>sp\|Q8N0Y7\|PGAM4_HUMAN Probable phosphoglycerate mutase 4 OS=Homo sapiens GN=PGAM4 PE=3 SV=1 | AAYK(1)LVLIR | 6 | 0.69 |
| O14828 | SCAM3 | >sp\|O14828\|SCAM3_HUMAN Secretory carrier-associated membrane protein 3 OS=Homo sapiens GN=SCAMP3 PE=1 SV=3 | K(1)LSPTEPK | 2 | 0.69 |
| P68036 | UB2L3 | >sp\|P68036\|UB2L3_HUMAN Ubiquitin-conjugating enzyme E2 L3 OS=Homo sapiens GN=UBE2L3 PE=1 SV=1 | TK(1)IYHPNIDEK | 1 | 0.69 |
| Q12846 | STX4 | >sp\|Q12846\|STX4_HUMAN Syntaxin-4 OS=Homo sapiens GN=STX4 PE=1 SV=2 | GQEHVK(0.997)TALENQK(0.003) | 1 | 0.68 |
| Q7KYR7 | BT2A1 | >sp\|Q7KYR7\|BT2A1_HUMAN Butyrophilin subfamily 2 member A1 OS=Homo sapiens GN=BTN2A1 PE=1 SV=3 | EIALK(1)ELEK | 12 | 0.66 |
| P01116 | RASK | >sp\|P01116\|RASK_HUMAN GTPase KRas OS=Homo | TVDTK(1)QAQDLAR | 2 | 0.66 |

| | | | | | |
|---|---|---|---|---|---|
| | | sapiens GN=KRAS PE=1 SV=1 | | | |
| Q9BQS8 | FYCO1 | >sp\|Q9BQS8\|FYCO1_HUMAN FYVE and coiled-coil domain-containing protein 1 OS=Homo sapiens GN=FYCO1 PE=1 SV=3 | TK(1)VEEVNR | 4 | 0.65 |
| Q15836 | VAMP3 | >sp\|Q15836\|VAMP3_HUMAN Vesicle-associated membrane protein 3 OS=Homo sapiens GN=VAMP3 PE=1 SV=3;>sp\|P63027\|VAMP2_HUMAN Vesicle-associated membrane protein 2 OS=Homo sapiens GN=VAMP2 PE=1 SV=3 | ADALQAGASQFETSAAK(0.809)LK(0.191) | 4 | 0.65 |
| Q8WTW3 | COG1 | >sp\|Q8WTW3\|COG1_HUMAN Conserved oligomeric Golgi complex subunit 1 OS=Homo sapiens GN=COG1 PE=1 SV=1 | ATAATSPALK(1)R | 2 | 0.65 |
| Q5T3U5 | MRP7 | >sp\|Q5T3U5\|MRP7_HUMAN Multidrug resistance-associated protein 7 OS=Homo sapiens GN=ABCC10 PE=1 SV=1 | TK(1)EGLEEEQSTSGR | 9 | 0.64 |
| Q8IVM0 | CCD50 | >sp\|Q8IVM0\|CCD50_HUMAN Coiled-coil domain-containing protein 50 OS=Homo sapiens GN=CCDC50 PE=1 SV=1 | VMK(1)EAVSTPSR | 1 | 0.63 |
| Q9BV40 | VAMP8 | >sp\|Q9BV40\|VAMP8_HUMAN Vesicle-associated membrane protein 8 OS=Homo sapiens GN=VAMP8 PE=1 SV=1 | NK(1)TEDLEATSEHFK | 13 | 0.63 |
| P05783 | K1C18 | >sp\|P05783\|K1C18_HUMAN Keratin, type I cytoskeletal 18 OS=Homo sapiens GN=KRT18 PE=1 SV=2 | VVSETNDTK(1)VLR | 2 | 0.63 |
| Q9BV40 | VAMP8 | >sp\|Q9BV40\|VAMP8_HUMAN Vesicle-associated membrane protein 8 OS=Homo sapiens GN=VAMP8 PE=1 SV=1 | TEDLEATSEHFK(1)TTSQK | 10 | 0.62 |
| P35670 | ATP7B | >sp\|P35670\|ATP7B_HUMAN Copper-transporting ATPase 2 OS=Homo sapiens GN=ATP7B PE=1 SV=4 | ALVK(1)FDPEIIGPR | 2 | 0.62 |
| P57053 | H2BFS | >sp\|P57053\|H2BFS_HUMAN Histone H2B type F-S | HAVSEGTK(1)AVTK | 1 | 0.62 |

| | | | | | |
|---|---|---|---|---|---|
| | | OS=Homo sapiens GN=H2BFS PE=1 SV=2;>sp\|O60814\|H2B1K_HUMAN Histone H2B type 1-K OS=Homo sapiens GN=HIST1H2BK PE=1 SV=3;>sp\|Q16778\|H2B2E_HUMAN Histone H2B type 2-E OS=Homo sapiens GN=HIST2H2BE PE=1 SV=3;>sp\|P33778\| | | | |
| O15126 | SCAM1 | >sp\|O15126\|SCAM1_HUMAN Secretory carrier-associated membrane protein 1 OS=Homo sapiens GN=SCAMP1 PE=1 SV=2 | TVQTAAANAASTAASSAAQNAFK(1)GNQI | 11 | 0.61 |
| O60664 | PLIN3 | >sp\|O60664\|PLIN3_HUMAN Perilipin-3 OS=Homo sapiens GN=PLIN3 PE=1 SV=3 | GAVQSGVDK(0.486)TK(0.514) | 1 | 0.60 |
| Q07954 | LRP1 | >sp\|Q07954\|LRP1_HUMAN Prolow-density lipoprotein receptor-related protein 1 OS=Homo sapiens GN=LRP1 PE=1 SV=2 | HSLASTDEK(1)R | 1 | 0.60 |
| Q9NQ84 | GPC5C | >sp\|Q9NQ84\|GPC5C_HUMAN G-protein coupled receptor family C group 5 member C OS=Homo sapiens GN=GPRC5C PE=1 SV=2 | GQSMFVENK(1)AFSMDEPVAAK | 5 | 0.60 |
| P78324 | SHPS1 | >sp\|P78324\|SHPS1_HUMAN Tyrosine-protein phosphatase non-receptor type substrate 1 OS=Homo sapiens GN=SIRPA PE=1 SV=2 | LHEPEK(1)NAR | 1 | 0.60 |
| P00441 | SODC | >sp\|P00441\|SODC_HUMAN Superoxide dismutase [Cu-Zn] OS=Homo sapiens GN=SOD1 PE=1 SV=2 | GDGPVQGIINFEQK(0.973)ESNGPVK(0.027) | 1 | 0.59 |
| P62888 | RL30 | >sp\|P62888\|RL30_HUMAN 60S ribosomal protein L30 OS=Homo sapiens GN=RPL30 PE=1 SV=2 | SGK(1)YVLGYK | 2 | 0.59 |
| O60488 | ACSL4 | >sp\|O60488\|ACSL4_HUMAN Long-chain-fatty-acid--CoA ligase 4 OS=Homo sapiens GN=ACSL4 PE=1 SV=2 | NHYLK(1)DIER | 1 | 0.58 |
| P62834 | RAP1A | >sp\|P62834\|RAP1A_HUMAN Ras-related protein Rap-1A OS=Homo sapiens GN=RAP1A PE=1 SV=1;>sp\|P61224\|RAP1B | SALTVQFVQGIFVEK(1)YDPTIEDSYRK | 2 | 0.58 |

| | | | | | |
|---|---|---|---|---|---|
| | | HUMAN Ras-related protein Rap-1b OS=Homo sapiens GN=RAP1B PE=1 SV=1 | | | |
| O15269 | SPTC1 | >sp\|O15269\|SPTC1_HUMAN Serine palmitoyltransferase 1 OS=Homo sapiens GN=SPTLC1 PE=1 SV=1 | LLK(1)EQEIEDQK | 1 | 0.57 |
| P61421 | VA0D1 | >sp\|P61421\|VA0D1_HUMAN V-type proton ATPase subunit d 1 OS=Homo sapiens GN=ATP6V0D1 PE=1 SV=1 | AK(1)IDNYIPIF | 10 | 0.55 |
| Q15286 | RAB35 | >sp\|Q15286\|RAB35_HUMAN Ras-related protein Rab-35 OS=Homo sapiens GN=RAB35 PE=1 SV=1 | DNLAK(1)QQQQQQNDVVK | 1 | 0.54 |
| Q13596 | SNX1 | >sp\|Q13596\|SNX1_HUMAN Sorting nexin-1 OS=Homo sapiens GN=SNX1 PE=1 SV=3 | SK(1)QFAVK | 1 | 0.54 |
| P46783 | RS10 | >sp\|P46783\|RS10_HUMAN 40S ribosomal protein S10 OS=Homo sapiens GN=RPS10 PE=1 SV=1 | SAVPPGADK(0.437)K(0.563) | 12 | 0.53 |
| P11717 | MPRI | >sp\|P11717\|MPRI_HUMAN Cation-independent mannose-6-phosphate receptor OS=Homo sapiens GN=IGF2R PE=1 SV=3 | SSNVSYK(0.957)YSK(0.043) | 2 | 0.53 |
| O60488 | ACSL4 | >sp\|O60488\|ACSL4_HUMAN Long-chain-fatty-acid--CoA ligase 4 OS=Homo sapiens GN=ACSL4 PE=1 SV=2 | SDQSYVISFVVPNQK(1)R | 1 | 0.53 |
| P61088 | UBE2N | >sp\|P61088\|UBE2N_HUMAN Ubiquitin-conjugating enzyme E2 N OS=Homo sapiens GN=UBE2N PE=1 SV=1 | IYHPNVDK(1)LGR | 3 | 0.51 |
| P55072 | TERA | >sp\|P55072\|TERA_HUMAN Transitional endoplasmic reticulum ATPase OS=Homo sapiens GN=VCP PE=1 SV=4 | ASGADSK(1)GDDLSTAILK | 13 | 0.51 |
| O00214 | LEG8 | >sp\|O00214\|LEG8_HUMAN Galectin-8 OS=Homo sapiens GN=LGALS8 PE=1 SV=4 | SFNVDLLAGK(0.345)SK(0.655) | 1 | 0.51 |
| P17301 | ITA2 | >sp\|P17301\|ITA2_HUMAN Integrin alpha-2 OS=Homo sapiens GN=ITGA2 PE=1 SV=1 | MTK(1)NPDEIDETTELSS | 3 | 0.49 |

| | | | | | |
|---|---|---|---|---|---|
| Q9UEU0 | VTI1B | >sp\|Q9UEU0\|VTI1B_HUMAN Vesicle transport through interaction with t-SNAREs homolog 1B OS=Homo sapiens GN=VTI1B PE=1 SV=3 | ASSAASSEHFEK(1)LHEIFR | 12 | 0.49 |
| Q96A25 | T106A | >sp\|Q96A25\|T106A_HUMAN Transmembrane protein 106A OS=Homo sapiens GN=TMEM106A PE=2 SV=1 | SILSSK(1)PAIGSK | 8 | 0.49 |
| Q07817 | B2CL1 | >sp\|Q07817\|B2CL1_HUMAN Bcl-2-like protein 1 OS=Homo sapiens GN=BCL2L1 PE=1 SV=1 | EVIPMAAVK(1)QALR | 1 | 0.47 |
| Q93050 | VPP1 | >sp\|Q93050\|VPP1_HUMAN V-type proton ATPase 116 kDa subunit a isoform 1 OS=Homo sapiens GN=ATP6V0A1 PE=1 SV=3 | VLQAAAK(1)NIR | 3 | 0.47 |
| Q9NR09 | BIRC6 | >sp\|Q9NR09\|BIRC6_HUMAN Baculoviral IAP repeat-containing protein 6 OS=Homo sapiens GN=BIRC6 PE=1 SV=2 | GSSYK(1)LLVEQAK | 1 | 0.46 |
| Q13404 | UB2V1 | >sp\|Q13404\|UB2V1_HUMAN Ubiquitin-conjugating enzyme E2 variant 1 OS=Homo sapiens GN=UBE2V1 PE=1 SV=2 | AATTGSGVK(1)VPR | 1 | 0.46 |
| P17096 | HMGA1 | >sp\|P17096\|HMGA1_HUMAN High mobility group protein HMG-I/HMG-Y OS=Homo sapiens GN=HMGA1 PE=1 SV=3 | SESSSK(1)SSQPLASK | 4 | 0.45 |
| Q9NQ84 | GPC5C | >sp\|Q9NQ84\|GPC5C_HUMAN G-protein coupled receptor family C group 5 member C OS=Homo sapiens GN=GPRC5C PE=1 SV=2 | GVGYETILK(1)EQK | 15 | 0.44 |
| Q6IAA8 | LTOR1 | >sp\|Q6IAA8\|LTOR1_HUMAN Ragulator complex protein LAMTOR1 OS=Homo sapiens GN=LAMTOR1 PE=1 SV=2 | K(1)LLLDPSSPPTK | 26 | 0.42 |
| P60866 | RS20 | >sp\|P60866\|RS20_HUMAN 40S ribosomal protein S20 OS=Homo sapiens GN=RPS20 PE=1 SV=1 | NVK(0.999)SLEK(0.001) | 1 | 0.40 |
| O95772 | MENTO | >sp\|O95772\|MENTO_HUMAN MLN64 N-terminal domain homolog OS=Homo | QDSEK(1)PLLEL | 3 | 0.39 |

| | | | | | |
|---|---|---|---|---|---|
| | | sapiens GN=STARD3NL PE=1 SV=1 | | | |
| P51149 | RAB7A | >sp\|P51149\|RAB7A_HUMAN Ras-related protein Rab-7a OS=Homo sapiens GN=RAB7A PE=1 SV=1 | QETEVELYNEFPEPIK(0.706)LDK(0.294) | 4 | 0.39 |
| P60866 | RS20 | >sp\|P60866\|RS20_HUMAN 40S ribosomal protein S20 OS=Homo sapiens GN=RPS20 PE=1 SV=1 | AFK(1)DTGK | 8 | 0.38 |
| Q9H3Z4 | DNJC5 | >sp\|Q9H3Z4\|DNJC5_HUMAN DnaJ homolog subfamily C member 5 OS=Homo sapiens GN=DNAJC5 PE=1 SV=1 | LALK(0.937)YHPDK(0.062)NPDNPEAADK(0.001) | 1 | 0.38 |
| Q9BTU6 | P4K2A | >sp\|Q9BTU6\|P4K2A_HUMAN Phosphatidylinositol 4-kinase type 2-alpha OS=Homo sapiens GN=PI4K2A PE=1 SV=1 | DTDWVVVK(1)EPVIK | 7 | 0.38 |
| P0CG47 | UBB | >sp\|P0CG47\|UBB_HUMAN Polyubiquitin-B OS=Homo sapiens GN=UBB PE=1 SV=1;>sp\|P0CG48\|UBC_HUMAN Polyubiquitin-C OS=Homo sapiens GN=UBC PE=1 SV=3;>sp\|P62979\|RS27A_HUMAN Ubiquitin-40S ribosomal protein S27a OS=Homo sapiens GN=RPS27A PE=1 SV=2;>sp\|P62987\|RL40_HUMA | TITLEVEPSDTIENVK(0.876)AK(0.124) | 19 | 0.36 |
| P57053 | H2BFS | >sp\|P57053\|H2BFS_HUMAN Histone H2B type F-S OS=Homo sapiens GN=H2BFS PE=1 SV=2;>sp\|O60814\|H2B1K_HUMAN Histone H2B type 1-K OS=Homo sapiens GN=HIST1H2BK PE=1 SV=3 | AVTK(1)YTSAK | 10 | 0.35 |
| P36543 | VATE1 | >sp\|P36543\|VATE1_HUMAN V-type proton ATPase subunit E 1 OS=Homo sapiens GN=ATP6V1E1 PE=1 SV=1 | ALSDADVQK(0.996)QIK(0.004) | 1 | 0.34 |
| Q96IV0 | NGLY1 | >sp\|Q96IV0\|NGLY1_HUMAN Peptide-N(4)-(N-acetyl-beta-glucosaminyl)asparagine amidase OS=Homo sapiens GN=NGLY1 PE=1 SV=1 | DTINGLNK(1)QR | 7 | 0.34 |

| | | | | | |
|---|---|---|---|---|---|
| Q16778 | H2B2E | >sp\|Q16778\|H2B2E_HUMAN Histone H2B type 2-E OS=Homo sapiens GN=HIST2H2BE PE=1 SV=3;>sp\|P33778\|H2B1B_HUMAN Histone H2B type 1-B OS=Homo sapiens GN=HIST1H2BB PE=1 SV=2;>sp\|P23527\|H2B1O_HUMAN Histone H2B type 1-O OS=Homo sapiens GN=HIST1H2BO PE=1 SV=3;>sp\|Q8N | AVTK(1)YTSSK | 58 | 0.33 |
| P35579 | MYH9 | >sp\|P35579\|MYH9_HUMAN Myosin-9 OS=Homo sapiens GN=MYH9 PE=1 SV=4 | EK(1)QLAAENR | 3 | 0.33 |
| P16104 | H2AX | >sp\|P16104\|H2AX_HUMAN Histone H2AX OS=Homo sapiens GN=H2AFX PE=1 SV=2 | K(1)TSATVGPK | 1 | 0.31 |
| Q9NVJ2 | ARL8B | >sp\|Q9NVJ2\|ARL8B_HUMAN ADP-ribosylation factor-like protein 8B OS=Homo sapiens GN=ARL8B PE=1 SV=1 | DLPNALDEK(1)QLIEK | 60 | 0.30 |
| Q9UI12 | VATH | >sp\|Q9UI12\|VATH_HUMAN V-type proton ATPase subunit H OS=Homo sapiens GN=ATP6V1H PE=1 SV=1 | ILTK(1)LLEVSDDPQVLAVAAHDVGEYVR | 1 | 0.30 |
| Q86WC4 | OSTM1 | >sp\|Q86WC4\|OSTM1_HUMAN Osteopetrosis-associated transmembrane protein 1 OS=Homo sapiens GN=OSTM1 PE=1 SV=1 | RLK(1)SSTSFANIQENSN | 6 | 0.27 |
| P62333 | PRS10 | >sp\|P62333\|PRS10_HUMAN 26S protease regulatory subunit 10B OS=Homo sapiens GN=PSMC6 PE=1 SV=1 | EQLK(0.999)ELTK(0.001) | 1 | 0.24 |
| Q96BM9 | ARL8A | >sp\|Q96BM9\|ARL8A_HUMAN ADP-ribosylation factor-like protein 8A OS=Homo sapiens GN=ARL8A PE=1 SV=1 | DLPGALDEK(1)ELIEK | 16 | 0.23 |
| P55072 | TERA | >sp\|P55072\|TERA_HUMAN Transitional endoplasmic reticulum ATPase OS=Homo sapiens GN=VCP PE=1 SV=4 | ASGADSKGDDLSTAILK(0.993)QK(0.007) | 3 | 0.19 |
| Q9UL40 | ZN346 | >sp\|Q9UL40\|ZN346_HUMAN Zinc finger protein 346 OS=Homo sapiens GN=ZNF346 PE=1 SV=1 | THAK(0.657)NLK(0.343) | 1 | 0.05 |

| | | | | | |
|---|---|---|---|---|---|
| Q86UF2 | CTGE6 | >sp\|Q86UF2\|CTGE6_HUMAN cTAGE family member 6 OS=Homo sapiens GN=CTAGE6 PE=2 SV=2;>sp\|A4D2H0\|CTGEF_HUMAN cTAGE family member 15 OS=Homo sapiens GN=CTAGE15 PE=2 SV=1 | LSGSAEPRSFK(1) | 10 | |
| O14786 | NRP1 | >sp\|O14786\|NRP1_HUMAN Neuropilin-1 OS=Homo sapiens GN=NRP1 PE=1 SV=3 | DK(1)LNTQSTYSEA | 1 | |
| O14983 | AT2A1 | >sp\|O14983\|AT2A1_HUMAN Sarcoplasmic/endoplasmic reticulum calcium ATPase 1 OS=Homo sapiens GN=ATP2A1 PE=1 SV=1 | TGTLTTNQMSVCK(1) | 2 | |
| O15320 | CTGE5 | >sp\|O15320\|CTGE5_HUMAN cTAGE family member 5 OS=Homo sapiens GN=CTAGE5 PE=1 SV=4;>sp\|Q96RT6\|CTGE2_HUMAN cTAGE family member 2 OS=Homo sapiens GN=CTAGE1 PE=1 SV=2 | LNASLK(1)TLEGER | 1 | |
| O43395 | PRPF3 | >sp\|O43395\|PRPF3_HUMAN U4/U6 small nuclear ribonucleoprotein Prp3 OS=Homo sapiens GN=PRPF3 PE=1 SV=2 | NLSNPAK(0.99)K(0.99)FK(0.021) | 1 | |
| O43395 | PRPF3 | >sp\|O43395\|PRPF3_HUMAN U4/U6 small nuclear ribonucleoprotein Prp3 OS=Homo sapiens GN=PRPF3 PE=1 SV=2 | NLSNPAK(0.99)K(0.99)FK(0.021) | 1 | |
| O60488 | ACSL4 | >sp\|O60488\|ACSL4_HUMAN Long-chain-fatty-acid--CoA ligase 4 OS=Homo sapiens GN=ACSL4 PE=1 SV=2 | EAANAMK(1)LER | 1 | |
| O60493 | SNX3 | >sp\|O60493\|SNX3_HUMAN Sorting nexin-3 OS=Homo sapiens GN=SNX3 PE=1 SV=3 | K(1)QGLEQFINK | 1 | |
| P57053 | H2BFS | >sp\|P57053\|H2BFS_HUMAN Histone H2B type F-S OS=Homo sapiens GN=H2BFS PE=1 SV=2;>sp\|O60814\|H2B1K_HUMAN Histone H2B type 1-K OS=Homo sapiens GN=HIST1H2BK PE=1 | LLLPGELAK(0.998)HAVSEGTK(0.002) | 1 | |

| | | | | | |
|---|---|---|---|---|---|
| | | SV=3;>sp\|Q16778\|H2B2E_HUMAN Histone H2B type 2-E OS=Homo sapiens GN=HIST2H2BE PE=1 SV=3;>sp\|P33778\| | | | |
| O95140 | MFN2 | >sp\|O95140\|MFN2_HUMAN Mitofusin-2 OS=Homo sapiens GN=MFN2 PE=1 SV=3 | FIDK(1)QLELLAQDYK | 1 | |
| O95183 | VAMP5 | >sp\|O95183\|VAMP5_HUMAN Vesicle-associated membrane protein 5 OS=Homo sapiens GN=VAMP5 PE=1 SV=1 | NNFGK(1)VLER | 1 | |
| P00451 | FA8 | >sp\|P00451\|FA8_HUMAN Coagulation factor VIII OS=Homo sapiens GN=F8 PE=1 SV=1 | IIVDDTSTQWSK(1) | 1 | |
| P02545 | LMNA | >sp\|P02545\|LMNA_HUMAN Prelamin-A/C OS=Homo sapiens GN=LMNA PE=1 SV=1 | LVEIDNGK(1)QR | 1 | |
| P02679 | FIBG | >sp\|P02679\|FIBG_HUMAN Fibrinogen gamma chain OS=Homo sapiens GN=FGG PE=1 SV=3 | YLQEIYNSNNQK(0.99)IVNLK(0.01) | 1 | |
| Q99878 | H2A1J | >sp\|Q99878\|H2A1J_HUMAN Histone H2A type 1-J OS=Homo sapiens GN=HIST1H2AJ PE=1 SV=3;>sp\|Q96KK5\|H2A1H_HUMAN Histone H2A type 1-H OS=Homo sapiens GN=HIST1H2AH PE=1 SV=3;>sp\|Q9BTM1\|H2AJ_HUMAN Histone H2A.J OS=Homo sapiens GN=H2AFJ PE=1 SV=1;>sp\|Q93077\|H2A1C_HU | VTIAQGGVLPNIQAVLLPK(0.5)K(0.5) | 5 | |
| P05023 | AT1A1 | >sp\|P05023\|AT1A1_HUMAN Sodium/potassium-transporting ATPase subunit alpha-1 OS=Homo sapiens GN=ATP1A1 PE=1 SV=1 | K(1)YGTDLSR | 1 | |
| P05026 | AT1B1 | >sp\|P05026\|AT1B1_HUMAN Sodium/potassium-transporting ATPase subunit beta-1 OS=Homo sapiens GN=ATP1B1 PE=1 SV=1 | EEGSWK(0.88)K(0.12) | 1 | |
| P05783 | K1C18 | >sp\|P05783\|K1C18_HUMAN Keratin, type I cytoskeletal 18 OS=Homo | VK(1)YETELAMR | 1 | |

| | | | | | |
|---|---|---|---|---|---|
| | | sapiens GN=KRT18 PE=1 SV=2;>P05784 SWISS-PROT:P05784 Tax_Id=10090 Gene_Symbol=Krt18 Keratin, type I cytoskeletal 18 | | | |
| P08034 | CXB1 | >sp\|P08034\|CXB1_HUMAN Gap junction beta-1 protein OS=Homo sapiens GN=GJB1 PE=1 SV=1 | QNEINK(1)LLSEQDGSLK | 1 | |
| P08238 | HS90B | >sp\|P08238\|HS90B_HUMAN Heat shock protein HSP 90-beta OS=Homo sapiens GN=HSP90AB1 PE=1 SV=4;>sp\|Q58FF7\|H90B3_HUMAN Putative heat shock protein HSP 90-beta-3 OS=Homo sapiens GN=HSP90AB3P PE=5 SV=1;>sp\|Q58FF8\|H90B2_HUMAN Putative heat shock protein HSP 90-be | LDSGK(0.996)ELK(0.004) | 1 | |
| P23634 | AT2B4 | >sp\|P23634\|AT2B4_HUMAN Plasma membrane calcium-transporting ATPase 4 OS=Homo sapiens GN=ATP2B4 PE=1 SV=2 | NEVPEEK(0.957)LYK(0.043) | 1 | |
| P25445 | TNR6 | >sp\|P25445\|TNR6_HUMAN Tumor necrosis factor receptor superfamily member 6 OS=Homo sapiens GN=FAS PE=1 SV=1 | NDNVQDTAEQK(1)VQLLR | 1 | |
| P31939 | PUR9 | >sp\|P31939\|PUR9_HUMAN Bifunctional purine biosynthesis protein PURH OS=Homo sapiens GN=ATIC PE=1 SV=3 | SLFSNVVTK(0.437)NK(0.563) | 1 | |
| Q14409 | GLPK3 | >sp\|Q14409\|GLPK3_HUMAN Putative glycerol kinase 3 OS=Homo sapiens GN=GK3P PE=5 SV=2;>sp\|P32189\|GLPK_HUMAN Glycerol kinase OS=Homo sapiens GN=GK PE=1 SV=3 | AASK(1)K(1)AVLGPLVGAVDQGTSSTR | 4 | |
| Q14409 | GLPK3 | >sp\|Q14409\|GLPK3_HUMAN Putative glycerol kinase 3 OS=Homo sapiens GN=GK3P PE=5 SV=2;>sp\|P32189\|GLPK_HUMAN Glycerol kinase | K(1)AVLGPLVGAVDQGTSSTR | 1 | |

| | | | | | |
|---|---|---|---|---|---|
| | | OS=Homo sapiens GN=GK PE=1 SV=3 | | | |
| P35998 | PRS7 | >sp\|P35998\|PRS7_HUMAN 26S protease regulatory subunit 7 OS=Homo sapiens GN=PSMC2 PE=1 SV=3 | YIINVK(0.979)QFAK(0.021) | 1 | |
| P40189 | IL6RB | >sp\|P40189\|IL6RB_HUMAN Interleukin-6 receptor subunit beta OS=Homo sapiens GN=IL6ST PE=1 SV=2 | SK(1)QVSSVNEEDFVR | 1 | |
| P43007 | SATT | >sp\|P43007\|SATT_HUMAN Neutral amino acid transporter A OS=Homo sapiens GN=SLC1A4 PE=1 SV=1 | K(1)GEQELAEVK | 1 | |
| P46783 | RS10 | >sp\|P46783\|RS10_HUMAN 40S ribosomal protein S10 OS=Homo sapiens GN=RPS10 PE=1 SV=1 | SAVPPGADK(0.5)K(0.5) | 12 | |
| P51797 | CLCN6 | >sp\|P51797\|CLCN6_HUMAN Chloride transport protein 6 OS=Homo sapiens GN=CLCN6 PE=1 SV=2 | SQSMK(1)SYPSSELR | 1 | |
| P55072 | TERA | >sp\|P55072\|TERA_HUMAN Transitional endoplasmic reticulum ATPase OS=Homo sapiens GN=VCP PE=1 SV=4 | LDQLIYIPLPDEK(1)SR | 1 | |
| P61088 | UBE2N | >sp\|P61088\|UBE2N_HUMAN Ubiquitin-conjugating enzyme E2 N OS=Homo sapiens GN=UBE2N PE=1 SV=1 | ICLDILK(0.279)DK(0.721) | 9 | |
| P84098 | RL19 | >sp\|P84098\|RL19_HUMAN 60S ribosomal protein L19 OS=Homo sapiens GN=RPL19 PE=1 SV=1 | LQAK(0.799)K(0.198)EEIIK(0.003) | 2 | |
| P86791 | CCZ1 | >sp\|P86791\|CCZ1_HUMAN Vacuolar fusion protein CCZ1 homolog OS=Homo sapiens GN=CCZ1 PE=1 SV=1;>sp\|P86790\|CCZ1B_HUMAN Vacuolar fusion protein CCZ1 homolog B OS=Homo sapiens GN=CCZ1B PE=1 SV=1 | DGK(1)PVIEYQEEELLDK | 1 | |
| Q01082 | SPTB2 | >sp\|Q01082\|SPTB2_HUMAN Spectrin beta chain, non-erythrocytic 1 OS=Homo sapiens GN=SPTBN1 PE=1 SV=2 | AK(1)TALPAQSAATLPAR | 1 | |
| Q13488 | VPP3 | >sp\|Q13488\|VPP3_HUMAN V-type proton ATPase | QEENK(1)AGLLDLPDASVNGWSSDEEK | 2 | |

| | | | | | |
|---|---|---|---|---|---|
| | | 116 kDa subunit a isoform 3 OS=Homo sapiens GN=TCIRG1 PE=1 SV=3 | | | |
| Q13772 | NCOA4 | >sp\|Q13772\|NCOA4_HUMAN Nuclear receptor coactivator 4 OS=Homo sapiens GN=NCOA4 PE=1 SV=1 | EVIEQTK(0.969)APK(0.031) | 1 | |
| Q14156 | EFR3A | >sp\|Q14156\|EFR3A_HUMAN Protein EFR3 homolog A OS=Homo sapiens GN=EFR3A PE=1 SV=2 | LTFYAVSAPEK(1)LDR | 1 | |
| Q14839 | CHD4 | >sp\|Q14839\|CHD4_HUMAN Chromodomain-helicase-DNA-binding protein 4 OS=Homo sapiens GN=CHD4 PE=1 SV=2 | ITQVAK(0.353)K(0.647) | 2 | |
| Q14849 | STAR3 | >sp\|Q14849\|STAR3_HUMAN StAR-related lipid transfer protein 3 OS=Homo sapiens GN=STARD3 PE=1 SV=2 | K(1)SFSAQER | 1 | |
| Q15147 | PLCB4 | >sp\|Q15147\|PLCB4_HUMAN 1-phosphatidylinositol 4,5-bisphosphate phosphodiesterase beta-4 OS=Homo sapiens GN=PLCB4 PE=1 SV=3 | TFASGK(1)TEK(1) | 1 | |
| Q15147 | PLCB4 | >sp\|Q15147\|PLCB4_HUMAN 1-phosphatidylinositol 4,5-bisphosphate phosphodiesterase beta-4 OS=Homo sapiens GN=PLCB4 PE=1 SV=3 | TFASGK(1)TEK(1) | 1 | |
| Q15166 | PON3 | >sp\|Q15166\|PON3_HUMAN Serum paraoxonase/lactonase 3 OS=Homo sapiens GN=PON3 PE=1 SV=3 | IQNVLSEK(1)PR | 1 | |
| Q52M93 | Z585B | >sp\|Q52M93\|Z585B_HUMAN Zinc finger protein 585B OS=Homo sapiens GN=ZNF585B PE=2 SV=1 | SYICMKCGLAFIRK(1) | 1 | |
| Q5FWF5 | ESCO1 | >sp\|Q5FWF5\|ESCO1_HUMAN N-acetyltransferase ESCO1 OS=Homo sapiens GN=ESCO1 PE=1 SV=3 | IIMVLPEDPK(0.012)YALK(0.988) | 1 | |
| Q6W2J9 | BCOR | >sp\|Q6W2J9\|BCOR_HUMAN BCL-6 corepressor OS=Homo sapiens GN=BCOR PE=1 SV=1 | LIVNK(1)NAGETLLQR | 1 | |
| Q86US8 | EST1A | >sp\|Q86US8\|EST1A_HUMAN Telomerase-binding protein EST1A OS=Homo | GLSSGGK(0.989)GSEK(0.011) | 1 | |

| | | | | | |
|---|---|---|---|---|---|
| | | sapiens GN=SMG6 PE=1 SV=2 | | | |
| Q86WA9 | S2611 | >sp\|Q86WA9\|S2611_HUMAN Sodium-independent sulfate anion transporter OS=Homo sapiens GN=SLC26A11 PE=2 SV=2 | GFQYFSTLEEAEK(1)HLR | 2 | |
| Q8NE01 | CNNM3 | >sp\|Q8NE01\|CNNM3_HUMAN Metal transporter CNNM3 OS=Homo sapiens GN=CNNM3 PE=1 SV=1 | GGGDPYSDLSK(1)GVLR | 1 | |
| Q8NHH9 | ATLA2 | >sp\|Q8NHH9\|ATLA2_HUMAN Atlastin-2 OS=Homo sapiens GN=ATL2 PE=1 SV=2 | EVAIK(1)QFR | 1 | |
| Q8WUM9 | S20A1 | >sp\|Q8WUM9\|S20A1_HUMAN Sodium-dependent phosphate transporter 1 OS=Homo sapiens GN=SLC20A1 PE=1 SV=1 | TVSFK(1)LGDLEEAPER | 1 | |
| Q96CW1 | AP2M1 | >sp\|Q96CW1\|AP2M1_HUMAN AP-2 complex subunit mu OS=Homo sapiens GN=AP2M1 PE=1 SV=2 | IVIEK(0.85)QGK(0.15) | 1 | |
| Q96HN2 | SAHH3 | >sp\|Q96HN2\|SAHH3_HUMAN Adenosylhomocysteinase 3 OS=Homo sapiens GN=AHCYL2 PE=1 SV=1 | YPNMFK(0.909)K(0.909)IK(0.181) | 1 | |
| Q96HN2 | SAHH3 | >sp\|Q96HN2\|SAHH3_HUMAN Adenosylhomocysteinase 3 OS=Homo sapiens GN=AHCYL2 PE=1 SV=1 | YPNMFK(0.909)K(0.909)IK(0.181) | 1 | |
| Q995336 | VAT1 | >sp\|Q99536\|VAT1_HUMAN Synaptic vesicle membrane protein VAT-1 homolog OS=Homo sapiens GN=VAT1 PE=1 SV=2 | VLLVPGPEK(1)EN | 2 | |
| Q996675 | CGRF1 | >sp\|Q99675\|CGRF1_HUMAN Cell growth regulator with RING finger domain protein 1 OS=Homo sapiens GN=CGRRF1 PE=1 SV=1 | DTK(1)IEDFGTVPR | 1 | |
| Q9BWH2 | FUND2 | >sp\|Q9BWH2\|FUND2_HUMAN FUN14 domain-containing protein 2 OS=Homo sapiens GN=FUNDC2 PE=1 SV=2 | SK(1)AEEVVSFVK | 1 | |
| Q9BYE9 | CDHR2 | >sp\|Q9BYE9\|CDHR2_HUMAN Cadherin-related family member 2 | K(1)TAAGVMPSAPAIPGTNMYNTER | 1 | |

| | | | | | |
|---|---|---|---|---|---|
| | | OS=Homo sapiens GN=CDHR2 PE=1 SV=2 | | | |
| Q9H2H9 | S38A1 | >sp\|Q9H2H9\|S38A1_HUMAN Sodium-coupled neutral amino acid transporter 1 OS=Homo sapiens GN=SLC38A1 PE=1 SV=1 | SLTNSHLEK(0.861)K(0.139) | 3 | |
| Q9NP58 | ABCB6 | >sp\|Q9NP58\|ABCB6_HUMAN ATP-binding cassette sub-family B member 6, mitochondrial OS=Homo sapiens GN=ABCB6 PE=1 SV=1 | AIQASLAK(1)VCANR | 2 | |
| Q9P0K7 | RAI14 | >sp\|Q9P0K7\|RAI14_HUMAN Ankycorbin OS=Homo sapiens GN=RAI14 PE=1 SV=2 | MKSLK(1)AK(1) | 1 | |
| Q9P0K7 | RAI14 | >sp\|Q9P0K7\|RAI14_HUMAN Ankycorbin OS=Homo sapiens GN=RAI14 PE=1 SV=2 | MKSLK(1)AK(1) | 1 | |
| Q9P243 | ZFAT | >sp\|Q9P243\|ZFAT_HUMAN Zinc finger protein ZFAT OS=Homo sapiens GN=ZFAT PE=1 SV=2 | NLIK(1)HIR | 1 | |
| Q9P2J5 | SYLC | >sp\|Q9P2J5\|SYLC_HUMAN Leucine--tRNA ligase, cytoplasmic OS=Homo sapiens GN=LARS PE=1 SV=2 | LSGLK(1)GK | 1 | |
| Q9UGQ2 | FLOWR | >sp\|Q9UGQ2\|FLOWR_HUMAN Calcium channel flower homolog OS=Homo sapiens GN=CACFD1 PE=1 SV=1 | QQADEEK(1)LAETLEGEL | 1 | |
| Q9UGQ3 | GTR6 | >sp\|Q9UGQ3\|GTR6_HUMAN Solute carrier family 2, facilitated glucose transporter member 6 OS=Homo sapiens GN=SLC2A6 PE=1 SV=2 | MQEPLLGAEGPDYDTFPEK(1)PPPSPGDR | 1 | |
| Q9UMX0 | UBQL1 | >sp\|Q9UMX0\|UBQL1_HUMAN Ubiquilin-1 OS=Homo sapiens GN=UBQLN1 PE=1 SV=2;>sp\|Q9UHD9\|UBQL2_HUMAN Ubiquilin-2 OS=Homo sapiens GN=UBQLN2 PE=1 SV=2 | EK(1)EEFAVPENSSVQQFK | 1 | |
| Q9UK28 | TM59L | >sp\|Q9UK28\|TM59L_HUMAN Transmembrane protein 59-like OS=Homo sapiens GN=TMEM59L PE=2 SV=1 | LK(1)LDLTKL | 1 | |

| | | | | | |
|---|---|---|---|---|---|
| Q9ULG1 | INO80 | >sp\|Q9ULG1\|INO80_HUMAN DNA helicase INO80 OS=Homo sapiens GN=INO80 PE=1 SV=2 | KEDELDGK(1)R | 1 | |
| Q9UPI3 | FLVCR2 | >sp\|Q9UPI3\|FLVC2_HUMAN Feline leukemia virus subgroup C receptor-related protein 2 OS=Homo sapiens GN=FLVCR2 PE=1 SV=1 | LQEEEEESNTSK(1)VPTAVSEDHL | 1 | |
| Q9Y287 | ITM2B | >sp\|Q9Y287\|ITM2B_HUMAN Integral membrane protein 2B OS=Homo sapiens GN=ITM2B PE=1 SV=1 | VTFNSALAQK(0.175)EAK(0.372)K(0.453) | 1 | |
| Q9Y5X4 | NR2E3 | >sp\|Q9Y5X4\|NR2E3_HUMAN Photoreceptor-specific nuclear receptor OS=Homo sapiens GN=NR2E3 PE=1 SV=1 | LLFMAVK(1)WAK(1) | 3 | |
| Q9Y5X4 | NR2E3 | >sp\|Q9Y5X4\|NR2E3_HUMAN Photoreceptor-specific nuclear receptor OS=Homo sapiens GN=NR2E3 PE=1 SV=1 | LLFMAVK(1)WAK(1) | 3 | |
| Q9Y6N7 | ROBO1 | >sp\|Q9Y6N7\|ROBO1_HUMAN Roundabout homolog 1 OS=Homo sapiens GN=ROBO1 PE=1 SV=1 | K(1)VPSFTFTPTVTYQR | 1 | |

**Supplemental Table 3-S2. GO analysis of cellular component (CC) and biological process (BP).**

| Category | Term | Count | % | PValue | Uniprot ID | ListTotal | PopHits | PopTotal | Fold Enrichment | Bonferroni | Benjamini | FDR |
|---|---|---|---|---|---|---|---|---|---|---|---|---|
| CC | GO:0005789~endoplasmic reticulum membrane | 44 | 36.666667 | 3.70E-27 | Q8TC12, O75915, P04114, Q16850, P49585, P55061, P49768, Q70UQ0, Q9Y5Z9, P08034, Q96QK8, P51572, P11021, Q9UNL2, O75845, O60427, Q96GF1, O75844, Q15800, P04844, Q9NZ01, P27824, Q9Y282, Q9NUQ2, Q9UBM7, P49326, Q7L5N7, Q9C0D9, Q9H3H5, P46977, Q99942, Q9Y5U4, Q9P0S3, P38435, Q15392, O95197, O95864, Q15041, Q96HR9, Q8TCT9, O00767, P48449, Q5I7T1, Q53GQ0 | 119 | 862 | 18224 | 7.82 | 7.37E-25 | 7.37E-25 | 4.64E-24 |
| CC | GO:0016021~integral component of membrane | 78 | 65 | 5.85E-17 | O75915, P55061, Q9Y3E5, Q96BD0, Q9BQA9, Q8NCU8, P21796, Q8TB61, P08034, Q96QK8, P51572, Q96B96, Q8WWT9, Q96GF1, P05023, O15173, P04844, Q9NZ01, Q9Y282, Q9NUQ2, P69849, Q6ZVX9, Q00765, Q7L5N7, Q07820, Q9C0D9, Q15155, P61619, P46977, Q9P0S3, O95197, Q15392, P0CK96, P48066, Q9NZS9, Q8TCT9, Q96HR9, O00767, Q5I7T1, Q8TC12, Q7Z3D4, Q16850, | 119 | 5163 | 18224 | 2.31 | 2.21E-14 | 1.11E-14 | 1.44E-13 |

| | | | | | | | | | | | | |
|---|---|---|---|---|---|---|---|---|---|---|---|---|
| | | | | | P49768, O95140, Q9UP95, P04920, Q70UQ0, Q9Y5Z9, Q8N2H4, Q96CS7, Q9NXW2, O75845, Q9UNL2, O60427, Q9H6A9, O75844, Q9BV81, Q9UPY5, Q15800, Q12846, Q9C0B5, O75387, Q9BWH2, Q9UBM7, P49326, P31641, Q9H3H5, Q86UQ4, Q99942, Q9H2H9, Q9Y5U4, P38435, P33527, O95864, Q15041, Q96B21, P55085, Q53GQ0 | | | | | | | |
| CC | GO:0016020~membrane | 51 | 42.5 | 8.75E-17 | O14495, O75915, Q9Y3E5, P55061, Q8NBX0, P21796, Q8TB61, P51572, P05023, P61978, O15173, P04844, P84090, P24001, Q9Y282, Q14677, Q07820, P61619, Q15155, P46977, P02649, Q15392, P67775, Q9NZS9, Q8TCT9, O00767, Q16850, P49768, Q9UP95, P04920, Q70UQ0, Q9Y5Z9, Q9NXW2, Q9Y679, P11021, O60427, O75844, Q9UPY5, Q12846, P27824, Q14254, Q9C0B5, P23458, Q9UBM7, Q9H3H5, P38435, P33527, O95864, Q15041, P63261, P48449 | 119 | 2200 | 18224 | 3.55 | 2.21E-14 | 7.33E-15 | 1.44E-13 |
| CC | GO:0005783~endoplasmic reticulum | 28 | 23.33333333 | 2.30E-12 | Q96CS3, O75915, Q16850, P55061, P49768, Q70UQ0, Q9Y5Z9, P51572, Q96QK8, P11021, Q96GF1, P05023, Q15800, P04844, Q9NZ01, P27824, Q99541, Q9UBM7, P49326, Q13501, Q7L5N7, P50454, P02649, Q15392, | 119 | 828 | 18224 | 5.18 | 4.57E-10 | 1.14E-10 | 2.88E-09 |

| | | | | | | | | | | | | |
|---|---|---|---|---|---|---|---|---|---|---|---|---|
| | | | | | O95197, Q9NZS9, Q8TCT9, O00767 | | | | | | | |
| CC | GO:0030176~integral component of endoplasmic reticulum membrane | 11 | 9.1666667 | 1.38E-09 | Q9NZ01, Q9Y679, Q9UBM7, Q8TB61, Q15041, Q9NZS9, P11021, O75844, Q9H3H5, Q9BV81, P61619 | 119 | 104 | 18224 | 16.20 | 2.74E-07 | 5.48E-08 | 1.73E-06 |
| CC | GO:0005811~lipid particle | 7 | 5.8333333 | 4.29E-06 | Q96CS3, Q99541, Q7L5N7, P51572, Q8NBX0, P48449, Q8N0X7 | 119 | 66 | 18224 | 16.24 | 8.54E-04 | 1.42E-04 | 5.38E-03 |
| CC | GO:0005791~rough endoplasmic reticulum | 6 | 5 | 1.94E-05 | P27824, P49768, Q8TCT9, P04844, P61619, Q9UPY5 | 119 | 51 | 18224 | 18.02 | 3.84E-03 | 5.50E-04 | 2.42E-02 |
| CC | GO:0036513~Derlin-1 retrotranslocation complex | 3 | 2.5 | 2.20E-03 | Q99942, Q8TCT9, Q96GF1 | 119 | 11 | 18224 | 41.77 | 3.55E-01 | 5.33E-02 | 2.72E+00 |
| CC | GO:0005741~mitochondrial outer membrane | 6 | 5 | 2.85E-03 | Q9NUQ2, O95140, Q07820, Q96GF1, P21796, Q8N0X7 | 119 | 149 | 18224 | 6.17 | 4.33E-01 | 6.12E-02 | 3.51E+00 |
| CC | GO:0043231~intracellular membrane-bounded organelle | 11 | 9.1666667 | 3.38E-03 | P04114, Q16850, Q99541, Q9UBM7, Q14677, O75845, O60427, P05023, Q9H3H5, Q86UQ4, O14964 | 119 | 558 | 18224 | 3.02 | 4.91E-01 | 6.52E-02 | 4.16E+00 |
| CC | GO:0070062~extracellular exosome | 30 | 25 | 6.26E-03 | O14495, O75915, P04114, Q9H444, P08134, O14964, P21796, Q9Y679, P11021, Q9H0E2, P05023, P61978, Q8WWT9, O75844, Q15843, P62745, Q12846, Q14254, P27824, P05787, Q00765, Q13501, P50454, Q9H2H9, P02649, P33527, O95197, P67775, P63261, P0CG47 | 119 | 2811 | 18224 | 1.63 | 7.13E-01 | 1.07E-01 | 7.56E+00 |

| | | | | | | | | | | | | |
|---|---|---|---|---|---|---|---|---|---|---|---|---|
| CC | GO:0030496~midbody | 5 | 4.166666667 | 9.89E-03 | P84090, P11021, Q9H444, Q8NBX0, Q8N0X7 | 119 | 129 | 18224 | 5.94 | 8.62E-01 | 1.52E-01 | 1.17E+01 |
| CC | GO:0005790~smooth endoplasmic reticulum | 3 | 2.5 | 1.22E-02 | P27824, P49768, P11021 | 119 | 26 | 18224 | 17.67 | 9.13E-01 | 1.71E-01 | 1.43E+01 |
| CC | GO:0005925~focal adhesion | 8 | 6.666666667 | 1.37E-02 | P62745, Q99755, Q14254, P23458, P04920, P63261, P11021, P61978 | 119 | 391 | 18224 | 3.13 | 9.36E-01 | 1.78E-01 | 1.59E+01 |
| CC | GO:0071556~integral component of lumenal side of endoplasmic reticulum membrane | 3 | 2.5 | 1.51E-02 | P27824, P51572, Q8TCT9 | 119 | 29 | 18224 | 15.84236453 | 9.51E-01 | 1.82E-01 | 1.73E+01 |
| CC | GO:0005768~endosome | 6 | 5 | 1.56E-02 | Q12846, Q14254, Q9H444, P05023, Q13114, O14964 | 119 | 225 | 18224 | 4.083809524 | 9.56E-01 | 1.77E-01 | 1.79E+01 |
| CC | GO:0043209~myelin sheath | 5 | 4.166666667 | 1.72E-02 | P27824, P63261, P11021, P05023, P21796 | 119 | 152 | 18224 | 5.037593985 | 9.68E-01 | 1.83E-01 | 1.95E+01 |
| CC | GO:0005887~integral component of plasma membrane | 17 | 14.16666667 | 2.02E-02 | O14495, P55061, Q96BD0, O75387, P49768, Q9UP95, P04920, P31641, Q9H2H9, P33527, O95864, P48066, Q9NZS9, P51572, P55085, Q8WWT9, Q9UPY5 | 119 | 4145 | 18224 | 1.839878849 | 9.83E-01 | 2.02E-01 | 2.25E+01 |
| CC | GO:0034363~intermediate-density lipoprotein particle | 2 | 1.666666667 | 2.57E-02 | P02649, P04114 | 119 | 4 | 18224 | 76.57142857 | 9.94E-01 | 2.38E-01 | 2.78E+01 |
| CC | GO:0005784~Sec61 translocon complex | 2 | 1.666666667 | 2.57E-02 | Q15041, P51572 | 119 | 4 | 18224 | 76.57142857 | 9.94E-01 | 2.38E-01 | 2.78E+01 |

| | | | | | | | | | | | | |
|---|---|---|---|---|---|---|---|---|---|---|---|---|
| CC | GO:0005886~plasma membrane | 37 | 30.8333333 | 2.87E-02 | O14495, O75915, P04114, Q16850, P49585, Q96BD0, P49768, Q9UP95, P04920, P08134, P21796, P11021, Q8WWT9, P05023, Q9UPY5, Q15800, P62745, Q12846, Q14254, Q9C0B5, O75387, Q99541, Q6ZVX9, P31641, Q8N0X7, Q99755, Q9H2H9, P02649, P33527, O95197, P67775, P63261, P48066, P55085, Q8TCT9, P0CG47, Q5I7T1 | 119 | 41211 | 182224 | 1.374978334 | 9.97E-01 | 2.52E-01 | 3.06E+01 |
| CC | GO:0016323~basolateral plasma membrane | 5 | 4.16666667 | 2.96E-02 | Q12846, Q14254, P33527, P04920, P05023 | 119 | 180 | 182224 | 4.253968254 | 9.97E-01 | 2.48E-01 | 3.14E+01 |
| CC | GO:0030173~integral component of Golgi membrane | 3 | 2.5 | 5.43E-02 | Q8TB61, Q9Y5Z9, Q8N2H4 | 119 | 58 | 182224 | 7.921182266 | 1.00E+00 | 3.97E-01 | 5.03E+01 |
| CC | GO:0005769~early endosome | 5 | 4.16666667 | 6.17E-02 | P62745, P02649, P04114, P55085, O14964 | 119 | 229 | 182224 | 3.343730505 | 1.00E+00 | 4.24E-01 | 5.50E+01 |
| CC | GO:0008250~oligosaccharyltransferase complex | 2 | 1.66666667 | 6.29E-02 | P04844, P46977 | 119 | 10 | 182224 | 30.62857143 | 1.00E+00 | 4.17E-01 | 5.57E+01 |
| CC | GO:0005829~cytosol | 29 | 24.16666667 | 7.75E-02 | P04114, Q9Y3E5, P49585, O95140, Q9H444, Q8N2H4, P08134, Q93034, O14964, O95816, P51572, Q9H0E2, Q13114, Q15843, P62745, Q12846, P23458, P24001, Q99541, Q13501, Q14677, Q07820, P61619, Q99755, Q15392, Q15041, P67775, P63261, P0CG47 | 119 | 33155 | 182224 | 1.339711269 | 1.00E+00 | 4.74E-01 | 6.36E+01 |

| | | | | | | | | | | | | |
|---|---|---|---|---|---|---|---|---|---|---|---|---|
| CC | GO:0005635~nuclear envelope | 4 | 3.33333333 | 8.44E-02 | P49585, Q9NUQ2, Q9H444, O15173 | 119 | 159 | 18224 | 3.852650494 | 1.00E+00 | 4.91E-01 | 6.69E+01 |
| CC | GO:0034362~low-density lipoprotein particle | 2 | 1.666666667 | 8.70E-02 | P02649, P04114 | 119 | 14 | 18224 | 21.87755102 | 1.00E+00 | 4.89E-01 | 6.80E+01 |
| CC | GO:0042627~chylomicron | 2 | 1.666666667 | 8.70E-02 | P02649, P04114 | 119 | 14 | 18224 | 21.87755102 | 1.00E+00 | 4.89E-01 | 6.80E+01 |
| CC | GO:0005739~mitochondrion | 14 | 11.66666667 | 8.94E-02 | Q9Y3E5, Q9NUQ2, Q9BWH2, P49768, O95140, Q8NBX0, Q07820, P21796, P67775, P51572, P11021, O60427, P0CG47, Q13114 | 119 | 1331 | 18224 | 1.610818933 | 1.00E+00 | 4.86E-01 | 6.91E+01 |
| CC | GO:0071682~endocytic vesicle lumen | 2 | 1.666666667 | 9.88E-02 | P02649, P04114 | 119 | 16 | 18224 | 19.14285714 | 1.00E+00 | 5.10E-01 | 7.28E+01 |
| BP | GO:0006695~cholesterol biosynthetic process | 6 | 5.00 | 3.53E-06 | Q9Y5U4, Q16850, Q15392, Q9UBM7, P48449, Q15800 | 105 | 38 | 16792 | 25.25112782 | 2.86E-03 | 2.86E-03 | 5.43E-03 |
| BP | GO:0033490~cholesterol biosynthetic process via lathosterol | 3 | 2.50 | 2.26E-04 | Q15392, Q9UBM7, O75845 | 105 | 4 | 16792 | 119.9428571 | 1.68E-01 | 8.77E-02 | 3.47E-01 |
| BP | GO:0033489~cholesterol biosynthetic process via desmosterol | 3 | 2.50 | 2.26E-04 | Q15392, Q9UBM7, O75845 | 105 | 4 | 16792 | 119.9428571 | 1.68E-01 | 8.77E-02 | 3.47E-01 |
| BP | GO:0055114~oxidation-reduction process | 13 | 10.83 | 2.96E-04 | Q8TC12, Q9NZ01, Q16850, Q15392, Q9UBM7, O95864, P49326, O75845, O00767, Q8NBX0, O60427, Q15800, Q53GQ0 | 105 | 592 | 16792 | 3.511840412 | 2.14E-01 | 7.71E-02 | 4.55E-01 |
| BP | GO:0055085~transmembrane transport | 8 | 6.67 | 8.06E-04 | P33527, O75387, Q9UP95, P08034, P48066, Q8WWT9, Q86UQ4, P61619 | 105 | 244 | 167 | 5.243403591 | 4.81E-01 | 1.51E-01 | 1.23E |

| | | | | | | | | | | | | |
|---|---|---|---|---|---|---|---|---|---|---|---|---|
| | | | | | | | | 92 | | | | +00 |
| BP | GO:0006865~amino acid transport | 4 | 3.33 | 1.31E-03 | Q9H2H9, O75387, P31641, Q9UPY5 | 105 | 35 | 167792 | 18.2770068 | 6.54E-01 | 1.91E-01 | 1.99E+00 |
| BP | GO:0006914~autophagy | 6 | 5.00 | 1.42E-03 | P55061, Q13501, Q9H444, Q9H0E2, Q96GF1, O14964 | 105 | 133 | 167792 | 7.214607948 | 6.85E-01 | 1.75E-01 | 2.16E+00 |
| BP | GO:0008654~phospholipid biosynthetic process | 4 | 3.33 | 1.93E-03 | Q99755, P49585, Q9NUQ2, O60427 | 105 | 40 | 167792 | 15.99238095 | 7.92E-01 | 2.01E-01 | 2.93E+00 |
| BP | GO:0043066~negative regulation of apoptotic process | 10 | 8.33 | 2.06E-03 | P55061, Q15392, P49768, Q15041, Q9NZS9, Q13501, P11021, Q07820, P61978, P0CG47 | 105 | 455 | 167792 | 3.514809001 | 8.12E-01 | 1.89E-01 | 3.12E+00 |
| BP | GO:0006986~response to unfolded protein | 4 | 3.33 | 2.22E-03 | Q96CS3, P55061, O95140, P50454 | 105 | 42 | 167792 | 15.230839 | 8.36E-01 | 1.82E-01 | 3.37E+00 |
| BP | GO:0006915~apoptotic process | 11 | 9.17 | 2.70E-03 | P62745, Q9Y3E5, O95197, Q15392, Q15041, P67775, O95140, Q9NZS9, Q13501, Q13114, P21796 | 105 | 567 | 167792 | 3.102578315 | 8.89E-01 | 1.97E-01 | 4.08E+00 |
| BP | GO:0034975~protein folding in endoplasmic reticulum | 3 | 2.50 | 2.83E-03 | P27824, P11021, Q9BV81 | 105 | 13 | 167792 | 36.90549451 | 9.00E-01 | 1.89E-01 | 4.27E+00 |
| BP | GO:0006629~lipid metabolic process | 6 | 5.00 | 2.93E-03 | Q9NZ01, O14495, Q9NUJ7, O95864, O75845, O60427 | 105 | 157 | 167792 | 6.111737944 | 9.08E-01 | 1.80E-01 | 4.42E+00 |
| BP | GO:0006636~unsaturated fatty acid biosynthetic process | 3 | 2.50 | 3.78E-03 | O95864, O00767, O60427 | 105 | 15 | 167792 | 31.9847619 | 9.54E-01 | 2.11E-01 | 5.67E+00 |
| BP | GO:1901214~regulation of neuron death | 3 | 2.50 | 4.86E-03 | P02649, Q15392, P0CG47 | 105 | 17 | 167792 | 28.22184874 | 9.81E-01 | 2.46E-01 | 7.22E+00 |

| | | | | | | | | | | | | |
|---|---|---|---|---|---|---|---|---|---|---|---|---|
| BP | GO:0030433~ER-associated ubiquitin-dependent protein catabolic process | 4 | 3.33 | 6.12E-03 | Q96CS3, Q9Y679, P11021, Q96GF1 | 105 | 60 | 16792 | 10.6615873 | 9.93E-01 | 2.83E-01 | 9.00E+00 |
| BP | GO:0016197~endosomal transport | 4 | 3.33 | 7.96E-03 | Q13501, Q9H444, P0CG47, O14964 | 105 | 66 | 16792 | 9.692352092 | 9.98E-01 | 3.33E-01 | 1.16E+01 |
| BP | GO:0033344~cholesterol efflux | 3 | 2.50 | 1.04E-02 | P02649, P04114, Q86UQ4 | 105 | 25 | 16792 | 19.19085714 | 1.00E+00 | 3.93E-01 | 1.48E+01 |
| BP | GO:0016236~macroautophagy | 4 | 3.33 | 1.17E-02 | O95140, Q13501, P0CG47, P21796 | 105 | 76 | 16792 | 8.417042607 | 1.00E+00 | 4.12E-01 | 1.66E+01 |
| BP | GO:0043311~positive regulation of eosinophil degranulation | 2 | 1.67 | 1.23E-02 | Q12846, P55085 | 105 | 2 | 16792 | 159.9238095 | 1.00E+00 | 4.12E-01 | 1.74E+01 |
| BP | GO:0042787~protein ubiquitination involved in ubiquitin-dependent protein catabolic process | 5 | 4.17 | 1.51E-02 | Q99942, Q9NZS9, Q96GF1, P0CG47, Q93034 | 105 | 153 | 16792 | 5.226268285 | 1.00E+00 | 4.61E-01 | 2.08E+01 |
| BP | GO:0006694~steroid biosynthetic process | 3 | 2.50 | 1.67E-02 | Q16850, P48449, Q53GQ0 | 105 | 32 | 16792 | 14.99285714 | 1.00E+00 | 4.79E-01 | 2.28E+01 |
| BP | GO:0045595~regulation of cell differentiation | 3 | 2.50 | 1.67E-02 | P67775, O60427, Q96CS7 | 105 | 32 | 16792 | 14.99285714 | 1.00E+00 | 4.79E-01 | 2.28E+01 |
| BP | GO:0045540~regulation of cholesterol biosynthetic process | 2 | 1.67 | 1.85E-02 | P04114, Q9UBM7 | 105 | 3 | 16792 | 106.615873 | 1.00E+00 | 4.97E-01 | 2.49E+01 |

| | | | | | | | | | | | | |
|---|---|---|---|---|---|---|---|---|---|---|---|---|
| BP | GO:0001568~blood vessel development | 3 | 2.50 | 2.31E-02 | O14495, P49768, Q9UBM7 | 105 | 38 | 16792 | 12.62556391 | 1.00E+00 | 5.62E-01 | 3.02E+01 |
| BP | GO:0042159~lipoprotein catabolic process | 2 | 1.67 | 2.45E-02 | P02649, P04114 | 105 | 4 | 16792 | 79.96190476 | 1.00E+00 | 5.69E-01 | 3.18E+01 |
| BP | GO:0071787~endoplasmic reticulum tubular network assembly | 2 | 1.67 | 2.45E-02 | O95197, Q15041 | 105 | 4 | 16792 | 79.96190476 | 1.00E+00 | 5.69E-01 | 3.18E+01 |
| BP | GO:0035338~long-chain fatty-acyl-CoA biosynthetic process | 3 | 2.50 | 2.79E-02 | Q9NZ01, O00767, Q53GQ0 | 105 | 42 | 16792 | 11.42312925 | 1.00E+00 | 6.00E-01 | 3.52E+01 |
| BP | GO:0006620~posttranslational protein targeting to membrane | 2 | 1.67 | 3.06E-02 | Q9H444, P61619 | 105 | 5 | 16792 | 63.96952381 | 1.00E+00 | 6.21E-01 | 3.80E+01 |
| BP | GO:0006979~response to oxidative stress | 4 | 3.33 | 3.09E-02 | P02649, Q15392, P49768, Q9UPY5 | 105 | 110 | 16792 | 5.815411255 | 1.00E+00 | 6.11E-01 | 3.83E+01 |
| BP | GO:0014070~response to organic cyclic compound | 3 | 2.50 | 3.70E-02 | Q15843, Q99541, O60427 | 105 | 49 | 16792 | 9.791253644 | 1.00E+00 | 6.65E-01 | 4.40E+01 |
| BP | GO:0006633~fatty acid biosynthetic process | 3 | 2.50 | 4.12E-02 | O75845, Q15800, Q53GQ0 | 105 | 52 | 16792 | 9.226373626 | 1.00E+00 | 6.92E-01 | 4.77E+01 |
| BP | GO:0015813~L-glutamate transport | 2 | 1.67 | 4.26E-02 | O75915, P49768 | 105 | 7 | 16792 | 45.69251701 | 1.00E+00 | 6.92E-01 | 4.88E+01 |
| BP | GO:0042987~amyloid precursor protein catabolic process | 2 | 1.67 | 4.85E-02 | Q15392, P49768 | 105 | 8 | 16792 | 39.98095238 | 1.00E+00 | 7.28E-01 | 5.34E+01 |

| | | | | | | | | | | | | |
|---|---|---|---|---|---|---|---|---|---|---|---|---|
| BP | GO:0042158~lipoprotein biosynthetic process | 2 | 1.67 | 5.44E-02 | P02649, P04114 | 105 | 9 | 16792 | 35.53862434 | 1.00E+00 | 7.58E-01 | 5.77E+01 |
| BP | GO:0008104~protein localization | 3 | 2.50 | 5.49E-02 | Q15843, Q15392, Q13501 | 105 | 61 | 16792 | 7.865105386 | 1.00E+00 | 7.51E-01 | 5.80E+01 |
| BP | GO:0001523~retinoid metabolic process | 3 | 2.50 | 5.49E-02 | Q8TC12, P02649, P04114 | 105 | 61 | 16792 | 7.865105386 | 1.00E+00 | 7.51E-01 | 5.80E+01 |
| BP | GO:0034374~low-density lipoprotein particle remodeling | 2 | 1.67 | 6.61E-02 | P02649, P04114 | 105 | 11 | 16792 | 29.07705628 | 1.00E+00 | 8.05E-01 | 6.51E+01 |
| BP | GO:0008203~cholesterol metabolic process | 3 | 2.50 | 6.65E-02 | P02649, Q9Y5U4, P04114 | 105 | 68 | 16792 | 7.055462185 | 1.00E+00 | 7.97E-01 | 6.53E+01 |
| BP | GO:0016192~vesicle-mediated transport | 4 | 3.33 | 6.84E-02 | Q12846, Q9Y282, O95197, Q14677 | 105 | 152 | 16792 | 4.208521303 | 1.00E+00 | 7.98E-01 | 6.64E+01 |
| BP | GO:0019068~virion assembly | 2 | 1.67 | 7.19E-02 | P02649, P0CG47 | 105 | 12 | 16792 | 26.65396825 | 1.00E+00 | 8.05E-01 | 6.82E+01 |
| BP | GO:0050921~positive regulation of chemotaxis | 2 | 1.67 | 7.19E-02 | Q12846, P55085 | 105 | 12 | 16792 | 26.65396825 | 1.00E+00 | 8.05E-01 | 6.82E+01 |
| BP | GO:0015909~long-chain fatty acid transport | 2 | 1.67 | 7.19E-02 | P02649, Q99541 | 105 | 12 | 16792 | 26.65396825 | 1.00E+00 | 8.05E-01 | 6.82E+01 |
| BP | GO:0071712~ER-associated misfolded protein catabolic process | 2 | 1.67 | 7.19E-02 | Q99942, Q96GF1 | 105 | 12 | 16792 | 26.65396825 | 1.00E+00 | 8.05E-01 | 6.82E+01 |

| | | | | | | | | | | | |
|---|---|---|---|---|---|---|---|---|---|---|---|
| BP | GO:0015807~L-amino acid transport | 2 | 1.67 | 7.19E-02 | Q9H2H9, O75387 | 105 | 12 | 16792 | 26.65396825 | 1.00E+00 | 8.05E-01 | 6.82E+01 |
| BP | GO:0009791~post-embryonic development | 3 | 2.50 | 7.52E-02 | P04114, P49768, Q9UBM7 | 105 | 73 | 16792 | 6.57221135 | 1.00E+00 | 8.12E-01 | 7.00E+01 |
| BP | GO:0015804~neutral amino acid transport | 2 | 1.67 | 7.76E-02 | Q9H2H9, O75387 | 105 | 13 | 16792 | 24.603663 | 1.00E+00 | 8.14E-01 | 7.11E+01 |
| BP | GO:0036109~alpha-linolenic acid metabolic process | 2 | 1.67 | 7.76E-02 | O95864, O60427 | 105 | 13 | 16792 | 24.603663 | 1.00E+00 | 8.14E-01 | 7.11E+01 |
| BP | GO:0043123~positive regulation of I-kappaB kinase/NF-kappaB signaling | 4 | 3.33 | 7.83E-02 | Q8TB61, P55085, P08134, P0CG47 | 105 | 161 | 16792 | 3.973262348 | 1.00E+00 | 8.09E-01 | 7.15E+01 |
| BP | GO:0006820~anion transport | 2 | 1.67 | 8.33E-02 | P04920, P21796 | 105 | 14 | 16792 | 22.8462585 | 1.00E+00 | 8.22E-01 | 7.38E+01 |
| BP | GO:0030970~retrograde protein transport, ER to cytosol | 2 | 1.67 | 8.33E-02 | Q96CS3, Q9Y679 | 105 | 14 | 16792 | 22.8462585 | 1.00E+00 | 8.22E-01 | 7.38E+01 |
| BP | GO:0033700~phospholipid efflux | 2 | 1.67 | 8.33E-02 | P02649, Q86UQ4 | 105 | 14 | 16792 | 22.8462585 | 1.00E+00 | 8.22E-01 | 7.38E+01 |
| BP | GO:0006488~dolichol-linked oligosaccharide biosynthetic process | 2 | 1.67 | 8.90E-02 | Q9H3H5, Q5I7T1 | 105 | 15 | 16792 | 21.3231746 | 1.00E+00 | 8.35E-01 | 7.62E+01 |
| BP | GO:0036503~ERAD pathway | 2 | 1.67 | 8.90E-02 | Q99942, Q96GF1 | 105 | 15 | 167 | 21.3231746 | 1.00E+00 | 8.35E-01 | 7.62E |

| | | | | | | | | | | | | |
|---|---|---|---|---|---|---|---|---|---|---|---|---|
| | | | | | | | | 92 | | | | +01 |
| BP | GO:0032469~endoplasmic reticulum calcium ion homeostasis | 2 | 1.67 | 8.90E-02 | P55061, P49768 | 105 | 15 | 16792 | 21.3231746 | 1.00E+00 | 8.35E-01 | 7.62E+01 |
| BP | GO:0034389~lipid particle organization | 2 | 1.67 | 8.90E-02 | Q96CS3, Q8N0X7 | 105 | 15 | 16792 | 21.3231746 | 1.00E+00 | 8.35E-01 | 7.62E+01 |
| BP | GO:0043122~regulation of I-kappaB kinase/NF-kappaB signaling | 2 | 1.67 | 8.90E-02 | Q13501, P55085 | 105 | 15 | 16792 | 21.3231746 | 1.00E+00 | 8.35E-01 | 7.62E+01 |
| BP | GO:2001234~negative regulation of apoptotic signaling pathway | 2 | 1.67 | 9.47E-02 | P55061, P49768 | 105 | 16 | 16792 | 19.99047619 | 1.00E+00 | 8.47E-01 | 7.83E+01 |
| BP | GO:0044257~cellular protein catabolic process | 2 | 1.67 | 9.47E-02 | Q99942, P04114 | 105 | 16 | 16792 | 19.99047619 | 1.00E+00 | 8.47E-01 | 7.83E+01 |

**Supplemental Table 3-S3. Predicted subcellular localizations of candidate ERAD substrates.**

| Uniprot ID | Amino acid length | Molecular weight | Subcellular location |
|---|---|---|---|
| Q15041 | 203 AA | 23363 MW | Endomembrane system {ECO:0000269\|PubMed:10995579}; Multi-pass membrane protein {ECO:0000269\|PubMed:10995579}. Endoplasmic reticulum membrane {ECO:0000269\|PubMed:12754298 ECO:0000269\|PubMed:24076029 ECO:0000269\|PubMed:24262037}; Multi-pass membrane protein {ECO:0000269\|PubMed:24076029}. Endoplasmic reticulum {ECO:0000250\|UniProtKB:Q9JKW0}. Note=Predominantly localized to intracytoplasmic membranes. Preferentially localizes at the ER tubules and the edge of the ER sheets both of which are characterized by a high membrane curvature. {ECO:0000269\|PubMed:24262037}. |
| Q92979 | 244 AA | 26720 MW | Nucleus nucleolus {ECO:0000269\|PubMed:11935223}. |
| P04114 | 4563 AA | 515605 MW | Cytoplasm {ECO:0000269\|PubMed:22580899}. Secreted {ECO:0000269\|PubMed:22580899 ECO:0000269\|PubMed:26224785}. |
| Q9UP95 | 1085 AA | 120650 MW | Membrane; Multi-pass membrane protein. |
| Q8WWT9 | 602 AA | 66841 MW | Cell membrane {ECO:0000269\|PubMed:17426067}; Multi-pass membrane protein {ECO:0000269\|PubMed:17426067}. |
| Q9H3H5 | 408 AA | 46090 MW | Endoplasmic reticulum membrane; Multi-pass membrane protein. |
| O00767 | 359 AA | 41523 MW | Endoplasmic reticulum membrane {ECO:0000269\|PubMed:15907797}; Multi-pass membrane protein {ECO:0000269\|PubMed:18765284 ECO:0000305}. |
| Q9NZS9 | 450 AA | 52738 MW | Endoplasmic reticulum membrane {ECO:0000269\|PubMed:10716992 ECO:0000269\|PubMed:14502241}; Multi- pass membrane protein {ECO:0000269\|PubMed:10716992 ECO:0000269\|PubMed:14502241}. |
| P0CG47 | 229 AA | 25762 MW | Ubiquitin: Cytoplasm {ECO:0000250}. Nucleus {ECO:0000250}. |
| Q9NXW2 | 375 AA | 41819 MW | Endoplasmic reticulum membrane {ECO:0000269\|PubMed:21148293 ECO:0000269\|PubMed:21150129 ECO:0000269\|PubMed:24732912 ECO:0000269\|PubMed:27916661}; Single- pass membrane protein {ECO:0000255}. Nucleus membrane {ECO:0000269\|PubMed:24732912}; Single-pass membrane protein {ECO:0000305}. Note=Localizes to the endoplasmic reticulum membrane (PubMed:21150129 PubMed:21148293 PubMed:24732912 PubMed:27916661). When overexpressed forms membranous structures in the nucleus (PubMed:24732912). {ECO:0000269\|PubMed:21148293 ECO:0000269\|PubMed:21150129 ECO:0000269\|PubMed:24732912 ECO:0000269\|PubMed:27916661}. |
| Q96QK8 | 99 AA | 10710 MW | 0 |
| Q96BD0 | 722 AA | 77193 MW | Cell membrane; Multi-pass membrane protein. |
| Q99942 | 180 AA | 19881 MW | Membrane; Multi-pass membrane protein. Mitochondrion membrane. Endoplasmic reticulum membrane. Note=Predominantly located in the plasma membrane with some localization occurring within cytoplasmic organelles. |
| Q9UPY5 | 501 AA | 55423 MW | Membrane {ECO:0000269\|PubMed:15151999}; Multi-pass membrane protein {ECO:0000269\|PubMed:15151999}. |

| | | | |
|---|---|---|---|
| Q9P0S3 | 153 AA | 17371 MW | Endoplasmic reticulum membrane {ECO:0000269\|PubMed:12093374}; Multi-pass membrane protein {ECO:0000269\|PubMed:12093374}. |
| Q70UQ0 | 350 AA | 39309 MW | Endoplasmic reticulum membrane {ECO:0000269\|PubMed:15389287}; Single-pass membrane protein {ECO:0000269\|PubMed:15389287}. Note=Isoform 4 deletion of the hydrophobic or transmembrane region between AA 45-63 results in uniform distribution throughout the cell suggesting that this region is responsible for endoplasmic reticulum localization. |
| O75915 | 188 AA | 21615 MW | Endoplasmic reticulum membrane {ECO:0000250\|UniProtKB:Q9ES40}; Multi-pass membrane protein {ECO:0000255}. Cell membrane {ECO:0000250\|UniProtKB:Q9ES40}; Multi-pass membrane protein {ECO:0000255}. Cytoplasm {ECO:0000250\|UniProtKB:Q9ES40}. Cytoplasm cytoskeleton {ECO:0000250\|UniProtKB:Q9ES40}. Note=Also exists as a soluble form in the cytoplasm. Associated with microtubules. {ECO:0000250\|UniProtKB:Q9ES40}. |
| P04844 | 631 AA | 69284 MW | Endoplasmic reticulum {ECO:0000250\|UniProtKB:F1PCT7}. Endoplasmic reticulum membrane; Multi-pass membrane protein {ECO:0000305}. |
| O60427 | 444 AA | 51964 MW | Isoform 1: Endoplasmic reticulum membrane {ECO:0000250\|UniProtKB:A4UVI1}; Multi-pass membrane protein {ECO:0000250\|UniProtKB:A4UVI1}. Mitochondrion {ECO:0000269\|PubMed:22619218}. |
| P04920 | 1241 AA | 137009 MW | Membrane; Multi-pass membrane protein. |
| P51572 | 246 AA | 27992 MW | Endoplasmic reticulum membrane {ECO:0000269\|PubMed:9334338 ECO:0000269\|PubMed:9396746}; Multi- pass membrane protein {ECO:0000255}. Endoplasmic reticulum-Golgi intermediate compartment membrane {ECO:0000269\|PubMed:11042173 ECO:0000269\|PubMed:9396746}; Multi-pass membrane protein {ECO:0000255}. Note=May shuttle between the ER and the intermediate compartment/cis-Golgi complex. {ECO:0000269\|PubMed:9396746}. |
| Q9Y5U4 | 225 AA | 24778 MW | Endoplasmic reticulum membrane {ECO:0000269\|PubMed:12242332}; Multi-pass membrane protein {ECO:0000269\|PubMed:12242332}. |
| Q13501 | 440 AA | 47687 MW | Cytoplasm cytosol {ECO:0000269\|PubMed:20168092}. Late endosome. Lysosome. Cytoplasmic vesicle autophagosome. Nucleus. Endoplasmic reticulum. Nucleus PML body {ECO:0000269\|PubMed:20168092}. Cytoplasm myofibril sarcomere {ECO:0000250}. Note=In cardiac muscle localizes to the sarcomeric band (By similarity). Commonly found in inclusion bodies containing polyubiquitinated protein aggregates. In neurodegenerative diseases detected in Lewy bodies in Parkinson disease neurofibrillary tangles in Alzheimer disease and HTT aggregates in Huntington disease. In protein aggregate diseases of the liver found in large amounts in Mallory bodies of alcoholic and nonalcoholic steatohepatitis hyaline bodies in hepatocellular carcinoma and in SERPINA1 aggregates. Enriched in Rosenthal fibers of pilocytic astrocytoma. In the cytoplasm observed in both membrane-free ubiquitin-containing protein aggregates (sequestosomes) and membrane-surrounded autophagosomes. Colocalizes with TRIM13 in the perinuclear endoplasmic reticulum. Co-localizes with TRIM5 in cytoplasmic bodies. When nuclear export is blocked by treatment with leptomycin B accumulates in PML bodies. {ECO:0000269\|PubMed:20168092}. |
| P0CK96 | 405 AA | 43777 MW | Membrane {ECO:0000305}; Multi-pass membrane protein {ECO:0000305}. |
| Q6ZVX9 | 377 AA | 42692 MW | Cell membrane {ECO:0000269\|PubMed:23161870}; Multi-pass membrane protein {ECO:0000255}. |

| | | | |
|---|---|---|---|
| Q9UBM7 | 475 AA | 54489 MW | Endoplasmic reticulum membrane {ECO:0000269\|PubMed:9878250}; Multi-pass membrane protein {ECO:0000269\|PubMed:9878250}. |
| Q99541 | 437 AA | 48075 MW | Membrane {ECO:0000305}; Peripheral membrane protein {ECO:0000305}. Lipid droplet {ECO:0000305\|PubMed:26357594}. |
| P50454 | 418 AA | 46441 MW | Endoplasmic reticulum lumen. |
| Q96GF1 | 192 AA | 20459 MW | Mitochondrion outer membrane {ECO:0000269\|PubMed:21931693}; Multi-pass membrane protein {ECO:0000305}. Endoplasmic reticulum membrane {ECO:0000269\|PubMed:24019521 ECO:0000269\|PubMed:27485036}; Multi- pass membrane protein {ECO:0000305}. |
| Q8TC12 | 318 AA | 35386 MW | Endoplasmic reticulum membrane {ECO:0000269\|PubMed:12036956}; Single-pass type II membrane protein {ECO:0000269\|PubMed:12036956}. |
| O15173 | 223 AA | 23818 MW | Membrane {ECO:0000305}; Single-pass membrane protein {ECO:0000305}. |
| Q9Y679 | 476 AA | 53028 MW | Endoplasmic reticulum membrane {ECO:0000269\|PubMed:12042322 ECO:0000269\|PubMed:18711132}; Single-pass type III membrane protein {ECO:0000269\|PubMed:12042322 ECO:0000269\|PubMed:18711132}; Cytoplasmic side {ECO:0000269\|PubMed:12042322 ECO:0000269\|PubMed:18711132}. |
| Q9Y5Z9 | 338 AA | 36831 MW | Endoplasmic reticulum membrane; Multi-pass membrane protein. Golgi apparatus membrane; Multi-pass membrane protein. Mitochondrion membrane. Cytoplasm. Nucleus. |
| O95864 | 444 AA | 52259 MW | Endoplasmic reticulum membrane {ECO:0000305}; Multi-pass membrane protein {ECO:0000305}. |
| O75845 | 299 AA | 35301 MW | Endoplasmic reticulum membrane {ECO:0000305}; Multi-pass membrane protein {ECO:0000305}. |
| Q8TB61 | 432 AA | 47515 MW | Golgi apparatus membrane {ECO:0000269\|PubMed:12716889}; Multi-pass membrane protein {ECO:0000269\|PubMed:12716889}. |
| P49768 | 467 AA | 52668 MW | Endoplasmic reticulum membrane {ECO:0000269\|PubMed:10593990 ECO:0000269\|PubMed:8574969 ECO:0000269\|PubMed:9738936 ECO:0000305\|PubMed:10037471 ECO:0000305\|PubMed:15274632}; Multi-pass membrane protein {ECO:0000269\|PubMed:25043039 ECO:0000269\|PubMed:25918421 ECO:0000269\|PubMed:26280335 ECO:0000269\|PubMed:26623517}. Golgi apparatus membrane {ECO:0000269\|PubMed:10593990 ECO:0000269\|PubMed:8574969 ECO:0000305\|PubMed:10037471 ECO:0000305\|PubMed:15274632}; Multi-pass membrane protein {ECO:0000269\|PubMed:25043039 ECO:0000269\|PubMed:25918421 ECO:0000269\|PubMed:26280335 ECO:0000269\|PubMed:26623517}. Cytoplasmic granule {ECO:0000269\|PubMed:11987239}. Cell membrane {ECO:0000269\|PubMed:10593990 ECO:0000269\|PubMed:11953314 ECO:0000269\|PubMed:11987239 ECO:0000269\|PubMed:21143716}. Note=Translocates with bound NOTCH1 from the endoplasmic reticulum and/or Golgi to the cell surface (PubMed:10593990). Colocalizes with CDH1/2 at sites of cell-cell contact. Colocalizes with CTNNB1 in the endoplasmic reticulum and the proximity of the plasma membrane (PubMed:9738936). Also present in azurophil granules of neutrophils (PubMed:11987239). Colocalizes with UBQLN1 in the cell membrane and in cytoplasmic juxtanuclear structures called aggresomes (PubMed:21143716). {ECO:0000269\|PubMed:10593990 ECO:0000269\|PubMed:11987239 ECO:0000269\|PubMed:21143716 ECO:0000269\|PubMed:9738936}. |
| Q16850 | 503 AA | 56806 MW | Endoplasmic reticulum membrane {ECO:0000250\|UniProtKB:Q64654}; Single-pass membrane protein {ECO:0000255}. Microsome membrane |

| | | | |
|---|---|---|---|
| | | | {ECO:0000250\|UniProtKB:Q64654}; Single-pass membrane protein {ECO:0000255}. |
| Q8NDN9 | 531 AA | 58252 MW | Nucleus {ECO:0000305}. |
| Q14677 | 625 AA | 68259 MW | Cytoplasm. Cytoplasm perinuclear region. Membrane; Peripheral membrane protein. Cytoplasmic vesicle clathrin-coated vesicle. Note=Found throughout the cell with the exception of the cell surface. Concentrated in the perinuclear region and associated with clathrin-coated vesicles close to the trans-Golgi network. |
| Q53GQ0 | 312 AA | 34324 MW | Endoplasmic reticulum membrane {ECO:0000269\|PubMed:12482854}; Multi-pass membrane protein {ECO:0000269\|PubMed:12482854}. |
| P63261 | 375 AA | 41793 MW | Cytoplasm cytoskeleton {ECO:0000269\|PubMed:28493397}. |
| Q15800 | 293 AA | 35216 MW | Endoplasmic reticulum membrane {ECO:0000305}; Multi-pass membrane protein {ECO:0000305}. |
| P55061 | 237 AA | 26538 MW | Endoplasmic reticulum membrane {ECO:0000269\|PubMed:21075086 ECO:0000269\|PubMed:22128171}; Multi- pass membrane protein {ECO:0000269\|PubMed:21075086 ECO:0000269\|PubMed:22128171}. |
| Q9NZ01 | 308 AA | 36034 MW | Endoplasmic reticulum membrane {ECO:0000269\|PubMed:12482854}; Multi-pass membrane protein {ECO:0000269\|PubMed:12482854}. |
| P61619 | 476 AA | 52265 MW | Endoplasmic reticulum membrane {ECO:0000269\|PubMed:27392076}; Multi-pass membrane protein {ECO:0000305}. Note=Localizes exclusively in granular structures in the endoplasmic reticulum (ER). {ECO:0000269\|PubMed:27392076}. |
| Q7Z3D4 | 306 AA | 34538 MW | Membrane {ECO:0000305}; Single-pass membrane protein {ECO:0000305}. |
| Q9Y282 | 383 AA | 43222 MW | Endoplasmic reticulum-Golgi intermediate compartment membrane {ECO:0000269\|PubMed:15308636}; Multi-pass membrane protein {ECO:0000269\|PubMed:15308636}. Golgi apparatus cis-Golgi network membrane {ECO:0000269\|PubMed:15308636}; Multi- pass membrane protein {ECO:0000269\|PubMed:15308636}. Endoplasmic reticulum membrane {ECO:0000269\|PubMed:15308636}; Multi-pass membrane protein {ECO:0000269\|PubMed:15308636}. Note=Cycles between the endoplasmic reticulum and the Golgi. |
| O95816 | 211 AA | 23772 MW | None Listed |
| P67775 | 309 AA | 35594 MW | Cytoplasm {ECO:0000269\|PubMed:16541025}. Nucleus {ECO:0000269\|PubMed:16541025}. Chromosome centromere {ECO:0000269\|PubMed:16541025}. Cytoplasm cytoskeleton spindle pole {ECO:0000269\|PubMed:16541025}. Note=In prometaphase cells but not in anaphase cells localizes at centromeres. During mitosis also found at spindle poles. Centromeric localization requires the presence of SGO2 (By similarity). {ECO:0000250}. |
| P84090 | 104 AA | 12259 MW | None Listed |
| Q9H0E2 | 274 AA | 30282 MW | Cytoplasm {ECO:0000305}. |
| Q9UNL2 | 185 AA | 21080 MW | Endoplasmic reticulum membrane; Multi-pass membrane protein. |
| P02649 | 317 AA | 36154 MW | Secreted {ECO:0000303\|PubMed:3283935}. |
| P49326 | 533 AA | 60221 MW | Microsome membrane. Endoplasmic reticulum membrane. |
| Q9BWH2 | 189 AA | 20676 MW | None Listed |

| | | | |
|---|---|---|---|
| Q00765 | 189 AA | 21493 MW | Membrane {ECO:0000255}; Multi-pass membrane protein {ECO:0000255}. Endoplasmic reticulum {ECO:0000269\|PubMed:23969831}. Note=Localizes to endoplasmic reticulum tubular network. {ECO:0000269\|PubMed:23969831}. |
| P46977 | 705 AA | 80530 MW | Endoplasmic reticulum {ECO:0000269\|PubMed:12887896}. Endoplasmic reticulum membrane {ECO:0000250\|UniProtKB:P46978}; Multi-pass membrane protein {ECO:0000250\|UniProtKB:P46978}. |
| Q9BV81 | 110 AA | 12017 MW | Membrane {ECO:0000269\|PubMed:22119785}; Multi-pass membrane protein {ECO:0000269\|PubMed:22119785}. |
| Q96HR9 | 211 AA | 23418 MW | Endoplasmic reticulum membrane {ECO:0000269\|PubMed:24098485 ECO:0000269\|PubMed:27889058}; Multi- pass membrane protein {ECO:0000255}. |
| P61956 | 95 AA | 10871 MW | Nucleus. Nucleus PML body. |
| Q86UQ4 | 5058 AA | 576159 MW | Membrane {ECO:0000305}; Multi-pass membrane protein {ECO:0000305}. |
| P61978 | 463 AA | 50976 MW | Cytoplasm {ECO:0000269\|PubMed:1729596}. Nucleus nucleoplasm {ECO:0000269\|PubMed:16360036 ECO:0000269\|PubMed:1729596 ECO:0000269\|PubMed:18775702 ECO:0000269\|PubMed:22721921}. Cell projection podosome {ECO:0000269\|PubMed:22721921}. Note=Recruited to p53/TP53- responsive promoters in the presence of functional p53/TP53 (PubMed:16360036). In case of ASFV infection there is a shift in the localization which becomes predominantly nuclear (PubMed:18775702). |
| Q9Y3E5 | 179 AA | 19194 MW | Mitochondrion. |
| Q15392 | 516 AA | 60101 MW | Endoplasmic reticulum membrane; Single-pass membrane protein. Golgi apparatus membrane; Single-pass membrane protein. |
| P11021 | 654 AA | 72333 MW | Endoplasmic reticulum lumen {ECO:0000269\|PubMed:21080038 ECO:0000269\|PubMed:21289099 ECO:0000269\|PubMed:23990668}. Melanosome {ECO:0000269\|PubMed:12643545}. Cytoplasm {ECO:0000250\|UniProtKB:P20029}. Note=Identified by mass spectrometry in melanosome fractions from stage I to stage IV. {ECO:0000269\|PubMed:12643545}. |
| Q8TCT9 | 377 AA | 41488 MW | Endoplasmic reticulum membrane {ECO:0000269\|PubMed:15998642}; Multi-pass membrane protein {ECO:0000305}. Membrane {ECO:0000269\|PubMed:12077416 ECO:0000269\|PubMed:15385547}; Multi-pass membrane protein {ECO:0000305}; Lumenal side {ECO:0000269\|PubMed:12077416 ECO:0000269\|PubMed:15385547}. |
| P27824 | 592 AA | 67568 MW | Endoplasmic reticulum membrane {ECO:0000269\|PubMed:22314232}; Single-pass type I membrane protein {ECO:0000255}. Endoplasmic reticulum {ECO:0000269\|PubMed:22314232}. Melanosome {ECO:0000269\|PubMed:12643545 ECO:0000269\|PubMed:17081065}. Note=Identified by mass spectrometry in melanosome fractions from stage I to stage IV (PubMed:12643545 PubMed:17081065). The palmitoylated form preferentially localizes to the perinuclear rough ER (PubMed:22314232). {ECO:0000269\|PubMed:12643545 ECO:0000269\|PubMed:17081065 ECO:0000269\|PubMed:22314232}. |
| Q7L5N7 | 544 AA | 60208 MW | Endoplasmic reticulum membrane {ECO:0000269\|PubMed:21498505}; Single-pass type II membrane protein {ECO:0000269\|PubMed:21498505}. Golgi apparatus membrane {ECO:0000250}; Single-pass type II membrane protein {ECO:0000250}. Lipid droplet {ECO:0000269\|PubMed:21498505}. |
| Q14254 | 428 AA | 47064 MW | Cell membrane {ECO:0000269\|PubMed:20682791}; Peripheral membrane protein {ECO:0000269\|PubMed:20682791}. Membrane caveola {ECO:0000269\|PubMed:20682791}; Peripheral membrane protein {ECO:0000269\|PubMed:20682791}. Endosome |

| | | | |
|---|---|---|---|
| | | | {ECO:0000269\|PubMed:20682791}. Membrane {ECO:0000305}; Lipid-anchor {ECO:0000305}. Note=Membrane-associated protein of caveolae. |
| Q8WUY1 | 208 AA | 23865 MW | Secreted {ECO:0000305}. |
| O75387 | 559 AA | 61477 MW | Membrane {ECO:0000305}; Multi-pass membrane protein {ECO:0000305}. |
| P31641 | 620 AA | 69830 MW | Cell membrane; Multi-pass membrane protein. |
| O95140 | 757 AA | 86402 MW | Mitochondrion outer membrane {ECO:0000269\|PubMed:11181170 ECO:0000269\|PubMed:11950885 ECO:0000269\|PubMed:12499352 ECO:0000269\|PubMed:23620051}; Multi- pass membrane protein {ECO:0000269\|PubMed:11181170 ECO:0000269\|PubMed:11950885 ECO:0000269\|PubMed:12499352 ECO:0000269\|PubMed:23620051}. Note=Colocalizes with BAX during apoptosis. {ECO:0000269\|PubMed:12499352}. |
| O75844 | 475 AA | 54813 MW | Endoplasmic reticulum membrane {ECO:0000269\|PubMed:23539603}; Multi-pass membrane protein {ECO:0000269\|PubMed:23539603}. Nucleus inner membrane {ECO:0000269\|PubMed:23539603}; Multi-pass membrane protein {ECO:0000269\|PubMed:23539603}. |
| Q96CS7 | 222 AA | 24736 MW | Recycling endosome membrane {ECO:0000269\|PubMed:21911378 ECO:0000269\|PubMed:22281740}; Peripheral membrane protein {ECO:0000269\|PubMed:21911378 ECO:0000269\|PubMed:22281740}. Note=Specifically detected in tubulovesicular structures and colocalizes with TFNR. |
| Q8NCU8 | 138 AA | 15608 MW | Membrane {ECO:0000305}; Single-pass membrane protein {ECO:0000305}. |
| Q8N2H4 | 156 AA | 17615 MW | Golgi apparatus membrane {ECO:0000269\|PubMed:15077113}; Multi-pass membrane protein {ECO:0000269\|PubMed:15077113}. |
| P62745 | 196 AA | 22123 MW | Late endosome membrane; Lipid-anchor. Cell membrane; Lipid-anchor. Nucleus. Cleavage furrow. Note=Late endosomal membrane (geranylgeranylated form). Plasma membrane (farnesylated form). Also detected at the nuclear margin and in the nucleus. Translocates to the equatorial region before furrow formation in a ECT2-dependent manner. |
| P05023 | 1023 AA | 112896 MW | Cell membrane sarcolemma {ECO:0000269\|PubMed:7711835}; Multi-pass membrane protein {ECO:0000255}. Melanosome {ECO:0000269\|PubMed:17081065}. Note=Identified by mass spectrometry in melanosome fractions from stage I to stage IV. {ECO:0000269\|PubMed:17081065}. |
| Q9C0D9 | 397 AA | 45229 MW | Membrane {ECO:0000305}; Multi-pass membrane protein {ECO:0000305}. |
| Q15843 | 81 AA | 9072 MW | Nucleus {ECO:0000269\|PubMed:9353319}. Note=Mainly nuclear. |
| Q9BQA9 | 187 AA | 20774 MW | Membrane {ECO:0000305}; Single-pass membrane protein {ECO:0000305}. |
| Q96LD4 | 638 AA | 69532 MW | Cytoplasm {ECO:0000269\|PubMed:11511098}. Nucleus {ECO:0000269\|PubMed:11511098}. |
| Q96B21 | 275 AA | 31826 MW | Membrane {ECO:0000305}; Multi-pass membrane protein {ECO:0000305}. |
| P05787 | 483 AA | 53704 MW | Cytoplasm {ECO:0000269\|PubMed:10973561 ECO:0000269\|PubMed:19188445}. Nucleus nucleoplasm {ECO:0000250}. Nucleus matrix {ECO:0000250}. |
| Q13114 | 568 AA | 64490 MW | Cytoplasm {ECO:0000305}. Endosome {ECO:0000250\|UniProtKB:Q60803}. Mitochondrion. Note=Undergoes endocytosis together with TLR4 upon LPS signaling (By similarity). Associated with mitochondria in response to virus. {ECO:0000250\|UniProtKB:Q60803}. |

| | | | |
|---|---|---|---|
| Q9NUQ2 | 364 AA | 42072 MW | Endoplasmic reticulum membrane {ECO:0000269\|PubMed:21173190}; Multi-pass membrane protein {ECO:0000269\|PubMed:21173190}. Nucleus envelope {ECO:0000269\|PubMed:21173190}. Mitochondrion {ECO:0000269\|PubMed:21173190}. |
| Q8NBX0 | 429 AA | 47151 MW | None Listed |
| P08034 | 283 AA | 32025 MW | Cell membrane; Multi-pass membrane protein. Cell junction gap junction. |
| Q96B96 | 161 AA | 17522 MW | Membrane {ECO:0000305}; Multi-pass membrane protein {ECO:0000305}. |
| P48066 | 632 AA | 70606 MW | Membrane; Multi-pass membrane protein. |
| P23458 | 1154 AA | 133277 MW | Endomembrane system; Peripheral membrane protein. Note=Wholly intracellular possibly membrane associated. |
| P38435 | 758 AA | 87561 MW | Endoplasmic reticulum membrane {ECO:0000269\|PubMed:10910912}; Multi-pass membrane protein {ECO:0000269\|PubMed:10910912}. |
| Q9H444 | 224 AA | 24950 MW | Cytoplasm cytosol {ECO:0000269\|PubMed:15511219}. Late endosome membrane {ECO:0000269\|PubMed:15511219 ECO:0000305\|PubMed:12860994}; Peripheral membrane protein {ECO:0000305}. Midbody {ECO:0000269\|PubMed:21310966 ECO:0000269\|PubMed:22422861}. Nucleus envelope {ECO:0000269\|PubMed:26040712}. Note=Recruited to the nuclear envelope by CHMP7 during late anaphase (PubMed:26040712). Localizes transiently to the midbody arms immediately before abscission (PubMed:22422861). {ECO:0000269\|PubMed:22422861 ECO:0000269\|PubMed:26040712}. |
| P55085 | 397 AA | 44126 MW | Cell membrane; Multi-pass membrane protein. |
| Q5I7T1 | 473 AA | 55448 MW | Cell membrane {ECO:0000250\|UniProtKB:O88788}; Multi-pass membrane protein {ECO:0000250\|UniProtKB:O88788}. |
| Q12846 | 297 AA | 34180 MW | Cell membrane {ECO:0000305}; Single-pass type IV membrane protein {ECO:0000305}. |
| Q07820 | 350 AA | 37337 MW | Membrane {ECO:0000305}; Single-pass membrane protein {ECO:0000305}. Cytoplasm. Mitochondrion. Nucleus nucleoplasm. Note=Cytoplasmic associated with mitochondria. |
| Q9NUJ7 | 323 AA | 36668 MW | Cytoplasm {ECO:0000269\|PubMed:22732399}. |
| O95197 | 1032 AA | 112611 MW | Endoplasmic reticulum membrane {ECO:0000269\|PubMed:12811824 ECO:0000269\|PubMed:15286784 ECO:0000269\|PubMed:16054885 ECO:0000269\|PubMed:16979658 ECO:0000269\|PubMed:17031492 ECO:0000269\|PubMed:17182608 ECO:0000269\|PubMed:17191123 ECO:0000269\|PubMed:24262037}; Multi- pass membrane protein {ECO:0000255}. Golgi apparatus membrane {ECO:0000269\|PubMed:15286784 ECO:0000269\|PubMed:16054885 ECO:0000269\|PubMed:16979658}; Multi-pass membrane protein {ECO:0000255}. |
| P33527 | 1531 AA | 171591 MW | Cell membrane {ECO:0000269\|PubMed:16230346}; Multi-pass membrane protein {ECO:0000255\|PROSITE-ProRule:PRU00441 ECO:0000269\|PubMed:16230346}. |
| Q9BUV8 | 137 AA | 15487 MW | None Listed |
| O14964 | 777 AA | 86192 MW | Cytoplasm {ECO:0000250\|UniProtKB:Q9JJ50}. Early endosome membrane {ECO:0000269\|PubMed:23166352 ECO:0000269\|PubMed:24790097}; Peripheral membrane protein {ECO:0000305\|PubMed:23166352 ECO:0000305\|PubMed:24790097}; Cytoplasmic side |

| | | | |
|---|---|---|---|
| | | | {ECO:0000305\|PubMed:23166352 ECO:0000305\|PubMed:24790097}. Endosome multivesicular body membrane {ECO:0000250\|UniProtKB:Q9JJ50}; Peripheral membrane protein {ECO:0000250\|UniProtKB:Q9JJ50}. Note=Colocalizes with UBQLN1 in ubiquitin-rich cytoplasmic aggregates that are not endocytic compartments. {ECO:0000269\|PubMed:16159959}. |
| Q99755 | 562 AA | 62633 MW | Cell membrane. Cytoplasm {ECO:0000250}. Nucleus speckle. Cell projection ruffle. Note=Colocalizes with RAC1 at actin-rich membrane ruffles. Localizes to nuclear speckles and associates with TUT1 to regulate polyadenylation of selected mRNAs. |
| P49585 | 367 AA | 41731 MW | Cytoplasm cytosol {ECO:0000250}. Membrane {ECO:0000250}; Peripheral membrane protein {ECO:0000250}. Note=It can interconvert between an inactive cytosolic form and an active membrane-bound form. {ECO:0000250}. |
| P24001 | 234 AA | 26676 MW | Secreted {ECO:0000269\|PubMed:15664165}. |
| Q8N0X7 | 666 AA | 72833 MW | Cytoplasm {ECO:0000269\|PubMed:19580544}. Midbody {ECO:0000269\|PubMed:20719964}. Note=Transiently associated with endosomes (PubMed:19580544). Colocalized with IST1 to the ends of Flemming bodies during cytokinesis (PubMed:20719964). {ECO:0000269\|PubMed:19580544 ECO:0000269\|PubMed:20719964}. |
| Q6UX53 | 244 AA | 27775 MW | None Listed |
| Q9C0B5 | 715 AA | 77545 MW | Cell membrane {ECO:0000250}; Multi-pass membrane protein {ECO:0000250}. |
| Q96CS3 | 445 AA | 52623 MW | Cytoplasm {ECO:0000269\|PubMed:12372427}. Lipid droplet {ECO:0000269\|PubMed:19773358 ECO:0000269\|PubMed:23297223}. Endoplasmic reticulum {ECO:0000269\|PubMed:18711132 ECO:0000269\|PubMed:23297223}. |
| Q9H6A9 | 2034 AA | 222039 MW | Membrane {ECO:0000305}; Multi-pass membrane protein {ECO:0000305}. |
| Q15155 | 1222 AA | 134324 MW | Membrane {ECO:0000305}; Single-pass type I membrane protein {ECO:0000305}. |
| Q9H2H9 | 487 AA | 54048 MW | Cell membrane {ECO:0000269\|PubMed:15054072}; Multi-pass membrane protein {ECO:0000269\|PubMed:15054072}. Note=Restricted to the somatodendritic compartment of neurons. Found in the cellular processes of neurons in the developing brain (By similarity). {ECO:0000250}. |
| O14495 | 311 AA | 35116 MW | Golgi apparatus trans-Golgi network membrane; Multi-pass membrane protein. Cell membrane; Multi-pass membrane protein. |
| P69849 | 1222 AA | 134134 MW | Membrane {ECO:0000305}; Single-pass type I membrane protein {ECO:0000305}. |
| P08134 | 193 AA | 22006 MW | Cell membrane {ECO:0000305}; Lipid-anchor {ECO:0000305}; Cytoplasmic side {ECO:0000305}. Cleavage furrow {ECO:0000269\|PubMed:16236794}. Note=Translocates to the equatorial region before furrow formation in a ECT2-dependent manner. |
| P48449 | 732 AA | 83309 MW | Endoplasmic reticulum membrane {ECO:0000269\|PubMed:14766201 ECO:0000269\|PubMed:15525992}; Peripheral membrane protein {ECO:0000269\|PubMed:14766201 ECO:0000269\|PubMed:15525992}. |
| P21796 | 283 AA | 30773 MW | Mitochondrion outer membrane {ECO:0000269\|PubMed:7539795}; Multi-pass membrane protein {ECO:0000269\|PubMed:18755977 ECO:0000269\|PubMed:18832158}. Cell membrane {ECO:0000269\|PubMed:25168729 ECO:0000269\|PubMed:25296756}; Multi-pass membrane protein {ECO:0000269\|PubMed:18755977 ECO:0000269\|PubMed:18832158}. Membrane raft |

| | | | |
|---|---|---|---|
| | | | {ECO:0000269\|PubMed:25168729}; Multi-pass membrane protein {ECO:0000269\|PubMed:18755977 ECO:0000269\|PubMed:18832158}. |
| Q93034 | 780 AA | 90955 MW | None Listed |